

**Carbon ($\delta^{13}\text{C}$) and Strontium ($^{87}\text{Sr}/^{86}\text{Sr}$)- based
chemostratigraphy of the Oxfordian series in the Lower
Saxony Basin of Northern Germany**

Von der Naturwissenschaftlichen Fakultät der
Gottfried Wilhelm Leibniz Universität Hannover

zur Erlangung des Grades

Doktor der Naturwissenschaften (Dr. rer. nat.)

genehmigte Dissertation

von

Deyan Zhang, Lixue shuoshi (Master of science)

(Chengdu University of Technology)

2023

Referent: Prof. Dr. Ulrich Heimhofer

Korreferent: Prof. Dr. Jörg Mutterlose

Tag der Promotion: 02. 08. 2023

Abstract

The Late Jurassic (ca. 161.5-145 Ma) witnessed significant changes in climate, sea-level, and global sedimentation patterns due to the break-up of the supercontinent Pangea. During this time, the Oxfordian interval in particular experienced multiple and pronounced perturbations of the global carbon cycle. To better understand these changes, shoal-water carbonate rocks, which archive important signatures of the biosphere's evolution, can be studied.

The Lower Saxony Basin (LSB) was located in the Boreal Realm during the Late Jurassic and was characterized by widespread shallow-marine carbonate deposition. Despite multiple biostratigraphic schemes that have been developed, the stratigraphy and subdivision of the Upper Jurassic rocks of the LSB are still poorly defined. Due to the scarcity of reliable biostratigraphic markers and numerous sedimentary gaps, the stratigraphic age assignment is still uncertain and hampers further studies on a basin-wide scale.

In order to reconstruct stratigraphic correlation and paleoclimatic interpretation, three well-accessible sections (Bisperode section, Osterwald section, Langenberg section) and a scientific borehole (Konrad #101 core) were studied within the LSB. A high-resolution carbonate microfacies and sequence stratigraphy are first analyzed, which form the baseline for the conceptualization of a reef-bearing carbonate ramp model. The supra-regional correlation of the observed sequences is discussed.

Chemostratigraphy represents a reliable technique for correlation and calibration of biostratigraphic schemes on local and global scales. However, new biocalcite-derived $^{87}\text{Sr}/^{86}\text{Sr}$ results from the Oxfordian Korallenoolith Formation in LSB fail to provide an improved age assignment, possibly due to environmental factors such as continental freshwater discharge affecting the seawater $^{87}\text{Sr}/^{86}\text{Sr}$ ratios recorded in the studied shell material. In addition, a high-resolution carbonate $\delta^{13}\text{C}_{\text{carb}}$ record is presented and compared with other existing records collected from the LSB as well as from Tethyan and proto-Atlantic sites. The $\delta^{13}\text{C}_{\text{carb}}$ data enable the refinement of the pre-existing biostratigraphic framework and the establishment of a high-resolution carbon isotope-based correlation scheme. The new framework improves the stratigraphic correlation between the western and eastern parts of the LSB and allows for a better assessment of the impact of carbon cycle disturbances on the shallow-marine carbonate systems in this area. The study provides critical insights into the global pacing of the Oxfordian carbon isotope excursions and the role of environmental factors in shaping them.

Keywords: Oxfordian; shallow-marine carbonate deposits; Lower Saxony Basin; sequence stratigraphy; chemostratigraphy

Kurzfassung

Die späte Jurazeit (ca. 161.5-145 Ma) war Zeuge bedeutender globaler Veränderungen des Klimas, des Meeresspiegels und der marinen Sedimentationsmuster infolge des Auseinanderbrechens des Superkontinents Pangäa. Während dieser Zeit kam es insbesondere im Oxfordium zu zahlreichen Störungen des globalen Kohlenstoffkreislaufs. Um diese Veränderungen besser zu verstehen, können Karbonatgesteine, die wichtige Archive der Entwicklung der Biosphäre darstellen, untersucht werden.

Das Niedersächsische Becken (NB) befand sich während des späten Jura im borealen Bereich und war durch kontinuierliche flachmarine Karbonatablagerung gekennzeichnet. Trotz mehrerer biostratigraphischer Zonierungen, die erstellt wurden, sind die Stratigraphie und Unterteilung der Gesteine des oberen Jura im NB immer noch schlecht definiert. Aufgrund des Mangels an biostratigraphischen Markern und zahlreicher Hiaten ist die stratigraphische Datierung nach wie vor unsicher und erschwert weitere Studien im gesamten Becken. Um die stratigraphische Korrelation und die paläoklimatische Interpretation zu rekonstruieren, wurden drei sedimentäre Abfolgen in Aufschlüssen (Bisperode, Osterwald, Langenberg) und eine wissenschaftliche Bohrung (Konrad-Kem #101) untersucht. Zunächst wurden eine hochauflösende Karbonat-Mikrofazies Analyse und eine sequenzstratigraphische Analyse durchgeführt, welche die Grundlage für die Konzeption eines riff-führenden Karbonat-Rampenmodells bilden. Die überregionale Korrelation der beobachteten Sequenzen wurde anschließend diskutiert.

Die Chemostratigraphie stellt ein zuverlässiges Mittel dar, biostratigraphische Schemata auf lokaler und globaler Ebene zu vergleichen und zu kalibrieren. Neue, aus Biocalcit gewonnene $^{87}\text{Sr}/^{86}\text{Sr}$ -Daten der Korallenoolith-Formation (Oxfordium) im NB konnten jedoch keine genaue Alterszuordnung liefern, was möglicherweise auf Umweltfaktoren wie kontinentalen Süßwassereintrag zurückzuführen ist, welche die aus Schalenmaterial abgeleiteten $^{87}\text{Sr}/^{86}\text{Sr}$ -Verhältnisse im Meerwasser beeinflussen. Um diese Einschränkungen zu beheben, wird eine hochauflösende C-Isotopen ($\delta^{13}\text{C}_{\text{carb}}$) Kurve präsentiert und mit anderen bestehenden Aufzeichnungen aus der Tethys und dem Proto-Atlantik verglichen. Die $\delta^{13}\text{C}$ -Daten ermöglichen die Verfeinerung des bereits bestehenden biostratigraphischen Rahmens und die Erstellung eines hochauflösenden stratigraphischen $\delta^{13}\text{C}_{\text{carb}}$ -Korrelationsdatensatzes. Der neue Rahmen verbessert die Korrelationsfähigkeit zwischen den westlichen und östlichen Teilen des NB und ermöglicht eine bessere Einschätzung der Auswirkungen von Störungen des Kohlenstoffkreislaufs auf die flachmarinen Karbonatsysteme im NB. Diese Studie liefert kritische Einblicke in das globale Tempo der Kohlenstoffisotopenexkursionen im Oxfordium und die Rolle von Umweltfaktoren bei ihrer Gestaltung.

Schlüsselwörter: Oxfordium; Flachmarine Karbonatablagerungen; Niedersächsisches Becken; Sequenzstratigraphie; Chemostratigraphie

Table of Contents

| | |
|---|-----------|
| Abstract | I |
| Kurzfassung..... | II |
| 1. Introduction..... | 1 |
| 1.1 Late Jurassic paleogeography and sea-level changes..... | 1 |
| 1.2 Chemostratigraphy..... | 3 |
| 1.2.1 Carbon isotope | 3 |
| 1.2.2 Strontium isotopes | 4 |
| 1.3 Geological setting..... | 5 |
| 1.3.1 Oxfordian strata in the LSB..... | 6 |
| 1.3.2 Biostratigraphy..... | 7 |
| 1.4 Main objectives..... | 8 |
| 1.5 General outline of the thesis..... | 9 |
| 1.6 References..... | 10 |
| 2. Carbonate microfacies and transgressive-regressive sequences of Oxfordian shallow-water limestones (Korallenoolith, Lower Saxony Basin) | 15 |
| 2.1 Abstract..... | 15 |
| 2.2 Introduction..... | 16 |
| 2.3 Geological setting..... | 16 |
| 2.3.1 Regional geology | 16 |
| 2.3.2 Stratigraphic framework..... | 18 |
| 2.4 Methods..... | 19 |
| 2.4.1 Fieldwork, sampling, and facies analysis | 19 |
| 2.4.2 Sequence stratigraphy | 19 |
| 2.5 Results and interpretation | 21 |
| 2.5.1 Lithostratigraphy | 21 |
| 2.5.2 Facies types | 22 |
| 2.5.3 Depositional model | 30 |
| 2.6 Sequence analysis..... | 32 |
| 2.6.1 Small-scale sequences | 32 |
| 2.6.2 Medium-scale sequences | 34 |
| 2.6.3 Large-scale sequences | 34 |
| 2.7 Discussion..... | 35 |
| 2.8 Conclusions..... | 37 |
| 2.9 Acknowledgments..... | 37 |
| 2.10 References..... | 37 |
| 3. First record of the Middle Oxfordian positive carbon isotope excursion within the Korallenoolith Formation, Lower Saxony Basin, Germany | 43 |

Table of contents

| | |
|--|-----------|
| 3.1 Abstract..... | 43 |
| 3.2 Introduction..... | 44 |
| 3.3 Geological setting and stratigraphy..... | 44 |
| 3.4 Methodology..... | 49 |
| 3.5 Results..... | 49 |
| 3.5.1 <i>Lithofacies and sediment composition</i> | 49 |
| 3.5.2 <i>Stable isotope results</i> | 50 |
| 3.6 Discussion | 51 |
| 3.6.1 <i>Significance of the $\delta^{13}\text{C}$ pattern</i> | 51 |
| 3.6.2 <i>Chemostratigraphic correlation with other Middle Oxfordian $\delta^{13}\text{C}$ records</i> | 52 |
| 3.6.3 <i>What triggered the major Middle Oxfordian carbon-isotope excursion?</i> | 55 |
| 3.7 Conclusions..... | 55 |
| 3.8 Acknowledgments | 56 |
| 3.9 References..... | 56 |
| 4. $^{87}\text{Sr}/^{86}\text{Sr}$ chemostratigraphy of Oxfordian carbonate deposits, Lower Saxony Basin, Northern Germany | 61 |
| 4.1 Abstract..... | 61 |
| 4.2 Introduction..... | 62 |
| 4.3 Geological setting..... | 63 |
| 4.4 Materials and methods | 65 |
| 4.4.1 <i>Materials</i> | 65 |
| 4.4.2 <i>Petrography and cathodoluminescence analyses of shell material</i> | 65 |
| 4.4.3 <i>Elemental and strontium-isotope analyses</i> | 65 |
| 4.5 Results and interpretation | 68 |
| 4.5.1 <i>Shell microstructure and cathodoluminescence characteristics</i> | 68 |
| 4.5.2 <i>Element concentrations and isotopic compositions</i> | 72 |
| 4.6 Discussion | 73 |
| 4.6.1 <i>Preservation of shells and reliability of strontium-isotope ratios</i> | 73 |
| 4.6.2 <i>Numerical age constraints</i> | 75 |
| 4.6.3 <i>Regional factors affecting mollusc shell $^{87}\text{Sr}/^{86}\text{Sr}$ ratios and their implications</i> | 77 |
| 4.7 Conclusions..... | 78 |
| 4.8 Acknowledgments | 78 |
| 4.9 References..... | 78 |
| 5. Carbon isotope stratigraphy of an Oxfordian carbonate ramp system, Lower Saxony Basin, Northern Germany | 83 |
| 5.1 Abstract..... | 83 |
| 5.2 Introduction..... | 84 |
| 5.3 Geological setting..... | 85 |
| 5.4 Lithostratigraphy and carbonate facies description | 87 |
| 5.4.1 <i>Bisperode section</i> | 87 |

Table of Contents

| | |
|---|------------|
| 5.4.2 Osterwald section | 89 |
| 5.4.3 Langenberg section | 90 |
| 5.5 Materials and methods | 90 |
| 5.5.1 Fieldwork and sampling..... | 90 |
| 5.5.2 Isotope analysis | 91 |
| 5.6 Stable isotope results | 91 |
| 5.6.1 Bisperode section | 91 |
| 5.6.2 Osterwald section | 92 |
| 5.6.3 Langenberg section | 92 |
| 5.7 Discussion | 92 |
| 5.7.1 Reliability of the carbonate carbon and oxygen isotope data | 92 |
| 5.7.2 Local environmental effects on carbon isotope signatures | 94 |
| 5.7.3 Carbon isotope-based correlation within the LBS | 97 |
| 5.8 Conclusions..... | 99 |
| 5.9 Acknowledgements | 100 |
| 5.10 References | 100 |
| 6. Conclusions | 107 |
| Appendix..... | 109 |
| Acknowledgments | 129 |
| Curriculum Vitae | 131 |
| Publications | 133 |

1. Introduction

Carbonate rocks hold the potential to preserve biological, chemical, or physical signatures of biosphere's evolution through time (Weissert 2000). Deep-time shallow-marine carbonates represent highly sensitive ecological systems and can provide powerful evidence to our understanding of the climate system, sea-level change, and response mechanisms of the biosphere to $p\text{CO}_2$ perturbations (Immenhauser et al. 2008; Huck and Heimhofer 2015; Lear et al. 2020). In the near future, large-scale changes of the global carbon cycle are predicted to continue (Lear et al. 2020), and studying the geologic past might offer some critical insights into potential consequences and solutions associated with anthropogenic $p\text{CO}_2$ increase. Research efforts to understand the long-term history of the global carbon cycle based on its carbon isotopic signature have been ongoing for many decades (Jeltsch-Thömmes and Joos 2020). For instance, the Late Jurassic corresponds to a unique time interval characterized by multiple perturbations of the global carbon cycle (Padden et al. 2001, 2002; Weissert and Erba 2004). During the Late Jurassic, the Oxfordian is a key period, for which the sedimentary record indicates significant changes in global climate and sea level (e.g. Hallam 2001; Dromart et al. 2003; Cecca et al. 2001; Collin et al. 2005; Louis-Schmid et al. 2007a, 2007b; Ramajo and Aurell 2008; Bouilila et al. 2010).

1.1 Late Jurassic paleogeography and sea-level changes

The Jurassic Period (ca. 201–144 Ma) constitutes the middle period of the Mesozoic Era and is named after the Jura Mountains in Switzerland, where limestone strata from this interval were first described (Gradstein et al. 2020). The Jurassic is subdivided into 11 stages based on ammonite biostratigraphy (Gradstein et al. 2020) and complemented by chemo-, magneto-, and cyclostratigraphy as well as by other biostratigraphic indicators (e.g., calcareous nannofossils). This time period is marked by fundamental reorganizations of paleogeography, paleoceanography, and ecosystems (Ziegler 1990). During the Late Jurassic, the break-up of the supercontinent Pangea continued with different spreading centers and oceanic rifts forming between North America, Eurasia, and Gondwana, and between the various segments of Gondwana itself (Ziegler 1990; Weissert and Mohr 1996; Padden et al. 2001, 2002; Hesselbo et al. 2020) (Fig. 1). This created more coastlines and shallow seas and shifted the climatic conditions from the continental dry Triassic climate towards more humid conditions prevailing during the Jurassic, indicated in the sedimentary record by the replacement of many arid areas into lush forests (Frakes et al. 1992).

In western Europe, Jurassic strata are well exposed with extensive and shallow-marine carbonate deposits and abundantly accessible outcrops. Good examples include the Jurassic Coast World Heritage Site in the UK, or the outcrops of Solnhofen, Langenberg, and Bisperode in Germany, where well exposed marine sequences indicate a time when much of the Central European continent was submerged under shallow tropical seas.

Chapter 1

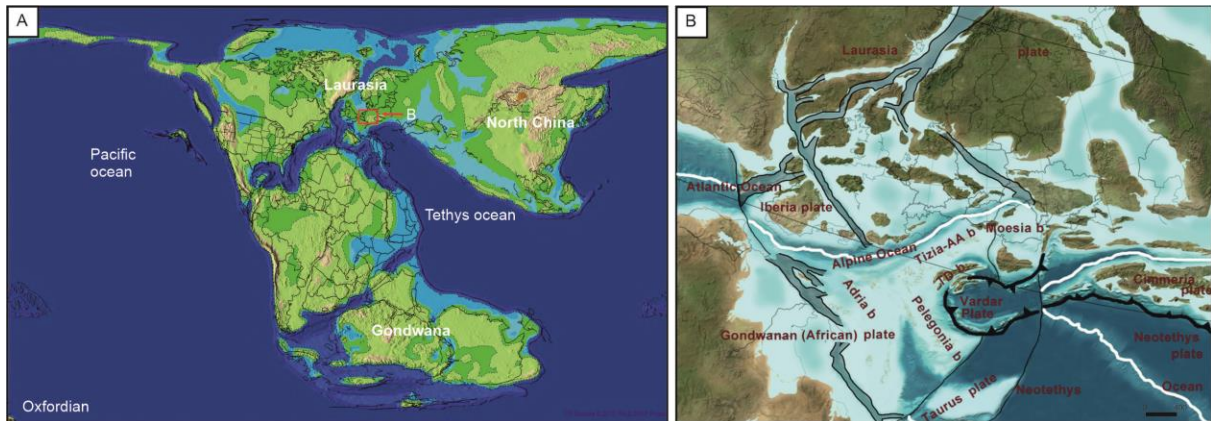


Fig. 1 - A) Paleogeographic map for the Late Jurassic (Oxfordian) (*PaleoDEM Resource - Scotese and Wright (2018) - EarthByte*). B) Enlargement of the area defined by the red box in (A) with the study area labeled with a red asterisk. (Map adapted from Jon Blakey, NAU Geology <https://www2.nau.edu/rcb7/>).

The Late Jurassic sea-level evolution was marked by a gradual rise, modulated by third-order sea-level changes. The maximum of the second-order transgressive trend was reached during the Late Kimmeridgian–Early Tithonian transition (Ponsot and Vail 1991; Hardenbol et al. 1998; Haq 2018). Climatic conditions paralleled sea-level evolution and are generally considered as an overall warm and equable climate with high atmospheric $p\text{CO}_2$ levels, punctuated by few cold snap episodes (Weissert and Mohr 1996; Dromart et al. 2003; Louis-Schmid et al. 2007a, 2007b; Sellwood et al. 2008) (Fig. 2). These relatively warm conditions are reflected in the development and wide distribution of shallow-marine carbonate platforms, ramps, and barrier reefs (Leinfelder et al. 2002; Dromart et al. 2003).

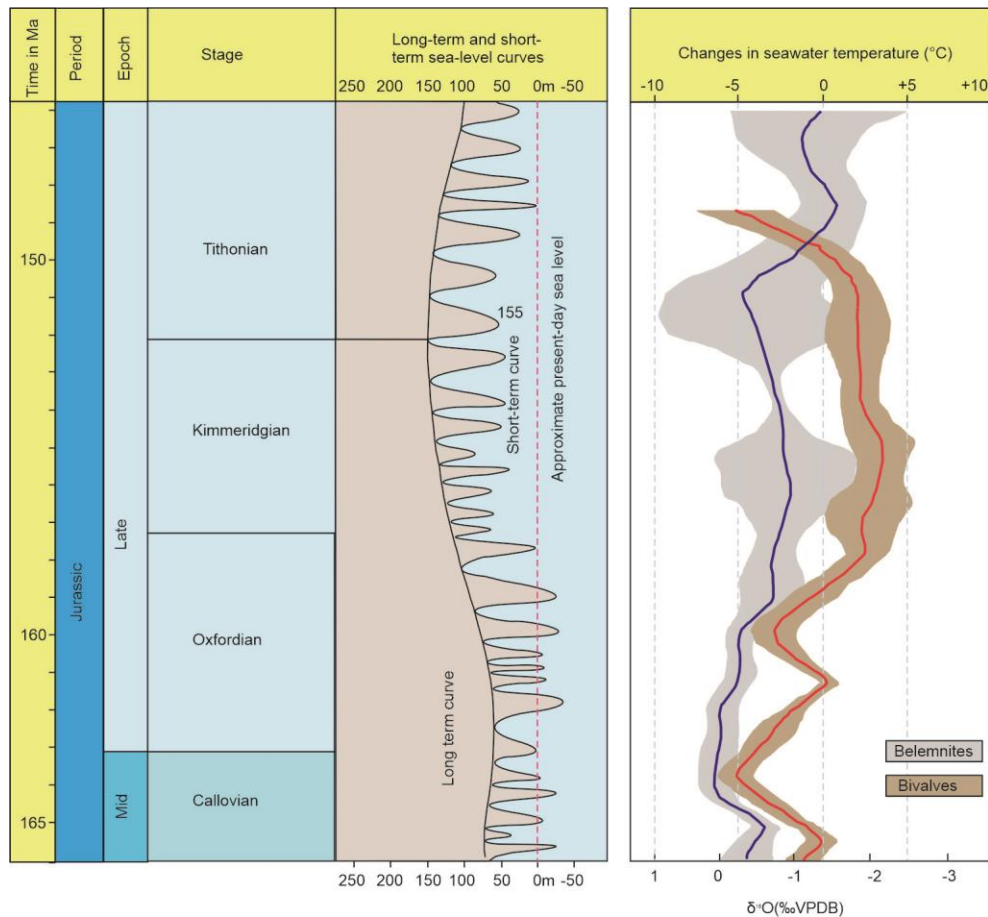


Fig. 2 - Global eustatic sea-level trend and marine paleotemperatures inferred from different types of shell material for the Late Jurassic (after Dera et al. 2011 and Haq 2018).

1.2 Chemostratigraphy

1.2.1 Carbon isotope

Carbon isotope ($\delta^{13}\text{C}_{\text{carb/org}}$) stratigraphy is central to our understanding of the connections within the ocean-atmosphere-biosphere system (Cramer and Jarvis 2020) and has been verified as a reliable way of contrasting and calibrating biostratigraphic schemes on local and global scales (Weissert 1989; Jenkyns et al. 2002; Hucket al. 2013; Frijia et al. 2015) (Fig. 3). Due to the potential of diagenetic alteration, using $\delta^{13}\text{C}$ bulk signatures for stratigraphic purposes can be problematic in shallow-water carbonates (Immenhauser et al., 2008). Generally, the pelagic bulk carbonate record stores valuable information allowing for reconstruction and a better understanding of disturbances of the exogenic carbon cycle (e.g. Scholle and Arthur 1980; Weissert 1989). However, more recent research showed that neritic carbonates can preserve a global marine $\delta^{13}\text{C}$ signature (e.g. Hucket al. 2011; Huck and Heimhofer 2015; Hucket al. 2017; Zuo et al. 2018).

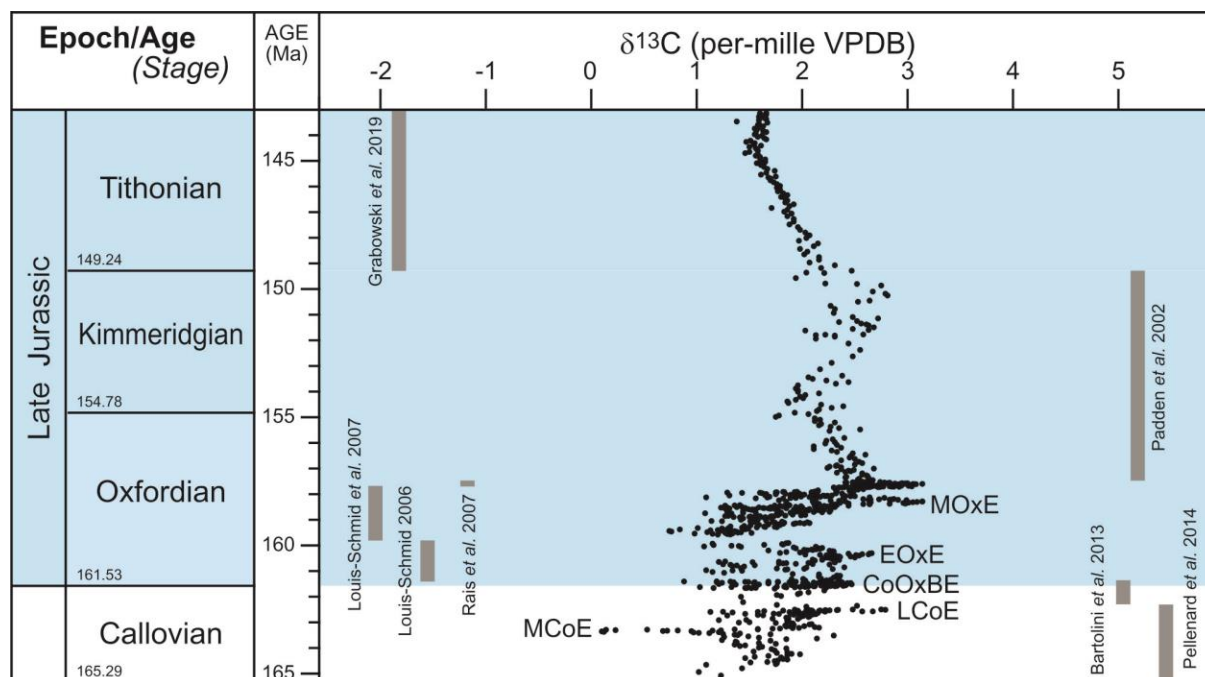


Fig. 3 - Late Jurassic composite $\delta^{13}\text{C}$ stratigraphy (adopted from Cramer and Jarvis, 2020).

Carbon isotope studies of Upper Jurassic strata have been carried out in both, pelagic and shallow-marine or neritic depositional environments in the Tethyan domain (e.g. Weissert and Mohr 1996; Cecca et al. 2001; Padden et al. 2002; Rais et al. 2007; Louis-Schmid et al. 2007b, 2007a; Coimbra et al. 2009; O'Dogherty et al. 2018; Eltom et al. 2018; Carmeille et al. 2020). Across this time interval, multiple $\delta^{13}\text{C}$ perturbations have been identified, incl. a pronounced positive $\delta^{13}\text{C}$ shift ($\sim 1.5\text{‰}$ to 4‰), termed the Middle Oxfordian Event (MOxE; Cramer and Jarvis 2020). However, with a few notable exceptions, most of these records are from the Tethyan domain (Cramer and Jarvis 2020; Eldrett 2022) and consist of relatively low-resolution datasets, which hampers precise correlations among different sections from other parts of the world. In order to better understand the response of carbonate producers to changing oceanographic and climate conditions during the Upper Jurassic, additional records need to be studied from more widespread geographic regions (Eldrett 2022). During the Late Jurassic, the Lower Saxony Basin (LSB) was located in the Boreal Realm and characterized by extensive shallow-marine carbonate deposition (Gramann et al. 1997). Hence, stratigraphic records from the LSB will enable a high-resolution investigation of the $\delta^{13}\text{C}$ trend, which will help to explore and re-evaluate the nature and origin of the Late Jurassic carbon isotope perturbations.

1.2.2 Strontium isotopes

Secular variations of the strontium isotope ratio ($^{87}\text{Sr}/^{86}\text{Sr}$) are widely used as a stratigraphic tool known as strontium isotope stratigraphy (SIS), which is important for correlation and dating of sedimentary sequences to obtain reliable geochronological information (Jones 1994; McArthur et al., 2001, 2012, 2020; Jenkyns et al., 2002; Hucket et al., 2013; Frijia et al., 2015; Kuznetsov et al. 2018). For the Jurassic Period, belemnite and oyster data have been faithfully used as a substrate, which is considered to preserve the contemporaneous seawater strontium isotope ratios (Jones 1992; Jones et al. 1994;

Schneider et al. 2009; Wierzbowski et al., 2017). Based on the available datasets the Jurassic strontium isotope curve has already been documented in considerable detail (Fig. 4). Most SIS studies with a focus on the Oxfordian have been carried out on pelagic deposits, whereas analyses from shallow-water carbonates are comparatively rare. Up to now, only a limited amount of SIS data is available for the Oxfordian (Jones 1992; Jones et al. 1994; McArthur et al. 2012; Wierzbowski et al. 2017). Within the LSB, Zuo et al. (2018) used SIS to successfully refine the Kimmeridgian stratigraphic framework. Although Bruhn et al. (2005) presented a limited number of $^{87}\text{Sr}/^{86}\text{Sr}$ ratios from bulk carbonate samples for the Oxfordian, a more precise dating and correlation for the Oxfordian within the LSB is still lacking. In this thesis, new data from the LSB (incl. material from the Bisperode section and Konrad #101 core) will be compared with the previously published $^{87}\text{Sr}/^{86}\text{Sr}$ records.

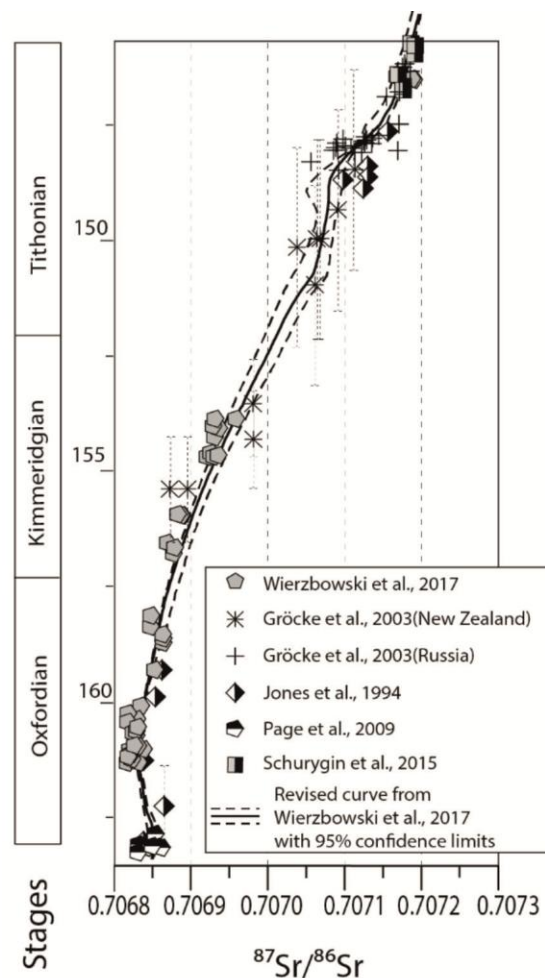


Fig. 4 - Strontium isotope trend of the Late Jurassic after Wierzbowski et al. (2017).

1.3 Geological setting

During the Late Jurassic, the Central European Basin System (CEBS) experienced extensional movements and moderate subsidence, induced by the crustal bulging of the 'North Sea Rift Dome' (Ziegler 1990). This instability resulted in extensive syn-sedimentary faulting in the CEBS with high subsidence in some areas and crustal uplifts in others (Betz et al. 1987). The LSB is located on the southern margin of the CEBS and represents one of several rifts- and wrench-induced "marginal

troughs”, that formed a series of E-W trending horst-and-graben structures (Betz et al. 1987; Ziegler 1990; Senglaub et al. 2006). The LSB has a length of ~300 km and a width of ~65 km and is bordered by the Rhenish Massif to the south and the Ringkøbing-Fyn High to the north. The sedimentary pile included within the LSB is estimated at ~4000 m in thickness (Betz et al. 1987; Mazur et al. 2005; Kästner et al. 2010) (Fig. 1). It represents the most important oil and gas province in Germany and one of the oldest oil-producing basins in the world (Boigk 1981; Binot et al. 1993). The evolution of the LSB began during the Permian with extensional movements and moderate subsidence, which reached its maximum in Late Jurassic to Early Cretaceous times (Betz et al. 1987; Kneucker et al. 2020). During the Late Cretaceous, a major inversion phase affected the entire LSB, which caused uplift and erosion of large parts of the sedimentary succession deposited during the Early and early Late Cretaceous (Senglaub et al. 2006). Uplift/erosion was most pronounced in the basin center and decreased towards the north (Petmecky et al. 1999). During the Early Cenozoic, sedimentation was reestablished, and marine shales and other deposits accumulated, which now unconformably overlie the deformed Cretaceous and Jurassic strata (Kneucker et al. 2020).

1.3.1 Oxfordian strata in the LSB

Lower Jurassic deposits are mainly exposed in the southeastern part of the LSB with spectacular outcrops in the low mountain ranges of southern Lower Saxony (Fig. 5). Three sections (Langenberg section, Bisperode section, Osterwald section) crop out south of Hannover, and all of them are well accessible. The Langenberg section can be studied in an active quarry about 5 km east of Godar, which represents one of the most important Jurassic fossil vertebrate localities in Europe (e.g. Sander et al. 2006). The Bisperode and Osterwald sections are both abandoned quarries located about 2 km southwest of Lauenstein, and about 3 km south of the village of Springe Holtensen, respectively. In addition, the scientific bore hole (Konrad #101 core) was studied, which was drilled close to the village Salzgitter-Beddingen (Fig. 5). In the LSB, the Upper Jurassic strata is represented by the lithological units of the Upper Omatenton Formation (Fm.) (Callovian–Oxfordian), Heersumer and Korallenoolith Fms. (Oxfordian), and the Upper Korallenoolith and Süntel Fms. (Kimmeridgian). This study specifically focuses on the Oxfordian Korallenoolith Fm. (Middle to Late Oxfordian). The Korallenoolith Fm. is essentially composed of oolitic and bioclastic limestones intercalated with marls and claystones, interspersed with coral patch reefs (Helm et al. 2001). Based on the faunal content and the lithological characteristics, the Korallenoolith Fm. is further subdivided into Lower, Middle, and Upper Korallenoolith (Schulze 1975).

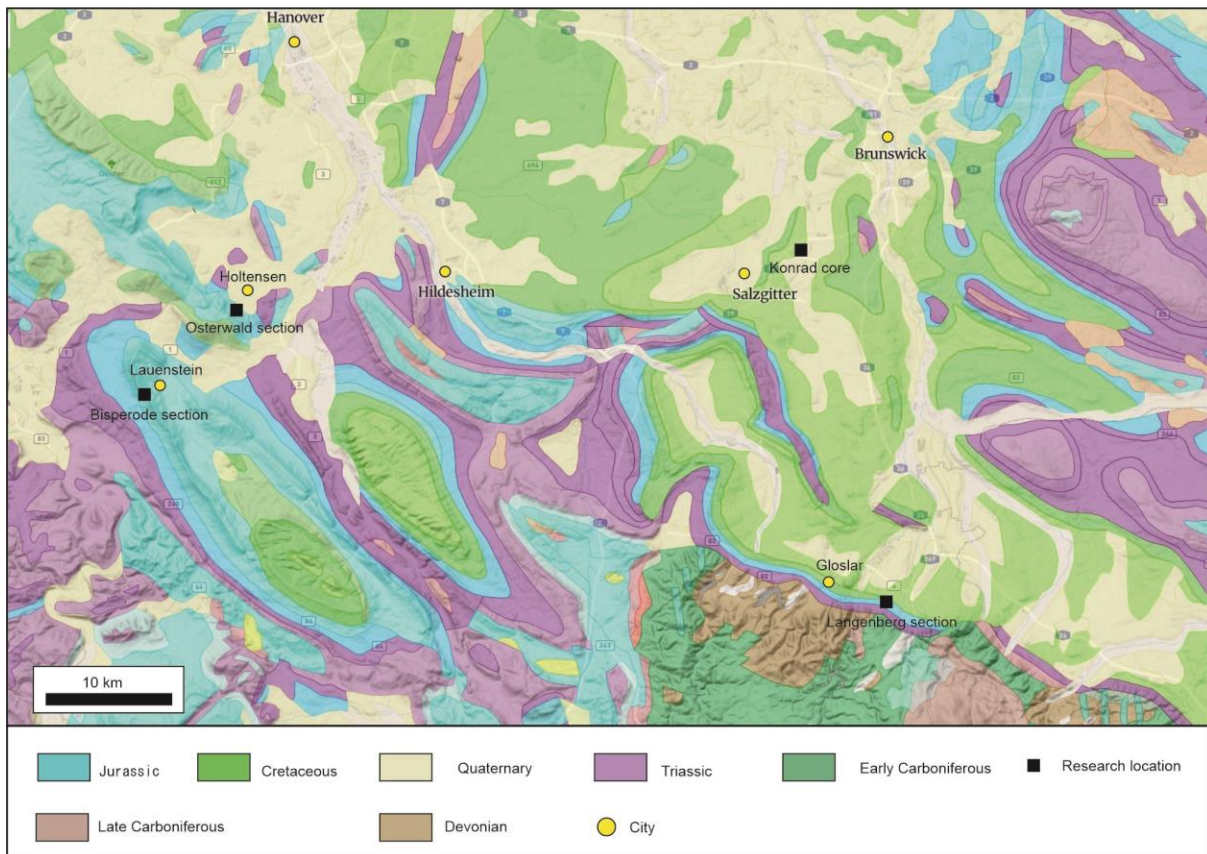


Fig. 5 - Geological map of the study area with the locations studied or used for comparison marked as black squares (modified from Kockel et al., 1996).

1.3.2 Biostratigraphy

The biostratigraphic subdivision of the Upper Jurassic strata in Northern Germany was developed based on ammonites, ostracods, dinoflagellate cysts, charophytes, foraminifera, spores and pollen (Schudack 1994; Weiß 1995; Gramann et al. 1997; Hardenbol et al. 1998). Due to the rare occurrence of age-diagnostic ammonites, the Oxfordian strata in the LSB is divided based on ostracods with the ostracod zones 1 to 8 covering the Ornatenton (zone 1), the Heersumer Fm. (zones 2 and 3), and the Korallenoolith Fm. (zones 4 to 8). The correlation between the ostracod zones from Gramann et al. (1997) and the sub-boreal ammonite zones is indicated in Fig. 6.

| Stage | Boreal realm Hardenbol et al. (1998) | | Ostracod zonation (LSB) | Lithostratigraphy Northwest Germany | |
|--------------|---|------------------------|----------------------------|--|-----------------------------|
| | Ammonites | Sequence | | | |
| Kimmeridgian | Cymodoce | JKi2 | Zone 9 | Süntel Fm | |
| | Baylei | JKi1 | Zone 8 | | |
| 154.8 | | JOx8 | Zone 7 | Humeralis-Schichten | |
| Oxfordian | Upper | Pseudocordata | JOx7 | Zone 6 | Upper Korallenoolith Fm. |
| | | | JOx6 | Zone 5 | |
| | | Cautisnigrae | | Zone 4 | |
| | Middle | Transversarium/Pumilus | JOx5 | Zone 3 | Lower Hersumer Fm. |
| | | Plicatilis | JOx4 | Zone 2 | |
| | | Cordatum | JOx3 | Zone 1 | |
| Lower | Mariae | JOx1 | Zone 1 | Upper Lower | |
| | Lamaerti | JCa6 | | | |
| 161.5 | | | | Ornatenton Fm. | |
| Callovian | | | | | |

Fig. 6 - Lithostratigraphic scheme of the Late Jurassic and its correlation with the standard zonation of the sub-boreal ammonite province (modified from Schulze 1975; Gramann et al. 1997; Hardenbol et al. 1998; Gradstein et al. 2020) and ostracod zonation (Schudack 1994; Weiß 1995).

1.4 Main objectives

This study focuses on refining the Oxfordian shallow-water deposits' sedimentology and stratigraphy in order to answer the following main scientific questions:

- 1) What was the carbonate depositional setting of the Korallenoolith Fm. within the LSB during the Oxfordian? Can the sequence stratigraphic pattern observed in the Korallenoolith Fm. be compared and correlated on a larger geographic scale?
- 2) What is the range of the $^{87}\text{Sr}/^{86}\text{Sr}$ ratios obtained from well-preserved bivalve shells from the Oxfordian Korallenoolith Fm.? Can the $^{87}\text{Sr}/^{86}\text{Sr}$ ratios be used to calibrate the existing biostratigraphic schemes on a local or even a global scale? If not, what processes affected the $^{87}\text{Sr}/^{86}\text{Sr}$ ratios derived from the Korallenoolith shell material?
- 3) How does the $\delta^{13}\text{C}$ stratigraphic trend from the LSB look like? Is the Oxfordian carbon isotope proxy obtained from the LSB useful for correlation with time-equivalent carbon isotope profiles from the Tethyan and proto-Atlantic domains? And what kind of carbon isotope trends and possible excursions can be identified? What are the underlying mechanisms behind the Oxfordian carbon isotope shift?

For this purpose, the following objectives have been defined:

- 1) Establish a potentially complete high-resolution sedimentary and sequence-stratigraphic framework for the Oxfordian deposits in the LSB. The above-mentioned sequence stratigraphic framework will complement preexisting biostratigraphic markers in order to fine-tune the chronostratigraphic constraint of the LSB. This approach will allow comparing the results collected in the LSB with other datasets from

lower latitude sections located in the Tethyan domain during the Oxfordian.

2) Develop a carbon and strontium isotope stratigraphic record for the Oxfordian successions in the LSB in order to refine the age assignment of the shallow-marine carbonates in the LSB. The carbon and strontium isotope chemostratigraphy will be integrated with sequence stratigraphic and biostratigraphic approaches.

3) The high-resolution $\delta^{13}\text{C}$ stratigraphic records from the LSB will be compared with existing carbon isotope curves from Tethyan and proto-Atlantic sites. Identification of the Middle Oxfordian carbon isotope excursion (MOxE) within the Korallenoolith Fm. will prompt a re-evaluation of the nature and origin of the globally observed MOxE.

1.5 General outline of the thesis

This thesis is subdivided into 6 individual chapters. Chapter 1 provides the introduction of the general topic of the thesis, and chapters 2 to 5 represent separate manuscripts, which are in preparation for publication in international peer-reviewed journals (except for chapter 4). Chapter 6 represents the conclusions.

Chapter 2 - Carbonate microfacies and transgressive-regressive sequences of Oxfordian shallow-water limestones (Korallenoolith, Lower Saxony Basin)

This chapter is planned to be submitted to the journal ZDGG. The present manuscript focuses on the shallow-marine limestones and marls of the Bisperode section located ~40 km SW of Hannover. This study provides a detailed carbonate microfacies analysis of the Bisperode section, which forms the baseline for the conceptualization of a reef-bearing carbonate ramp model. Following the accommodation to sediment supply ratio (A/S) concept, three different orders of sequences were distinguished in the studied section, resulting in the recognition of three large-, 8 medium-, and 15 small-scale sequences. The supra-regional correlation of the observed sequences is discussed.

Chapter 3 - First record of the Middle Oxfordian positive carbon isotope excursion within the Korallenoolith Formation, Lower Saxony Basin, Germany

This chapter is planned to be submitted to the journal Terra Nova. In the manuscript, a new high-resolution inorganic carbon isotope record is presented, which stems from a scientific borehole (Konrad #101 core) in the LSB. The $\delta^{13}\text{C}$ stratigraphic pattern is compared with existing carbon isotope curves from Tethyan and proto-Atlantic sites. Based on stratigraphic constraints, the Middle Oxfordian carbon isotope excursion (MOxE) can be identified. The new findings are discussed with regard to carbon cycle dynamics and the paleoenvironmental conditions prevailing during the Oxfordian.

Chapter 4 - $^{87}\text{Sr}/^{86}\text{Sr}$ chemostratigraphy of Oxfordian carbonate deposits, Lower Saxony Basin, Northern Germany

Within chapter 4, the $^{87}\text{Sr}/^{86}\text{Sr}$ ratios obtained from well-preserved skeletal materials (low-Mg calcite

Chapter 1

brachiopods, oysters, echinoderm, *trichites* bivalves, and shell fragments) are presented. A multi-methods approach (morphological examination, cathodoluminescent microscopy, and trace elements) is used to assess the preservation state of the studied shells used for seawater $^{87}\text{Sr}/^{86}\text{Sr}$ reconstruction. In the following, numerical age constraints obtained from Sr-isotope analysis and regional factors affecting shell $^{87}\text{Sr}/^{86}\text{Sr}$ variability are discussed.

Chapter 5 - Carbon isotope stratigraphy of an Oxfordian carbonate ramp system, Lower Saxony Basin, Northern Germany

In this chapter, high-resolution $\delta^{13}\text{C}$ analyses of bulk carbonate samples from three outcrop sections (Langenberg, Osterwald, and Bisperode) and one scientific borehole (Konrad #101 core) are studied and compared. Based on litho- and biostratigraphic constraints, a $\delta^{13}\text{C}$ record correlation is presented for the southern LSB for the Oxfordian interval. The chemostratigraphic data presented in this study enables the refinement of the pre-existing biostratigraphic framework and the establishment of a composite high-resolution $\delta^{13}\text{C}$ stratigraphic record. The $\delta^{13}\text{C}$ records improve the correlation ability between the western and eastern parts of the LSB. Overall, the new framework also allows to better assess the impact of carbon cycle disturbances on the shallow-marine carbonate systems in the LSB. Chapter 5 will also be submitted to an international peer-reviewed journal.

1.6 References

- Betz, D., Führer, F., Greiner, G., & Plein, E.M. (1987). Evolution of the Lower Saxony Basin. *Tectonophysics*, 137, 127–170.
- Binot, F., Gerling, P., Hiltmann, W., Kockel, F., & Wehner, H. (1993). The Petroleum System in the Lower Saxony Basin. In: Spencer, A.M. (eds) *Generation, Accumulation and Production of Europe's Hydrocarbons III*. Special Publication of the European Association of Petroleum Geoscientists, vol 3. Springer, Berlin, Heidelberg.
- Boigk, H., (1981). *Erdöl und Erdölgas in der Bundesrepublik Deutschland: Erdölprovinzen, Felder, Förderung, Vorräte, Lagerstättentechnik*. Enke, Stuttgart (330 pp.).
- Boulila, S., Galbrun, B., Hinnov, L. A., Collin, P. Y., Ogg, J. G., Fortwengler, D., & Marchand, D. (2010). Milankovitch and sub-Milankovitch forcing of the Oxfordian (Late Jurassic) Terres Noires Formation (SE France) and global implications. *Basin Research*, 22(5), 717–732.
- Bruhn, F., Veizer, J., Buhl, D., & Meijer, J. (2005). Diagenetic history of the Korallenoolith (Malm) of northwestern Germany: Implications from in-situ trace element and isotopic studies. *Nuclear Instruments & Methods in Physics Research Section B-beam Interactions With Materials and Atoms* 231, 518–523.
- Carmeille, M., Bourillot, R., Pellenard, P., Dupias, V., Schnyder, J., Riquier, L., Mathieu, O., Brunet, M.F., Énay, R., Grossi, V., Gaborieau, C., Razin, P., & Visscher, P.T. (2020). Formation of microbial organic carbonates during the Late Jurassic from the Northern Tethys (Amu Darya Basin, Uzbekistan): Implications for Jurassic anoxic events. *Global and Planetary Change*, 186, 103–127.
- Cecca, F., Savary, B., Bartolini, A., Remane, J., & Cordey, F. (2001). The Middle Jurassic–Lower Cretaceous Rosso Ammonitico succession of Monte Inici (Trapanese Domain, western Sicily);

- sedimentology, biostratigraphy and isotope stratigraphy. *Bulletin de la Société Géologique de France*, 172, 647–659.
- Collin, P., Loreau, J.P., & Courville, P. (2005). Depositional environments and iron ooid formation in condensed sections (Callovian–Oxfordian, south - eastern Paris basin, France). *Sedimentology*, 52, 969–985.
- Coimbra, R., Immenhauser, A., & Olóriz, F. (2009). Matrix micrite $\delta^{13}\text{C}$ and $\delta^{18}\text{O}$ reveals synsedimentary marine lithification in Upper Jurassic Ammonitico Rosso limestones (Betic Cordillera, SE Spain). *Sedimentary Geology*, 219, 332–348.
- Cramer, B.D., Jarvis, I., (2020). Carbon isotope stratigraphy. In F. M. Gradstein, J. G. Ogg, M. D. Schmitz, G. M. Ogg (Eds.). *Geologic time scale*, Elsevier.
- Dera, G., Brigaud, B., Monna, F., Laffont, R., Pucéat, E., Deconinck, J.F., Pellenard, P., Joachimski, M.M., & Durllet, C. (2011). Climatic ups and downs in a disturbed Jurassic world. *Geology*, 39, 215–218.
- Dromart, G., Garcia, J., Picard, S., Atrops, F., Lécuyer, C., & Sheppard, S.M. (2003). Ice age at the Middle–Late Jurassic transition? *Earth and Planetary Science Letters*, 213, 205–220.
- Eldrett, J.S., (2022). Middle Oxfordian carbon cycle perturbation expressed in the Smackover Formation, Gulf of Mexico. *Geology*, 50, 500–505.
- Eltom, H.A., González, L.A., Hasiotis, S.T., Rankey, E.C., & Cantrell, D.L. (2018). Paleogeographic and paleo-oceanographic influences on carbon isotope signatures: Implications for global and regional correlation, Middle-Upper Jurassic of Saudi Arabia. *Sedimentary Geology*, 364, 89–102.
- Frakes, L.A., Francis, J.E., & Syktus, J. (1992). *Climate Modes of the Phanerozoic*. Cambridge University Press
- Frijia, G., Parente, M., Lucia, M.D., & Mutti, M. (2015). Carbon and strontium isotope stratigraphy of the Upper Cretaceous (Cenomanian–Campanian) shallow-water carbonates of southern Italy: Chronostratigraphic calibration of larger foraminifera biostratigraphy. *Cretaceous Research*, 53, 110–139.
- Gradstein, F.M., Ogg, J.G., Schmitz, M.D. and Ogg, G. M., eds. (2020). *The Geologic Time Scale 2020*. Elsevier.
- Gramann, F., Heunisch, C., Klassen, H., Kockel, F., Dulce, G., Harms, F., Katschorek, T., Mönnig, E., Schudack, M.E., Schudack, U., Thies, D., Weiss, M., Hinze, C. (1997). Das Niedersächsische Oberjura-Becken – Ergebnisse interdisziplinärer Zusammenarbeit. *Zeitschrift der Deutschen Geologischen Gesellschaft*, 148(2), 165–236.
- Hallam, A. (2001). A review of the broad pattern of Jurassic sea-level changes and their possible causes in the light of current knowledge. *Palaeogeography, Palaeoclimatology, Palaeoecology*, 167(1–2), 23–37.
- Haq, B.U. (2018). Jurassic Sea-Level Variations: A Reappraisal. *GSA Today*, 4–10.
- Hardenbol J., Thierry J., Farley M.B., Jacquin T., de Graciansky P.C., Vail P.R. (1998). Jurassic chronostratigraphy. In: de Graciansky P.C., Hardenbol J., Jacquin T., Vail P.R. (eds) *Mesozoic and Cenozoic sequence stratigraphy of European Basins*. SEPM Special Publication, Tulsa, pp 3–13.
- Helm, C., Schülke, I., Fischer, I. (2001). Paläobiogeographie des Korallenooliths (Mittleres Oxfordium Unteres Kimmeridgium): Tethyale Faunen und Florenelemente auf höherer Paläobreite (Niedersächsisches Becken, NW-Deutschland). *Geologische Beiträge Hannover* 2, 51–64.
- Hesselbo, S.P., Ogg, J.G., Ruhl, M., Hinnov, L.A., & Huang, C. (2020). The Jurassic Period. *Geologic*

Chapter 1

Time Scale.

- Huck, S., Heimhofer, U., Rameil, N., Bodin, S., & Immenhauser, A. (2011). Strontium and carbon-isotope chronostratigraphy of Barremian–Aptian shoal-water carbonates: Northern Tethyan platform drowning predates OAE 1a. *Earth and Planetary Science Letters*, 304, 547–558.
- Huck, S., & Heimhofer, U. (2015). Improving shallow-water carbonate chemostratigraphy by means of rudist bivalve sclerochemistry. *Geochemistry, Geophysics, Geosystems*, 16, 3111–3128.
- Huck, S., Wohlwend, S.P., Coimbra, R., Christ, N., & Weissert, H. (2017). Disentangling shallow-water bulk carbonate carbon isotope archives with evidence for multi-stage diagenesis: An in-depth component-specific petrographic and geochemical study from Oman (mid-Cretaceous). *The Depositional Record*, 3, 233–257.
- Huck, S., Heimhofer, U., Immenhauser, A., & Weissert, H. (2013). Carbon-isotope stratigraphy of Early Cretaceous (Urgonian) shoal-water deposits: Diachronous changes in carbonate-platform production in the north-western Tethys. *Sedimentary Geology*, 290, 157–174.
- Immenhauser, A., C. Holmden, and W. P. Patterson (2008). Interpreting the carbon-isotope record of ancient shallow epeiric seas: Lessons from the recent, in *Dynamics of Epeiric Seas*. Geological Association of Canada - Special Paper, 48, 135–174.
- Jeltsch-Thömmes, A., & Joos, F. (2020). Modeling the evolution of pulse-like perturbations in atmospheric carbon and carbon isotopes: The role of weathering–sedimentation imbalances. *Climate of the Past*, 16(2), 423–451.
- Jenkyns, H.C., Jones, C.E., Gröcke, D.R., Hesselbo, S.P., & Parkinson, D.N. (2002). Chemostratigraphy of the Jurassic System: applications, limitations and implications for palaeoceanography. *Journal of the Geological Society*, 159, 351–378.
- Jones, C. E. (1992). Strontium isotopes in Jurassic and early Cretaceous seawater (Doctoral dissertation, University of Oxford).
- Jones, C.E., Jenkyns, H.C., Coe, A.L., & Stephen, H.P. (1994). Strontium isotopic variations in Jurassic and Cretaceous seawater. *Geochimica et Cosmochimica Acta*, 58, 3061–3074.
- Kästner, M., Schülke, I., Winsemann, J., & Böttcher, J. (2010). High-resolution sequence stratigraphy of a Late Jurassic mixed carbonate-siliciclastic ramp, Lower Saxony Basin, Northwestern Germany. *Zeitschrift Der Deutschen Gesellschaft Für Geowissenschaften*, 161, 263–283.
- Kneucker, T., Blumenberg, M., Strauss, H., Dohrmann, R., Hammer, J., & Zulauf, G. (2020). Structure, kinematics and composition of fluid-controlled brittle faults and veins in Lower Cretaceous claystones (Lower Saxony Basin, Northern Germany): Constraints from petrographic studies, microfabrics, stable isotopes and biomarker analyses. *Chemical Geology*, 540, 119501.
- Kockel, F., Baldschuhn, R., and Frisch, U. (1996). *Tectonic Atlas of NW-Germany*: Federal Institute for Geosciences and Natural Resources, Hannover.
- Kuznetsov, A., Semikhatov, M.A., & Gorokhov, I.M. (2018). Strontium Isotope Stratigraphy: Principles and State of the Art. *Stratigraphy and Geological Correlation*, 26, 367–386.
- Lear, C.H., Anand, P., Blenkinsop, T.G., Foster, G.L., Gagen, M.H., Hoogakker, B., Larter, R.D., Lunt, D.J., McCave, I.N., McClymont, E.L., Pancost, R.D., Rickaby, R.E., Schultz, D.M., Summerhayes, C., Williams, C.J., & Zalasiewicz, J. (2020). Geological Society of London Scientific Statement: what the geological record tells us about our present and future climate. *Journal of the Geological Society*, 178.

- Leinfelder, R., Schmid, D.U., Nose, M., & Werner, W. (2002). Jurassic Reef Patterns—The Expression of a Changing Globe.
- Louis-Schmid, B., Rais, P., Schaeffer, P., Bernasconi, S.M., & Weissert, H. (2007a). Plate tectonic trigger of changes in $p\text{CO}_2$ and climate in the Oxfordian (Late Jurassic): Carbon isotope and modeling evidence. *Earth and Planetary Science Letters*, 258, 44–60.
- Louis-Schmid, B., Rais, P., Bernasconi, S.M., Pellenard, P., Collin, P., & Weissert, H. (2007b). Detailed record of the mid-Oxfordian (Late Jurassic) positive carbon-isotope excursion in two hemipelagic sections (France and Switzerland): A plate tectonic trigger? *Palaeogeography, Palaeoclimatology, Palaeoecology*, 248, 459–472.
- Mazur, S., Scheck-Wenderoth, M., & Krzywiec, P. (2005). Different modes of the Late Cretaceous–Early Tertiary inversion in the North German and Polish basins. *International Journal of Earth Sciences*, 94, 782–798.
- McArthur, J.M., Howarth, R.J., & Bailey, T.R. (2001). Strontium Isotope Stratigraphy: LOWESS Version 3: Best Fit to the Marine Sr-Isotope Curve for 0–509 Ma and Accompanying Look-up Table for Deriving Numerical Age. *The Journal of Geology*, 109, 155–170.
- McArthur, J.M. (2012). Strontium Isotope Stratigraphy. *Geologic Time Scale 2012*.
- McArthur, J.M. (2020). Strontium Isotope Stratigraphy. *Geologic Time Scale 2020*.
- O'Dogherty, L., Aguado, R., Baumgartner, P.O., Bill, M., Goričan, Š., Sandoval, J., & Sequeiros, L. (2018). Carbon-isotope stratigraphy and pelagic biofacies of the Middle–Upper Jurassic transition in the Tethys–Central Atlantic connection. *Palaeogeography, Palaeoclimatology, Palaeoecology*, 507, 129–144.
- Padden, M., Weissert, H., Rafelis, M.D. (2001). Evidence for Late Jurassic release of methane from gas hydrate. *Geology*, 29, 223–226.
- Padden, M., Weissert, H., Funk, H., Schneider, S. and Gansner, C. (2002). Late Jurassic lithological evolution and carbon-isotope stratigraphy of the western Tethys. *Eclogae Geologicae Helvetiae*, 95(3), pp.333–346.
- Petmecky, S., Meier, L.A., Reiser, H., & Littke, R. (1999). High thermal maturity in the Lower Saxony Basin: intrusion or deep burial? *Tectonophysics*, 304, 317–344.
- Ponsot, C.M., & Vail, P.R. (1991). Sequence Stratigraphy of the Jurassic: New Data from the Paris-London Basin Compiled on Well Logs. *AAPG Bulletin*, 75.
- Rais, P., Louis-Schmid, B., Bernasconi, S.M., & Weissert, H. (2007). Palaeoceanographic and palaeoclimatic reorganization around the Middle–Late Jurassic transition. *Palaeogeography, Palaeoclimatology, Palaeoecology*, 251, 527–546.
- Ramajo, J., & Aurell, M. (2008). Long-term Callovian–Oxfordian sea-level changes and sedimentation in the Iberian carbonate platform (Jurassic, Spain): possible eustatic implications. *Basin Research*, 20(2), 163–184.
- Schneider, S., Fürisch, F. T., Werner, W. (2009). Sr-isotope stratigraphy, of the Upper Jurassic of central Portugal (Lusitanian Basin) based on oyster shells. *International Journal of Earth Science*, 98(8), 1949–1970
- Schudack, U. (1994). Revision, Dokumentation und Stratigraphie der Ostracoden des Nordwestdeutschen Oberjura und Unter-Berriasium. Selbstverlag Fachbereich Geowissenschaften, FU Berlin, p. 1–192.

Chapter 1

- Schulze, K-H. (1975). Mikrofazielle, geochemische und technologische Eigenschaften von Gesteinen der Heersumer Schichten und des Korallenoolith (Mittleres und Oberes Oxfordium NW Deutschlands) zwischen Weser und Leine. *Geologisches Jahrbuch*, D11, 3–102.
- Scholle, P.A., & Arthur, M.A. (1980). Carbon Isotope Fluctuations in Cretaceous Pelagic Limestones: Potential Stratigraphic and Petroleum Exploration Tool. *AAPG Bulletin*, 64, 67–87.
- Sellwood, B.W., Valdes, P.J. (2008). Jurassic climates. *Proceedings of the Geologists' Association*, 119(1), 5e17.
- Sander, P.M., Mateus, O., Laven, T., & Knötschke, N. (2006). Bone histology indicates insular dwarfism in a new Late Jurassic sauropod dinosaur. *Nature*, 441, 739–741.
- Senglaub, Y., Little, R., & Brix, M.R. (2006). Numerical modeling of burial and temperature history as an approach for an alternative interpretation of the Bramsche anomaly, Lower Saxony Basin. *International Journal of Earth Sciences*, 95, 204–224.
- Weissert, H. (2000). Deciphering methane's fingerprint. *Nature*, 406, 356–357.
- Weissert, H., & Erba, E. (2004). Volcanism, CO₂ and palaeoclimate: a Late Jurassic–Early Cretaceous carbon and oxygen isotope record. *Journal of the Geological Society*, 161, 695–702.
- Weissert, H., Mohr, H.M. (1996). Late Jurassic climate and its impact on carbon cycling. *Palaeogeography, Palaeoclimatology, Palaeoecology*, 122, 27–43.
- Weissert, H., & Channell, J.E. (1989). Tethyan carbonate carbon isotope stratigraphy across the Jurassic-Cretaceous boundary: An indicator of decelerated global carbon cycling? *Paleoceanography*, 4, 483–494.
- Weiß, M. (1995). Stratigraphie und Mikrofauna im Kimmeridge SE-Niedersachsens unter besonderer Berücksichtigung der Ostracoden. *Clausthaler Geowissenschaftliche Dissertationen*, 48, 1–274.
- Wierzbowski, H., Anczkiewicz, R., Pawlak, J., Rogov, M.A., & Kuznetsov, A. (2017). Revised Middle–Upper Jurassic strontium isotope stratigraphy. *Chemical Geology*, 466, 239–255.
- Ziegler, P. A. (1990). *Geological Atlas of Western and Central Europe*. 2nd Edition, Shell International Petroleum Mij. B.V. and Geological Society, London.
- Zuo, F., Heimhofer, U., Huck, S., Bodin, S., Erbacher, J., & Bai, H. (2018). Coupled $\delta^{13}\text{C}$ and $^{87}\text{Sr}/^{86}\text{Sr}$ chemostratigraphy of Kimmeridgian shoal-water deposits: A new composite record from the Lower Saxony Basin, Germany. *Sedimentary Geology*, 376, 18–31.

2. Carbonate microfacies and transgressive-regressive sequences of Oxfordian shallow-water limestones (Korallenoolith, Lower Saxony Basin)

Deyan Zhang, François-Nicolas Krencker, Stefan Huck, Ulrich Heimhofer

Institute of Geology, Leibniz University Hannover, Germany.

2.1 Abstract

During the Oxfordian, the Lower Saxony Basin (LSB) was covered by a shallow epicontinental sea, in which a thick succession of marine limestones and marls was deposited. The scarcity of open-marine biostratigraphic marker fossils and numerous sedimentary gaps make it difficult to correlate strata from the LSB with Oxfordian deposits elsewhere in the world. This study focuses on the Oxfordian Korallenoolith Formation, which is well exposed in the Bisperode section located ~40 km SW of Hannover. The ~126 m-thick section was described bed-by-bed during fieldwork and complemented by 73 thin sections that were analyzed for their carbonate microfacies. Based on differences in allochem and orthochem composition and primary sedimentary fabrics, an integrated log of the Bisperode quarry was constructed. Seven lithofacies types (FTs) and fourteen microfacies types (MF-types) are characterized upon which a reef-bearing carbonate ramp model was built. Following the accommodation to sediment supply ratio (A/S) concept, three orders of sequences are distinguished in the studied section, resulting in the recognition of 3 large-, 8 medium-, and 15 small-scale sequences. The large-scale sequences correlate well to the established sequence-stratigraphic model and the medium-scale sequences point to a possible control of their stacking pattern by Milankovitch long eccentricity cycles. For their part, small-scale sequences were most likely controlled by autocyclic processes. This study is important because it helps to better understand the link between the stacking pattern of Oxfordian strata in the LSB and allocyclic processes, allowing future global chemo- and sequence-stratigraphic correlations.

Keywords: Lower Saxony Basin, Oxfordian, carbonate microfacies, sequence stratigraphy, sedimentary depositional model

2.2 Introduction

The Upper Jurassic succession of the Lower Saxony Basin (LSB) has attracted significant interest amongst geologists and paleontologists as the strata contains rich invertebrate and vertebrate assemblages and significant reservoir suitable for oil extraction (Lotze 1968; Pape 1970; Weiß, 1995; Sander et al. 2006, see also English et al. 2017 and references herein). Unfortunately, the scarcity of open-marine biostratigraphic markers, the occurrence of multiple sedimentary gaps and the poor lateral continuity of the strata make it difficult to build a precise litho- and biostratigraphy that allows correlation within the LSB, and worldwide. During the Oxfordian, the LSB was covered by a shallow epicontinental sea, in which a thick succession of alternating marine limestones and marls was deposited (Ziegler 1990; Betzler et al. 2007; Kästner et al. 2008). Some excellent and undeformed Upper Jurassic sections are exposed along the southern margin of the LSB, including the Langenberg quarry outcrop, which is considered one of the most important fossil vertebrate localities in Europe for the Late Jurassic (Sander et al., 2006).

Up to now, several biostratigraphic, lithostratigraphic, and sequence stratigraphic papers on the Oxfordian Korallenoolith Formation (Fm.) have been published. Helm et al. (1998, 2003, 2006) worked on several sections within the LSB, mainly focusing on coral reefs assemblages. Kästner et al. (2008; 2010) studied eight well-exposed sections of the LSB (Süntel area, Wesergebirge, and eastern part of the Wiehengebirge), providing detailed information about lithofacies and lateral thickness variations of the Oxfordian to basal Kimmeridgian carbonate ramp deposits. In terms of sequence stratigraphy, Bai et al. (2017) interpreted the Eulenflucht 1 core, which is located in the Süntel area, covering Oxfordian to Kimmeridgian strata.

The present study focuses on the shallow-marine limestones and marls of the Bisperode section, which are well-exposed in an abandoned limestone quarry located in the Ith Mountains. Here, the thickness of the Korallenoolith Fm. is estimated as being twice the thickness of most Oxfordian outcrop sections in the LSB. Based on facies variation and gamma-ray logs, Betzler et al. (2007) developed a depositional model for the lower part of the Bisperode section. In a follow-up study by Cäsar (2012), the Bisperode record was compared with time-equivalent sections from the south-eastern LSB. The upper part of the section, assigned to the Kimmeridgian Süntel Fm., was studied by Zuo et al. (2017) using a combined approach including sedimentological observation and stable isotope chemostratigraphy.

This study aims to provide a detailed carbonate microfacies analysis of the Bisperode section, which is the first essential step to propose this section as an Oxfordian reference section for future chemostratigraphic studies. Its exceptional thickness points towards a rather complete Oxfordian shallow-marine record. The newly acquired sedimentological data combined and compared with the previous work of Betzler et al. (2007) and Cäsar (2012) allow a better assessment of the depositional environment of the Bisperode section and the LSB filling succession during the Oxfordian.

2.3 Geological setting

2.3.1 Regional geology

The LSB represents a sub-basin of the North German Basin located in Central Europe (Ziegler 1977). During the Late Jurassic, the LSB was bounded by the Ringkøbing Fyn High to the north and the London Brabant, the Rhenish, and the Bohemian massifs to the south (Ziegler 1990). The LSB is described as a 300 km long and 65 km wide Late Jurassic to Early Cretaceous trough, which parallels the northern margin of the Rhenish Massif, and which formed part of an epicontinental sea (Betz et al. 1987; Betzler et al. 2007; Fig 1). The basin-fill comprises a ~4500 m-thick sequence of Upper Paleozoic and Mesozoic strata (Bombien et al., 2012; LBEG 2013). Differential subsidence in the LSB controlled by syn-sedimentary faults and salt tectonics began during the Late Triassic (Betz et al. 1987; Gramann et al., 1997; Hoyer, 1965). Consequently, the deposit thicknesses can vary by tens of meters over short distances (Hoyer 1965). During the Oxfordian, the LSB was located at a paleolatitude of ~35°N, most likely within the subtropical paleoclimatic belt (Smith et al. 1994; Helm et al. 2001), and connected with the Boreal Ocean via the Viking Corridor (Ziegler, 1988).

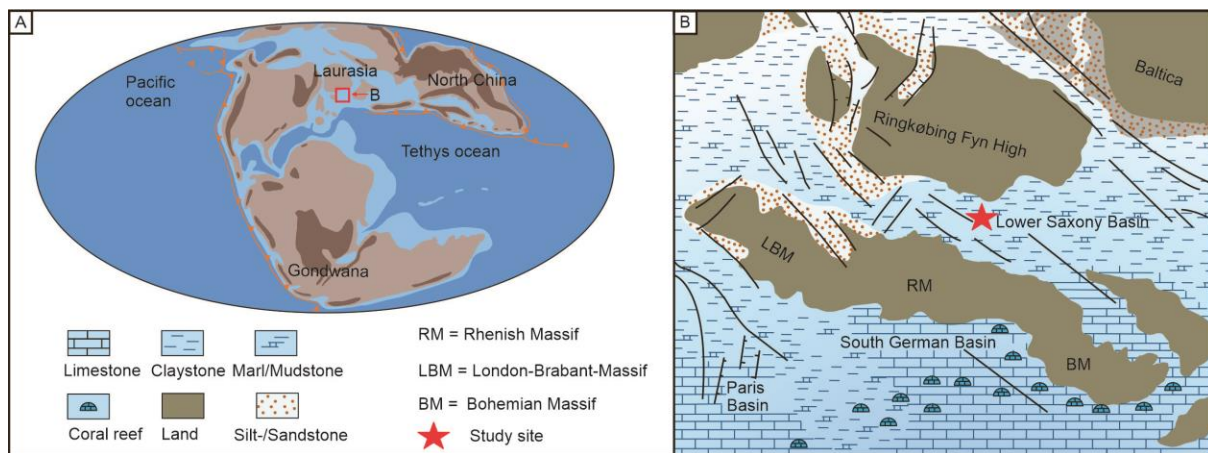


Fig. 1 (A) Global and (B) Central Europe palaeogeographic reconstruction of the Late Jurassic (152 Ma, modified after Tang, 2021). Major landmasses and general marine facies distribution are shown. RM = Rhenish Massif, LBM = London-Brabant Massif; BM = Bohemian Massif. Map modified after Ziegler (1990). Approximate position of the studied outcrop in the Lower Saxony Basin is marked with a red asterisk.

The Korallenoolith Fm. is restricted to the south-eastern part of the LSB (Gramann et al. 1997) and has been described from many outcrops in the mountainous areas of Lower Saxony including Wiehen- and Wesergebirge, Süntel, Deister, Osterwald, Ith and Subherzynian Basin (Helm et al. 2003). The Korallenoolith Fm. itself consists of oolitic limestones with intercalated bioherms, assigned to a shallow-marine environment with a limited terrestrial influx. Stratigraphically, it belongs to the NW German Malm Group (Helm et al. 2003; Betzler et al. 2007; Kästner et al. 2008; Cäsar et al. 2012; Zuo et al. 2017). Schulze (1975) subdivided the Korallenoolith Fm. into Lower, Middle, and Upper Korallenoolith based on characteristic microfacies assemblages and diagenetic features. More recently, the Korallenoolith Fm. has been subdivided into only two units separated by a well-developed unconformity, the "Hauptemersionsfläche", showing clear evidence of subaerial exposure (Helm 1998; Schülke et al. 2004, Kästner et al. 2008; Cäsar 2012).

2. 3.2 Stratigraphic framework

The biostratigraphic subdivision of the Upper Jurassic in Northern Germany was developed based on ammonites, ostracods, dinoflagellate cysts, charophytes, spores and pollen (Schudack 1994; Weiß 1995; Gramann et al. 1997; Hardenbol et al. 1998). The Oxfordian strata in the LSB is assigned to the ostracod zones 1 to 6 and includes the Ornatenton (zone 1), the Heersum (zones 2 and 3), and the Korallenoolith (zones 4 to 8) Fms. The correlation between the ostracod zones from Gramann et al. (1997) and the Sub-Boreal ammonite zones are indicated in Fig. 2.

| Stage | Boreal realm Hardenbol et al. (1998) | | Ostracod zonation (LSB) | Lithostratigraphy Northwest Germany | |
|--------------|---|------------------------|-------------------------------|--|--|
| | Ammonites | Sequence | | | |
| Kimmeridgian | Cymodoce | JKi2 | Zone 9 | Süntel Fm. | |
| | Baylei | JKi1 | Zone 8 | | |
| 154.8 | | JOX8 | Zone 7 | Humeralis-Schichten | |
| Oxfordian | Upper | Pseudocordata | JOX7 | Zone 6 | Upper Middle Lower Korallenoolith Fm. |
| | | | JOX6 | Zone 5 | |
| | | Cautisnigrae | | Zone 4 | |
| | Middle | Transversarium/Pumilus | JOX5 | Zone 3 | Upper Lower Heersum Fm. |
| | | Plicatilis | JOX4 | | |
| | | Cordatum | JOX3 JOX2 | | |
| Lower | Mariae | JOX1 | Zone 2 | | |
| | Lamaerti | JCa6 | Zone 1 | Ornatenton Fm. | |
| 161.5 | | | | | |
| Callovian | | | | | |

Fig. 2 Lithostratigraphic scheme of the Late Jurassic and its correlation with the standard zonation of the sub-boreal ammonite province (modified from Gramann et al. 1997; Hardenbol et al. 1998; Schulze 1975; Gradstein and Ogg 2020) and ostracod zonation (Schudack 1994; Weiß 1995).

Gramann et al. (1997) suggested that the Korallenoolith Fm. covers the interval from the upper *Perisphinctes plicatilis* (*Perisphinctes antecedens* subzone) to the lowermost *Pictonia baylei* ammonite zones. The Bisperode section has been considered to encompass the Lower to Upper Korallenoolith Fm. (Weiß 1995, Mönnig 2002). Weiß (1995) developed a biostratigraphic framework for the upper part of the Bisperode section based on ostracod biostratigraphy, which was refined by Zuo et al. (2017) for the Süntel Fm. forming the uppermost part of the Bisperode section. A stratigraphic assignment is only available for the Upper Korallenoolith ("Humeralis-Schichten"). According to Zuo et al. (2017), the onset of ostracod zone 7 can be placed at 125.5 m (hardground surface). As a consequence, a certain part of the Upper Korallenoolith can be placed within ostracod zone 6, but the lower boundary of zone 6 remains unclear (Cäsar 2012).

The *Florigemma*-Bank reef association is another stratigraphic marker in the marginal marine facies of the Korallenoolith Fm. From the *Florigemma*-Bank, a few poorly preserved ammonite findings are reported (Helm et al. 1998), further assisting the stratigraphic attribution. The "Hauptemersionsfläche" at or near the top of the *Florigemma*-Bank is the only regional marker bed within the Korallenoolith Fm., which can be traced over a large lateral extent in the Weser-Leine area (Hoyer 1965; Helm 1998;

Kästner et al. 2008). Kaiser (1979) placed the *Florigemma*-Bank of the Hohenstein area (locality “Grüner Altar”) in the *Perisphinctes variocostatus* subzone (*Perisphinctes cautisnigrae* ammonite zone), which would indicate an early Late Oxfordian age. In the Bisperode section, the *Florigemma*-Bank and the “Hauptemersionsfläche” are not clearly identified. However, based on their resemblance, many studies suggested that the coral-rich interval (5.0–45.0 m) and the hardground (~50.0 m) described in the lower part of the Bisperode section are equivalent to the *Florigemma*-Bank and the “Hauptemersionsfläche”, respectively (Betzler et al. 2007; Căsar 2012; Bai et al., 2020). In the Bisperode section, the “Hauptemersionsfläche” equivalent (Surface D in Căsar 2012) is capped by a marly limestone interval (53.0–60.0 m) including the first occurrence of the foraminifera *Alveosepta jaccardi* (Betzler et al. 2007) indicative of the *Ringsteadia pseudocordata* ammonite zone in the LSB (Gramann 1997).

2.4 Methods

2.4.1 Fieldwork, sampling, and facies analysis

The Bisperode section covers shallow-marine carbonate deposits ranging from Oxfordian (Korallenoolith Fm.) to Kimmeridgian (Süntel Fm.) and is accessible in an abandoned quarry (52°04'00.09"N, 9°32'36.47"E) located ~2 km southwest of the village Lauenstein, Lower Saxony, Germany. Limestones of the Korallenoolith Fm. are exposed in a ~126 m-thick succession, showing slightly tilted bedding (Fig. 3). A total of 258 rock samples were taken approximately every 50 cm, accompanied by a detailed lithological description. A total of 73 petrographic thin sections for carbonate microfacies analysis were produced. Carbonate microfacies was analyzed using an Olympus BX53 microscope equipped with an Olympus SC50 camera. The classification scheme of Dunham (1962) with the modifications of Embry and Klovan (1971) was applied.

2.4.2 Sequence stratigraphy

The sequence stratigraphic arrangement follows the concept of accommodation to sediment supply (or production) ratio (A/S) concept (Cross et al. 1993; Cross and Lessenger 1998; Homewood et al. 1999, Schlager 2005; Catuneanu et al. 2011). The A/S ratio controls the facies record and the stratigraphic architectures. Discontinuity surfaces (e.g., hardgrounds, karstified and erosional surfaces, paleosols) help to identify environmental changes (like subaqueous erosion or subaerial exposure) and to understand the changes in A/S leading to hiatuses. Based on the combination of the vertical stacking pattern of microfacies types (MF-types), changes in bed thickness, and the occurrence of diagnostic surfaces, three orders of sequences were differentiated in the studied section, including small-, medium-, and large-scale sequences. The hierarchy between small-, medium-, and large-scale sequences is based upon the significance of facies shift and the magnitude of the deepening/shallowing trends.

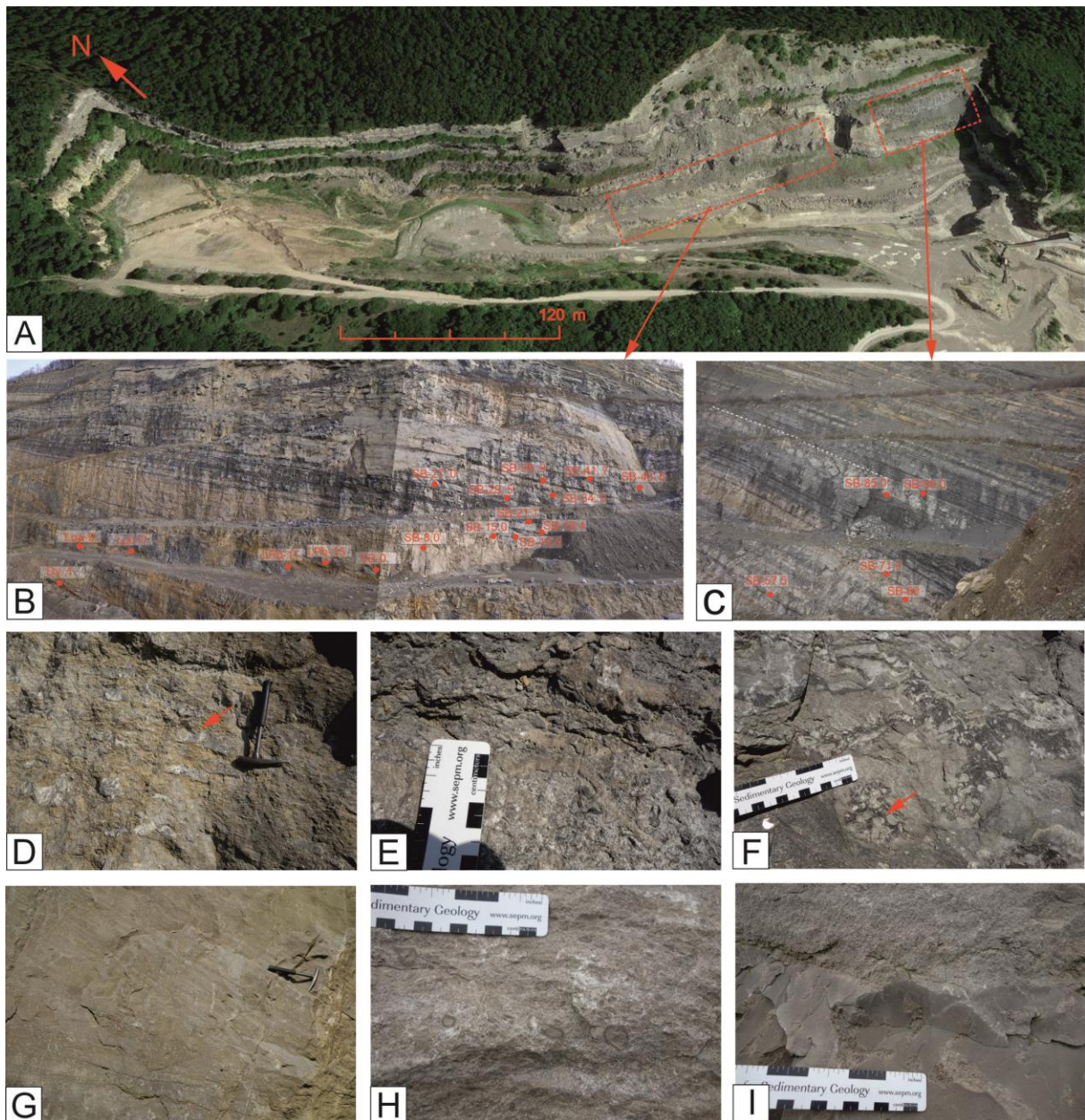


Fig. 3 Field view and selected sedimentary features exposed in the Upper Jurassic succession of the Bisperode section. (A) Aerial view of the Bisperode quarry (Google Earth imagery). (B) and (C) Enlargements of the area defined by the two stippled red boxes marked in (A), which show views of the steep quarry cliff with selected sample positions. (D) Coral-rich boundstone facies containing flat, sheet-like and strongly recrystallized corals (at 22.0 m). (E) Sharp-based bioclastic-rich rudstone with abundant coral fragments showing fining-upward sequences and cross-bedding (at 9.0 m). (F) Stalk-shaped bafflestone bored by bivalves (molds of bivalves) fossilized in life position. Note how the borings are filled with fine-grained material including second generation of bivalve borings (at 31.0 m). (G) Ooid-rich grainstone facies showing well-developed medium-scale cross-stratification (at 40.0 m). (H) Oncoid-rich rudstone including coarse individual oncoids (0.2 to 2 cm) with a distinctive concentric but irregular cortex (between 51.2 to 52.0 m). (I) Well-developed hardground with borings, which corresponds to the white stippled line in (C) and marks the top of the studied section (at 125.5 m).

2.5 Results and interpretation

2.5.1. Lithostratigraphy

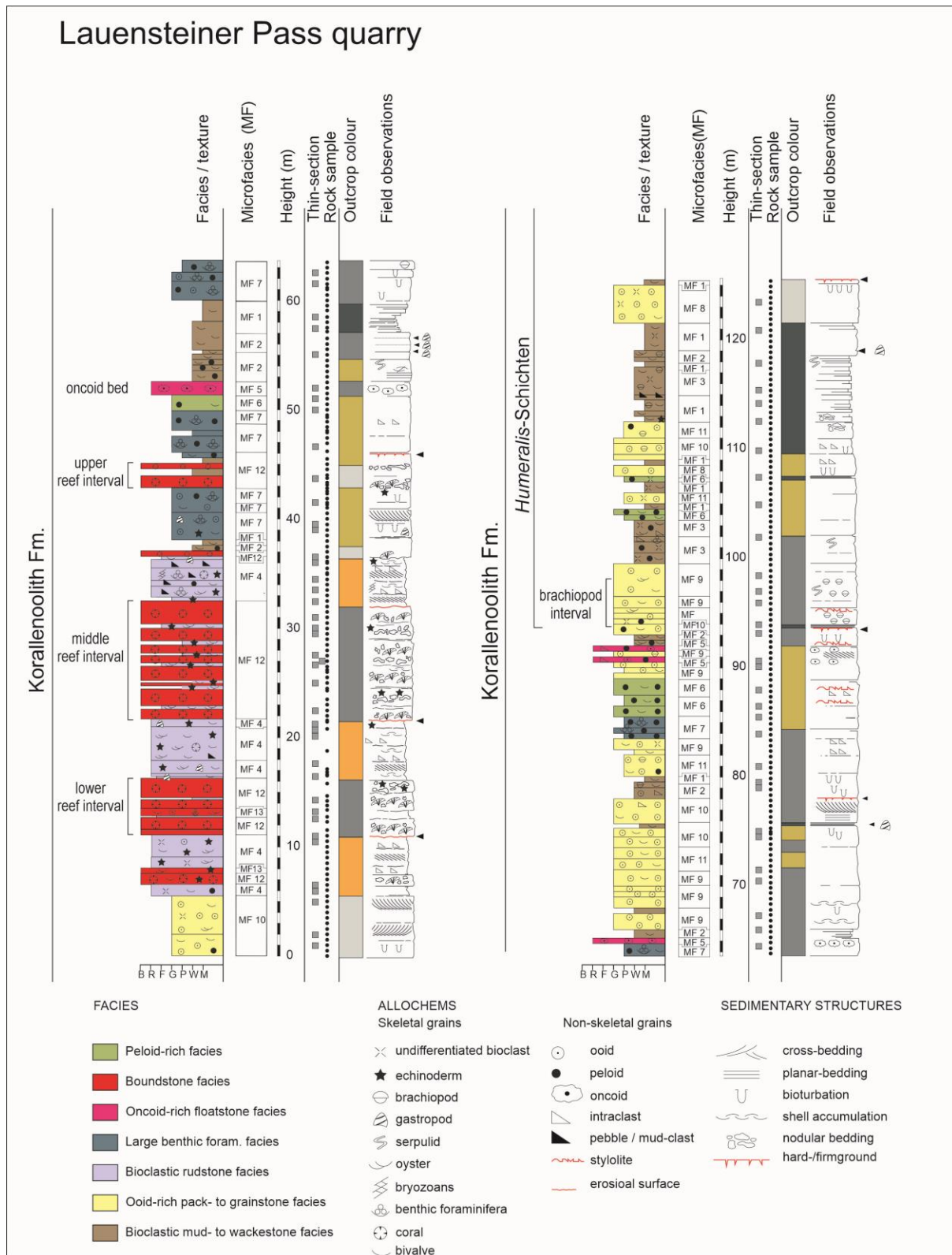


Fig. 4 High-resolution log description of the Bisperode section showing lithology, thin section sample distribution, height (m), and erosional profile.

Chapter 2

Here we focus on the lower 126 m of the accessible section (Fig. 4), assigned to the Korallenoolith Fm. (Betzler et al. 2007; Cäsar 2012). The base of the section is characterized by ~5.5 m of ooid-rich grainstones including rare to common iron ooids. The ooid-rich grainstone lithologies belong to the Hauptoolith Member (Mbr.) (Klöpffel 1931; Stinder 1991; Schülke 1993; Helm et al. 2003). Above, five boundstone horizons alternate with bioclastic-rich rudstone between 5.5 and 45.0 m. The top reefal boundstone layer is considered to represent the equivalent of the *Florigemma*-Bank (Cäsar 2012; Bai et al. 2020). Based on different growth forms of corals (ramose, flat sheet-like, dome-shaped, hemispheric), different ecological associations were distinguished by Betzler et al. (2007) and Cäsar (2012). Above the middle reef interval, grain- and packstone textures dominate the succession (45.0–65.0 m), with some intervals showing a high portion (>50%) of *Reophacidae* cf. *Reophax* foraminifera. The marl-limestone alternation intervals at 52.6–60.0 m, 99.5 m–103.5, and 112.5 m–121.5 m are characterized by wacke- to mudstone beds. The upper part of the section (66.0 to 125.5 m) is essentially composed of ooid-rich pack- and grainstones with intercalations of bioclastic-rich wackestone.

2.5.2. Facies types

A total of 7 facies types (FTs) including 14 different microfacies types (MFs) are distinguished for the Bisperode section (Table 1).

Table 1 Facies types and microfacies types in the present study

| Facies types (FT) | Microfacies types (MF) | Description | Depositional environment and interpretation | Energy |
|---|---|---|--|------------------|
| FT 1 Bioclastic wackestone to mudstone facies | MF 1 Thin-bedded mudstone with bioclastic | This MF-type is gray bioclastic mudstone composed of micrite, rich in argillaceous, quartz, organic matter, and scattered pyrite. The main skeletal components are fine molluscan bioclasts, benthic foraminifera, a few ostracods, and crinoid stem (Fig. 5A, B). | Open marine | Low |
| | MF 2 Bioturbated wackestone | This MF-type is wackestone containing shell fragments derived from benthic foraminifera, brachiopod, and serpulid. Two types of foraminifera species have different shapes and sizes; the foraminifera chamber is filled with black organic materials, so the chamber structure is unclear. The brachiopod shells microstructure reveals both punctuated (terebratula-like) and non-punctuated (rhyconella-like) specimens (Fig. 5C). | Open marine | Low to moderate |
| | MF 3 wackestone with shell fragments | In this MF-type. Bioclasts include shell fragments of juvenile gastropod, echinoderm, and brachiopod shell fragments, and thin filamentous shells representing potential mollusk larval stages (Fig. 5-E). Abundant angular to subangular smaller detrital grains, agglutinated foraminifera, and some organic matters are recognized (Fig. 5D, E). | Open marine | Low to moderate |
| FT 2 Bioclastic-rich facies | MF 4 Bioclastic | This MF-type is dominated by micritized (coated) bioclasts, which account for >50 % of the particle. The biofabric with imbrication structure and the elongated bioclasts vary in a clear orientation, resulting in very poor sorting. Bioclasts are derived from coral fragments, gastropods, bivalves, echinoderms, brachiopods, and foraminifera; besides, peloids and rare ooids are observed, most grains are cortoids comprising coated bioclasts. Selective dissolution is visible amongst the bioclasts, with some of them showing the original structure, whereas some are just keeping the stable micrite envelopes and encrustations (Fig 5F). | Bioclastic sand bar or open marine? storm deposits | Moderate to high |

| Facies types (FT) | Microfacies types (MF) | Description | Depositional environment and interpretation | Energy |
|---|---|---|---|-----------------|
| FT 3 Oncoid-rich facies | MF 5 Oncoid-rich rudstone | MF-type 5 is composed of oncoids with distinctive concentric but irregular cortex; Individual oncoids are 2 mm to 20 mm in diameter. The oncoids are elliptical, lobate, and with knobby surfaces, the surface irregular organism-bearing <i>Bacinella-Lithocodium</i> laminations. They have formed around gastropods, bivalve fragments, foraminifera, and the shape of the core strongly influences the body of the oncoids. Some of the oncoids show clear signs of compaction and dissolution along their outer face, and serpulid worm tubes within the cortex, some sparry patches (dissolved organism?) within the cortex, and fine-grained sediments are also trapped on the oncoïd surface by the organism. The intra-oncoids have a continuous micritic lamination (Fig. 5G, Fig. 5H). | Lagoon, storm events | Moderate |
| FT 4 Peloid rich facies | MF 6, Bahamite type peloids | With various shapes and sizes, with a relic internal structure and a black lamina envelope surrounding it, these may be heavily micritic bioclasts. Brachiopod fragments are also present (Fig. 5I). The peloids show a typical ellipsoidal shape including in rare occurrences slightly larger particles. The peloids are stained in brown by organic matter, probably fecal in origin (Fig. 6A). | Semi-open lagoon | Moderate |
| FT 5 Large benthic foraminifera-rich facies | MF 7 Foraminiferal-rich packstone to grainstone | The main component is <i>Reophacidae cf. Reophax</i> foraminifera accounts for up to 50% of the total grains. Other bioclasts (~20 %) include fragments of bivalves, brachiopods, and gastropods, as well as the rare crinoid stem. The foraminiferal are large, often exceed 0.5 mm in diameter, and show a complex internal structure, all of them agglutinated ooids or peloids as their wall structure, and their chambers are filled with fine-grained carbonate mud micrite (Fig. 6B). | Lagoon | Low to moderate |
| FT 6 Ooid rich facies | MF 8 Radial oolitic grainstone | Aggregate of radial oolitic lithoclasts and radial ooids with grain sizes ranging between 0.4 and 1.75 mm in diameter. They are made up of radial fibrous calcite crystals and weak concentric banding, evenly dispersed within the sparry calcite cement. By the close packing of the ooids, the radial microstructure indicated a quiet water depositional environment. (Fig. 6C). | Oolitic bar | High |
| | MF 9 Bioclastic oolitic grainstone | This MF-type contains an estimated ooid portion of 80%. Ooids with a tangential structure are present and have different shapes and sizes. Other components are shell fragments derived from bivalves, brachiopods, echinoderms, and agglutinated foraminifera. Few intraclasts and oncoids are also present. Some of the ooids, bioclasts, and oncoids have gone through intensive micritization, but we can still see the original individual structure under the microscope. The interspace between the grains is filled with fine-grained carbonate micrite or sparry calcite cement. The nuclei are entirely calcareous and include opaque micritic grains (peloids) of rather large size compared to the thickness of the cortex (Fig. 6D). | Ooids-bioclastic bar | High |
| | MF 10 Superficial oolitic grainstone | MF-type 11 is grains that are subspherical to subelongated, with the shape being related to the size of the bioclastic nucleus, benthic foraminifera, and gastropods are abundant. Ooids are 0.3 to 0.8 mm in diameter, well-rounded, and show a concentric structure with smaller skeletal or non-skeletal cores. Some ooids show selective dissolution features with dissolution affecting coatings and the ooid cores, and some of them still keep original organic concentric lamination, some are entirely dissolved, and some have completely formed neomorphosed oolite. The interparticle space is filled with sparry calcite. Other components are mainly represented by benthic foraminifera and mollusk fragments (Fig. 6E). | Ooid bar | High |

Chapter 2

| Facies types (FT) | Microfacies types (MF) | Description | Depositional environment and interpretation | Energy |
|------------------------|-----------------------------|--|---|--------|
| | MF 11 Oolitic packstone | The ooids have peloidal nuclei and numerous cortical coatings. The nuclei are opaque micritic grains (peloids) of rather large size compared to the thickness of the cortex, and some are micritized bioclastic cores (Fig. 6F). | Ooids bar | High |
| FT 7 Boundstone facies | MF 12 Boundstone | This MF-type is mainly composed of in-situ preserved stromatoporoids and rare scleractinian corals. Between the stromatoporoids or corals space are filled with intraclast containing ooids, echinoid spines, coral fragment, bivalves, gastropods, and rare peloid, which are very poorly sorted. Some coral fragments show bioerosion structures and have been bored by sponges or bivalves and were subsequently filled with fine-grained carbonate sediment—longitudinal sections of the colonial coral show a well-preserved margin, with a slightly thickened wall structure. The stromatoporoid and rare dendritic scleractinian corals underwent selective dissolution, resulting in numerous, partially irregular-shaped vugs. Subsequent hydrothermal dolomitization as indicated by the formation of saddle dolomite can be observed in some vugs. Some vugs were filled by fine-grained carbonate sediment, a well-developed geopetal structure, with black fine lime at the bottom and cementation at the top (Fig. 6G, H). | Reefs, open marine | High |
| | MF 13 Reef-flank bioclastic | Poorly sorted and densely packed bioclasts in the micritic matrix with mainly remains of sessile benthic organisms, angular to subangular clasts of reworked reefs (coral head), and some bioclasts including skeletal fragments derived from echinoids, bivalves, oysters, bryozoans and benthic foraminifera (Fig. 6I). | Open marine, or Open lagoon | High |

FT-1 – Bioclastic mud-to wackestone facies

Description: FT-1 is characterized by alternating marl-limestone beds between 52.6–60.0 m and wacke- and mudstone beds between 37.0–38.2 m, 65.5–66.5 m, 78.0–80.0 m, 92.0–93.0 m, 99.5–103.5 m, 104.4–105.0 m, 106.0–107.0 m, 108.5–109.0 m, 112.5–121.5 m. Facies type-1 comprises 3 MF-types (MF-1, MF-2, MF-3). Individual marl-limestone couplets show an average thickness of ~30–50 cm and are composed of a brown mud ribbon (marl) and a resistant limestone cap. The brown mud ribbon is made up of clay- and silt-rich marls, typically several centimeters in thickness. The limestone beds of the marl-limestone couplets are 20–30 cm-thick and made up of dark, grey wacke- to mudstones rich in finely disseminated pyrite. The different MFs are distinguished based on the amount and type of bioclastic material, with MF-1 representing a mudstone with small-size bioclasts (Fig. 5A, B). MF-2 corresponds to a bioturbated wackestone with fragments derived predominantly from benthic foraminifera, and brachiopods (Fig. 5C). MF-3 represents a wackestone composed of thin filamentous mollusc shells, echinoderms, and brachiopod fragments (Fig. 5D, E).

Paleoenvironmental interpretation: In FT-1, the dominant mud-and-wackestone texture points to a low hydrodynamic regime supported by the common occurrence of thin filamentous mollusk shells (Flügel, 2004). Moreover, nerineoid gastropods formed semi-sessile communities, which colonized stable seafloor surfaces and maybe grazed on algae or microbial mats in quiet environments. These gastropod communities were sensitive to disturbance and coastal hypoxia (Gallmetzer et al. 2017; Tomašových et al. 2018) and are therefore considered to represent useful paleoecological indicators (Waite et al. 2008).

Mass accumulations of nerineoid gastropods could indicate well-oxygenated mesotrophic conditions prevailing in shallow-shelf sea areas (Schlager et al. 1981; Nebelsick et al. 2019). Based on the above-mentioned sedimentary characteristics and faunal content, FT-1 is best assigned to an outer ramp (open marine) setting with limited water oscillation and including carbonate-dominated storm deposits reworked from inner or mid-ramp settings.

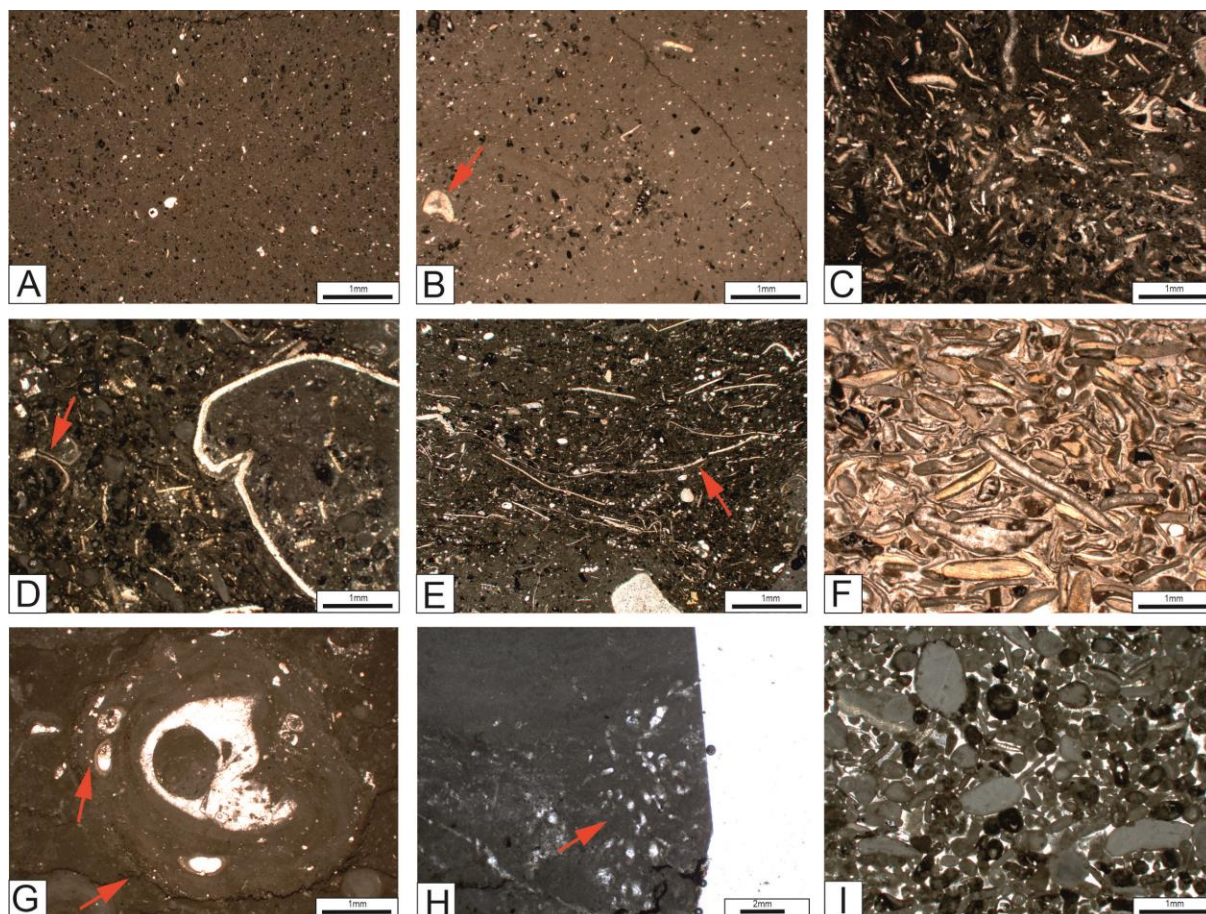


Fig. 5 Oxfordian MF-types defined in the study areas (1). MF-1 Mudstone includes (A) scattered organic matter and pyrite (at 58.5 m) and (B) fine-grain bioclasts of crinoids, ostracods, and foraminifera. The red arrow points at a crinoid arm plate (at 107.5 m). (C) MF-2 bioturbated wackestone, with very common shell bioclast, including brachiopod shells, and small benthic forams (at 118.0 m). (D, E) MF-3 bioclastic-rich wackestone including (D) encrusting serpulids (red arrow) and a brachiopod (at 54.4 m); (E) MF-2 bioturbated wackestone with common echinoderm fragments and oriented filamentous bivalve shells (red arrow, at 114.0 m). (F) MF-4 bioclast-rich rudstone with superficially micritized components (at 21.0 m). (G) MF-5 oncooid-rich rudstone with individual oncooids formed around gastropod clasts characterized by crenulated cortices including serpulids (red arrow, at 52.0 m). (H) MF-5 oncooid. Note that the oncooid cortices are composed of crenulated *Bacinella-Lithocodium* bearing laminations (at 52.0m). (I) MF-6, peloid-, foraminifera-rich grainstone (at 107.5 m).

FT-2 – Bioclastic rich facies

Description: FT-2 occurs commonly in the lower part of the section (5.5–6.5 m, 7.5–11 m, 12.5–13.5 m,

16.3–21.5 m, and 32.5–36.5 m) in the form of massive bioclastic-rich beds (>1 m thickness) often associated with an erosive base (Fig. 5F). FT-2 includes a single MF-type (MF-4). Individual beds typically show fining-upward units and trough cross-bedding. Thin sections reveal that bioclasts are very poorly to fairly sorted from the base to the top of individual beds, often showing a preferred orientation (incl. imbrication structure). The faunal content includes coral fragments, and debris of gastropods, bivalves, echinoderms, brachiopods, and benthic foraminifera, most of the bioclasts being superficially micritized. Secondary allochem grains include peloids, rare ooids (mostly superficial). Moldic porosity is visible among the bioclasts, with some bioclasts showing their original internal structure, whereas others preserve only the stable micrite envelopes and encrustations.

Paleoenvironmental interpretation: Large-scale cross-bedding clearly shows deposition above the fairweather wave-base (Betzler et al. 2007). The poor sorting with angular clasts and a high abundance of coral debris indicate that FT-2 was deposited nearby reefal structures. Between 16.3 m and 21.5 m, intense recrystallization of FT-2 is observed, which might support the previous interpretation that this interval has been affected by subaerial exposure as inferred from regional sequence stratigraphic correlation (Betzler 2007; Cesar 2012). Between 32.5 m and 36.5 m, the micrite content increases and indicates transport and redeposition of coarse reworked reef debris within a lower energy environment (Flügel 1982), which is likely to be associated with an open lagoonal setting. FT-2 is interpreted as coarse-grain tempestite reworked from and deposited near coral reefs (Flügel 2004). The composition and high diversity of the fossil assemblage (incl. large echinoderm and coral fragments) indicate a high-energy, open marine environment with normal salinity (Flügel 2004).

FT-3 – Oncoid-rich facies

Description: Oncoid-rich facies (FT-3) occurs in the form of distinct, well-defined, and sharp-based 0.5 to 1 m-thick layers (Fig. 3 H). FT-3 comprises MF-5 only (51.2–52.7 m, 64.9–65.3 m, 90.5–91.5 m). From base to top, the individual beds often show a gradual decrease in oncoïd size. Observed micrite-dominated oncoïds range from 2–20 mm in diameter and show a predominantly ovoidal shape with an irregular knobby surface. Most oncoïd nuclei correspond to gastropods, bivalve fragments, or foraminifera. Locally, serpulids or fine-grained sediment are observed within the cortex. The oncoïds are characterized by a distinctive concentric and irregular cortex (Fig. 5G). *Bacinella-Lithocodium*-like oncoïds (Védrine et al., 2007; Védrine, 2008) floating in a carbonate-dominated matrix are also observed (Fig. 5H).

Paleoenvironmental interpretation: The composition and lamination types of the oncoïds reflect environmental factors that control microbial and algal growth as well as encrusting communities (light, salinity, water energy, sediment input; Flügel 2004). Given the similarity in surface morphology and structure of the cortex, the MF-5 oncoïds resemble type-2 oncoïds described from the Upper Oxfordian Hauptmumienbank Mbr. of the Swiss Jura (Gygi 2000; Védrine et al. 2007). According to Védrine et al. (2007), this type of micrite-dominated oncoïd shows ellipsoidally smooth to lobate growth form and was generated under open-marine and strong wave-energy conditions. In the Hauptmumienbank Mbr., type-2 oncoïds preferentially occur around sequence boundaries and transgressive deposits where higher energy conditions prevailed in relatively shallow water. The occurrence of oncoïds, as well as the irregular wavy base of the fining-upward rudstone beds, suggest high-energy depositional conditions

most likely triggered by storm activity (Betzler et al. 2007; Căsar et al. 2012). MF-5 is assigned to a lagoonal depositional environment and influenced by storm-induced bottom currents, able to episodically rework microbially bound and cemented sediments (Wilson 1975; Flügel 2004, Védine et al. 2007; Betzler et al. 2007).

FT-4 – Peloid-rich facies

Description: FT-4 includes MF-6 and rarely occurs in the section (50.0–51.0 m, 85.5–89.0 m, 103.5–104.5 m). MF-6 resembles the Bahamite peloid type-3 of Flügel (2004) with poorly sorted spherical to ellipsoidal peloids ranging from 0.2–1.0 mm in diameter. Strongly micritized bioclasts with internal structures coated by black lamina are commonly found in association with the peloids. Secondary allochems include benthic foraminifera and brachiopod fragments (Fig. 5-I, 6A).

Paleoenvironmental interpretation: Peloid-rich grainstones are a conspicuous constituent of high-energy shallow-marine platform carbonates. The term “Bahamite peloid” (type-3 peloid) was introduced by Gygi (1969) for structureless peloids of Jurassic platform carbonates, which closely resemble peloids found in the interior lagoon of the Bahama banks. This type of peloid originates from intensive micritization of ooids, bioclasts, or aggregation of micrite from disaggregation of calcareous algae leading to the complete loss of the microstructure of the grain.

FT-5 – Large benthic agglutinated foraminifera-rich facies

Description: FT-5 includes a single MF-type (MF-7) occurring at several intervals (38.2–42.5 m, 46.0–50.0 m, 60.0–64.5 m, 83.5–85.5 m). MF-8 is composed of grain- and packstones containing large-size (0.6 cm) agglutinated uniserial *Reophacidae* cf. *Reophax* foraminifera (> 50%). Other typical components include bivalve (mainly oysters), brachiopod and gastropod shell fragments, rare ooids as well as peloids and lithoclasts (Fig. 6B). The foraminifera exhibit a complex internal structure, with the individual chambers often being filled with fine-grained carbonate mud. The agglutinated wall structure often contains small-sized ooids, peloids, and bioclasts.

Paleoenvironmental interpretation: In the literature, the genus *Reophax* (Ordovician to present) has been documented in multiple and very different depositional environments such as high-energy shoal deposits (France; Lower Cretaceous; Amaud-Vanneau 1980), warm-water lagoonal settings (Austria; upper Coniacian; Schlagintweit et al., 2007), and coral-stromatoporoid patch-reef platform margins (Austria; Upper Jurassic; Schlagintweit et al., 2007). In the past, *Reophax* depositional environment reconstruction has been based on the building constituent of the foraminifera test. Following the same strategy, it is possible to infer an open-marine lagoonal depositional environment most likely located nearby some ooid shoals.

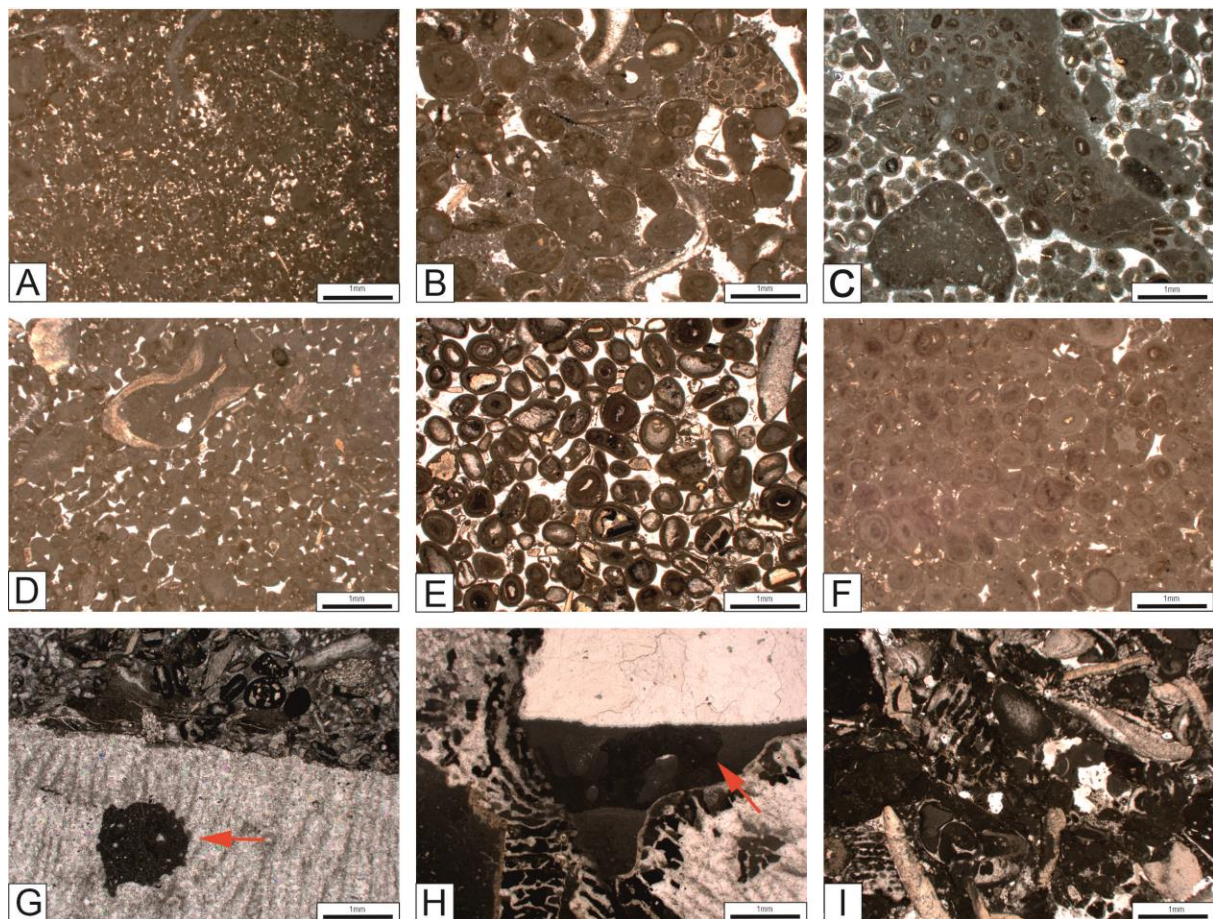


Fig. 6 Oxfordian MF-types defined in the study areas (2). (A) MF-6, peloid-rich packstone, with peloids accounting for more than 50% of all components, with rare ooid and micritised shells (at 51.0 m). (B) MF-7 foraminifera-rich pack- and grainstone, including large benthic *Reophacidae* cf. *Reophax foraminifera* (red arrow a) with agglutinated walls composed of peloids, ooids, bioclasts, and lithoclasts (red arrow b) (at 41.5 m). (C) MF-8 ooid-rich grainstone including radial ooids and large ooid-rich packstone intraclasts (at 123.5 m). (D) MF-9 bio-, ooid-rich grainstone dominated by micritized tangential ooids (Bahamite-like ooids, at 104.5 m). (E) MF-10 ooid-rich grainstone, oosparite including ooids showing several growth generations partially iron-enriched (1.0 m). (F) MF-11 ooid-rich pack- to grainstone including Bahamite-like ooids (at 96.0 m). (G) MF-11 coral-rich rudstone belonging to the reef-bearing interval with common boring occurrences (red arrow, at 12.3 m). (H) MF-11 coral-rich boundstone with geopetal fabric (red arrow, at 31.0 m). (I) MF-12 Coral-rich rudstone including large irregular badly sorted coral debris and diverse bioclasts (at 34.5 m).

FT-6 – Ooid-rich pack- and grainstone facies

Description: Oolitic limestones form a significant portion of the lowermost (0.0–5.5 m) and the upper half of the section (66.0–78.0 m, 80.0–83.5 m, 89.0–90.5 m, 90.0–90.5 m, 93.0–99.5 m, 105.0–106.0 m, 107.5–108.0 m, 109.0–112.5 m, 121.5–124.5 m), and are represented by well-sorted, gray or brownish thick limestone beds, often with distinct high-angle cross-bedding (Fig. 3G). Based on ooid type and size, a total of 4 different MFs are distinguished (MF-8, MF-9, MF-10, MF-11).

MF-8 corresponds to ooid-rich grainstones composed of radial ooids ranging between 0.4–0.6 mm in diameter (Fig. 6C). Besides, abundant lithoclasts (up to 8 mm) represent reworked consolidated ooid-

rich packstones. Individual ooids are made up of radial fibrous calcite crystals resulting in a concentric banding and the interparticle pores between the ooids is filled with sparry calcite cement.

MF-9 includes bioclastic ooid-rich grainstones containing ~50 to 80 % ooid grains (Fig. 6D). Individual ooids are relatively small (0.2–0.5 mm) and dominated by concentric ooids. The nuclei often consist of peloids. Additional components include shell fragments derived from bivalves, brachiopods, echinoderms, and agglutinated foraminifera. Secondary allochems include intraclasts and oncoids. Some grains have gone through intensive micritization, but the original structure is still recognizable. The intergranular space is filled with sparry calcite cement.

MF-10 corresponds to ooid-rich grainstones composed of significantly larger-size ooids (0.3–0.8 mm in diameter) than in MF-8; between 0.0–5.5 m iron-rich ooids have been observed. The individual grains have a subspherical or subelongate shape and often show a well-developed concentric rim around the bioclastic nucleus (Fig. 6E). Other components include primarily benthic foraminifers and mollusk fragments. Some ooids show selective dissolution features, which affect both the coatings and ooid cores. Some still keep the original concentric lamination, some are entirely dissolved, and some represent wholly formed neomorphic ooids.

MF-11 includes bioclastic-, ooid-rich packstone, with individual ooids showing mostly peloidal nuclei and numerous cortical coatings (Fig. 6F). Ooids are well-sorted and range between 0.3–0.8 mm in diameter. Nuclei are of relatively large size compared to the thickness of the cortex. The interparticle pores were filled with fine-grained calcareous mud, with only a few pores being filled with sparite.

Paleoenvironmental interpretation: Ooids typically form in Ca oversaturated, agitated shallow-marine subtropical waters influenced by waves and currents above the fairweather wave-base (Tucker and Wright, 1990; Flügel, 2004). Regular sorting, lack of bioturbation, and abundant large-scale cross-bedding support a high-energy depositional setting (oolitic bar). Radial aggregate ooid-rich grainstone (MF-8) is restricted to an interval in the uppermost part of the section (121.5 m–125.5 m). Radial ooids are more abundant in relatively lower-energy shallow-marine settings (Strasser 1986; Diaz et al., 2019). Oolitic and bioclastic shoals commonly separate more restricted lagoonal environments from deeper ramp environments and may act as wide and extensive barriers to currents and waves (Flügel, 2004).

FT-7 – Boundstone facies

Description: In the lower part of the studied section, coral-stromatoporoid boundstones (FT-7) represent the main portion of the succession (Betzler et al. 2007) and occur in the form of several, often m-thick stratiform layers (e.g., 6.5–7.5 m, 11.0–12.5 m, 13.5–16.3 m, 21.5–32.0 m, 36.5–37.0 m, 42.8–46.0 m). These layers show distinct variations in terms of texture and dominant builders. FT-7 is composed of two MFs, including coral boundstone facies (MF-12) and patch-reef flank bioclastic facies (MF-13). The lower boundstone intervals (11.0–12.5 m, 13.5–16.3 m) are dominated by flat, sheet-like, and strongly recrystallized corals (Fig. 3D, E). Between 6.5–7.5 m platy corals in growth position are embedded in fine-grained micrite (Fig. 3D). Stalk-shaped bafflestones dominate the thick interval between 21.5–32.0 m with distinct bioerosional structures (Fig. 3F). The latter include distinct circular borings produced by bivalves. Often, the bivalves are preserved in life positions with intact shells. Borings have been filled with fine-grained sediment, and certain bivalves have been rebored by other organisms. The

Chapter 2

boundstone interval between 42.8–46.0 m is composed of dome-shaped to hemispheric patch-reef structures, surrounded by a debris apron. This interval of the reef facies has been interpreted to be equivalent to the *Florigemma-Bank* (Cäsar 2012; Bai et al. 2020).

MF-12 is mainly composed of in-situ preserved stromatoporoids and rare dendritic scleractinian corals. The space between the stromatoporoids or corals is filled with coarse-grained and poorly sorted debris containing ooids, echinoid spines, coral fragments, bivalves, gastropods, and rare peloids. Certain coral fragments show bioerosion structures and have been bored by sponges or other organisms (Fig. 6G). The resulting cavities were subsequently filled with fine-grained carbonate sediment. In some layers, the stromatoporoid and rare dendritic scleractinian corals underwent selective dissolution, resulting in numerous, partially irregular-shaped vugs. Some dissolution vugs were partially filled by fine-grained geopetal carbonate sediment (Fig. 6H). Saddle dolomite cement filled the residual pore space of these vugs.

Paleoenvironmental interpretation: The reef structures of the Bisperode section did provide a suitable environment for highly diverse reef-dwelling fauna (incl. lithophaga, bivalves, oysters, gastropods, echinoids), indicative of normal-marine conditions. The occurrence of reworked reefal rubble and erosional surfaces indicates episodic storm events. The coarse-grained bioclastic texture of reef-flank deposits implies that the hydrodynamic conditions were sufficient to wash out any fine-grained lime mud (Fig. 6I). The water depth of this depositional environment was probably at or around the fair-weather wave base and the reef structures were located in a mid-ramp setting (Dupraz and Strasser 2002; Carpentier et al. 2007; Betzler et al. 2007).

2.5.3 Depositional model

Based on the facies distribution and previous research on the Korallenoolith Fm. (Helm 1998; Betzler et al. 2007; Cäsar 2012; Bai et al. 2020), a gently inclined carbonate ramp morphology is inferred (Fig. 7).

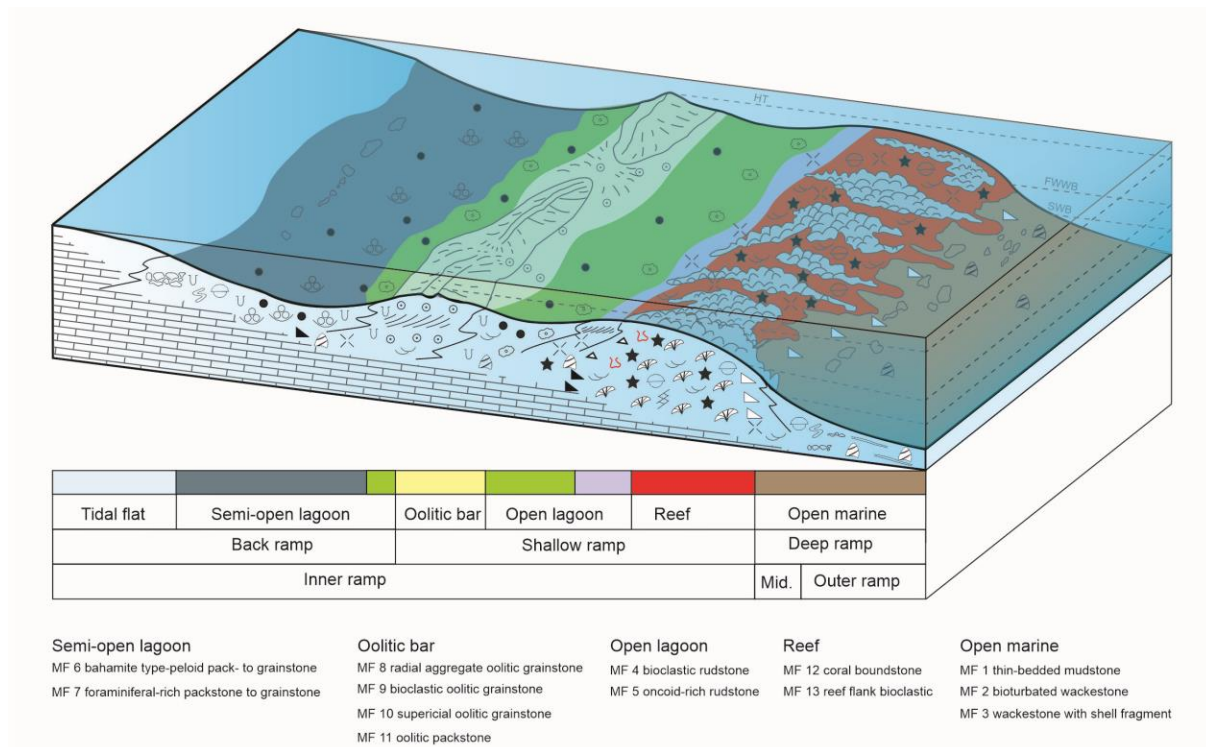


Fig. 7 Conceptual depositional environment model used for the sequence stratigraphic interpretation of the Bisperode section.

Five main depositional environments are differentiated throughout the section based on their characteristics and vertical distribution. A proximal/distal transect includes the following juxtaposed environments: open marine, patch reef, open lagoon, shoal, and semi-open lagoon. This proximal/distal succession reflects a hydrodynamic energy gradient. The open marine facies deposited below the storm wave-base is characterized by a large proportion of fine grain-size particles within a micrite matrix. The main textures are wackestone and mudstone, which formed the marl-limestone couplets bed with abundant bioturbation, indicating very low energy conditions. Stenohaline organisms (e.g., brachiopods and echinoderms) are indicative of normal-marine conditions (Strasser et al. 2012; MF-1, MF-2, MF-3). The patch-reef depositional environment is mainly composed of coral-rich boundstones and embedded reefal debris, reflecting a high-energy environment and isolating a lagoon from the open ocean. In this transitional zone (between open marine and open lagoon), storm waves and storm-induced currents lead to abrupt changes by redistributing sediment in large quantities, and by reworking corals (Flügel 2004; Strasser et al. 2012; MF-12, MF-13). Open lagoon facies deposited behind the reefs are characterized by diverse normal-marine fossils (bioclastic-rich rudstone, MF-4) deposited during episodic storm events. Oncoids were formed in the open lagoonal environment and subsequently reworked and redeposited during episodic storm events (MF-5). The oolitic bar corresponds to a higher energy environment with a high lateral variability due to tidal and long-shore currents. Some inlet cut through the sand bar and allow tidal currents to transport sediment and water into and out of the lagoon (Védrine and Strasser 2009). The texture is dominated by ooid-rich grainstone, confirming constant high-energy conditions (MF-8, MF-9, MF-10, MF-11). A semi-open lagoon, characterized by more restricted conditions with higher salinity, might have formed behind the high-energy facies of the oolitic

bar. Foraminiferal-rich peloid packstone-to-grainstone implies a low-energy environment with rare ooids washed in from the oolitic bars (MF-6, MF-7).

2.6 Sequence analysis

2.6.1 Small-scale sequences

Throughout the studied stratigraphic section, a total of 15 small-scale sequences were recognized with thicknesses ranging from 2.0 to 15.0 m (Fig. 8). The lowermost small-scale sequence (SS-1) is formed by thick-bedded, partly cross-bedded, oolitic-rich grainstones (0.0–5.5 m) interpreted as a regressive hemisequence including the stacking of coarsening upward trends (Betzler et al. 2007). The overlying SS-2 (5.5–12.5 m), SS-3 (11.0–21.5 m), and SS-4 (21.5–36.5 m) represent the superposition of deepening-shallowing hemisequences characterized by the transition from bioclastic rudstone facies (MF-4) at its base, grading upward into reef deposits (MF-12 and MF-13) back to bioclastic rudstones. The top of SS-3 is bound by a pronounced iron-stained exposure surface (surface B+C in Cäsar 2012) characterized by microkarst structure. SS-4 contains the most common occurrence of coral-rich boundstone over a ~10 m-thick interval and corresponds to the “middle reef interval” (Betzler et al. 2007). SS-4 is capped by a sharp erosional surface recognized as well in Betzler et al. (2007). SS-5 (36.5–43.0 m) and SS-6 (43.0–51.2 m) show a very similar thickness and composition made up of coral-rich boundstone at the base grading upward into the foraminifera-rich pack- and grainstones. SS-6 includes the last occurrence of coral-rich boundstone in the section interpreted as the top of the *Florigemma-Barke* equivalent (Cäsar 2012; Bai et al., 2020) or the “upper reef interval” of Betzler et al. (2007). SS-6 is capped by an erosion surface correlative to the “Hauptemersionsfläche” based on its stratigraphic positioning (capping the coral boundstone-rich interval) and its gamma-ray signature (Betzler et al. 2007; Cäsar 2012; Bai et al. 2020). The overlying SS-7 (51.2–65.0 m) is characterized by transgressive and regressive hemisequences grading from an oncoid-rich rudstone into open-marine deposits (MF-1 and MF-2) evolving upward into the foraminifera-rich pack- and grainstones, respectively. The interval between 52.6–57.6 m contains some abundant, up to 3 cm-long nerineoid gastropods. In this interval, pronounced nodular bedding composed of individual ovoid-shaped nodules is prevalent. SS-7 is capped by a firmground (Surface E; Cäsar 2012) including intense bioturbation, possibly indicative of reduced sedimentation rates associated with a transgressive surface. SS-8 (65.0–75.5 m), SS-9 (75.5–78.0 m), SS-10 (78.0–90.5 m), and SS-11 (90.5–100.0 m) constitute the ooid-rich grainstone (MF-8 to MF-11) interval of the section. Their transgressive and regressive hemisequences depict a facies belt migration from an oolitic bar into open-marine conditions back to an ooidal bar. SS-10 shows a slight difference with more regressive semi-open lagoonal deposits (MF-6 and MF-7). Each sequence is separated by distinctive surfaces interpreted as hardgrounds based on the strong bioturbation and fossil density and the common occurrence of dark-coloured mineralization. Noteworthy, the top of SS-9 and SS-10 correspond to surfaces F and G from Cäsar (2012). SS-12 (100.0–106.0 m), SS-13 (106.0–108.5 m), SS-14 (108.5–112.5 m), and SS-15 (112.5–125.5 m) show similar composition and facies belt fluctuations than SS-8 to SS-11, but with thicker mud- to wackestone intervals (MF-1 to MF-3).

characteristic of the *Humeralis Schichten*. Apart from the top of SS-15, which is characterized by a karstified surface, the other sequence boundaries are unspecific.

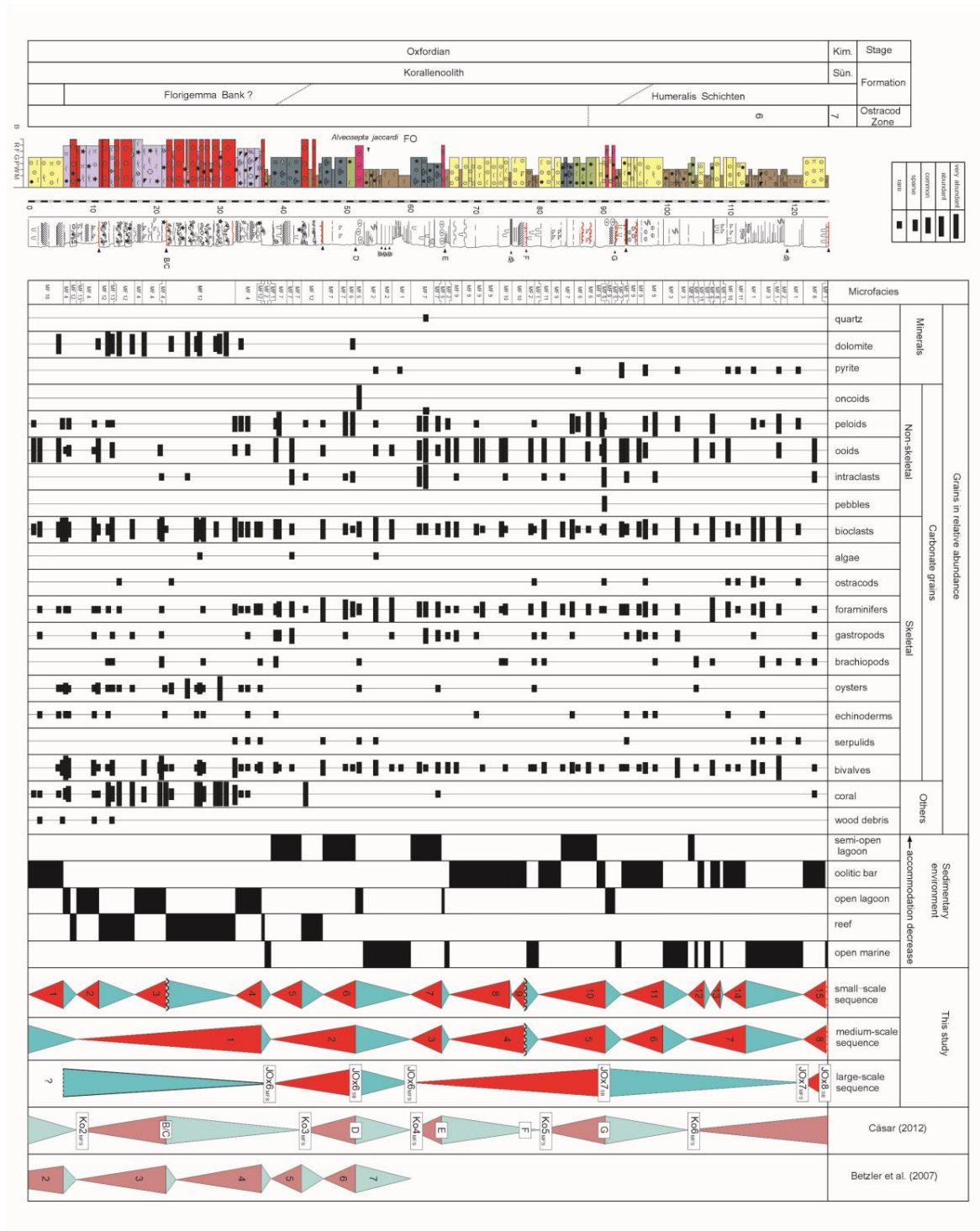


Fig. 8 Sedimentological description, depositional settings and sequence stratigraphic interpretation of the Bisperode section including semi-quantitative allochem composition.

2.6.2. Medium-scale sequences

Eight medium-scale sequences (MS) were recognized, showing a thickness range from 6 to 32 m. The number of SS sequences per MS sequence varies from 1 to 4. MS-1 (0.0–39.0 m; SS-1 to SS-4) is the thickest MS recorded in the Bisperode section and starts with a transgressive hemisequence depicting a facies shift from MF-11 to MF-13. Its regressive hemisequence includes most of the coral-boundstone interval and starts and finishes with MF-13 corresponding to an aggradational stacking pattern indicating that A/S roughly equals one. The MS-2 (39.0–51.2 m; SS-5 and SS-6) transgressive hemisequence corresponds to a shift from MF-13 to MF-1 and marks the first occurrence of the most distal facies recorded in the Bisperode section (MF-1). The MS-2 regressive hemisequence starts with MF-1 and is capped with the erosional surface (51.2 m) interpreted as the “Hauptemersionsfläche” (Betzler et al. 2007; Cäsar 2012; Bai et al. 2020). The MS-3 (51.2–65.0 m; SS-7) transgressive hemisequence is the second thickest transgressive interval composed of the most distal facies MF-2 and MF-1, which indicates one of the smallest A/S ratios of the entire section. Its regressive hemisequence is the thinnest described in the Bisperode section and corresponds to a facies shift from MF-1 to MF-8 within less than 5 m. The MS-4 (65.0–78.0 m; SS-7 to SS-9) transgressive hemisequence corresponds to a facies shift from MF-7 to MF-2. Its regressive hemicycle marks the reappearance of ooid-rich grainstones after a ~60 m stratigraphic gap. MS-5 (78.0–90.5 m) and MS-6 (90.5–100.0 m) are equivalent to SS-10 and SS-11 and the regressive hemisequences depict a facies shift from MF-1 to MF-11 and MF-2 to MF-9, respectively. The *Humeralis Schichten* include MS-7 (100.0–112.5 m; SS-12 to SS-14) and MS-8 (112.5–125.5 m; SS-15). The MS-8 transgressive hemisequence is the thickest and includes the most distal facies (MF-1 and MF-2), which indicate the lowest A/S values.

2.6.3 Large-scale sequences

Three large-scale sequences (LS) with an average thickness of ~45 m are recognized in the Bisperode section. All LS show a similar amplitude of facies belt migration interpreted to range from subaerial exposure to open-marine depositional environments. LS-1 (0.0–51.2 m; MS-1 to MS-2) is the thickest LS recorded in the Bisperode section. The base of LS-1 is not accessible in the studied area but is interpreted to correspond to the transition between the Heersum and the Korallenoolith Fms. Its regressive hemisequence ends with the sharp erosional surface (51.2 m) interpreted as the “Hauptemersionsfläche” (Betzler et al. 2007; Cäsar 2012). The LS-2 (51.2–90.5 m; MS-3 to MS-5) transgressive hemisequence corresponds to the first occurrence of a thick (> 5 m) interval of deposits characteristic of an open-marine depositional environment. The top of LS-2 corresponds to the hardground correlative to the surface G of Cäsar (2012) located 7.5 m below the base of the *Humeralis Schichten*. LS-3 (90.5–125.5 m; MS-6 to MS-8) covers the entire *Humeralis Schichten*. The LS-3 transgressive hemisequence is characterized by the progressive thickening of open-marine deposits from MS-6 (1.0 m), MS-7 (3.0 m) and MS-8 (8.0 m) transgressive hemisequences. The LS-3 transgressive hemisequence is interfingered with MS-6 and MS-7 regressive hemisequences including ooid-rich grainstone shoreface deposits. This trend of progressive thickening of transgressive hemisequences indicates an overall increase of the A/S ratio with the largest value reached at 122.0 m.

LS-7 ends at 125.5 m which corresponds to the karstified surface characteristic of the top of the *Humeralis Schichten*.

2.7 Discussion

Sequence-stratigraphic regional and supra-regional correlations

Betzler et al. (2007) suggested a subdivision of the lower part of the Bisperode section (0.0–60.0 m) into 7 “long-term” sequences, a scheme showing minor divergences with the present interpretation. Comparatively, the follow-up study from Căsar (2012) subdivided the exposed Oxfordian strata of the Bisperode section into 6 sequences (Ko1 to Ko6; Fig. 8) of which one (Ko1) is not accessible anymore and therefore, is not described in this study. Ko2 to Ko6 broadly correlate with our LS-sequences LS-1 to LS-3. The differences between Căsar (2012) and our study is due to the fact that Ko2 and Ko3 as well as Ko4 and Ko5 have been merged into our LS-1 and LS-2, respectively. The last difference and probably the most significant one is the interpretation by Căsar (2012) of the mud-dominated intervals at 51.2–60.0 m and 112.5–122.0 m to be supratidal and open- to restricted-lagoon depositional environments respectively. A supratidal origin for the interval 51.2–60.0 m is unlikely based on the presence of ooids and marine fauna (e.g., oysters) revealed by our MF-analysis within this interval. Concerning the strata between 112.5–122.0 m, the occurrences of stenohaline organisms such as brachiopods and echinoderms do not support the interpretation of a restricted-lagoon depositional environment for this interval. However, the interpretation of possible open-marine lagoon deposits cannot be ruled out. A more conservative approach is applied in this study by considering both intervals to be formed in a similar depositional environment based on their sedimentological characteristics and their resemblance with the mud-dominated interval located between 100.0–103.5 m interpreted in here and in Căsar (2012) as open marine deposits.

According to the sequence-stratigraphic chart of Hardenbol et al. (1998), the Late Jurassic was characterized by a second-order transgressive trend starting in the *Quenstedtoceras mariae* (lowermost Oxfordian; JOx1_{SB}) and ending in the *Aulacostephanus euxodus* (uppermost Kimmeridgian; JKi6_{MFS}) ammonite zones, respectively. The latter second-order trend was subdivided, in the Oxfordian, into 8 higher-order sequences with five major sequence boundaries (SBs) recorded within the *Q. mariae* (JOx1_{SB}), the uppermost *P. plicatilis* (JOx5_{SB}), the uppermost *P. cautisnigrae* (JOx6_{SB}), the *R. pseudocordata* (JOx7_{SB}), the lowermost *P. baylei* (JOx8_{SB}) and four major maximum-flooding surfaces (MFSs) documented within the uppermost *P. mariae* (JOx1_{MFS}), the *P. cautisnigrae* (JOx5_{MFS}), and the lower and upper *R. pseudocordata* (JOx6_{MFS} and JOx7_{MFS}). Maximum regressive surfaces (MRSs) and MFSs ages are expected to be diachronous in each basin due to their strong dependence on sedimentation supply and regional subsidence change. Subaerial unconformities (SUs) on the contrary are much more reliable as chronostratigraphic markers since they are defined as the onset of base-level fall (Csato and Catuneanu 2012; Krencker et al. 2022). In the Bisperode section, we propose that no/or a reduced Lowstand Systems Tract and a Falling Stage Systems Tract are preserved following the assumption from Betzler et al. (2007). This implies that SBs documented in our work coincide with SUs. Even though the accurate dating of the Korallenoolith Fm. is still challenging, it is interesting to notice

Chapter 2

that some of the key stratigraphic markers of the LSB and our large-scale SBs can be correlated to Hardenbol et al. (1998) sequence-stratigraphic chart. This indicates that eustatic sea-level fluctuations were likely the main driver behind the building of at least the LS-sequences recorded in the Bisperode section despite different subsidence and sediment supply histories specific to each basin.

First, in the LSB the Callovian/Oxfordian transition is described as an erosional surface cutting through the offshore claystone from the Omatenton Fm., which in the south-eastern part of the basin is directly overlain by the shallow-marine Korallenoolith Fm. (Mönnig 1989; Fischer 1991). The timing and the nature of this regionally-significant surface match well JOx1_{SB} characteristics. Second, even though the transition from the Heersum to the Korallenoolith Fm. is diachronous between Wesergebirge and the Heersum type section (Siegfried 1954; Stinder 1991), it is noticeable that the major sedimentological change from outer ramp (Heersum Fm.) to inner ramp (Korallenoolith Fm.) depositional setting is recorded around the uppermost *P. plicatilis* zone (Siegfried, 1954) at the Middle/Upper Oxfordian boundary correlating to JOx5_{SB}. The “Hauptemersionsfläche” (Kästner et al., 2010) (LS-1_{SB} in this study) is capping the coral-rich boundstones interval, which might correspond to the *Florigemma Bank* (Căsar 2012; Bai et al. 2020). Following this interpretation implies that the “Hauptemersionsfläche” belongs to the uppermost *P. cautisnigrae* zone (see chapter 2.1), similar to JOx6_{SB}. This interpretation is in agreement with the chemo- and sequence stratigraphy of Bai et al. (2017; 2020). The interval located between LS-1_{SB} (surface D, Căsar 2012) and LS-3_{SB} belongs to the *R. pseudocordata* zone based on the occurrence of *A. jaccardi*, and *Galliaecytheridea dissimilis* and *G. mandelstami*, at 53.0 and 125.5 m, respectively. Our LS-sequence-stratigraphic analysis indicates two remaining SBs within this interval at 90.5 and 125.5 m corresponding to LS-2_{SB} and LS-3_{SB}, respectively. LS-2_{SB} and LS-3_{SB} could correlate to JOx7_{SB} and JOx8_{SB} based on their sedimentological characteristics and chronostratigraphical assignment (Hardenbol et al. 1998).

Last but not least, a duration of ~3.8 Myr can be suggested based on the GTS2020 (Hesselbo et al. 2020) for the deposition of the Korallenoolith Fm. dated from the base of the *P. antecedens* subzone (158.6 Ma) to the top of the *R. pseudocordata* zone (154.8 Ma). Assuming an equal duration of the 8 MS-sequences, and acknowledging that the transition between the Heersum and the Korallenoolith Fms is missing in the Bisperode section, an average duration in the order of the long eccentricity cycle (i.e., 405 kyr) can be deduced for these sequences. This suggests that MS-sequences are in line with the scheme proposed by Gygi (2000c) and ultimately that those sequences could be driven by orbital forcing. Even though it is clear that the calculation of the duration is subject to many caveats (e.g., stratigraphic gaps) it is still interesting to see that the obtained result is compatible with Milankovitch cycles as potential controlling mechanism of the MS-sequences. This interpretation is also in line with the sequence-stratigraphic interpretation of the Upper Oxfordian–Kimmeridgian succession in the southern German Jurassic Basin by Ruf et al. (2005), who suggested that their medium-scale sequences (3–10 m-thick) reflect the long eccentricity as well. Altogether, MS- and LS-sequences tend to indicate a potential control of allocyclic processes on their stacking pattern.

2.8 Conclusions

Based on detailed field observations, slab, and thin section analysis, a total of seven superordinate facies types - composed of 14 different microfacies types - were distinguished in the Bisperode section and attributed to different paleoenvironments. Through the paleoenvironmental analysis, a homoclinal ramp setting composed of different juxtaposed facies belts, ranging from semi-open lagoonal to open marine settings, is supported. On the basis of microfacies, diagnostic bedding surfaces, and the vertical lithofacies stacking pattern, a total of 15 small-, 8 medium-, and 3 large-scale sequences are identified. Detailed facies analysis and sequence stacking pattern of the Bisperode section suggest that eustatic fluctuations might have controlled the medium- and large-scale sequences preserved within the Korallenoolith Fm. based on their good match with the well-established eustatic model (e.g., Hardenbol, 1998). Regional synsedimentary salt tectonism and sedimentation rate fluctuations may have played a role in relative sea-level changes in the LSB and as such influence most of the small-scale sequences. Although it is clear that the lack of strong biostratigraphic markers hampers the confidence in the correlation between regional and global sequence-stratigraphic model in the LSB, this work provides a general framework, which will help to better understand the link between the stacking pattern of Oxfordian strata in the LSB and allocyclic processes allowing future chemo- and sequence-stratigraphic correlations.

2.9 Acknowledgments

This research was financed by the CSC scholarship (201808510183) granted to Deyan Zhang. Fritz Stoepke is thanked for his support during fieldwork sessions and for the thin section preparation. The first author would like to express his gratitude to Prof. Fang Xiang for her help with microfacies analysis and to Dr. Julia Gravenyck for her help proofreading the manuscript.

2.10 References

- Amaud-Vanneau, A. (1980). L'Urgonien du Vercors septentrional et de la Chartreuse. *Géol. Alpine, Mém.* 11, 1–874, Grenoble.
- Bai, H., Betzler, C., Erbacher, J., Reolid, J., & Zuo, F. (2017). Sequence stratigraphy of Upper Jurassic deposits in the North German Basin (Lower Saxony, Süntel Mountains). *Facies*, 63, 1–20. <https://doi.org/10.1007/s10347-017-0501-4>
- Betzler, C., Pawellek, T., Abdullah, M.A., & Kossler, A. (2007). Facies and stratigraphic architecture of the Korallenoolith Formation in North Germany (Lauensteiner Pass, Ith Mountains). *Sedimentary Geology*, 194, 61–75. <https://doi.org/10.1016/j.sedgeo.2006.05.002>
- Bai, H., Betzler, C., Huang, W., Zuo, F., & Wu, F. (2020). Sequence stratigraphy of the Upper Jurassic mixed siliciclastic-carbonate deposits in the North German Basin (Lower Saxony, Hildesheimer Wald). *International Journal of Earth Sciences*, 109, 893–910.

Chapter 2

- Betz, D., Führer, F., Greiner, G., & Plein, E.M. (1987). Evolution of the Lower Saxony Basin. *Tectonophysics*, 137, 127-170. [https://doi.org/10.1016/0040-1951\(87\)90319-2](https://doi.org/10.1016/0040-1951(87)90319-2)
- Bombien, H., Hoffers, B., Breuckmann, S., Helms, M., Lademann, M., Lange, M., Oelrich, A., Reimann, R., Rienäcker, J., Schmidt, C., Slaby, M., Ziesch, J. (2012). Der Geotektonische Atlas von Niedersachsen und dem deutschen Nordseesektor als geologisches 3D-Modell. *Geowissenschaftliche Mitteilungen*, 48, 6–13.
- Cross, T.A., Baker, M.R., Chapin, M.A., Clark, M.S., Gardner, M.H., Hanson, M.S., Lessenger, M.A., Little, L.D., McDonough, K.-J., Sonnenfeld, M.D., Valasek, D.W., Williams, M.R., Witter, D.N. (1993). Applications of high-resolution sequence stratigraphy to reservoir analysis. In: Eschard R, Doligez B (Eds.) *Subsurface Reservoir Characterization from Outcrop Observations*. Éditions Technip, Paris, pp 11–33.
- Cross, T.A., Lessenger, M.A. (1998). Sediment volume partitioning: rationale for stratigraphic model evaluation and high-resolution stratigraphic correlation. In: Gradstein FM, Sandvik KO, Milton NJ (Eds.), *Sequence Stratigraphy—Concepts and Applications*. Elsevier Science B.V, Amsterdam, pp. 171–195.
- Carpentier, C., Lathuilière, B., Ferry, S., & Sausse, J. (2007). Sequence stratigraphy and tectono-sedimentary history of the Upper Jurassic of the Eastern Paris Basin (Lower and Middle Oxfordian, Northeastern France). *Sedimentary Geology*, 197, 235-266. <https://doi.org/10.1016/j.sedgeo.2006.10.004>
- Catuneanu, O., Galloway, W.E., Kendall, C.G., Miall, A.D., Posamentier, H.W., Strasser, A., & Tucker, M.E. (2011). Sequence Stratigraphy: Methodology and Nomenclature. *Newsletter on Stratigraphy*, 44, 173-245. DOI: 10.1127/0078-0421/2011/0011
- Cäsar, S. (2012). Sequenzstratigraphie und sedimentologie oberjurassischer Karbonate von Norddeutschland (Oxfordium/Kimmeridium, Niedersächsisches Becken). Dissertation, Universität Hamburg.
- Csato, I., Catuneanu, O. (2012). System tract successions under variable climatic and tectonic regimes: A quantitative approach. *Stratigraphy*, 9, 109–130.
- Dunham, R.J. (1962). Classification of carbonate rocks according to depositional texture. *AAPG Mem*, 1, 108–121.
- Diaz, M.R., & Eberli, G.P. (2019). Decoding the mechanism of formation in marine ooids: A review. *Earth-Science Reviews*, 190, 536–556. <https://doi.org/10.1016/j.earscirev.2018.12.016>
- Embry, A.F., & Klovan, J.E. (1971). A Late Devonian Reef Tract on Northeastern Banks Island, N.W.T. *Bulletin of Canadian Petroleum Geology*, 19, 730–781.
- Dupraz, C., & Strasser, A. (2002). Nutritional Modes in Coral: Microbialite Reefs (Jurassic, Oxfordian, Switzerland): Evolution of Trophic Structure as a Response to Environmental Change. *PALAIOS*, 17(5), 449–471. <http://www.jstor.org/stable/3515720>
- Englich, B., Hühne, C., Joger, U., Knötschke, N., Knolle, F., Röhling, H.G. et al. (2017). Jurassic Harz. Dinosaurier von Oker bis Wyoming.
- Fischer, R. (1991). Die Oberjura-Schichtfolge vom Langenberg bei Oker. *Arbeitskreis Paläontologie Hannover*, 107, 21–52.
- Flügel, E. (2004). *Microfacies of carbonate rocks*. Springer, Berlin.

- Flügel, E. (1982). *Microfacies of carbonate rocks*. Springer, Berlin.
- Gramann, F., Heunisch, C., Klassen, H., Kockel, F., Dulce, G., Harms, F., Katschorek, T., Mönnig, E., Schudack, M., Schudack, U., Thies, D., Weiss, M. (1997). Das Niedersächsische Oberjura-Becken-Ergebnisse Interdisziplinärer Zusammenarbeit. *Zeitschrift der Deutschen Geologischen Gesellschaft*, 148, 165–236.
- Gallmetzer, I., Haselmair, A., Tomašových, A., Stachowitsch, M., & Zuschin, M. (2017). Responses of molluscan communities to centuries of human impact in the northern Adriatic Sea. *PLoS ONE*, 12, 1–31. <https://doi.org/10.1371/journal.pone.0180820>
- Gygi, R.A. (2000). Integrated stratigraphy of the Oxfordian and Kimmeridgian (Late Jurassic) in northern Switzerland and adjacent southern Germany. *Denkschriften der Schweizerischen Akademie der Naturwissenschaften*, 104, 1–151
- Hoyer, P. (1965). Fazies, Paläogeographie und Tektonik des Malm im Deister-Osterwald und Süntel. *Beih Geol Jb*, 61, 249.
- Homewood, P., Mauriaud, P., Lafont, F. (1999). Best practices in sequence stratigraphy for explorationists and reservoir engineers. *Bull Cent Rech Explor Prod Elf Aquitaine, Mém*, 25, 81.
- Hardenbol, J., Thierry, J., Farley, M.B., Jacquin, T., de Graciansky, P.C., Vail, P.R. (1998). Jurassic chronostratigraphy. In: de Graciansky PC, Hardenbol J, Jacquin T, Vail PR (eds) *Mesozoic and Cenozoic sequence stratigraphy of European Basins*. SEPM Special Publication, Tulsa, pp 3–13.
- Helm, C., Schülke, I. (1998). A coral-microbialite patch reef from the Late Jurassic (Florigemma-Bank Oxfordian) of NW Germany (Süntel Mountains). *Facies*, 39, 75–104. <https://doi.org/10.1007/BF02537012>
- Helm, C., Schülke, I., Fischer, I. (2001). Paläobiogeographie des Korallenooliths (Mittleres Oxfordium Unteres Kimmeridgium): Tethyale Faunen und Florenelemente auf höherer Paläobreite (Niedersächsisches Becken, NW-Deutschland). *Geol Beitr Hannover*, 2, 51–64.
- Helm, C., Reuter, M., Schülke, I. (2003). Die Korallenfauna des Korallenooliths (Oxfordium, Oberjura, NW-Deutschland): Zusammensetzung, Stratigraphie und regionale Verbreitung. *Paläontologische Zeitschrift*, 77, 77–94.
- Helm, C., Schülke, I., & Schlagintweit, F. (2003). Calcareous algae (“Porostromata”, rhodophyta dasycladales) and microproblematica with algal affinity from the NW German Korallenoolith Formation (Oxfordian, Süntel Mountains). *Facies*, 49, 61–86.
- Helm, C., Schülke, I. (2006). Patch reef development in the Florigemma-Bank Member (Oxfordian) from the Deister Mts (NW Germany): a type example for Late Jurassic coral thrombolite thickets. *Facies*, 52, 441–467. <https://doi.org/10.1007/s10347-006-0078-9>
- Hesselbo, S.P., Ogg, J.G., Ruhl, M., Hinnov, L.A., Huang, C.J. (2020). Chapter 26—The Jurassic Period. *Geologic Time Scale 2020*, Elsevier, pp. 955–1021.
- Kästner, M., Schülke, I., & Winsemann, J. (2008). Facies architecture of a Late Jurassic carbonate ramp: the Korallenoolith of the Lower Saxony Basin. *International Journal of Earth Sciences*, 97, 991–1011. <https://doi.org/10.1007/s00531-007-0282-z>
- Kästner, M., Schülke, I., Winsemann, J., Böttcher, J. (2010). High-resolution sequence stratigraphy of a Late Jurassic mixed carbonate-siliciclastic ramp, Lower Saxony Basin, Northwestern Germany. *Z Dtsch Ges Für Geowiss*, 161, 263–2.

Chapter 2

- Krencker, F., Fantasia, A., El Ouali, M., Kabiri, L., & Bodin, S. (2021). The effects of strong sediment-supply variability on the sequence stratigraphic architecture: Insights from early Toarcian carbonate factory collapses. *Marine and Petroleum Geology*, 136, 105469.
- Klüpfel, W. (1931). Stratigraphie der Weserkette (Oberer Dogger und Malm unter besonderer Berücksichtigung des Ober-Oxford). *Abh preuß-geol L-Anst, NF Berlin*, 129, 13-423.
- Kaiser, C. (1979). Einführung in die Geologie des Naturschutzgebietes Hohenstein. 82 S, Hessisch-Oldendorf (Nds Lforstverw, Staatl Forstamt Oldendorf)
- LBEG. (2013). Geologisches 3D-Modell des tieferen Untergrundes von Niedersachsen (GTA3D), ggf. Kachel HAM [Hameln]–NIBIS® Kartenserver, Landesamt für Bergbau, Energie und Geologie (LBEG), Hannover, ggf. Link <https://3d.lbeg.de/webgui/?viewHash=7d294484ccb2bdfd564c893b56049c1>
- Lotze, F. (1968). Zum Jura des Langenberges zwischen Oker und Bad Harzburg (nördl. Harzrand). *Neues Jahrbuch für Geologie und Paläontologie, Monatshefte*, 730–732.
- Medwedeff, D.A., Wilkinson, B.H. (1983). *Cortical Fabrics in Calcite and Aragonite Ooids* Springer, Berlin.
- Mönnig, E. (2002). *Exkursionsführer, Jahrestagung Subkommission für Jurastratigraphie Springe am Deister*, 74.
- Mönnig, E. (1989). *Stratigraphie und Fazies des Calloviums in NW-Deutschland. Clausthaler Geowiss Diss.*, 37, 1–183.
- Nebelsick, J.H., Rasser, M.W., Höltnke, O., Thompson, J.R., & Bieg, U. (2020). Turritelline mass accumulations from the Lower Miocene of southern Germany: implications for tidal currents and nutrient transport within the North Alpine Foreland Basin. *Lethaia*, 53, 280–293.
- Pape, H. (1970). Die Malmschichtfolge von Langenberg bei Oker (nördl. Harzvorland). In: *Die Geologie der Mittelrät-Schichten von Velpke (nördl. Helmstedt)/ von Mohamed-Husni Zeino-Mahmalat*. Hannover: Universität Hannover. Institut für Geologie und Paläontologie. Mitteilungen aus dem Geologischen Institut der Universität Hannover 9, S, 41–137.
- Ruf, M., Link, E., Pross, J., & Aigner, T. (2005). Integrated sequence stratigraphy: Facies, stable isotope and palynofacies analysis in a deeper epicontinental carbonate ramp (Late Jurassic, SW Germany). *Sedimentary Geology*, 175, 391–414. <https://doi.org/10.1016/j.sedgeo.2004.12.023>
- Schulze, K.H. (1975). Mikrofazielle, geochemische und technologische Eigenschaften von Gesteinen der Oberen Heersumer Schichten und des Korallenoolith (Mittleres bis Oberes Oxfordium NW Deutschlands) zwischen Weser und Leine. *Geol Jahrb Reihe D*, 11, 1–102.
- Schülke, I., Helm, C., Kästner, M., Winsemann, J. (2004). The basal Upper Jurassic of the Süntel area: a key for facies development and sequence stratigraphic analysis of the Lower Saxony Basin. *Terra Nostra*
- Sander, P.M., Mateus, O., Laven, T., & Knötschke, N. (2006). Bone histology indicates insular dwarfism in a new Late Jurassic sauropod dinosaur. *Nature*, 441, 739–741.
- Stinder, T. (1991). Mikropaläontologie und Biostratigraphie des Unteren Malm (Korallenoolith) im Wesergebirge (Norddeutschland). *Boch Geol Geotech Arb*, 35, 1–319.
- Strasser, A., Védrine, S., & Stienne, N. (2012). Rate and synchronicity of environmental changes on a shallow carbonate platform (Late Oxfordian, Swiss Jura Mountains). *Sedimentology*, 59, 185–211. <https://doi.org/10.1111/j.1365-3091.2011.01236.x>

- Strasser, A. (1986). Ooids in Purbeck limestones (lowermost Cretaceous) of the Swiss and French Jura. *Sedimentology*, 33, 711–727.
- Schudack, U. (1994). Revision, Dokumentation und Stratigraphie der Ostracoden des Nordwestdeutschen Oberjura und Unter-Berriasium. *Berliner Geowissenschaftliche Abhandlungen*, 11, 1–193.
- Smith, A.G., Smith, D.G., Funnell, B.M. (1994). *Atlas of Cenozoic and Mesozoic coastlines* Cambridge University Press, Cambridge
- Schüllke, I. (1993). Die Oxford-Schichtfolge im Steinbruch Riesenberg (NW Hameln). *Arbeitskreis Palaontologie Hannover*, 21, 38–48.
- Schlager, W., & Ginsburg, R.N. (1981). Bahama carbonate platforms—The deep and the past. *Marine Geology*, 44, 1–24. [https://doi.org/10.1016/0025-3227\(81\)90111-0](https://doi.org/10.1016/0025-3227(81)90111-0)
- Schlager, W. (2005). *Carbonate Sedimentology and Sequence Stratigraphy*: SEPM Society for Sedimentary Geology
- Schlagintweit, F., Auer, M.K., & Gawlick, H. (2007). *Reophax? rhaxelloides n. sp.*, a new benthic foraminifer from Late Jurassic reefal limestones of the Northern Calcareous Alps (Austria). *Journal of Alpine Geology*, 48, 57–69.
- Siegfried, P. (1954). Die Heersumer Schichten im Hildesheimer Jura-Zug. In *Geologisches Jahrbuch* 67, pp. 273–360.
- Tucker, M.E., Wright, V.P. (1990). *Carbonate Sedimentology*. Blackwell, Oxford
- Tomašových, A., Gallmetzer, I., Haselmair, A., Kaufman, D.S., Kralj, M., Cassin, D., Zonta, R., & Zuschin, M. (2018). Tracing the effects of eutrophication on molluscan communities in sediment cores: outbreaks of an opportunistic species coincide with reduced bioturbation and high frequency of hypoxia in the Adriatic Sea. *Paleobiology*, 44, 575–602.
- Védrine, S. (2008). Co-occurrence of the foraminifer *Mohlerina basiliensis* with *Bacinnella-Lithocodium* oncoids: palaeoenvironmental and palaeoecological implications (Late Oxfordian, Swiss Jura). *Journal of Micropalaeontology*, 27, 35–44.
- Védrine, S., Strasser, A., & Hug, W. (2007). Oncoid growth and distribution controlled by sea-level fluctuations and climate (Late Oxfordian, Swiss Jura Mountains). *Facies*, 53, 535–552.
- Wilson, J.L. (1975). *Carbonate facies in geologic history*. Springer, Berlin.
- Weiß, M. (1995). Stratigraphie und Mikrofauna im Kimmeridge SE-Niedersachsens unter besonderer Berücksichtigung der Ostracoden. *Clausthaller Geowiss Diss*, 48, 1–274.
- Waite, R.I., Wetzell, A., Meyer, C.A., & Strasser, A. (2008). The paleoecological significance of neineoid mass accumulations from the Kimmeridgian of the Swiss Jura Mountains. *Palaios*, 23, 548–558. <http://dx.doi.org/10.2110/palo.2007.p07-048r>
- Zuo, F., Heimhofer, U., Huck, S., Luppold, F.W., Wings, O., & Erbacher, J. (2017). Sedimentology and depositional sequences of a Kimmeridgian carbonate ramp system, Lower Saxony Basin, Northern Germany. *Facies*, 64, 1–25. <https://doi.org/10.1007/s10347-017-0513-0>
- Ziegler, P.A. (1977). Geology and Hydrocarbon Provinces of the North Sea. *GeoJournal*, 1, 7–31.
- Ziegler, P.A. (1988). Evolution of the Arctic-North Atlantic and Western Tethys. *AAPG Mem*, 43, 1–198.
- Ziegler, P.A. (1990). *Geological Atlas of Western and Central Europe*. 2nd Edition, Shell International Petroleum Mij. B.V. and Geological Society, London

3. First record of the Middle Oxfordian positive carbon isotope excursion within the Korallenoolith Formation, Lower Saxony Basin, Germany

Deyan Zhang¹, François-Nicolas Krencker¹, Stefan Huck¹, Philipp Ulke¹, Michael Schramm²,
Ulrich Heimhofer¹

1 Institute of Geology, Leibniz University Hannover, Germany

2 Federal Institute for Geosciences and Natural Resources, Hannover, Germany

3.1 Abstract

The Middle Oxfordian *Transversarium* ammonite Zone is characterized by pronounced changes in the carbon isotope ($\delta^{13}\text{C}$) trend, recorded from various marine and terrestrial organic and inorganic substrates. These carbon isotope events have been associated with climate fluctuations, changes in marine carbonate production, and long-term sea-level rise. A new high-resolution inorganic $\delta^{13}\text{C}$ record illustrating the same chemostratigraphic feature is obtained from a scientific borehole (Konrad #101 core) located in the Lower Saxony Basin (LSB). The record is interpreted to reflect synchronous changes in the global marine dissolved inorganic carbon pool, probably in response to Middle Oxfordian reef proliferation caused by climatic changes. This is the first record of the Middle Oxfordian positive $\delta^{13}\text{C}$ excursion within the Korallenoolith Formation in the LSB. Our high-resolution data set prompts a re-evaluation of the nature and origin of Middle Oxfordian $\delta^{13}\text{C}$ excursions.

Keywords: Chemostratigraphy, Oxfordian, Carbon stable isotope, Boreal Realm, Middle Oxfordian MOxE

3.2 Introduction

The Oxfordian stage (Late Jurassic; 161.5–154.8 Myrs, Gradstein et al. 2020) was a time interval of widespread and significant changes in climate, sea-level, and marine sedimentation patterns and associated with marked fluctuations of the global carbon isotope ($\delta^{13}\text{C}$) trend (Padden et al. 2001, 2002; Dromart et al. 2003a; Rais et al. 2007; Louis-Schmid et al. 2007a). A pronounced positive carbon isotope excursion (CIE) has been identified in the Middle Oxfordian (Jenkyns 1996; Weissert and Mohr 1996; Padden et al. 2001, 2002; Rais et al. 2007; Louis-Schmid et al. 2007a, 2007; O'Dogherty et al. 2018; Eltom et al. 2018; Carmeille et al. 2020; Eldrett 2022), recorded in both pelagic and shallow marine ramp carbonates. However, with a few exceptions, most of these records are from the Tethyan realm (Cramer and Jarvis 2020, Eldrett 2022). Due to this spatial restriction, combined with often low sample density, and poor biostratigraphic control, the global $\delta^{13}\text{C}$ trend across this interval still remains equivocal. In order to explore temporal changes in the isotopic composition of the global marine dissolved inorganic carbon pool during the Late Jurassic, additional and continuous high-resolution stable carbon isotope of the carbonate phase ($\delta^{13}\text{C}$) are needed.

During the Late Jurassic, the Lower Saxony Basin (LSB) was located in the Boreal realm and characterized by continuous shallow-marine carbonate deposition (Gramann et al. 1997) (Fig. 1). An ostracod biostratigraphic scheme enables correlation of the Oxfordian strata in the LSB with the Boreal standard ammonite zonation (Schudack, 1994; Weiß 1995; Gramann et al. 1997). The few existing stable isotope studies on Oxfordian LSB strata suffer from limited biostratigraphic control and ambiguous stratigraphic $\delta^{13}\text{C}$ trends (Kästner et al. 2008; Bai et al. 2017), which limits regional calibration of carbonate strata and global correlations. Here, a high-resolution carbonate $\delta^{13}\text{C}$ record from a scientific drill core (Konrad #101 core) is presented and compared with other existing records collected from Tethyan and proto-Atlantic sites, in order to better understand the global pacing of the Oxfordian CIEs.

3.3 Geological setting and stratigraphy

The LSB is an elongate basin covering large parts of northern Germany with an up to 4500 m -thick Permian-Cenozoic succession. During the Oxfordian stage, the basin was located at a paleolatitude of $\sim 35^\circ$ to 40°N within the northern hemisphere subtropical climate belt (Smith et al. 1994; van Hinsbergen et al. 2015) and covered by a shallow epicontinental sea (Ziegler, 1990) (Fig. 1). Along the southeastern margin of the basin, sedimentation was predominantly characterized by shallow-marine carbonates deposited on a homoclinal to moderately steepened epeiric ramp (Betzler et al. 2007). In the LSB, the Middle to Late Oxfordian succession is assigned to the Korallenoolith Formation (Fm.) and essentially composed of oolitic and bioclastic limestones with intercalated marls and claystones interspersed with coral patch reefs (Helm et al. 2001).

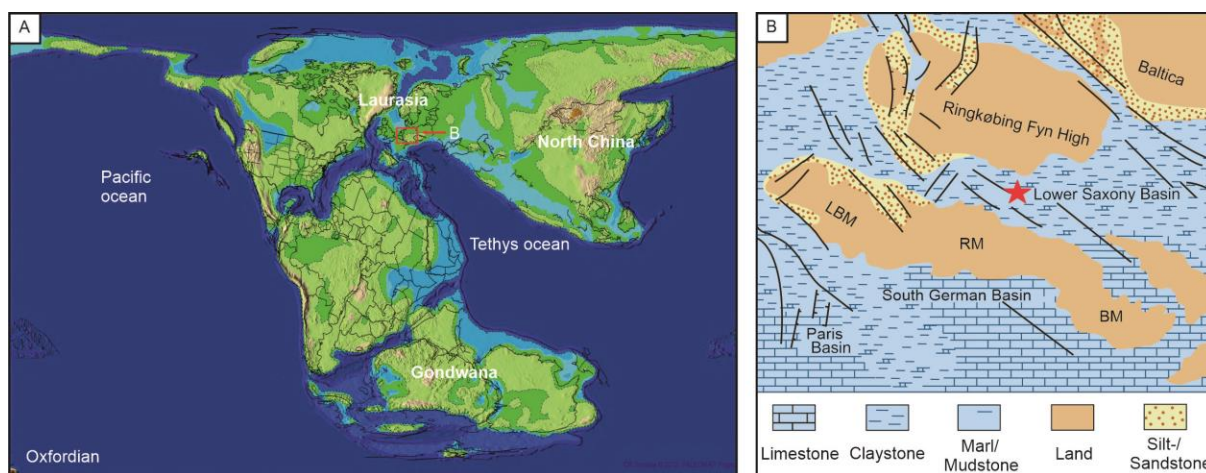


Fig. 1. (A) Global paleogeography for the Late Jurassic (~152 Ma, modified after Scotese 2014). (B) Paleogeographic reconstruction of Central Europe for the Oxfordian. Major landmasses and general marine facies distribution are shown. RM = Rhenish Massif, LBM = London-Brabant Massif; BM = Bohemian Massif. Map modified after Ziegler (1990). The approximate position of the studied outcrop in the Lower Saxony Basin is marked with a red asterisk.

Based on lithological characteristics, the Korallenoolith Fm. is further subdivided into Lower, Middle, and Upper Korallenoolith (Schulze 1975). In the Gifhomer Trough, a depression located in the eastern part of the LSB, sediment accumulation during the Late Jurassic was enhanced due to salt diapirism (Brink et al., 1992). In this area, the Korallenoolith Fm. reaches considerable thickness and contains distinct horizons of sedimentary iron ores (known as “Unteres Lager” and “Oberes Lager”), which have been mined in the subsurface until the 1970s (Berg et al. 1987).

The studied scientific Konrad #101 core was drilled in 1985 within the “management of radioactive wastes” project and is located close to the village Salzgitter-Beddingen about 500 m from the Konrad 2 mine shaft (Berg et al. 1987). Between 635.0–774.1 mbs, the core covers a ~139.1 m-thick succession of the Korallenoolith Fm (Fig. 2). The biostratigraphic framework of the Konrad #101 core is based on ostracod and foraminifera findings (Kemper 1985; Weiss 1985) and on lithostratigraphic correlation. Occurrences of age-diagnostic ostracods and foraminifera and their respective stratigraphic ranges (Gramann, 1997; Whittaker and Hart, 2009) are reported in Fig. 3. The dating of the different horizons was done by combining the stratigraphic ranges of the different specimens found together within the same horizon.

In the Konrad #101 core the Callovian/Oxfordian boundary is placed at 774.1 m, within the uppermost Omatenton Fm “Gryphäenbank” (Fig. 2). The occurrence at 785.9 m of the ostracods *Palaeocytheridea (P.) parabakirovi* and *Lophocythere (L.) karpiskii* indicates that the uppermost Omatenton Fm. is latest Middle Callovian in age (*Coronatum* Zone). The Middle part of the Lower Korallenoolith Fm. at 745.5 m includes the ostracod and foraminifera *Galliaecytheridea (G.) dissimilis* and *Trocholina (T.) nodulosa*, respectively, which assemblage indicates the latest Middle Oxfordian (*Pumilus* Zone). The Oxfordian/Kimmeridgian boundary is placed at 646.50 m within the Upper Korallenoolith Fm. at the first

Chapter 3

occurrence of the ostracods *Amphicythere* (*A.*) *plena* and *Eocytheropteron* (*E.*) *decoratum*. The presence of *Paranotacythere* (*P.*) cf. *extendata* and *Macrodentina* (*P.*) *pulchra* directly below the boundary, which is in agreement with a Late Oxfordian age (*Pseudocordata* Zone) for the Upper Korallenoolith Fm.

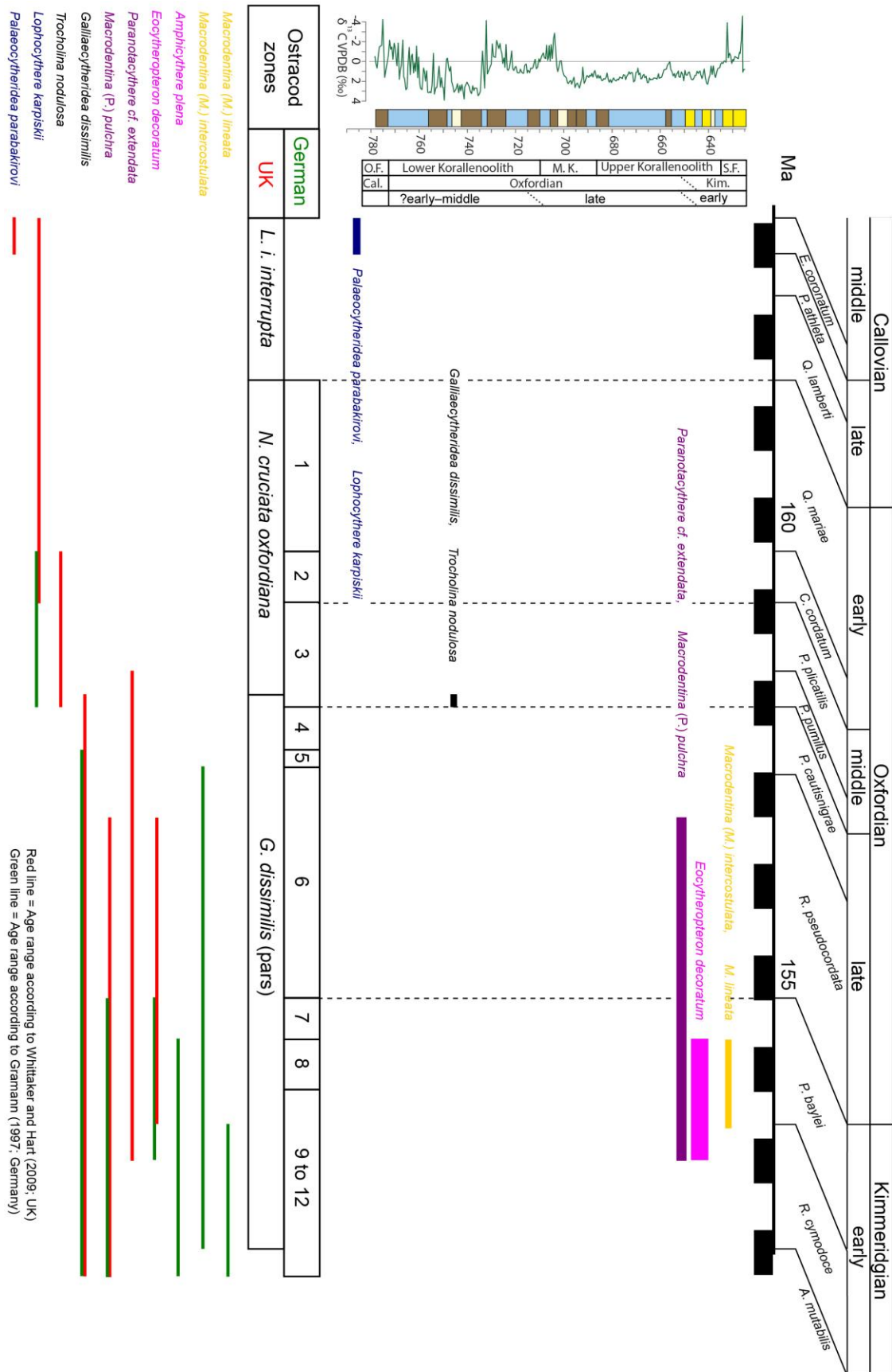


Fig. 3 Ostracod biostratigraphy of the Konrad 101 core. Range of indicative ostracod taxa is shown against stratigraphic age. Zonation schemes for northern Germany (green) and UK (red) are compared.

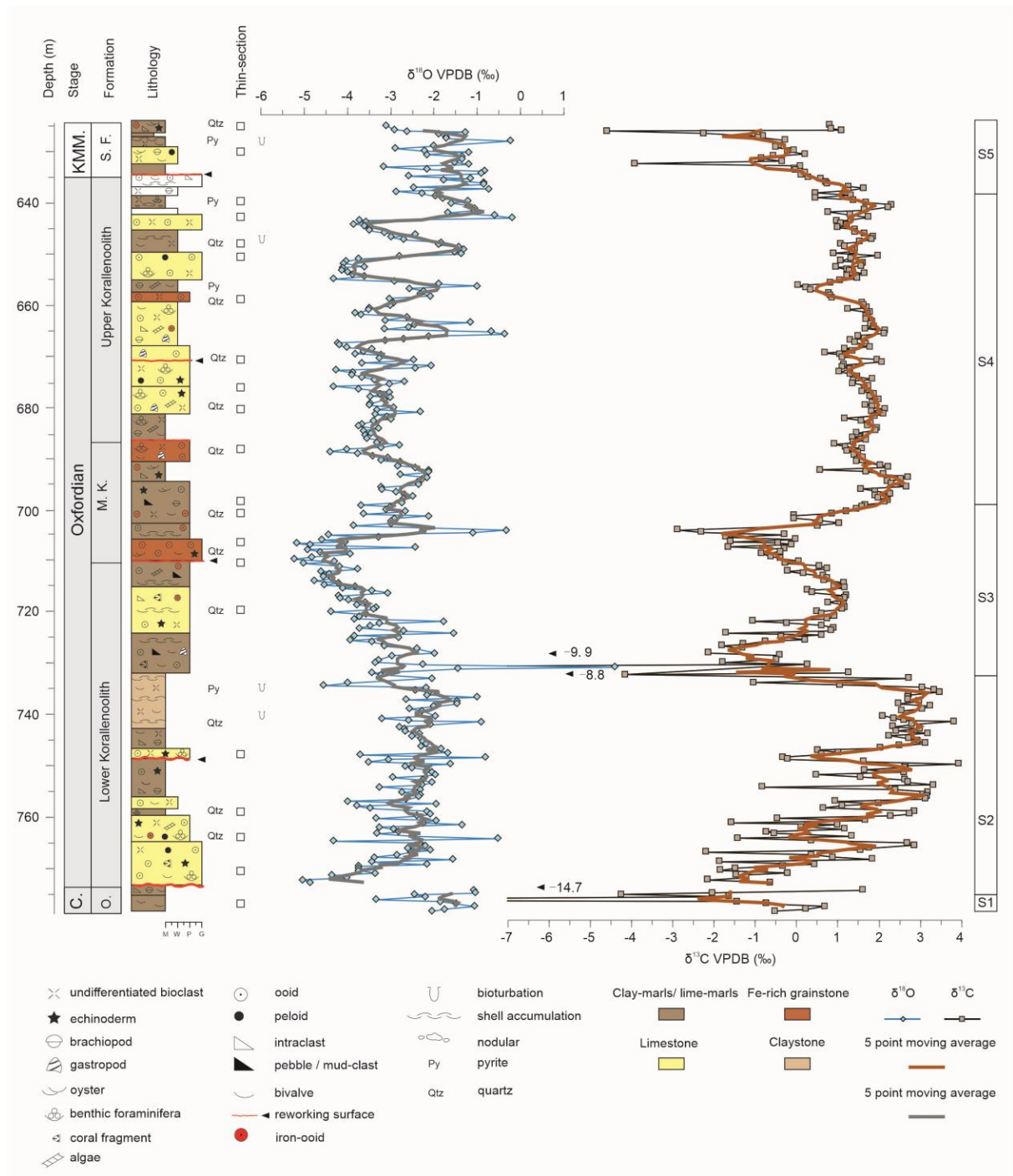


Fig. 2 Lithostratigraphy and high-resolution stable isotope stratigraphy ($\delta^{18}\text{O}$, $\delta^{13}\text{C}$) of the Konrad #101 core, Lower Saxony Basin, Germany. Stratigraphy is based on the BGR report. Intervals S1 to S5 correspond to chemostratigraphic segments of the $\delta^{13}\text{C}$ trend, where thick red line indicates a 5-point moving average. The thick gray line indicates a $\delta^{18}\text{O}$ 5-point moving average. Lithology is based on core observation and petrographic thin-section analysis. Carbonate classification follows Dunham (1962). C., Callovian; KMM., Kimmeridgian; O. Ornatenton; M.K., Middle Korallenoolith; S.F., Süntel Formation.

3.4 Methodology

The Konrad #101 core is stored at the Federal Institute for Geosciences and Natural Resources (BGR) core repository in Grubenhagen, Germany. In this study, the depth interval from 624.0 to 778.0 mbs was studied, which stratigraphically covers the uppermost Omatenton Fm. (778.0–774.1 mbs), Korallenoolith Fm. (774.1–635.0 mbs) and lowermost Süntel Fm. (635.0–624.0 mbs). A total of 154 m was logged bed-by-bed on a dm-scale with a special emphasis on lithology, depositional texture, faunal content and sedimentary structures. A total of 350 samples were analyzed for bulk carbonate $\delta^{13}\text{C}$ and $\delta^{18}\text{O}$ isotopes (at a spacing of ~50 cm or less) at the stable isotope laboratory of the Institute of Geology, Leibniz University Hannover and 21 petrographic thin-sections were investigated. For more details on the analytical procedure, we refer to Huck, et al. (2011). For the purpose of chemostratigraphic correlation, a five-point moving average was calculated from all measured $\delta^{13}\text{C}$ values.

3.5 Results

3.5.1 Lithofacies and sediment composition

Unconformably overlying claystone of Callovian age, the Lower Korallenoolith Fm. (710.7–774.1 mbs) is composed of oolitic pack- to grainstones (Figs. 4A, B) rich in bioclastic material, which pass into clayey marls and claystones with varying sand content (Fig. 4C) and interspersed limestone beds. The upper part of the Lower Korallenoolith Fm. is made up of packstones characterized by abundant shell debris layers and an increasing abundance of Fe-rich ooids (Fig. 4D). The Middle Korallenoolith Fm. (686.9–710.7 mbs) is characterized by two distinct ironstone layers located at the bottom (706.1–710.7 mbs, “Unteres Lager”, Fig. 4E) and top (686.9–691.2 mbs, “Oberes Lager”) of this unit. The stratigraphic interval between the iron-rich layers is dominated by clay- and quartz-rich marls with abundant bioclastic debris and dispersed Fe-ooids. The Upper Korallenoolith Fm. (635.0–686.9 mbs) includes well-sorted oolitic pack- and grainstones (Fig. 4F) intercalating with wackestones poor in bioclasts (Fig. 4G), and interspersed beds rich in Fe-rich ooids (Fig. 4H; I). The topmost of the Korallenoolith Fm. is marked by a reworking surface, overlain by the Süntel Fm.

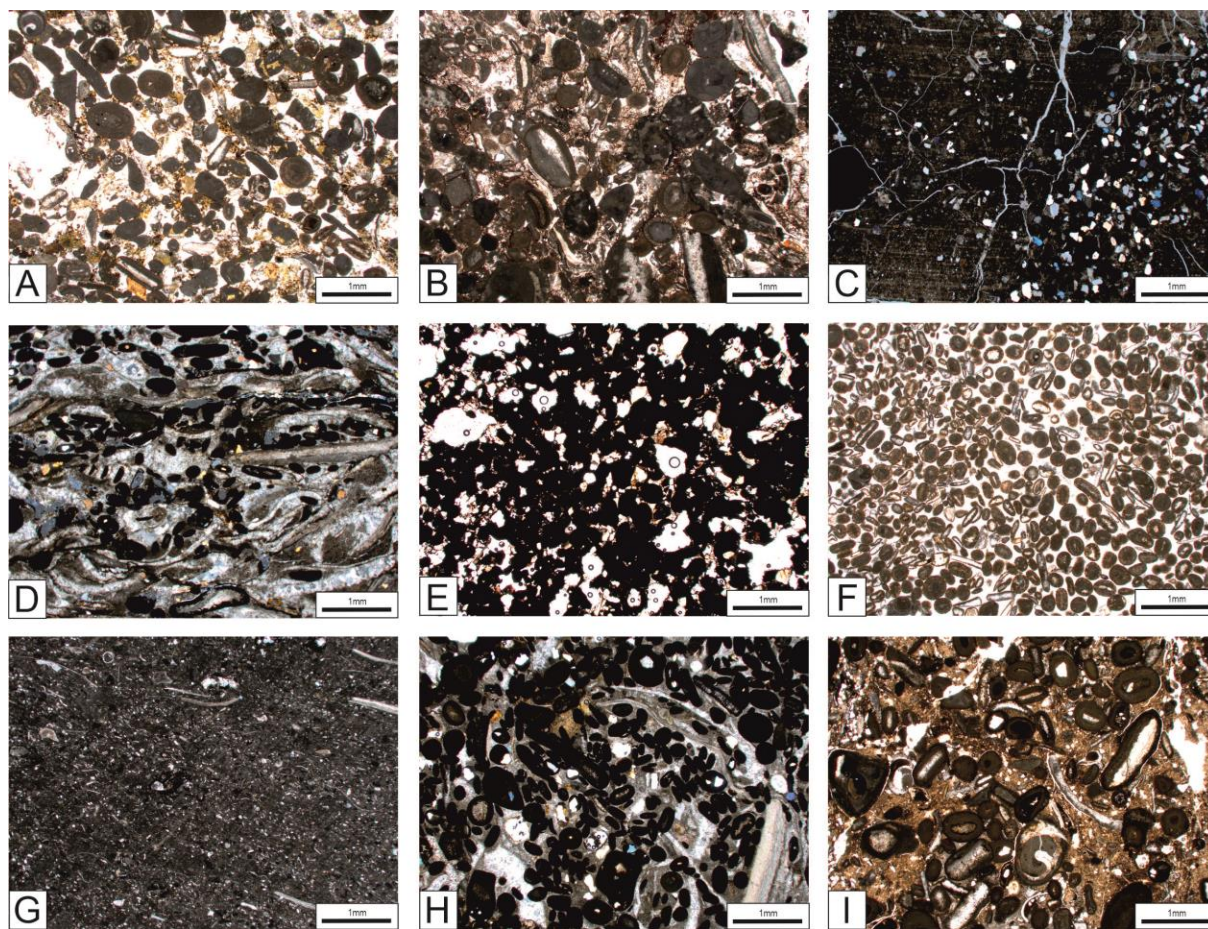


Fig. 4 Photomicrographs of characteristic carbonate microfacies associations of the Oxfordian Korallenoolith Fm. in the Konrad #101 core. (A) Loosely-packed oolitic grainstone containing large amounts of glauconite (771.0 mbs). (B) Agglutinated foraminifera-rich pack- to grainstone (763.0 mbs). (C) Argillaceous mudstone with abundant silt-sized quartz grains (759.4 mbs). (D) Bioclastic packstone showing preferred orientation and umbrella structure of bivalve shells (720.0 mbs). (E) Iron-rich oolitic grainstone of the "Unteres Lager" with individual ooids being completely replaced by iron minerals. Other components are primarily represented by well-rounded quartz grains (706.0 mbs). (F) Well-sorted oolitic grainstone with the small-sized ooids being characterized by radial fibrous calcite crystals and weak concentric banding (643.5 mbs). (G) Argillaceous mudstone comprising detrital silt-sized quartz and skeletal debris (649.0 mbs). (H) Oolitic grainstone composed of iron-rich ooids (~60-70% of the total components) (659.0 mbs). (I) Packstone composed of a mixture of iron-rich ooids and coated bioclasts, the matrix shows a mass of various sizes of skeletal material (681.0 mbs).

3.5.2 Stable isotope results

The high-resolution $\delta^{13}\text{C}$ record shows significant fluctuations through the Middle to Late Oxfordian of the Konrad #101 core (Fig. 3). Bulk $\delta^{13}\text{C}$ values vary between -4.6‰ and 3.9‰ (mean: 0.97‰ , three outlier data were discarded: -14.7‰ , -9.9‰ , -8.8‰). Based on distinct changes of the stratigraphic $\delta^{13}\text{C}$ trend, the $\delta^{13}\text{C}$ record is divided into 5 chemostratigraphic segments. The basal segment S1 (778.0–775.8 mbs) is characterized by a sharp negative peak reaching values of -4.3‰ . Segment S2

(775.8–732.1 mbs) displays multiple negative and positive small-amplitude excursions that are superimposed on a pronounced positive trend reaching maximum values of 3.9 ‰. A sharp negative shift in $\delta^{13}\text{C}$ values marks the onset of segment S3 (732.1–698.5 mbs), which exhibits two pronounced negative $\delta^{13}\text{C}$ excursions with amplitudes of -4.2 ‰ and -2.9 ‰, respectively. Segment S4 (698.5–637.5 mbs) starts above the $\delta^{13}\text{C}$ excursion characterizing the upper part of segment S3. Segment S4 displays a relatively constant $\delta^{13}\text{C}$ mean values of ~1.5 ‰ modulated by $\delta^{13}\text{C}$ oscillations of ~1 ‰ in amplitude. The uppermost segment S5 (637.5–624.0 mbs) shows a stepwise decrease towards more negative $\delta^{13}\text{C}$ values from a value of ~1.6 ‰ and reaching a minimum value of -4.6 ‰.

The $\delta^{18}\text{O}$ values range between -0.2 ‰ and -5.3 ‰ (mean: -2.8 ‰, one outlier data was discarded: 2.2 ‰). The $\delta^{18}\text{O}$ curve displays strong oscillations and certain parts of the $\delta^{18}\text{O}$ trend are clearly linked to lithological changes (e.g. marl-carbonate couplets). The lowermost part of the $\delta^{18}\text{O}$ curve (778.0–735.0 mbs) displays a stepwise positive trend, followed by a pronounced negative trend (735.0–705.0 mbs), reaching values of -5.2 ‰. Up-section (705.0–667.0 mbs), the $\delta^{18}\text{O}$ record fluctuates around values of ~-3 ‰. In the upper part (667.0–643.0 mbs), high-amplitude fluctuations are observed (amplitude <3.5 ‰). The uppermost part of the $\delta^{18}\text{O}$ curve (643.0–624.0 mbs) displays relatively stable values fluctuating around ~-1.5 ‰. In general, the $\delta^{18}\text{O}$ composition of the bulk rock carbonate is influenced by many factors (e.g. temperature, salinity), which can alter the original isotopic composition of the bulk rock (Mitchell et al., 1997). Hence, the $\delta^{18}\text{O}$ values will not be further discussed in this study.

3.6 Discussion

3.6.1 Significance of the $\delta^{13}\text{C}$ pattern

In order to use $\delta^{13}\text{C}$ trends for the purpose of stratigraphic correlation, potential diagenesis of the studied strata has to be assessed. Skeletal carbonate lithologies formed in shallow-marine settings are particularly prone to post-depositional alteration given their high primary porosities combined with the frequent occurrence of subaerial exposure (Immenhauser et al. 2003; Schmitt et al. 2019). The lithology of the Konrad #101 core is mainly composed of limestone, marl and claystone beds with the $\delta^{13}\text{C}$ trend showing no clear relationship with lithology across the studied core (Fig. 3). The majority of the analyzed bulk carbonate isotope values overlap with signatures obtained from well-preserved Oxfordian low-Mg shell calcite (Nunn et al. 2009; Wierzbowski 2015) and fine-grained open-marine carbonates exhibiting no signs of strong diagenetic overprint (Marshall 1992; Louis-Schmid et al. 2007). A cross-plot of $\delta^{13}\text{C}$ and $\delta^{18}\text{O}$ values reveals overall low covariance ($r^2 = 0.004$), with the individual chemostratigraphic segments showing similarly weak correlation coefficients (S1: $r^2 = 0.291$; S2: $r^2 = 0.156$; S3: $r^2 = 0.062$; S4: $r^2 = 0.004$; S5: $r^2 = 0.040$, Fig. 5). The lack of pronounced trends in C/O isotope cross-plots, which is typically caused by the addition of porosity-filling cement to skeletal carbonate (Li et al. 2006) points to the absence of strong diagenetic alteration of the Konrad #101 core stable isotope signatures. However, some pronounced short-lasting negative shifts in the $\delta^{13}\text{C}$ stratigraphic pattern are observed, which may indicate diagenetic host rock alteration by local processes. Strata directly underlying a discontinuity surface separating the Callovian Ornatenton Fm. from the overlying Korallenoolith Fm.

Chapter 3

shows low $\delta^{13}\text{C}$ values (as low as -14.7‰) indicative of meteoric diagenesis or remineralization of organic matter, probably associated with subaerial exposure (Marshall 1992). Another abrupt negative $\delta^{13}\text{C}$ shift (segment S3, reaching values of -9.9‰) marks the transition from claystones to fossiliferous packstones at 732.1 mbs. The claystones and clay-rich marlstones of the Konrad #101 core contain well-preserved bioclasts, showing no re-crystallization or overgrowth. Such lithologies are usually compacted during the very early stage of diagenesis resulting in low porosity and permeability, preventing later-stage diagenetic modification (Elton et al. 2018). Despite some evidence for local diagenetic overprinting, the general trend of the bulk $\delta^{13}\text{C}$ record is interpreted to reflect a primary marine signal, which can be used for chemostratigraphic correlation.

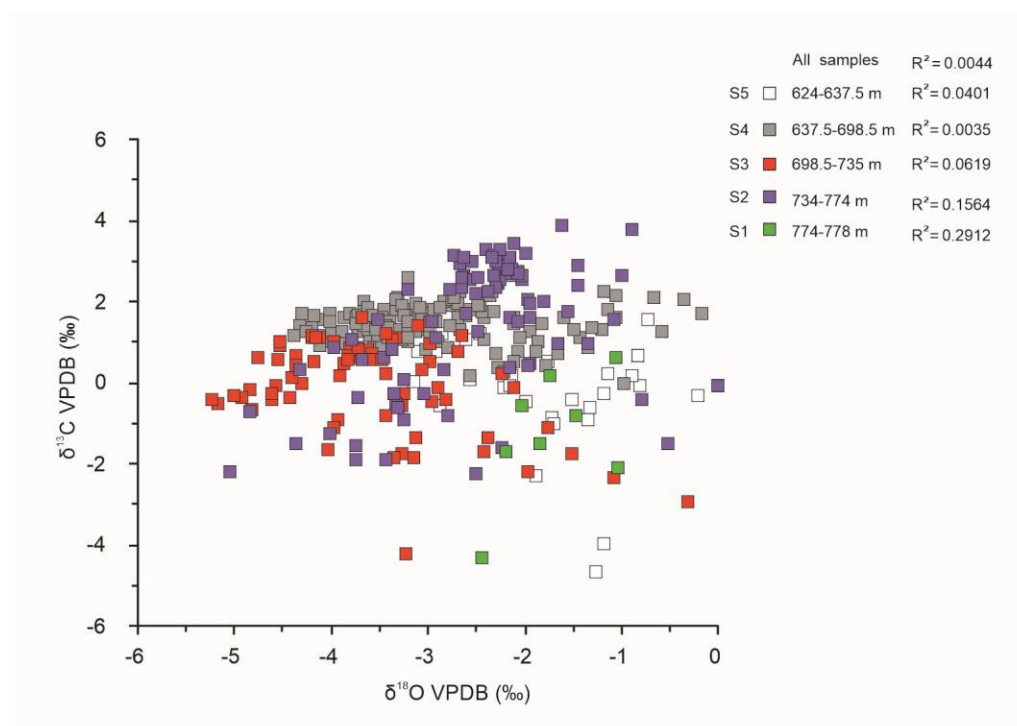


Fig. 5 Covariance plot of carbonate carbon ($\delta^{13}\text{C}$) and oxygen ($\delta^{18}\text{O}$) isotope values of bulk rock material derived from the Konrad #101 core. Coloring reflects groups of samples from different chemostratigraphic segments S1 to S5. Note the generally weak correlation coefficient of the analyzed stable isotope values.

3.6.2 Chemostratigraphic correlation with other Middle Oxfordian $\delta^{13}\text{C}$ records

The overall pattern of the Middle Oxfordian $\delta^{13}\text{C}$ record is characterized by a distinct positive CIE (MOxE) that starts at the earliest Middle Oxfordian (*Plicatilis* Zone), and reaches a maximum value ($> 3.0\text{‰}$) (*Transversarium* Zone) before being interrupted by a negative CIE within the latest Middle Oxfordian (*Transversarium* Zone). Then reaching back to the pre-excursion value during the Late Oxfordian, and shows a progressive decreasing ($\sim 1\text{‰}$) trend toward the Oxfordian/Kimmeridgian boundary (Cramer and Jarvis 2020). Similar magnitude CIEs have been reported from marine carbonates and/or organic substrates from Europe, western Asia, and the Gulf of Mexico (Jenkyns 1996; Weissert and Mohr 1996; Padden et al. 2001, 2002; Rais et al. 2007; Louis-Schmid et al. 2007a; Martinez and Dera 2015;

O'Dogherty et al. 2018; Eltom et al. 2018; Carmeille et al. 2020; Eldrett 2022) (Fig 5). The MOxE coincides with a climatic warming trend recorded in the Paris Basin, France (Brigaud et al., 2008) and was coupled with an episode of widespread tropical carbonate sedimentation and a global spread of coral reefs (Leinfelder 2001; Helm et al. 2001; Martin-Garin et al. 2012).

In the Konrad #101 core, foraminifera and ostracod biostratigraphy enable constraining the age of the pronounced positive shift in segment S2 (Fig. 2). The foraminifera *T. nodulosa* and ostracod *G. dissimilis*, have been reported at 745.5 m within the uppermost part of segment S2. The stratigraphic ranges of *T. nodulosa* and *G. dissimilis* correspond to the *Cordatum–Pumilus* and *Pumilus–Mutabilis* sub-boreal ammonite Zones, respectively. The overlap of both biostratigraphic marker ranges indicates that the bed at 745.5 mbs is most likely *Pumilus* in age (partially equivalent to the *Transversarium* Tethyan ammonite Zone; Middle to Late Oxfordian).

A pronounced facies change at 732.1 mbs is interpreted to correspond to a regionally traceable disconformity, known as “Hauptemersionsfläche” in LSB (Klüpfel 1931; Schulze 1975), which has been assigned to the *Cautisnigrae* Zone.

The high-resolution $\delta^{13}\text{C}$ record shows a distinct positive CIE (S2 segment) in the Lower Korallenoolith Fm. followed by two negative CIEs (S3 segment), which gives rise to a relatively stable trend in the Upper Korallenoolith Fm. This $\delta^{13}\text{C}$ trend is similar in shape and magnitude to what is characteristically observed in Middle Oxfordian carbonate carbon isotope profiles from Europe, western Asia, and the Gulf of Mexico (Fig. 6). Based on the existing microfossil biostratigraphic constraints, the positive CIE in the Lower Korallenoolith Fm. (S2 segment) is interpreted to correspond to the Middle Oxfordian MOxE, and thus can be used as an accurate stratigraphic marker within the poorly dated Korallenoolith Fm. in the LSB.

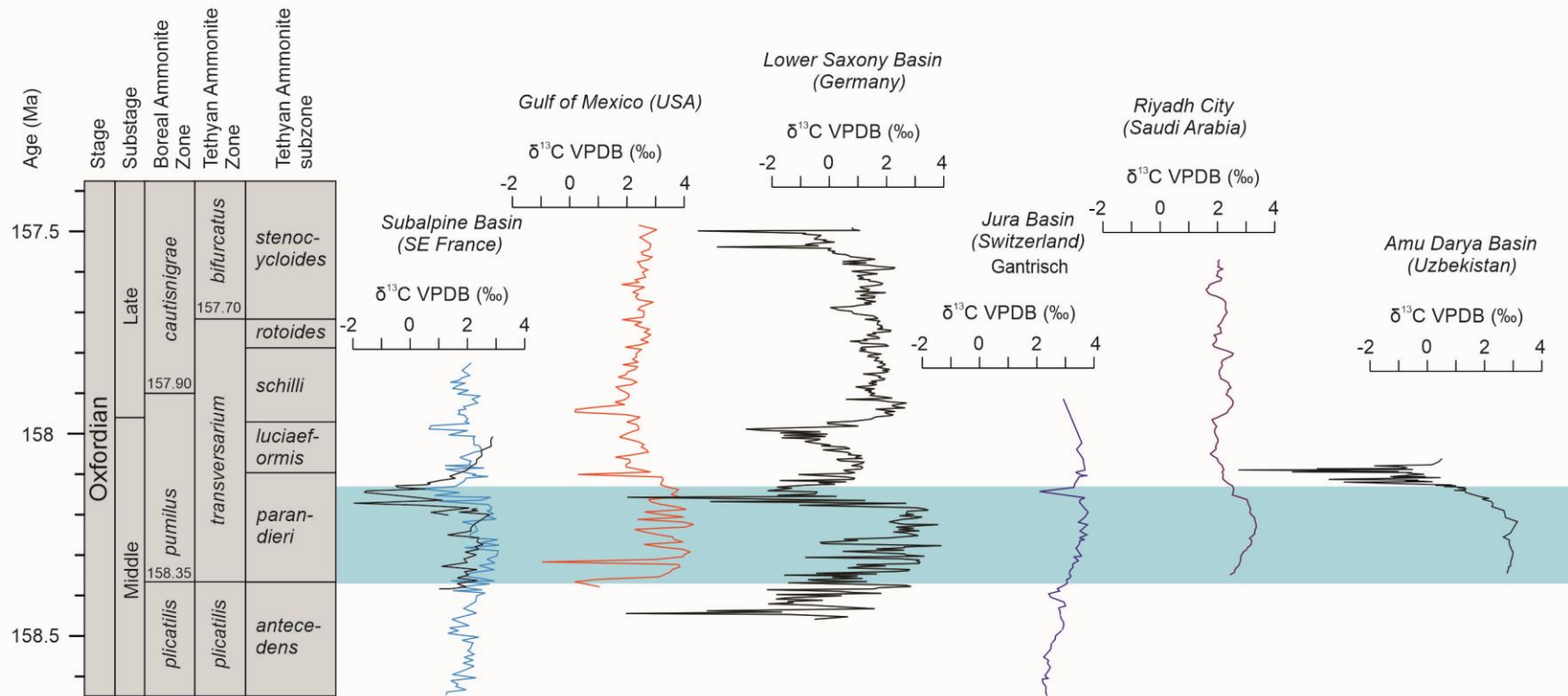


Fig. 6 Correlation panel showing a comparison of Middle to Late Oxfordian carbonate isotope records from the Lower Saxony Basin (Germany, this study) with published $\delta^{13}\text{C}$ data from the Subalpine Basin (France; Louis-Schmid et al. 2007), Gulf of Mexico (USA; Eldrett 2022), Jura Basin (Switzerland; Padden et al. 2001), Riyadh City (Saudi Arabia; Eltom et al. 2018), and Amu Darya Basin (Uzbekistan; Carneille et al. 2020). The Blue horizontal bar corresponds to the positive carbonate CIE assigned to the lower Transversarium Zone.

3.6.3 What triggered the major Middle Oxfordian carbon-isotope excursion?

The Middle Oxfordian was a time of reef proliferation accompanied by increased organic carbon burial (Budyko et al., 1987; Weissert and Mohr 1996; Leinfelder 2001; Helm et al. 2001; Louis-Schmid et al., 2007a; Martin-Garin et al. 2012; Pearce et al. 2005; Nunn et al. 2009; Carmeille et al. 2020). The $\delta^{13}\text{C}$ pattern is characterized by a major positive shift (MOxE) observed in carbonate and organic carbon (Pearce et al. 2005; Nunn et al. 2009; Carmeille et al. 2020; Eldrett 2022). Differences in absolute values and amplitudes of the different records and substrates may be caused by local environmental effects and/or diagenesis (Husinec et al. 2022). The underlying causes for the positive MOxE are still unclear, as there is no evidence for large-scale volcanism (Rampino and Stothers, 1988; Louis-Schmid et al. 2007). In previous studies, a transgression during the Middle Oxfordian has been related to the MOxE (Jenkyns 1996; Weissert and Mohr 1996; Louis-Schmid et al., 2007a). In contrast, Pearce et al. (2005) reported that the increasing trend in $\delta^{13}\text{C}$ values corresponds to a decreasing relative sea level. However, Martinez and Dera (2015) interpreted this coincides with a maximum eccentricity of the 9 Myr orbital cycle, which altered the climatic conditions and triggered the paleoenvironmental changes. More recently, marine organic carbon burial has been put forward as a causal mechanism for the positive CIE, which coincides with a gentle second-order transgressive sea-level trend in the Middle Oxfordian (O'Dogherty et al. 2018). In turn, these paleoenvironmental changes may have been responsible for the $\delta^{13}\text{C}$ trends and excursions (Louis-Schmid et al., 2007a).

Our new high-resolution data set shows three pronounced negative CIEs. The negative CIE located at top of the S1 segment is considered to be related to a sedimentary hiatus. In the LSB the Callovian/Oxfordian transition is described as an erosional surface (Mönnig 1989; Fischer 1991). Another clear negative CIE is observed within the lowermost part of the S3 segment. This shorter-term negative excursion immediately above the positive CIE may correspond to the negative $\delta^{13}\text{C}$ excursion ($\sim -2\text{‰}$) recorded in the uppermost (*Perisphinctes parandieri-luciaiformis* Tethyan ammonite subzones (partial *Transversarium* Tethyan ammonite Zone) from sections in Europe (Padden et al., 2001; Louis-Schmid et al., 2007a), Gulf of Mexico (Eldrett 2022) and western Asia (Carmeille et al., 2020). The extreme values (-8.8‰ and -9.9‰) might be related to OM remineralization processes. Padden et al. (2001) interpreted a pronounced negative $\delta^{13}\text{C}$ shift in the Oxfordian *Transversarium* Zone as the consequence of isotopically light carbon injected into the ocean-atmosphere reservoir due to the dissociation of marine methane hydrates, associated with oceanographic reorganization. The negative anomaly in the uppermost part of S3, which is mirrored in the lower ironstone layer, may represent an early-stage diagenetic modification of the carbonates (OM mineralization?). The reason behind this discrepancy of the Middle Jurassic CIE probably lies within the limited sedimentological and geochemical data available for the Oxfordian stratigraphic interval. Additional higher-resolution analysis of other geochemical proxies (e.g. $\delta^{13}\text{C}_{\text{org}}$, nitrogen isotopes, etc.) would help to disentangle between those different ideas and help to better characterize what triggered the MOxE.

3.7 Conclusions

Chapter 3

Our $\delta^{13}\text{C}$ record is the first record of the Middle Oxfordian positive $\delta^{13}\text{C}$ excursion within the Korallenoolith Fm. in the LSB and is interpreted to reflect global $\delta^{13}\text{C}$ changes in the carbon cycle. The positive CIE observed in the Konrad #101 core is an important chemostratigraphic indicator for the inter-basinal correlation of the Lower Korallenoolith Fm. and considered to be synchronous with the globally recorded Middle Oxfordian carbon isotope excursion (MOxE). Our dataset with well-defined tie points further proves the usefulness of shallow-water isotope variations recorded in bulk carbonate as chemostratigraphic proxy. In addition, our new dataset supports the composite carbon isotope stratigraphy of the GTS 2020 compiled by Cramer and Jarvis (2020).

3.8 Acknowledgments

This research was supported by a CSC scholarship (201808510183) and by an LUH Ph.D. completion grant at LUH to Deyan Zhang. Fritz Stoepke is thanked for his support with the preparation of petrographic thin-sections. The authors thank Christiane Wenske (Leibniz University Hannover) for assistance with stable isotope analysis.

3.9 References

- Ahrlrichs, N., Hübscher, C., Noack, V., Schnabel, M., Damm, V., & Krawczyk, C.M. (2020). Structural Evolution at the Northeast North German Basin Margin: From Initial Triassic Salt Movement to Late Cretaceous-Cenozoic Remobilization. *Tectonics*, 39.
- Bai, H., Betzler, C., Erbacher, J., Reolid, J., & Zuo, F. (2017). Sequence stratigraphy of Upper Jurassic deposits in the North German Basin (Lower Saxony, Süntel Mountains). *Facies*, 63, 1–20.
- Berg, H.P., Brennecke, P.W., Thomauske, B.R. (1987). The German Konrad repository project, *Progress in Nuclear Energy*, 20, 255–307.
- Betzler, C., Pawellek, T., Abdullah, M., Kossler, A. (2007). Facies and stratigraphic architecture of the Korallenoolith Formation in North Germany (Lauensteiner Pass, Ith Mountains). *Sedimentary Geology*, 194, 61–75.
- Brigaud, B., Pucéat, E., Pellenard, P., Vincent, B., & Joachimski, M.M. (2008). Climatic fluctuations and seasonality during the Late Jurassic (Oxfordian–Early Kimmeridgian) inferred from $\delta^{18}\text{O}$ of Paris Basin oyster shells. *Earth and Planetary Science Letters*, 273, 58–67.
- Brink, H., Dürschner, H., & Trappe, H. (1992). Some aspects of the late and post-Variscan development of the Northwestern German Basin. *Tectonophysics*, 207, 65–95.
- Budyko, M.I., Ronov, A.B., Yanshin, A.L. (1987). *History of the Earth's atmosphere*. Springer Heidelberg.
- Carneille, M., Bourillot, R., Pellenard, P., Dupias, V., Schnyder, J., Riquier, L., Mathieu, O., Brunet, M.F., Énay, R., Grossi, V., Gaborieau, C., Razin, P., Visscher, P.T. (2020). Formation of microbial organic carbonates during the Late Jurassic from the Northern Tethys (Amu Darya Basin, Uzbekistan): Implications for Jurassic anoxic events. *Global and Planetary Change*, 186, 103127.
- Cramer, B.D., Jarvis, I. (2020). Carbon isotope stratigraphy. In F. M. Gradstein, J. G. Ogg, M. D. Schmitz, G. M. Ogg (Eds.), 2020. *Geologic time scale*, Elsevier.

- Dromart, G., Garcia, J., Picard, S., Atrops, F., Lécuyer, C., Sheppard, S.M. (2003). Ice age at the Middle–Late Jurassic transition? *Earth and Planetary Science Letters*, 213, 205–220.
- Eldrett, J.S. (2021). Middle Oxfordian carbon cycle perturbation expressed in the Smackover Formation, Gulf of Mexico. *Geology*, 50, 500–505.
- Eltom, H.A., González, L.A., Hasiotis, S.T., Rankey, E.C., Cantrell, D.L. (2018). Paleogeographic and paleoceanographic influences on carbon isotope signatures: Implications for global and regional correlation, Middle–Upper Jurassic of Saudi Arabia. *Sedimentary Geology*, 364, 89–102.
- Fischer R. (1991). Die Oberjura-Schichtfolge vom Langenberg bei Oker. *Arbeitskreis Paläontologie Hannover*, 107 (2) 21–52.
- Gradstein, J. G. Ogg, M. D. Schmitz, G. M. Ogg (Eds.), 2020. *Geologic time scale*, Elsevier.
- Gramann, F., Heunisch, C., Klassen, H., Kockel, F., Dulce, G., Harms, F., Katschorek, T., Mönnig, E., Schudack, M., Schudack, U., Thies, D., Weiss, M. (1997). Das Niedersächsische Oberjura-Becken. Ergebnisse Interdisziplinärer Zusammenarbeit. *Zeitschrift der Deutschen Geologischen Gesellschaft*, 148, 165–236.
- Helm, C., Schülke, I., Fischer, I. (2001). Paläobiogeographie des Korallenooliths (Mittleres Oxfordium Unteres Kimmeridgium): Tethyale Faunen und Florenelemente auf höherer Paläobreite (Niedersächsisches Becken, NW-Deutschland). *Geologische Beiträge Hannover*, 2, 51–64.
- Husinec, A., Leslie, S.A. (2022). Continuous record of Upper Ordovician (Katian) to lower Silurian (Telychian) global $\delta^{13}\text{C}$ excursions in the Williston Basin. *Terra Nova*, 34, 314–322.
- Huck, S., Heimhofer, U., Rameil, N., Bodin, S., Immenhauser, A. (2011). Strontium and carbon-isotope chronostratigraphy of Barremian–Aptian shoal-water carbonates: Northern Tethyan platform drowning predates OAE 1a. *Earth and Planetary Science Letters*, 304, 547–558.
- Jenkyns, H.C. (1996). Relative sea-level change and carbon isotopes: data from the Upper Jurassic (Oxfordian) of central and Southern Europe. *Terra Nova*, 8, 75–85.
- Kemper, E. (1985). Paläontologischer Bericht über die Kernbohrung Konrad 101. Bundesanstalt für Geowissenschaften und Rohstoffe (BGR), Hannover, 7 pp.
- Kästner, M., Schülke, I., Winsemann, J. (2008). Facies architecture of a Late Jurassic carbonate ramp: The Korallenoolith of the Lower Saxony Basin. *International Journal of Earth Sciences*, 97, 991–1011.
- Klüpfel, W. (1931). Stratigraphie der Weserkette (Oberer Dogger und Malm unter besonderer Berücksichtigung des Ober-Oxford). *Abhandlungen der Preußischen Geologischen Landesanstalt, NF Berlin* 129, 13–423.
- Leinfelder, R.R. (2001). Jurassic reef ecosystems, in Stanley, G.D., Jr. (ed.), *The History and Sedimentology of Ancient Reef Systems*: Boston, Springer, p. 251–309.
- Louis-Schmid, B., Rais, P., Schaeffer, P., Bernasconi, S.M., Weissert, H. (2007a). Plate tectonic trigger of changes in $p\text{CO}_2$ and climate in the Oxfordian (Late Jurassic): Carbon isotope and modeling evidence. *Earth and Planetary Science Letters*, 258, 44–60.
- Louis-Schmid, B., Rais, P., Bernasconi, S.M., Pellenard, P., Collin, P., Weissert, H. (2007). Detailed record of the mid-Oxfordian (Late Jurassic) positive carbon-isotope excursion in two hemipelagic sections (France and Switzerland): A plate tectonic trigger? *Palaeogeography, Palaeoclimatology,*

Chapter 3

- Palaeoecology, 248, 459–472.
- Marshall, J.D. (1992). Climatic and oceanographic isotopic signals from the carbonate rock record and their preservation. *Geological Magazine*, 129, 143–160.
- Martin-Garin, B., Lathuilière, B., & Geister, J. (2012) The shifting biogeography of reef corals during the Oxfordian (Late Jurassic). A climatic control. *Palaeogeography, Palaeoclimatology, Palaeoecology*, 365, 136–153.
- Martinez, M., Dera, G. (2015). Orbital pacing of carbon fluxes by a ~9-My eccentricity cycle during the Mesozoic. *Proceedings of the National Academy of Sciences*, 112, 12604–12609.
- Mitchell, S.F., Ball, J.D., Crowley, S.F., Marshall, J.D., Paul, C.R.C., Veltkamp, C.J., et al. (1997). Isotope data from Cretaceous chalks and foraminifera: environmental or diagenetic signals? *Geology*, 25 (8), 691–694
- Mönnig, E. (1989). Stratigraphie und Fazies des Calloviums in NW-Deutschland. *Clausthaler Geowissenschaftliche Dissertationen*, 37: 1–183
- Nunn, E.V., Price, G.D., Hart, M.B., Page, K.N., Leng, M.J. (2009). Isotopic signals from Callovian–Kimmeridgian (Middle–Upper Jurassic) belemnites and bulk organic carbon, Staffin Bay, Isle of Skye, Scotland. *Journal of the Geological Society*, 166, 633–641.
- O’Dogherty, L., Aguado, R., Baumgartner, P.O., Bill, M., Goričan, Š., Sandoval, J., Sequeiros, L. (2018). Carbon-isotope stratigraphy and pelagic biofacies of the Middle–Upper Jurassic transition in the Tethys–Central Atlantic connection. *Palaeogeography, Palaeoclimatology, Palaeoecology*, 507, 129–144.
- Padden, M., Weissert, H., Rafelis, M.D. (2001). Evidence for Late Jurassic release of methane from gas hydrate. *Geology*, 29, 223–226.
- Pearce, C.R., Hesselbo, S.P., Coe, A.L. (2005). The mid-Oxfordian (Late Jurassic) positive carbon-isotope excursion recognised from fossil wood in the British Isles. *Palaeogeography, Palaeoclimatology, Palaeoecology*, 221, 343–357.
- Rais, P., Louis-Schmid, B., Bernasconi, S.M., Weissert, H. (2007). Palaeoceanographic and palaeoclimatic reorganization around the Middle–Late Jurassic transition. *Palaeogeography, Palaeoclimatology, Palaeoecology*, 251, 527–546.
- Rampino, M.R., Stothers, R.B. (1988). Flood Basalt Volcanism During the Past 250 Million Years. *Science*, 241, 663–668.
- Schudack, U. (1994). Revision, Dokumentation und Stratigraphie der Ostracoden des Nordwestdeutschen Oberjura und Unter-Berriasium. *Berliner geowissenschaftliche Abhandlungen*, E11, 1–193.
- Schulze, K. H. (1975). Mikrofazielle, geochemische und technologische Eigenschaften von Gesteinen der Oberen Heersumer Schichten und des Korallenoolith (Mittleres bis Oberes Oxfordium NW Deutschlands) zwischen Weser und Leine. *Geologisches Jahrbuch*. D11, 3–102.
- Scotese, C. (2014). Atlas of Jurassic Paleogeographic Maps. Scotese, C.R., Atlas of Jurassic Paleogeographic Maps, PALEOMAP Atlas for ArcGIS, Volume 3, The Jurassic and Triassic, Maps 32–42, Mollweide Projection, PALEOMAP Project, Evanston, IL.
- Smith, A. G., Smith, D. G., Funnell, B. M. (1994). Atlas of Cenozoic and Mesozoic coastlines Cambridge

University Press, Cambridge.

- Van Hinsbergen, D.J., de Groot, L.V., van Schaik, S.J., Spakman, W., Bijl, P.K., Sluijs, A., Langereis, C.G., & Brinkhuis, H. (2015). A Paleolatitude Calculator for Paleoclimate Studies. *PLoS ONE*, 10.
- Weiß, M. (1995). Stratigraphie und Mikrofauna im Kimmeridge SE-Niedersachsens unter besonderer Berücksichtigung der Ostracoden. *Clausthaler Geowissenschaftliche Dissertationen*, 48, 1–274
- Weiss, W. (1985). Mikropaläontologischer Bericht. Bundesanstalt für Geowissenschaften und Rohstoffe (BGR), Hannover, 4 pp.
- Weisert, H., Mohr, H.M. (1996). Late Jurassic climate and its impact on carbon cycling. *Palaeogeography, Palaeoclimatology, Palaeoecology*, 122, 27–43.
- Whittaker, J. E., Hart, M. B. (2009). *Ostracods in British Stratigraphy*. Geological Society of London.
- Wierzbowski, H. (2015). Seawater temperatures and carbon isotope variations in central European basins at the Middle–Late Jurassic transition (Late Callovian–Early Kimmeridgian). *Palaeogeography, Palaeoclimatology, Palaeoecology*, 440, 506–523.
- Ziegler, P. A. (1990). *Geological Atlas of Western and Central Europe*. 2nd Edition, Shell International Petroleum Mij. B.V. and Geological Society, London.

4. $^{87}\text{Sr}/^{86}\text{Sr}$ chemostratigraphy of Oxfordian carbonate deposits, Lower Saxony Basin, Northern Germany

Deyan Zhang, François-Nicolas Krencker, Stefan Huck, Ulrich Heimhofer

Institute of Geology, Leibniz University Hannover

4.1 Abstract

During the Oxfordian, the Lower Saxony Basin was covered by a shallow epicontinental sea, in which a thick succession of alternating marine limestones and marls was deposited. Due to the scarcity of biostratigraphic markers and numerous sedimentary gaps, the stratigraphic dating is still uncertain and hampers further studies on a basin-wide scale. Chemostratigraphy represents a reliable means of contrasting and calibrating biostratigraphic schemes on local and global scales. New biocalcite-derived $^{87}\text{Sr}/^{86}\text{Sr}$ data for 11 well-preserved shells and shell fragments from the Oxfordian Korallenoolith Fm. of Lower Saxony Basin are used to identify secular trends in seawater and to constrain the depositional age of the Korallenoolith Formation. Unfortunately, the analyzed data deviate significantly from the Oxfordian open marine Sr-isotope signature and fail to provide a more precise age assignment. We discuss possible environmental factors that may have affected the $^{87}\text{Sr}/^{86}\text{Sr}$ ratios derived from shell material of the Korallenoolith Fm. The new findings indicate that continental freshwater discharge was the most likely controlling factor for the observed seawater $^{87}\text{Sr}/^{86}\text{Sr}$.

Keywords: Shell Geochemistry, Oxfordian, Strontium stable isotope, Boreal realm, Late Jurassic

4.2 Introduction

During the Oxfordian stage (Late Jurassic; 161.5–154.8 Myrs), the Lower Saxony Basin (LSB) was covered by a shallow epicontinental sea, which facilitated the accumulation of carbonate-rich sediments (Ziegler, 1990). These shallow-marine deposits are composed of alternating limestones, marls, and coral reef-bearing horizons and correspond to the Korallenoolith Formation (Fm.). Despite multiple biostratigraphic schemes that have been constructed, the stratigraphy and subdivision of the Upper Jurassic rocks of the LSB are still poorly defined. The shallow-marine carbonates of the Korallenoolith Fm. probably formed under varying salinity regimes that lack typical marine index fossils. Due to the scarcity of biostratigraphic markers and numerous sedimentary gaps, the stratigraphic dating is still uncertain and hampers further studies on a basin-wide scale. As ammonites are scarce or lacking, other biostratigraphic schemes have been developed, including ostracods, benthic foraminifera, charophytes, terrestrial and marine palynomorphs, and vertebrate remains (Schudack, 1994; Weiß, 1995; Gramann et al., 1997; Mudroch et al., 1999; Luppold, 2003). However, most of these organism groups are endemic due to the restricted palaeogeographic position of the LSB, which had limited exchange with the open ocean. Given this poor dating, a correlation on supra-regional and/or global scales remains ambiguous and imprecise (Jach et al., 2014; Zuo, 2017). As a result, a stratigraphic age assignment of the Korallenoolith Fm. in the LSB remains difficult, although some excellent and undeformed Upper Jurassic sections are exposed in the LSB, including the Bisperode section (Ith syncline).

At any given time, Strontium has a long ocean residence time of $\sim 2.4 \cdot 10^6$ years (Jones and Jenkyns 2001) and can be viewed as a global signal, with its isotopic composition reflecting the relative input of Sr from rivers (continental flux with high, radiogenic $^{87}\text{Sr}/^{86}\text{Sr}$ ratios) and from submarine hydrothermal systems (mantle flux with relatively low $^{87}\text{Sr}/^{86}\text{Sr}$ ratios) (Faure, 1986; Bruhn and Veizer, 2005). Secular variations of the $^{87}\text{Sr}/^{86}\text{Sr}$ ratio are used as a tool for strontium isotope stratigraphy (SIS), which represents a reliable means of contrasting and calibrating the divergent biostratigraphic schemes on local and global scales (McArthur et al., 2001, 2012, 2020; Jenkyns et al., 2002; Hucket et al., 2013; Fijija et al., 2015). Low-Mg calcite shells are considered an ideal geochemical archive for capturing contemporaneous seawater $^{87}\text{Sr}/^{86}\text{Sr}$ ratios due to their resistance to diagenesis (Popp et al., 1986; Brand et al., 2011; Hucket et al. 2011). Previous studies have demonstrated that low-Mg calcite shells are a valuable tool for age assignment of shallow marine strata (Schneider et al. 2009, Heimhofer et al. 2012, Horikx et al. 2014; Zuo et al. 2018; Schmitt et al. 2020). Most existing SIS studies dealing with the Oxfordian interval focus on pelagic and hemipelagic deposits whereas data from shallow-water carbonates is comparatively rare. Overall, only a limited amount of SIS data is available for the Oxfordian (Wierzbowski et al., 2017; McArthur et al., 2020). In addition, crucial Sr isotope data is still lacking for the Oxfordian–Kimmeridgian transition, and for some other intervals of the Middle–Upper Jurassic, which makes the precise determination of seawater strontium isotope ratios during these periods difficult (Wierzbowski et al. 2017). Within the LSB, Zuo et al. (2018) used SIS to establish a refined stratigraphic framework for the Kimmeridgian Süntel Fm. Although Bruhn et al. (2005) presented $^{87}\text{Sr}/^{86}\text{Sr}$ ratios from bulk rock samples from the Oxfordian Korallenoolith Fm., precise dating and correlation for Oxfordian strata within the LSB based on pristine shell material are still lacking.

The aim of this study is to develop a composite Sr-isotope stratigraphic record for the Oxfordian limestone successions in the LSB. From the Bisperode section and the Konrad #101 core, well-described high-resolution lithological logs with detailed sedimentological information of the Korallenoolith Fm. have been built (Betzler et al. 2007; Cäsar 2012; Zuo, et al. 2017; Zhang et al. 2023). We combine morphological preservation, CL characteristics, and trace element threshold values to assess the preservation of fossil shell material, which is subsequently analyzed for $^{87}\text{Sr}/^{86}\text{Sr}$ ratios. The new Sr-isotope data from the Oxfordian part of the Bisperode section and Konrad #101 core will be compared with previously published $^{87}\text{Sr}/^{86}\text{Sr}$ records (Wierzbowski et al., 2017; McArthur et al., 2020). Based on these new results, the existing stratigraphic age assignment of the Korallenoolith Fm. in the LSB will be critically assessed. Finally, a supra-regional stratigraphic correlation with other successions in the peri-Tethyan and western Tethyan domains can be proposed.

4.3 Geological setting

The LSB, located on the southern margin of the Central European Basin, is one of several rift- and wrench-induced “marginal troughs”, that formed a series of E-W trending horst-and-graben structures (Betz et al., 1987; Ziegler 1990; Senglaub et al., 2006). With a length of ~300 km and a width of ~65 km, the LSB formed an elongate, E-W trending basin bordered by the Rhenish Massif to the South and the Ringkøbing-Fyn High to the North (Fig. 1). The LSB contains a maximum sedimentary thickness of ~4500 m (Betz et al. 1987; Mazur et al. 2005; Kästner et al., 2010). Stratigraphic sections located on the uplifted horst areas may show less stratigraphic thickness and contain fewer small- and medium-scale cycles compared to the adjacent graben areas (Kästner et al. 2008). During the Oxfordian, the LSB was located at a palaeolatitude of about ~35°N (van Hinsbergen et al. 2015) and can be viewed as a tributary sea of the Tethys, which resulted in the interchange of fauna and flora between the Boreal and the Tethyan Realms (Helm et al. 2001; Cäsar, 2012). In the LSB, the middle to late Oxfordian succession is assigned to the Korallenoolith Fm., which belongs to the NW German Malm Group (Helm et al. 2003). The Korallenoolith Fm. consists of reef-bearing oolitic limestones, which were formed within a shallow-marine subtropical environment with limited terrestrial influx. Deposition took place on a homoclinal carbonate ramp setting (Helm et al. 2003; Betzler et al. 2007; Kästner et al. 2008; Cäsar 2012; Zuo et al. 2017; Zhang et al. 2023).

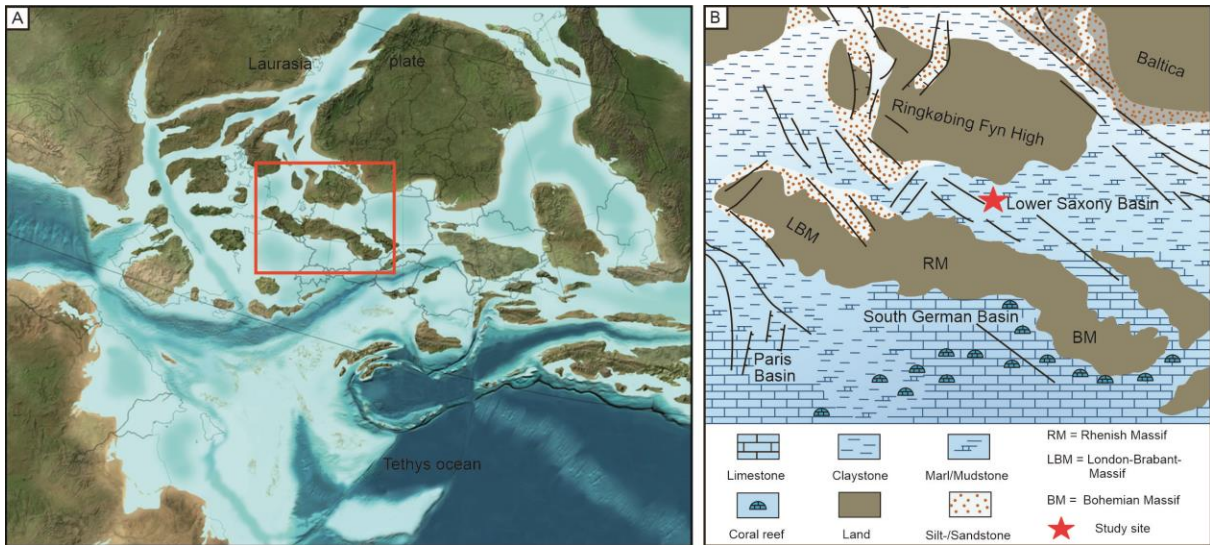


Fig. 1. (A) Paleogeographic maps of Europe and adjacent regions for the Late Jurassic (150 Ma, modified after Blakey, 2011). (B) Paleogeographic reconstruction of Central Europe for the Oxfordian. Major landmasses and general marine facies distribution are shown. The approximate position of the studied outcrop in the Lower Saxony Basin is marked with a red asterisk.

The studied sites are situated in northern Germany (Fig. 2). and include an abandoned quarry (Bisperode section) located ~2 km southwest of the village Lauenstein and a scientific drill core (Konrad #101 core) located close to the village Salzgitter-Beddingen about 500 m of the Konrad 2 mine shaft (Berg et al. 1987). The lithology is essentially composed of oolitic and bioclastic limestones with intercalated marls and claystone, interspersed with coral patch reefs in the Bisperode section. More detailed information on the sedimentary facies and depositional settings encountered in the Bisperode section and the Konrad #101 core can be found in chapters 2 and 3.

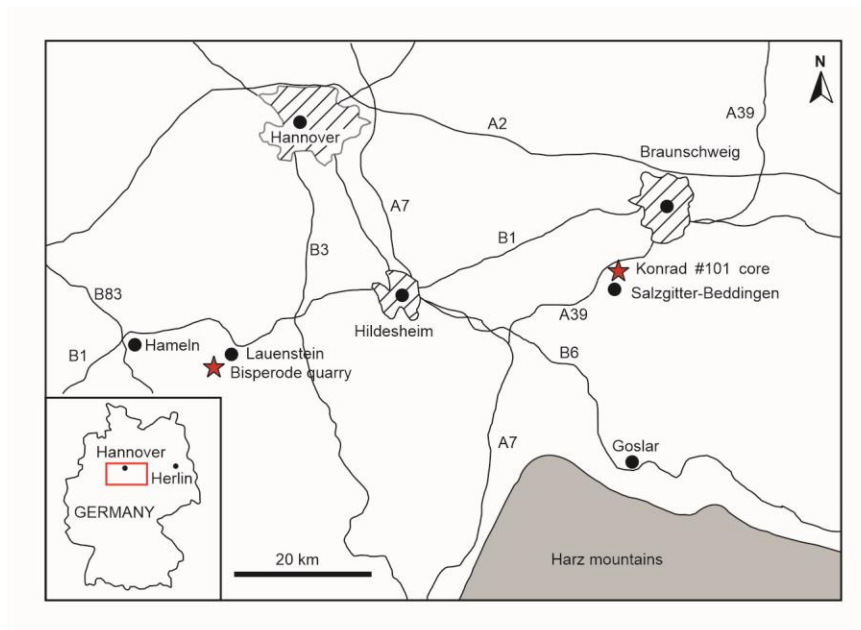


Fig. 2. Location of the studied sites in northeast Niedersachsen, Germany, The Bisperode quarry and Konrad #101 core location are marked with asterisks.

4.4 Materials and methods

4.4.1 Materials

A total of 30 shells were collected for SIS from the Bisperode section and an additional 16 shell fragments were obtained from the Konrad #101 core, respectively. The shells and shell fragments from the Bisperode section are mainly derived from brachiopods, oysters, *trichites* bivalves (a group related to *Pinnidae*), and rarely from echinoderms. Brachiopods are represented by *Zeilleriidae* and *Lobidothyrididae*, which both belong to the *Terebratulida* order (Gervais, 1987; Fischer, 1991). The shell fragments from the Konrad #101 core are very small (< 10 mm) and do not allow identification on a taxonomic level. In consequence, all samples from the Konrad #101 core are grouped simply as shell fragments without further differentiation.

Given the potential alteration of primary shell calcite during early and later-stage diagenesis, it is necessary to use multiple methods (visual inspection, petrographic thin-section and cathodoluminescent microscopy, and trace element geochemistry) to assess the preservation state of the studied shells used for seawater $^{87}\text{Sr}/^{86}\text{Sr}$ reconstruction (Brand et al., 2012a; Korte et al. 2006; McArthur et al., 2012; Immenhauser et al., 2016; Wang et al., 2018).

4.4.2 Petrography and cathodoluminescence analyses of shell material

Before further processing, all of the sampled shells have been visually inspected to avoid bio-eroded parts, cement infills, and other impurities. Subsequently, the shells were thin-sectioned in order to analyze the internal shell structure, using an Olympus BX53 microscope equipped with an Olympus SC50 camera, at Institute for Geology, Leibniz University Hannover. In addition, cathodoluminescence (CL) microscopy was carried out at Aarhus University using a cold cathodoluminescence (Nuclide ELM2) operating at 12 kV with a beam current of 3 mA. Exposure to the electronic beam (before taking the photo) was limited to 15~30 seconds. Photographic exposure time was set to 2-4 s and to be uniform for consistency.

Visible growth increments, compact fibrous microstructure and negligible impact of bioerosion and fracturing are considered morphological criteria indicative of well-preserved mollusc shell material (Schmitt et al. 2020, 2022). Following Garbelli et al. (2019), the luminescence characteristics of the shells were classified as non-luminescent (NL), slightly luminescent (SL), and bright luminescent (L). Non-luminescent shells showing rare bright microfractures are assigned to the first category (NL), but if the fissures occur more frequently, the samples are categorized as SL. Only the most pristine shells (showing visible growth increments and compact fibrous microstructure of the outer shell layer, and predominantly non-luminescent shell areas) were selected for further geochemical analysis.

4.4.3. Elemental and strontium-isotope analyses

Following the strict petrographic screening, 23 shell samples from Bisperode (7 oysters, 4 brachiopods, 9 *trichites* bivalves, and 1 echinoderm fragment), and 14 shell fragments from the Konrad #101 core

Chapter 4

were selected for subsequent trace element measurement (Table 1). For major and trace element analyses, several milligrams (~10) of powder were micro-drilled from different positions of each shell. The powders were analyzed for Ca, Mg, Mn, Fe, and Sr in order to assess the potential diagenetic alteration of the low-Mg shell material. Analyses were performed using inductively coupled plasma-atomic emission spectrometry (ICP-AES) at the isotope laboratory of the Institute of Geology, Mineralogy and Geophysics at the Ruhr-University Bochum, Germany. For more details on the analytical procedure compare Hucket al. (2011).

Based on the petrographic and element geochemical results, 11 well-preserved shells and shell fragments were selected for analysis of $^{87}\text{Sr}/^{86}\text{Sr}$ ratios at the Ruhr-University Bochum, Germany, using a thermal ionization mass spectrometer (Finnigan MAT 262) in dynamic mode. For more details on the analytical procedure, please refer to Hucket al. (2011). In order to be consistent with the normalization used for the compilation of the SIS reference curve of McArthur et al. (1997), the $^{87}\text{Sr}/^{86}\text{Sr}$ ratios of the samples were adjusted to a value of 0.709175 for the USGS EN-1 standard.

Table 1. Analytical results (Sr-isotope and trace elements) of low-Mg calcite shells from Bisperode sections and Konrad #101 core

| Locality | Fossils | Height(m) | Sample No. | Mg Sr Fe Mn (ppm) | | | | | $^{87}\text{Sr}/^{86}\text{Sr}$ | $^{87}\text{Sr}/^{86}\text{Sr}$ |
|------------|------------|-----------|------------|-------------------|------|-------|----------|----------|---------------------------------|---------------------------------|
| | | | | Mg | Sr | Fe | Mn | | | |
| Bisperode | brachiopod | 44 | SB7.7 | 2697 | 606 | 69 | 16 | 0.706954 | 5 | |
| | brachiopod | 45 | SB8.5-B | 1785 | 576 | 221 | 19 | 0.706913 | 5 | |
| | brachiopod | 45 | SB8.5-D | 1689 | 563 | 98 | 12 | - | - | |
| | brachiopod | 24.5 | LPb-3 | 1811 | 458 | 698 | 31 | - | - | |
| | trichtes | 45 | SB8.5-A | 5705 | 170 | 488 | 106 | - | - | |
| | trichtes | 61.5 | SB25.2 | 4173 | 706 | 220 | 35 | 0.706909 | 5 | |
| | trichtes | 94 | SB57.2 | 1469 | 631 | 115 | 7 | - | - | |
| | trichtes | 95 | SB58.5 | 3688 | 433 | 1324 | 75 | - | - | |
| | trichtes | 101.5 | SB65-A | 4025 | 290 | 109 | 57 | - | - | |
| | trichtes | 101.5 | SB65-B | 3816 | 192 | 273 | 77 | - | - | |
| | trichtes | 101.5 | SB65-C | 3702 | 197 | 337 | 73 | - | - | |
| | trichtes | 119 | D82.5-A | 6266 | 632 | 3945 | 71 | - | - | |
| | trichtes | 119 | D82.5-B | 5237 | 685 | 259 | 29 | 0.706914 | 5 | |
| | oyster | 10 | DY10 | 1400 | 551 | 301 | 23 | - | - | |
| | oyster | 12.15 | DY11.5 | 745 | 623 | 336 | 13 | 0.706887 | 5 | |
| | oyster | 97 | SB60.5-A | 2064 | 470 | 196 | 21 | - | - | |
| | oyster | 97 | SB60.5-B | 1077 | 617 | 90 | 9 | 0.706923 | 5 | |
| | oyster | 28 | LPb-6.5A | 814 | 574 | 565 | 64 | - | - | |
| | oyster | 28 | LPb-6.5B | 2186 | 588 | 222 | 24 | - | - | |
| | oyster | 30 | LPb-8.5A | 708 | 532 | 321 | 34 | - | - | |
| oyster | 30 | LPb-8.5B | 1209 | 610 | 279 | 29 | 0.706914 | 5 | | |
| oyster | 30 | LPb-8.5C | 6207 | 53 | 1620 | 104 | - | - | | |
| echinoderm | 45 | SB8.5-C | 3937 | 105 | 283 | 48 | - | - | | |
| Konrad | shell | 649.5 | K649.5A | 1905 | 688 | 2141 | 102 | 0.706981 | 5 | |
| | shell | 649.5 | K649.5B | 3501 | 853 | 6155 | 150 | 0.707193 | 5 | |
| | shell | 655.79 | K655.79A | 3889 | 312 | 26463 | 398 | - | - | |
| | shell | 655.79 | K655.79B | 2913 | 485 | 12874 | 259 | - | - | |
| | shell | 748.2 | K748.2 | 1386 | 983 | 4387 | 409 | 0.706950 | 5 | |
| | shell | 753.5 | K753.5 | 740 | 620 | 3442 | 275 | 0.706966 | 5 | |
| | shell | 766.48 | K776.48 | 268 | 550 | 254 | 57 | - | - | |
| | shell | 776.7 | K776.7 | 382 | 505 | 1387 | 60 | - | - | |
| | shell | 777.45 | K777.45 | 3842 | 598 | 10662 | 150 | - | - | |
| | shell | 777.7 | K777.7 | 452 | 517 | 597 | 70 | - | - | |
| | shell | 778.40A | K778.40 | 642 | 522 | 682 | 77 | - | - | |
| | shell | 778.40B | K778.40 | 513 | 507 | 5105 | 79 | - | - | |

4.5 Results and interpretation

4.5.1 Shell microstructure and cathodoluminescence characteristics

Under the petrographic microscope, most of the brachiopod and oyster shell specimens show detailed prismatic layers and growth lines, with a clearly visible alternation of light to dark lamellae, indicating good preservation (Fig. 3). Examples include oyster shells exhibiting near-horizontally foliated orientations of prismatic layers (specimen DY11.5, Fig. 3A). Stacked growth bundles with different orientations are clearly visible in a shell fragment of questionable brachiopod origin (specimen K735.5, Fig. 3B). Two types of foliated wall structures with different foliation orientation are observed in a shell fragment of uncertain taxonomic assignment (specimen K753.5, Fig. 3C). Well-preserved brachiopod shells are characterized by a parallel fibrous wall structure oriented at a low angle to the shell margin (specimen SB 8.5B, Fig. 3D) and by a well developed foliated structure (specimen SB7.7, Fig. 3E). In contrast, *trichites* shells show a prismatic shell structure composed of coarse and well-developed calcite prisms, well visible under cross-polarized light (specimen D 82.2, Fig. 3F). The coarseness and inclusion-rich nature of the calcite prisms may indicate that the shell has undergone some diagenetic modification.

Most of the analyzed specimens (brachiopods, oysters) remain non-luminescent in most parts of the shell. Comparison of CL and transmitted-light microscopy illustrates well the non-luminescent (NL) character of well-preserved brachiopod shells, which contrast with the strongly luminescent, fine-grained matrix (Fig. 4A, B). Here, only rare luminescent fissures occur, which correspond to growth lines (Fig. 4C, D). The visually well-preserved *trichites* shells document often different levels of luminescence. Several samples show significant luminescence variability within the shell, including parts being slightly luminescent (SL) (Fig. 5A). Here, luminescence occurs between individual calcite prisms (Fig. 5B). In other parts of the shells, more prevalent bright luminescence (L) indicates diagenetic alteration due to cement infill (Fig. 5C). In contrast, strongly diagenetically altered *trichites* shells show bright luminescence (L) encompassing the entire shell (Fig. 6A) and uncovering the individual growth bands (Fig. 6B, C).

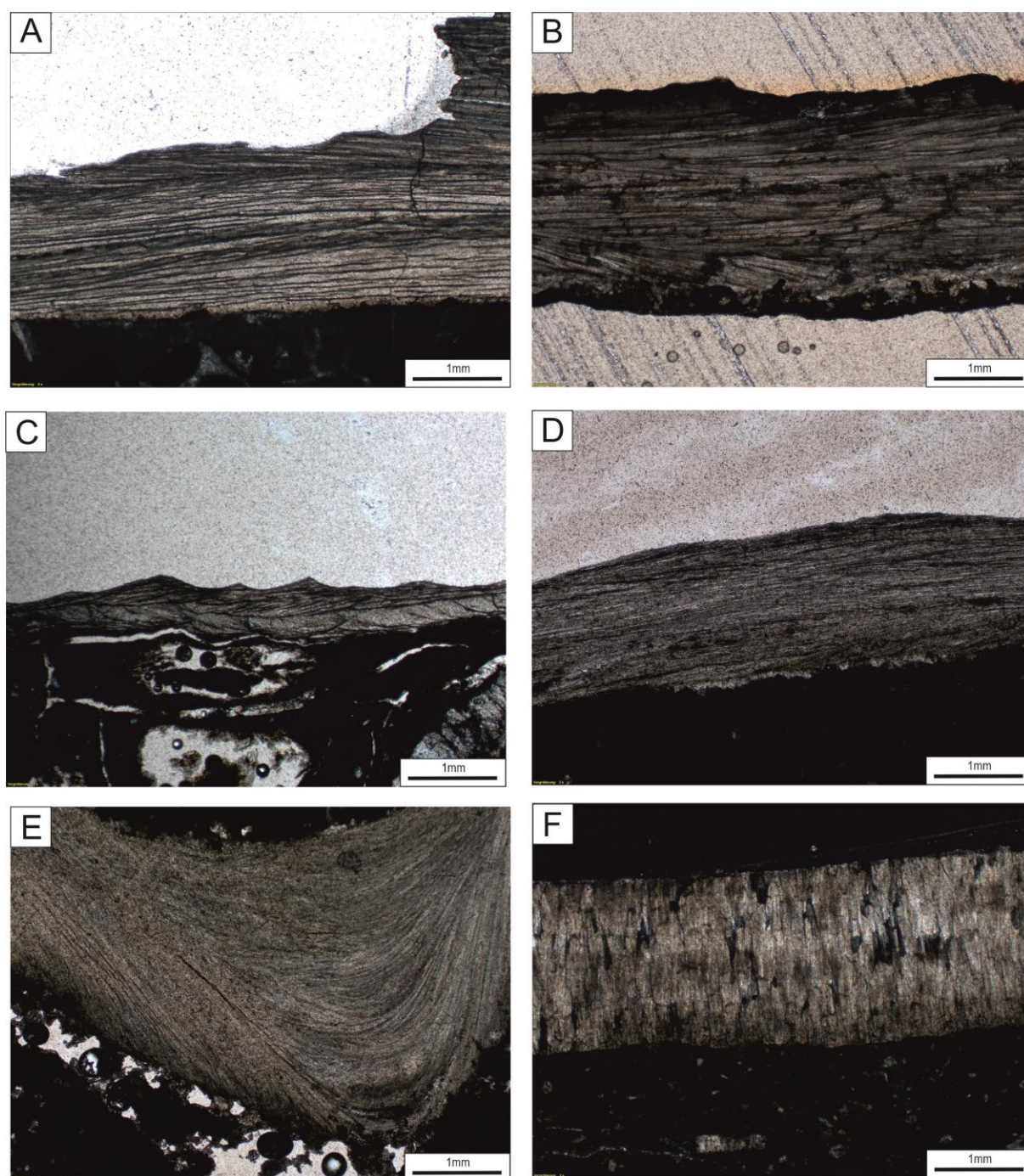


Fig. 3. Petrographic thin-section photomicrographs of selected brachiopod, oyster, and trichites shells from Bisperode quarry section and Konrad #101 core. (A) Specimen DY11.5 shows an oyster shell composed of individual calcite layers with near-horizontally foliated orientation. (B) Specimen K735.5 is tentatively assigned to represent a brachiopod shell fragment showing stacked calcitic bundles with different orientations. (C) Specimen K753.5 is tentatively assigned to represent a brachiopod shell fragment showing two types of foliated wall structure. The two layers exhibit different foliation orientations. (D) Specimen SB 8.5B represents a brachiopod shell with a well-developed parallel fibrous wall structure oriented at a low angle to the shell margin. (E) Specimen SB7.7 provides a detailed view of the foliated structure of a brachiopod shell. (F) Specimen D 82.2 shows a trichites shell under cross-polarized light with its characteristic coarsely prismatic structure.

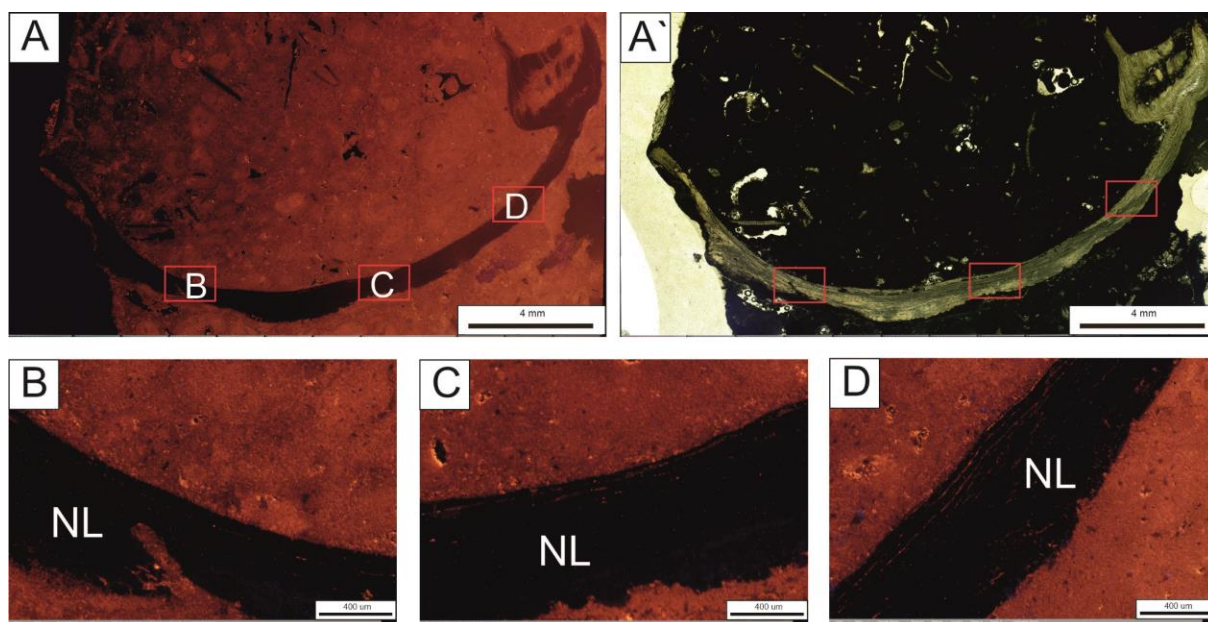


Fig. 4. Detailed view of brachiopod specimen SB8.5-B (Bisperode section) under CL (A) and transmitted light (A'). Enlargements of selected shell areas are marked by the red boxes labeled B, C, D. (B) Non-luminescent (NL) shell area with a bioerosion structure permeated by luminescent diagenetic cement. (C, D) Non-luminescent (NL) areas show thin luminescent fissures on the inner side of the shell parallel to growth lines.

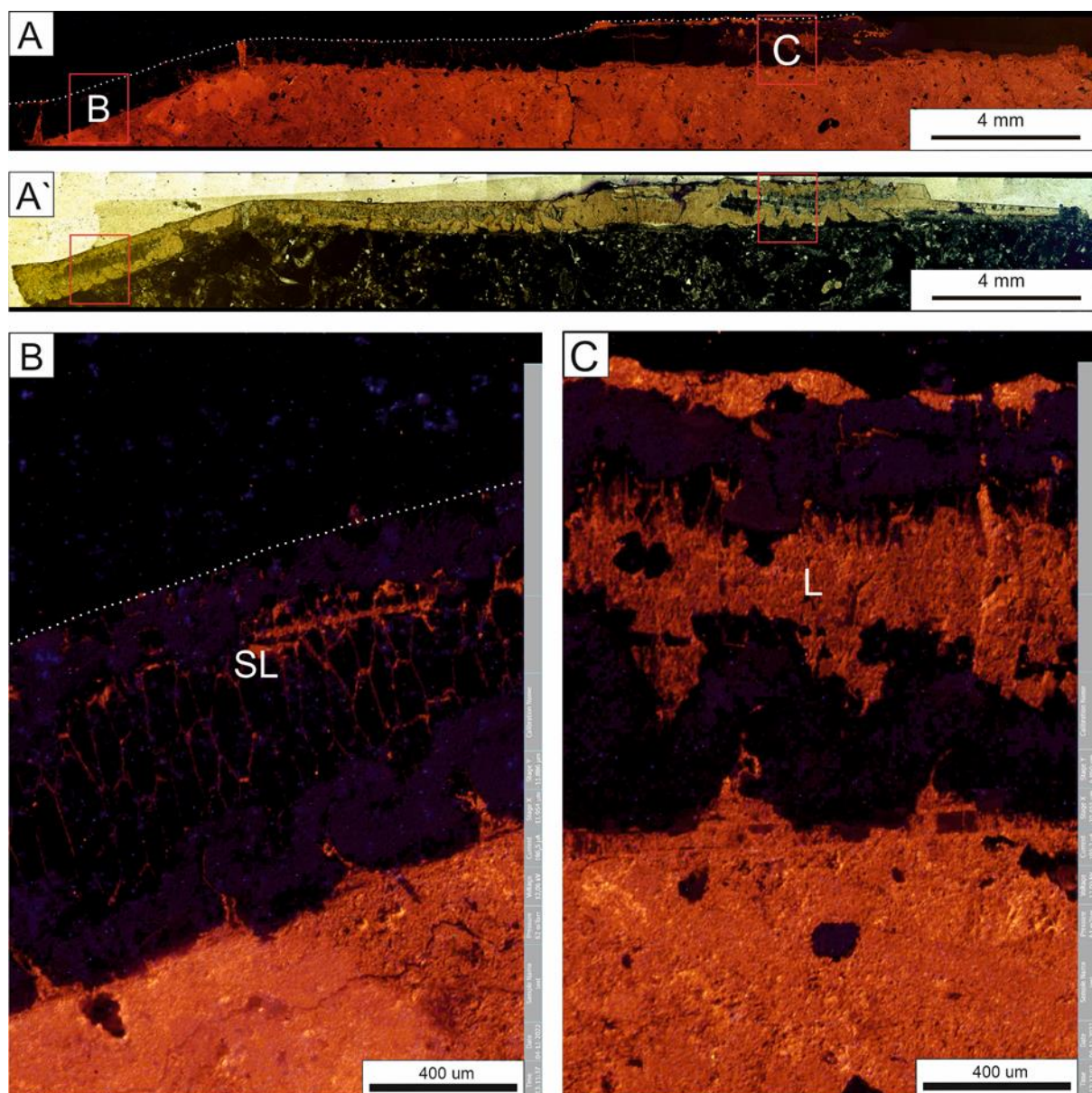


Fig. 5. Detailed view of trichites specimen SB25.2 (Bisperode section) under CL (A) and transmitted light (A') illustrating different levels of preservation. Enlargements of selected shell areas are marked by the red boxes labeled B, C. (B) Coarsely prismatic shell structure showing luminescent boundaries between individual calcite prisms. (C) Shell area showing widespread bright luminescence (L) indicating cementation/recrystallization during diagenesis.

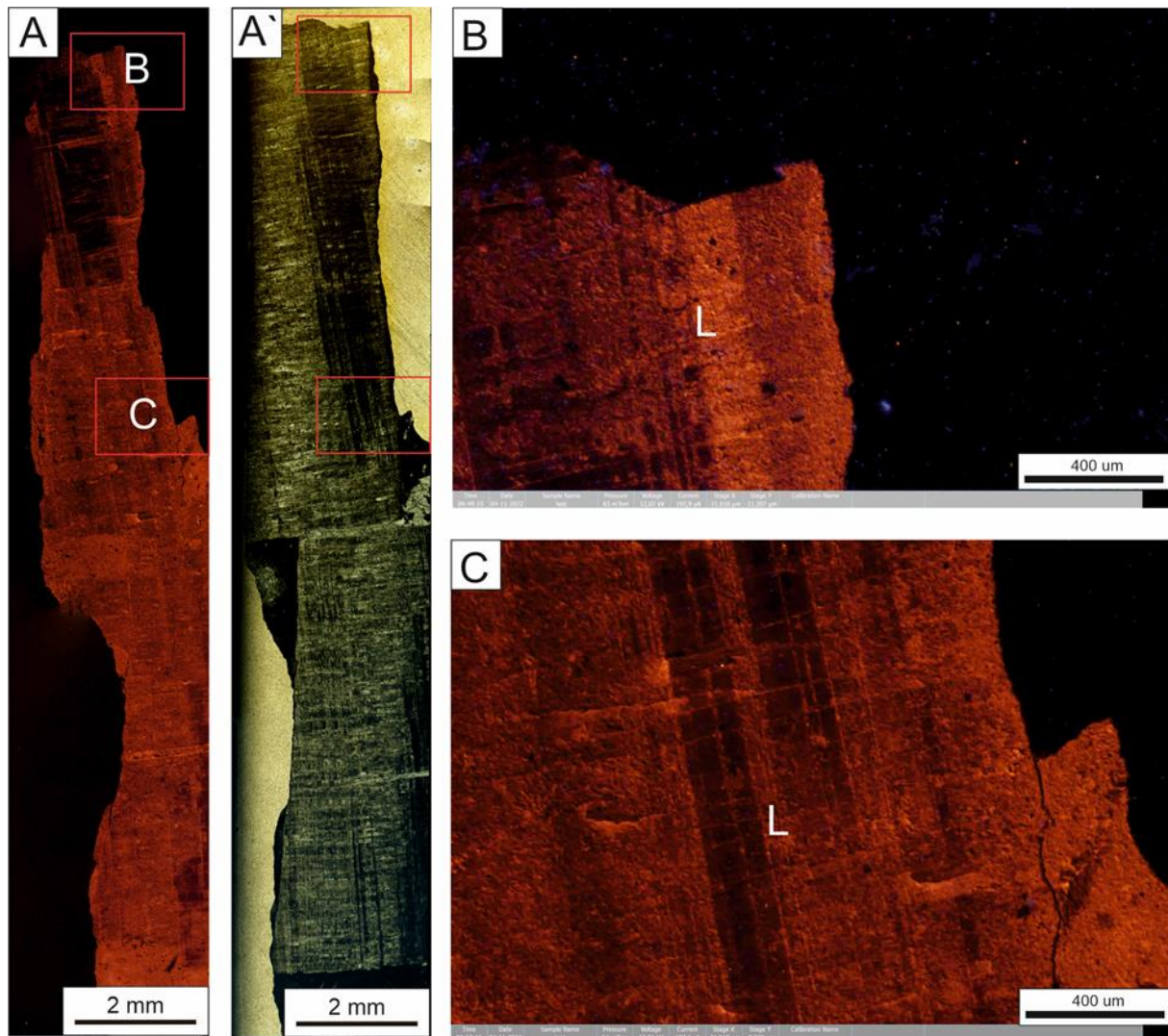


Fig. 6. Detailed view of trichites specimen SB 65 (Bisperode section) under CL (A) and transmitted light (A') showing strong luminescence (L) across the entire shell. Enlargements of selected shell areas are marked by the red boxes labeled B, C. (B, C) Bright luminescence covering the entire trichites shell indicates strong diagenetic alteration and loss of the primary geochemical information.

4.5.2 Element concentrations and isotopic compositions

The oyster shell samples from Bisperode show the following ranges of major and trace element contents. Mn varies between 9 and 104 ppm (n=9), Fe between 90 and 1.620 ppm, Sr between 53 and 623 ppm, and Mg between 708 and 6.207 ppm. Brachiopod shell material from Bisperode (n=4) shows variations of Mn between 12 and 31 ppm, Fe between 69 and 698 ppm, Sr between 458 and 606 ppm, and Mg between 1.689 and 2.697 ppm. *Trichites* shell specimens from Bisperode (n=9) exhibit Mn concentrations between 7 and 106 ppm, Fe between 109 and 3945 ppm, Sr between 170 and 706 ppm, and Mg between 1.469 and 6.266 ppm. For a single echinoderm fragment, concentrations are Mn 48 ppm, Fe 283 ppm, Sr 105 ppm, and Mg 3.927 ppm. The different shells fragments (n=14) obtained from the Konrad #101 core show concentrations of Mn between 57 and 409 ppm, Fe between 57 and 26.463

ppm, Sr between 312 and 983 ppm, and Mg between 268 and 3.889 ppm. All major and trace element results are shown in Table 1.

Only shell samples showing element concentrations below the defined cut-off values (discussed in section 5.1) were analyzed for their $^{87}\text{Sr}/^{86}\text{Sr}$ ratios (Table 1). The Sr-isotope ratios obtained from different types of shells located in the same or adjacent stratigraphic horizons show very similar values ranging between 1×10^{-6} and 9×10^{-6} (Zuo 2018). Sr-isotope values ($n=7$) from the Bisperode quarry section vary between $0.706887 \pm 5 \times 10^{-6}$ to $0.706954 \pm 5 \times 10^{-6}$, which is generally within the range of values reported for Late Jurassic sea water (McArthur et al., 2020). Besides, 4 Sr-isotope values ($0.706950 \pm 5 \times 10^{-6}$ to $0.707193 \pm 5 \times 10^{-6}$) from the Konrad #101 core have been obtained. One value ($0.707193 \pm 5 \times 10^{-6}$) is highly radiogenic compared to Late Jurassic global seawater proxy (McArthur et al. 2020) and this data was excluded from further interpretation. Three of the values fall within the Sr isotope range reported for Late Jurassic seawater (Rais 2007; Wierzbowski et al. 2017; McArthur et al. 2020), but more radiogenic compared to the values from the Oxfordian. This data will be discussed further in 5.1.

4.6 Discussion

4.6.1 Preservation of shells and reliability of strontium-isotope ratios

Only marine precipitates that have retained the original Sr-isotope ratio of the ocean will give correct SIS ages (Frijia et al., 2015). Oysters mineralize a primarily low-Mg-calcitic shell usually comprised of prismatic and foliate layers (Carter 1990). The specific mineralogy makes them less prone to diagenetic processes, which potentially can alter the primary chemical composition of the shell material (Schneider et al. 2009, Heimhofer et al. 2012, Horikx et al. 2014). Modern brachiopod shells show little taxonomic or vital effects on their $^{87}\text{Sr}/^{86}\text{Sr}$ composition (e.g., El Meknassi et al., 2018; Immenhauser et al., 2016; Zaky et al., 2019) and previous studies have considered brachiopod shells to be one of the best archives for capturing the Sr-isotopic signature of ancient ocean waters due to their resistance to diagenesis (Brand et al., 2011; Popp et al., 1986; Wang et al. 2020). *Trichites* shells represent a novel substrate for chemostratigraphic applications, and geochemical information on shell composition is essentially lacking (Brigaud et al., 2009, Zuo et al. 2018). *Trichites* and oyster shells that have been recovered from the same stratigraphic levels display similar Sr-isotope values (Brigaud et al. 2009). Zuo et al. (2018) reported *trichites* shells showing elemental contents comparable with brachiopod and oyster low-Mg calcite. These studies suggest the absence of strong vital effects and indicate a rather limited diagenetic overprint for the investigated *trichites* shells (Brigaud et al., 2009, Zuo et al. 2018). In summary, all the collected shells (oyster, brachiopod, and *trichites*) can potentially be used as archives for ancient seawater $^{87}\text{Sr}/^{86}\text{Sr}$ reconstruction. However, diagenesis may have influenced the primary $^{87}\text{Sr}/^{86}\text{Sr}$ signal of the shell, so it is fundamental to evaluate the preservation state of materials used for seawater $^{87}\text{Sr}/^{86}\text{Sr}$ reconstruction (Brand et al., 2012a; Korte et al., 2006; McArthur et al., 2012; Immenhauser et al., 2016; Wang et al., 2018, 2021). Shell samples are considered well-preserved when their shell structure shows good preservation under the petrographic microscope and absence of luminescence

Chapter 4

under CL (Horikx et al. 2014; Zuo et al. 2018; Wang et al., 2018, 2021). In addition, the trace element concentrations of shell calcite are widely used to further distinguish the preservation state of shells.

The degree of diagenetic alteration of primary shell calcite of carbonate-secreting organisms is verified by using Sr, Fe, and Mn abundances (Brand and Veizer 1980, Al-Aasm and Veizer 1986, Veizer et al. 1999, Huck et al. 2011, Horikx et al. 2014). High Mn and Fe concentrations in skeletal calcite are considered to indicate recrystallization in a reducing environment, involving the partial or complete equilibration of the Sr-isotope ratio with that of the diagenetic fluid, also resulting in low Sr concentrations (Al-Aasm and Veizer, 1986). Brand et al. (2011) suggested dynamic limits for trace elemental concentrations to differentiate preserved and altered shell materials. For low-Mg brachiopod calcite shells precipitated from normal marine waters, Mn values of < 100 ppm and Sr values > 600 ppm have been proposed as cut-off values, reflecting insignificant diagenetic overprint (van Geldern et al., 2006; Wierzbowski, 2015). In this study, well-preserved brachiopod samples are defined in comparison to typical threshold elemental values used by other authors (e.g., van Geldern et al., 2006; Wierzbowski, 2015) with a single exception. Sample SB8.5-B is considered as well preserved despite a Sr content (576 ppm) slightly below the threshold value. For Fe concentrations, we follow Zuo et al. (2018), who proposed values of < 700 ppm for brachiopod calcite obtained from the LSB, which is higher than the typical threshold values used by other authors (e.g., van Geldern et al., 2006; Wierzbowski, 2015). For oyster shell calcite, Schneider et al. (2009) analyzed Late Jurassic oysters in the Lusitanian Basin and proposed threshold values < 100 ppm for Mn and < 700 ppm for Fe. For Sr concentrations, Zuo et al. (2018) suggested threshold values > 600 for samples derived from the LSB based on a comparison with Schneider et al. (2009). In the present study, we follow the proposed values (Mn < 100 ppm, Fe < 700 ppm, Sr > 600 ppm) for oyster shell calcite considered to reflect insignificant diagenetic overprint (Fig. 7). *Trichites* shell material represents a novel substrate for chemostratigraphic applications, and geochemical information on shell composition is rare. Here we follow the cut-off values proposed by Zuo et al. (2018), which are Mn < 100 ppm, Fe < 700 ppm, and Sr > 600 ppm. Sample SB 57.2 is discarded as it only contains 7 ppm Mn. Echinoderm biocalcite is discarded as the original porous stereome is typically filled with diagenetic cement resulting in alteration of its primary geochemical composition. Based on their shell microstructure, the small shell fragments from the Konrad #101 core are tentatively assigned to be derived from brachiopods. Despite showing good structural preservation, the Konrad #101 core shell material does not fulfill the necessary geochemical criteria to be considered as well preserved. None of the fragments shows Mn concentrations < 100 ppm together with Sr concentrations > 600 ppm (Fig. 8). Fe concentrations are exceptionally high and reach values > 1000 ppm. However, the increased Fe may reflect a signature of the depositional environment given that the succession is rich in Fe-bearing ooids reaching exploitable concentrations in certain layers (Berg et al. 1987). In the Konrad #101 core, the shell containing host rock shows higher clay content compared to Bisperode, typically resulting in better shell calcite preservation. On the other hand, the small size of the analyzed shell fragments may have promoted diagenetic overprint.

In summary, combining morphological preservation, CL characteristics, and trace element threshold values, 7 samples from Bisperode (2 brachiopods, 2 trichites, 3 oysters,) were classified as well-preserved and analyzed for strontium-isotope ratios. Although all shell fragments from the Konrad #101

core show signs of diagenetic alteration, we still selected 4 shell fragments with Sr concentrations > 600 ppm for strontium-isotope analysis (Table 1).

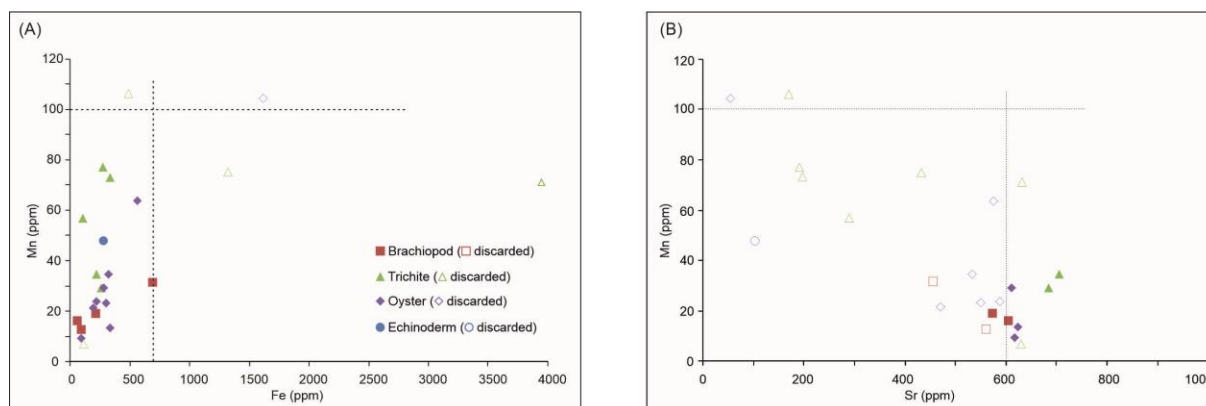


Fig. 7. Trace element composition of different shell materials derived from Bisperode displayed in scatter plots. (A) Mn vs. Fe concentration (in ppm) and (B) Mn vs. Sr concentration (in ppm) for shell material incl. brachiopods, oysters, trichites and echinoderms. Dashed lines in (A) indicate thresholds for Mn at 100 ppm and for Fe at 700 ppm. The dashed line in (B) indicates the threshold for Sr at 600 ppm. Filled symbols refer to samples fulfilling the threshold criteria, and hollow symbols represent samples, which are discarded for further analysis based on trace element composition.

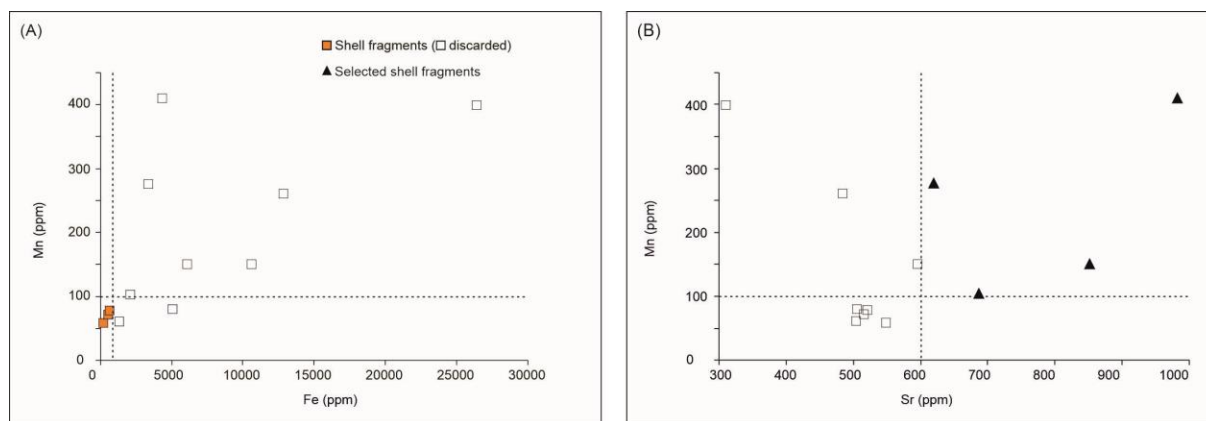


Fig. 8. Trace element composition of different shell fragments derived from Konrad #101 core displayed in scatter plots. (A) Mn vs. Fe concentration (in ppm) and (B) Mn vs. Sr concentration (in ppm) for shell fragments of the unknown taxonomic assignment. Dashed lines in (A) indicate thresholds for Mn at 100 ppm and for Fe at 700 ppm. The dashed line in (B) indicates the threshold for Sr at 600 ppm. Filled symbols refer to samples fulfilling the threshold criteria, and hollow symbols represent samples, which are discarded for further analysis based on trace element composition. Filled triangle symbols selected sample for strontium-isotope analysis.

4.6.2 Numerical age constraints

Chapter 4

Bruhn et al. (2005) presented $^{87}\text{Sr}/^{86}\text{Sr}$ ratios of echinoid fragments and interparticle cement from the Korallenoolith Fm. with $^{87}\text{Sr}/^{86}\text{Sr}$ ratios varying from 0.706910 to 0.708064, which have been interpreted to represent the original marine water composition. Rais (2007) performed $^{87}\text{Sr}/^{86}\text{Sr}$ ratio analyzes on well-dated belemnites covering Late Callovian to Oxfordian strata derived from Switzerland, France, and northern Italy. In their study, $^{87}\text{Sr}/^{86}\text{Sr}$ ratios range between 0.706897 and 0.706821. The observed Sr-isotope trend in our study is in good agreement with the lower ratios of Bruhn et al. (2005) and in the same range as the data of Rais (2007), which corresponds to a Late Jurassic age range. Compared to the Late Jurassic open ocean Sr-isotope curve of McArthur et al. (2020), all the data points from the LSB deviate from the open marine Sr-isotope record and fail to provide a definitive age assignment (Fig. 9; Fig. 10). Hence, the Sr-isotope data obtained from Bisperode and the Konrad #101 core cannot be used to confirm or refine the existing biostratigraphic age assignment of the Korallenoolith Fm.

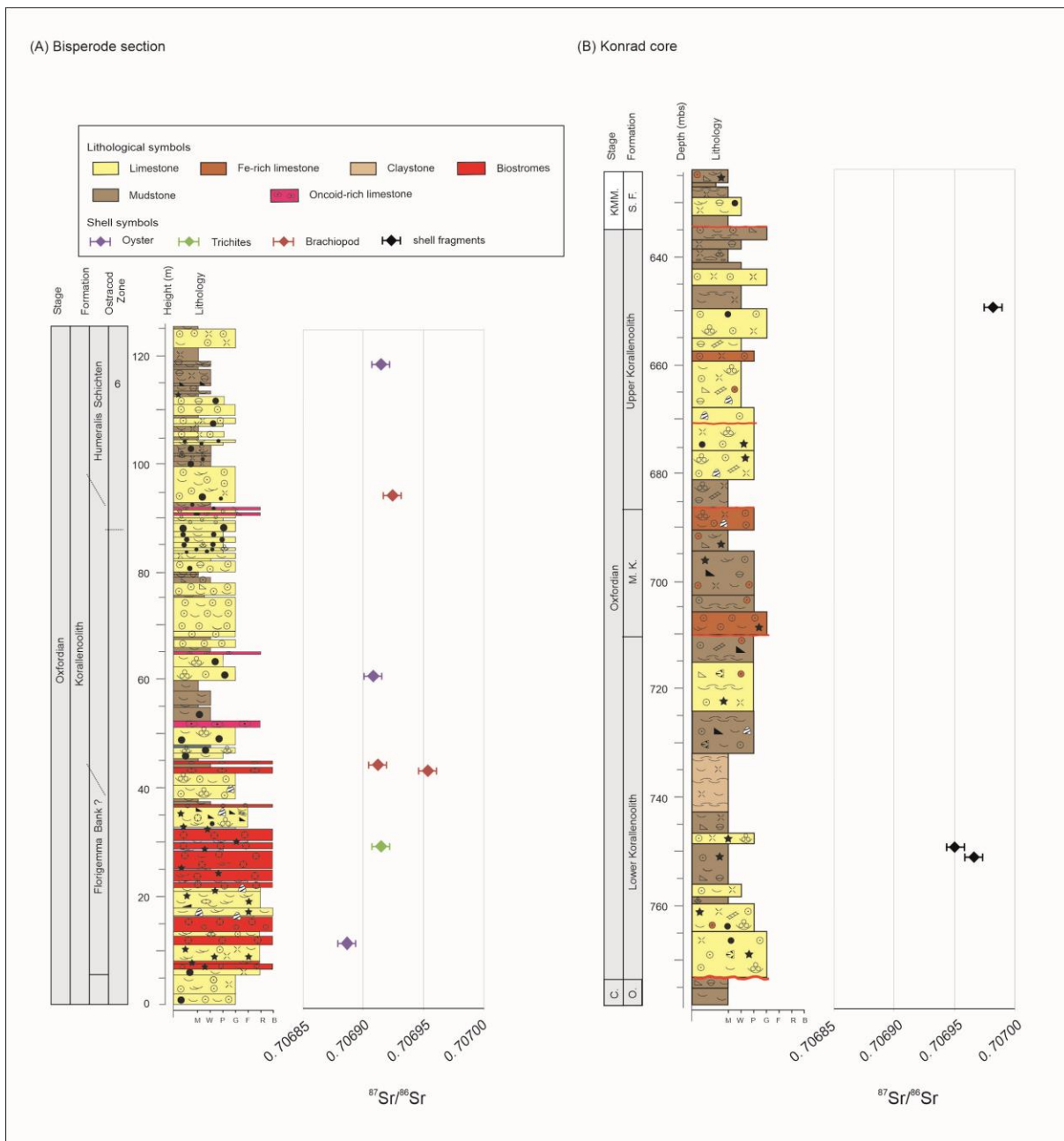


Fig. 9. Lithostratigraphy versus $^{87}\text{Sr}/^{86}\text{Sr}$ ratios of selected calcite shell materials for (A) Bisperode section and (B) Konrad #101 core. For details of sedimentary log symbols, see Chapter 2 and Chapter 3.

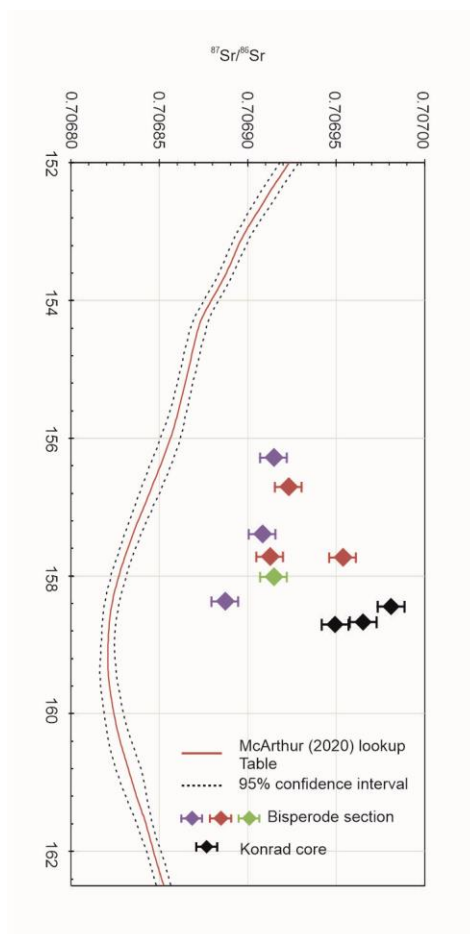


Fig. 10. Analyzed $^{87}\text{Sr}/^{86}\text{Sr}$ ratios obtained from the Oxfordian Korallenoolith Fm. (Bisperode section and Konrad #101 core, LSB) compared to the LOWESS best-fit curve of McArthur et al. (2020). Y-axis shows age in millions of years.

4.6.3 Regional factors affecting mollusc shell $^{87}\text{Sr}/^{86}\text{Sr}$ ratios and their implications

During the Oxfordian stage, the LSB was surrounded by emerged land masses (incl. the Ringkøbing Fyn High to the north and the London-Brabant, Rhenish, and Bohemian massifs to the south). The marine waters of the LSB could have been easily affected by the input of freshwaters carrying a continental radiogenic Sr-isotope signature to the basin. The deposition of the Korallenoolith Fm. occurred coeval to changes in climatic conditions, forcing the erosion of the hinterland and leading to increased nutrient input into the depositional setting (Gramann et al. 1997; Kästner et al. 2010). This could have significantly influenced the $^{87}\text{Sr}/^{86}\text{Sr}$ composition of local marine waters, in particular in areas close to freshwater discharge. Consequently, inputs of more radiogenic Sr from rivers (continental flux with high radiogenic $^{87}\text{Sr}/^{86}\text{Sr}$ ratios) may have resulted in slightly more radiogenic Sr-isotope ratios in the analyzed shell materials. In the LSB, all the measured $^{87}\text{Sr}/^{86}\text{Sr}$ ratios are highly radiogenic compared to Oxfordian global open ocean $^{87}\text{Sr}/^{86}\text{Sr}$ isotopic signatures (McArthur et al. 2020). Hence, the observed pattern from the LSB is best assigned to freshwater mixing. Alteration due to diagenetic

Chapter 4

fluids is an alternative explanation for the slightly more radiogenic values observed in the shell calcite. The LSB underwent tectonic inversion (Ziegler, 1987, 1995; Sippel et al., 2009; Kneucker et al. 2020), which was accompanied by to strong uplift, the development of fracture systems and salt diapirism, which all together could have enhanced fluid flow and sediment alteration. However, the strong diagenetic overprint of the studied shell material is not supported by the good structural preservation of shell calcite and by the trace element result.

4.7 Conclusions

In this paper, we present a new calcite shell-based $^{87}\text{Sr}/^{86}\text{Sr}$ data-set based on well-preserved skeletal materials. The new $^{87}\text{Sr}/^{86}\text{Sr}$ values stem from low-Mg calcite brachiopods, oysters, and *trichites* bivalves and are within the range of values reported for Late Jurassic seawater. However, closer inspection shows a distinct deviation from the Oxfordian marine Sr-isotope signal, indicating that the depositional setting was probably influenced by freshwaters with a continental Sr-isotope signature. The analysed shells may have captured local, more radiogenic $^{87}\text{Sr}/^{86}\text{Sr}$ signatures derived from riverine waters. Our $^{87}\text{Sr}/^{86}\text{Sr}$ results indicate that shells from shallow marine settings showing no diagenetic overprint can still show deviation from the normal marine Sr isotope signature.

4.8 Acknowledgments

This research was supported by a CSC scholarship (201808510183) granted and by an LUH Ph.D. completion grant to Deyan Zhang. Alexandra Rühmkorf is thanked for her support with the preparation of petrographic thin-section. The authors thank Philipp Ulke for collecting the shell fragments from Konrad #101 core, and Dr. Michael Schramm from the BGR for access to the Konrad #101 core. Professor Stéphane Bodin is thanked for his support of the cathodoluminescence microscope access.

4.9 References

- Al-Aasm, I.S., & Veizer, J. (1986). Diagenetic Stabilization of Aragonite and Low-mg Calcite, I. Trace Elements in Rudists. *Journal of Sedimentary Research*, 56, 138–152.
- Berg, H.P., Brennecke, P.W., Thomauske, B.R. (1987). The German Konrad repository project, *Progress in Nuclear Energy*, 20, 255–307.
- Betz, D., Führer, F., Greiner, G., & Plein, E.M. (1987). Evolution of the Lower Saxony Basin. *Tectonophysics*, 137, 127–170.
- Betzler C., Pawellek T., Abdullah M., Kossler A. (2007). Facies and stratigraphic architecture of the Korallenoolith Formation in North Germany (Lauensteiner Pass, Ith Mountains). *Sediment Geol* 194:61–75.
- Brand, U., Jiang, G., Azmy, K., Bishop, J.W., & Montañez, I.P. (2012). Diagenetic evaluation of a Pennsylvanian carbonate succession (Bird Spring Formation, Arrow Canyon, Nevada, U.S.A.) — 1: Brachiopod and whole rock comparison. *Chemical Geology*, 308, 26–39.
- Brand, U., Logan, A., Bitner, M.A., Griesshaber, E., Azmy, K., Buhl, D. (2011). What is the ideal proxy of Palaeozoic seawater chemistry? *Mem. Assoc. Austral. Palaeontolog.* 41, 9–14.

- Brand, U., & Veizer, J. (1980). Chemical Diagenesis of a Multicomponent Carbonate System--1: Trace Elements. *Journal of Sedimentary Research*, 50, 1219–1236.
- Brigaud, B., Durllet, C., Deconinck, J.F., Vincent, B., Pucéat, E., Thierry, J., & Trouiller, A. (2009). Facies and climate/environmental changes recorded on a carbonate ramp: A sedimentological and geochemical approach on Middle Jurassic carbonates (Paris Basin, France). *Sedimentary Geology*, 222, 181–206.
- Bruhn, F., Veizer, J., Buhl, D., & Meijer, J. (2005). Diagenetic history of the Korallenoolith (Malm) of northwestern Germany: Implications from in-situ trace element and isotopic studies. *Nuclear Instruments & Methods in Physics Research Section B-beam Interactions With Materials and Atoms*, 231, 518–523.
- Carter, J. G. (1990). Evolutionary significance of shell microstructure in the Palaeotaxodonta, Pteriomorpha and Isofilibranchia (Bivalvia: Mollusca). *Skeletal biomineralization: patterns, processes and evolutionary trends*, 1, 135–296.
- Cäsar S. (2012). Sequenzstratigraphie und sedimentologie oberjurassischer Karbonate von Norddeutschland (Oxfordium/Kimmeridgium, Niedersächsisches Becken). Dissertation, Universität Hamburg.
- Faure, G. (1977). *Principles of isotope geology*.
- Fischer, R. (1991). Die Oberjura-Schichtfolge vom Langenberg bei Oker. *Arbeitskreis Paläontologie Hannover*, pp. 21–36.
- Frijia, G., Parente, M., Lucia, M.D., & Mutti, M. (2015). Carbon and strontium isotope stratigraphy of the Upper Cretaceous (Cenomanian-Campanian) shallow-water carbonates of southern Italy: Chronostratigraphic calibration of larger foraminifera biostratigraphy. *Cretaceous Research*, 53, 110–139.
- Geldern, R.V., Joachimski, M.M., Day, J., Jansen, U., Alvarez, F., Yolkin, E.A., & Ma, X. (2006). Carbon, oxygen and strontium isotope records of Devonian brachiopod shell calcite. *Palaeogeography, Palaeoclimatology, Palaeoecology*, 240, 47–67.
- Gervais. (1987). Die Brachiopoden aus dem niedersächsischen Malm der Sammlung Hubert REIM. *Arbeitskreis Paläontologie Hannover*, pp. 76–80.
- Gramann F., Heunisch C., Klassen H., Kockel F., Dulce G., Harms F., Katschorek T., Mönning E., Schudack M., Schudack U., Thies D., Weiss M. (1997). Das Niedersächsische Oberjura-Becken-Ergebnisse Interdisziplinärer Zusammenarbeit. *Zeitschrift der Deutschen Geologischen Gesellschaft* 148:165–236.
- Heimhofer, U., Hochuli, P.A., Burla, S., Oberli, F., Adatte, T., Dinis, J., & Weissert, H. (2012). Climate and vegetation history of western Portugal inferred from Albian near-shore deposits (Galé Formation, Lusitanian Basin). *Geological Magazine*, 149, 1046–1064.
- Helm, C., Schülke, I., Fischer, I. (2001). Paläobiogeographie des Korallenooliths (Mittleres Oxfordium Unteres Kimmeridgium): Tethyale Faunen- und Florenelemente auf höherer Paläobreite (Niedersächsisches Becken, NW-Deutschland). *Geologische Beiträge Hannover*, 2:51–64.
- Helm, C., Reuter, M., Schülke, I. (2003). Die Korallenfauna des Korallenooliths (Oxfordium, Oberjura, NW-Deutschland): Zusammensetzung, Stratigraphie und regionale Verbreitung. *Paläontologische Zeitschrift* 77:77–94.

Chapter 4

- Horikx, M., Heimhofer, U., Dinis, J., & Huck, S. (2014). Integrated stratigraphy of shallow marine Albian strata from the southern Lusitanian Basin of Portugal. *Newsletters on Stratigraphy*, 47, 85–106.
- Huck, S., Heimhofer, U., Rameil, N., Bodin, S., & Immenhauser, A. (2011). Strontium and carbon-isotope chronostratigraphy of Barremian–Aptian shoal-water carbonates: Northern Tethyan platform drowning predates OAE 1a. *Earth and Planetary Science Letters*, 304, 547–558.
- Immenhauser, A., Schöne, B.R., Hoffmann, R., & Niedermayr, A. (2016). Mollusc and brachiopod skeletal hard parts: Intricate archives of their marine environment. *Sedimentology*, 63(1), 1–59.
- Jach, R., Djerić, N., Goričan, Š., & Reháková, D. (2014). Integrated stratigraphy of the Middle–Upper Jurassic of the Krížna Nappe, Tatra Mountains. *Annales Societatis Geologorum Poloniae*, 84, 1–33.
- Jenkyns, H.C., Jones, C.E., Gröcke, D.R., Hesselbo, S.P., & Parkinson, D.N. (2002). Chemostratigraphy of the Jurassic System: applications, limitations and implications for palaeoceanography. *Journal of the Geological Society*, 159, 351–378.
- Jones, C.E., & Jenkyns, H.C. (2001). Seawater strontium isotopes, oceanic anoxic events, and seafloor hydrothermal activity in the Jurassic and Cretaceous. *American Journal of Science*, 301, 112–149.
- Kästner, M., Schülke, I., Winsemann, J., & Böttcher, J. (2010). High-resolution sequence stratigraphy of a Late Jurassic mixed carbonate-siliciclastic ramp, Lower Saxony Basin, Northwestern Germany. *Zeitschrift Der Deutschen Gesellschaft Für Geowissenschaften*, 161, 263–283.
- Kästner, M., Schülke, I., & Winsemann, J. (2008). Facies architecture of a Late Jurassic carbonate ramp: the Korallenoolith of the Lower Saxony Basin. *International Journal of Earth Sciences*, 97, 991–1011.
- Kneucker, T., Blumenberg, M., Strauss, H., Dohrmann, R., Hammer, J., & Zulauf, G. (2020). Structure, kinematics and composition of fluid-controlled brittle faults and veins in Lower Cretaceous claystones (Lower Saxony Basin, Northern Germany): Constraints from petrographic studies, microfabrics, stable isotopes and biomarker analyses. *Chemical Geology*, 540, 119501.
- Korte, C., Jasper, T., Kozur, H.W., Veizer, J., (2006). $^{87}\text{Sr}/^{86}\text{Sr}$ record of Permian seawater. *Palaeogeography, Palaeoclimatology, Palaeoecology*, 240 (1–2), 89–107.
- Luppold, F.W. (2003). Neue und seltene Index-Foraminiferen und-Ostrakoden aus dem Jura NW-Deutschlands. *Senckenb Lethaea*, 83:15–37.
- Mazur, S., Scheck-Wenderoth, M., & Krzywiec, P. (2005). Different modes of the Late Cretaceous–Early Tertiary inversion in the North German and Polish basins. *International Journal of Earth Sciences*, 94, 782–798.
- McArthur, J.M., Howarth, R.J., Bailey, T.R. (2001). Strontium Isotope Stratigraphy LOWESS Version 3: best fit to the Marine Sr-isotope curve for 0-509 Ma and accompanying look-up table for deriving numerical age. *The Journal of Geology*, 109, 155–170.
- McArthur, J.M., Howarth, R.J., Shields, G.A. (2012). Strontium isotope stratigraphy. In: Gradstein, F.M., Ogg, J.G., Schmitz, M.D., Ogg, G.M. (Eds.), *The Geological time scale*.
- McArthur, J.M., Howarth, R.J., Shields, G.A., Zhou, Y. (2020). Strontium Isotope Stratigraphy. *Geologic Time Scale 2020*, 211–238.
- Meknassi, S.E., Dera, G., Cardone, T., Rafélis, M.D., Brahmi, C., & Chavagnac, V. (2018). Sr isotope ratios of modern carbonate shells: Good and bad news for chemostratigraphy. *Geology*, 46(11), 1003–1006.

- Mudroch, A., Thies D. (1996). Knochenfchzähne (Osteichthyes, Actin opterygii) aus dem Oberjura (Kimmeridgian) des Langenbergs bei Oker (Norddeutschland). *Geologica Palaeontologica*, 30:239–265.
- Popp, B.N., Podosek, F.A., Brannon, J.C., Anderson, T.F., & Pier, J.G. (1986). $^{87}\text{Sr}/^{86}\text{Sr}$ ratios in Permian-Carboniferous sea water from the analyses of well-preserved brachiopod shells. *Geochimica et Cosmochimica Acta*, 50, 1321–1328.
- Rais, P. (2007). Evidence for a major paleoceanographic reorganization during the Late Jurassic; insights from sedimentology and geochemistry. Diss. Naturwissenschaften, Eidgenössische Technische Hochschule ETH Zürich, Nr. 16932: 149 p.
- Schmitt, K.E., Huck, S., Krummacker, M., de Winter, N.J., Godet, A., Claeys, P., & Heimhofer, U. (2022). Radiolitic rudists: an underestimated archive for Cretaceous climate reconstruction? *Lethaia*, 55(4), pp.1–21.
- Schmitt, K.E., Heimhofer, U., Frijia, G., Lucia, M.D., & Huck, S. (2020). Deciphering the fragmentary nature of Cretaceous shallow-water limestone archives: A case study from the subtropical Apennine carbonate platform. *Newsletters on Stratigraphy*, 53, 389–413.
- Schneider, S., Fürsich, F.T., & Werner, W. (2009). Sr-isotope stratigraphy of the Upper Jurassic of central Portugal (Lusitanian Basin) based on oyster shells. *International Journal of Earth Sciences*, 98, 1949–1970.
- Schudack, U. (1994). Revision, Dokumentation und Stratigraphie der Ostracoden des Nordwestdeutschen Oberjura und Unter-Berriasium. *Berliner geowissenschaftliche Abhandlungen*, E11, 1–193.
- Senglaub, Y., Littke, R., & Brix, M.R. (2006). Numerical modeling of burial and temperature history as an approach for an alternative interpretation of the Bramsche anomaly, Lower Saxony Basin. *International Journal of Earth Sciences*, 95, 204–224.
- Sippel, J., Scheck-Wenderoth, M., Reicherter, K., & Mazur, S. (2009). Paleostress states at the southwestern margin of the Central European Basin System—Application of fault-slip analysis to unravel a polyphase deformation pattern. *Tectonophysics*, 470, 129–146.
- Van Hinsbergen, D.J., de Groot, L.V., van Schaik, S.J., Spakman, W., Bijl, P.K., Sluijs, A., Langereis, C.G., & Brinkhuis, H. (2015). A Paleolatitude Calculator for Paleoclimate Studies. *PLoS ONE*, 10.
- Veizer, J., Ala, D., Azmy, K., Bruckschen, P., Buhl, D., Bruhn, F., Carden, G.A., Diener, A., Ebner, S., Goddérís, Y., Jasper, T., Korte, C., Pawellek, F., Podlaha, O.G., & Strauss, H. (1999). $^{87}\text{Sr}/^{86}\text{Sr}$, $\delta^{13}\text{C}$ and $\delta^{18}\text{O}$ evolution of Phanerozoic seawater. *Chemical Geology*, 161, 59–88.
- Wang, W., Garbelli, C., Zheng, Q., Chen, J., Liu, X., Wang, W., & Shen, S. (2018). Permian $^{87}\text{Sr}/^{86}\text{Sr}$ chemostratigraphy from carbonate sequences in South China. *Palaeogeography, Palaeoclimatology, Palaeoecology*, 500, 84–94.
- Wang, W., Garbelli, C., Zhang, F., Zheng, Q., Zhang, Y., Yuan, D., Shi, Y., Chen, B., & Shen, S. (2020). A high-resolution Middle to Late Permian paleotemperature curve reconstructed using oxygen isotopes of well-preserved brachiopod shells. *Earth and Planetary Science Letters*, 540, 116245.
- Wang, W., Katchinoff, J.A., Garbelli, C., Immenhauser, A., Zheng, Q., Zhang, Y., Yuan, D., Shi, Y., Wang, J., Planavsky, N.J., & Shen, S. (2021). Revisiting the Permian seawater $^{87}\text{Sr}/^{86}\text{Sr}$ record: New perspectives from brachiopod proxy data and stochastic oceanic box models. *Earth-Science*

Chapter 4

Reviews, 218, 103679.

- Weiß, M. (1995). Stratigraphie und Mikrofauna im Kimmeridge SE-Niedersachsens unter besonderer Berücksichtigung der Ostracoden. *Clausthaler Geowissenschaftliche Dissertationen*, 48:1–274.
- Wierzbowski, H. (2015). Seawater temperatures and carbon isotope variations in central European basins at the Middle–Late Jurassic transition (Late Callovian–Early Kimmeridgian). *Palaeogeography, Palaeoclimatology, Palaeoecology*, 440, 506–523.
- Wierzbowski, H., Anczkiewicz, R., Pawlak, J., Rogov, M.A., & Kuznetsov, A. (2017). Revised Middle–Upper Jurassic strontium isotope stratigraphy. *Chemical Geology*, 466, 239–255.
- Zaky, A.H., Brand, U., Buhl, D., Blamey, N.J., Bitner, M.A., Logan, A., Gaspard, D., & Popov, A.M. (2019). Strontium isotope geochemistry of modern and ancient archives: tracer of secular change in ocean chemistry. *Canadian Journal of Earth Sciences*, 56(3), 245–264.
- Zhang et al. (2023). Carbonate microfacies and transgressive-regressive sequences of Oxfordian shallow water limestones (Korallenoolith, Lower Saxony Basin).
- Ziegler P. A. (1990). *Geological Atlas of Western and Central Europe*. 2nd Edition, Shell International Petroleum Mij. B.V. and Geological Society, London.
- Ziegler, P. A. (1987). Late Cretaceous and Cenozoic intra-plate compressional deformations in the Alpine foreland—a geodynamic model. *Tectonophysics*, 137, 389–420.
- Ziegler, P.A. (1995). Geodynamics of compressional intra-plate deformations: a comparison with the Alpine foreland. *Nova Acta Leopoldina* 291, 265–300.
- Zuo, F., Heimhofer, U., Huck, S., Luppold, F.W., Wings, O., & Erbacher, J. (2018). Sedimentology and depositional sequences of a Kimmeridgian carbonate ramp system, Lower Saxony Basin, Northern Germany. *Facies* 64:1–25.
- Zuo, F., Heimhofer, U., Huck, S., Bodin, S., Erbacher, J., & Bai, H. (2018). Coupled $\delta^{13}\text{C}$ and $^{87}\text{Sr}/^{86}\text{Sr}$ chemostratigraphy of Kimmeridgian shoal-water deposits: A new composite record from the Lower Saxony Basin, Germany. *Sedimentary Geology*, 376, 18–31.

5. Carbon isotope stratigraphy of an Oxfordian carbonate ramp system, Lower Saxony Basin, Northern Germany

Deyan Zhang, François-Nicolas Krencker, Stefan Huck, Ulrich Heimhofer

Institute of Geology, Leibniz University Hannover, Germany

5.1 Abstract

Shallow carbonate deposits represent highly sensitive ecological systems and can provide valuable information for understanding the climate system and sea-level changes in the geological past. However, decoding these archives can be challenging due to the low stratigraphic resolution achieved through biostratigraphy. This is particularly the case for the Late Jurassic carbonate deposits of the Lower Saxony Basin, where the lack of typical index fossils hinders precise correlations between different sections. Carbon isotope ($\delta^{13}\text{C}$) stratigraphy has been applied as a reliable tool for comparing and calibrating biostratigraphic schemes on both, local and global scales. In this study, high-resolution $\delta^{13}\text{C}$ analyses of bulk carbonate from three outcrop sections are investigated and a $\delta^{13}\text{C}$ chemostratigraphy correlation panel is presented for the Oxfordian Korallenoolith Formation. The chemostratigraphic data presented here enable the confirmation and refinement of the pre-existing biostratigraphic data and the establishment of a composite high-resolution stratigraphic framework enhancing the correlation ability between the western and eastern part of the LSB. Overall, this framework allows also to better comprehend what might have been the impact of the carbon cycle disturbances on the Late Jurassic shallow-marine carbonate systems.

Keywords: Shallow-water carbonates, Carbon isotope stratigraphy, Oxfordian, Lower Saxony Basin

5.2 Introduction

During the Oxfordian stage (154.8-161.5 Ma, Gradstein et al. 2020), the Lower Saxony Basin (LSB) was covered by a shallow epicontinental sea under a subtropical climate (Ziegler, 1990). The shallow-marine deposits are sedimentary successions composed of alternating limestones, marls, and recifal carbonates and correspond to the Korallenoolith Formation (Fm.). Despite multiple biostratigraphic schemes that have been developed over the years, the detailed stratigraphy and subdivision of the Upper Jurassic rocks of the LBS are still poorly defined (Schudack, 1994; Weiß, 1995; Gramann et al., 1997; Mudroch et al., 1999; Luppold, 2003). The shallow-marine strata lack typical open-marine index fossils and the prevalence of sedimentary gaps in the Korallenoolith Fm. further hampers any lithostratigraphic subdivision of the Korallenoolith sequence (Gramann et al. 1997). As ammonites are very scarce or lacking, other biostratigraphic schemes have been developed, including schemes based on ostracods, benthic foraminifera, charophytes, terrestrial and marine palynomorphs, and vertebrate remains (e.g., Schudack, 1994; Weiß, 1995; Gramann et al., 1997; Mudroch et al., 1999; Luppold, 2003). However, most of those organism groups are endemic, and due to the facies-controlled restriction, any correlation on a supra-regional and/or global scale remains ambiguous and imprecise (Jach et al., 2014). As a result, a precise stratigraphic age assignment of the Korallenoolith Fm. in the LSB is still difficult, although some excellent Upper Jurassic sections are exposed in the LSB, including the Bisperode section (Ith syncline), the Osterwald section and the outcrops of the Langenberg quarry.

Carbon isotope ($\delta^{13}\text{C}$) records obtained from Mesozoic shallow-water carbonates have been widely used as a proxy for secular changes in ocean chemistry. Unfortunately, carbonate $\delta^{13}\text{C}$ signatures derived from shallow-water settings are often afflicted with large uncertainties, compared with hemipelagic and pelagic succession (Huck et al., 2011; Horikx et al., 2014; Frijia et al., 2015; Huck and Heimhofer, 2015; Bover-Arnal et al., 2016; Zuo et al. 2018). Post-depositional diagenetic alteration and/or environmental controls on the $\delta^{13}\text{C}$ signature need to be treated carefully. In addition, shallow-water carbonates may record local seawater carbon isotope signatures (Patterson and Walter, 1994; Immenhauser et al., 2003), and the signals extracted from shallow-water carbonates, especially those from lagoonal and peritidal settings, make the application of carbon isotope stratigraphy even more challenging (Coimbra et al., 2016). Despite these obstacles, many studies using $\delta^{13}\text{C}$ values from shallow marine carbonates demonstrate the preservation of a global marine carbon isotope signature and support a correlation between shallow-water and deep-water successions for stratigraphic purposes (Vahrenkamp, 1996; Weissert et al. 1998; Glumac and Walker, 1998; Grötsch et al.1998; Huck et al. 2011; Buonocunto et al. 2002; Immenhauser et al. 2002; Krullet al. 2004; Swart and Eberli, 2005; Huck and Heimhofer 2015; Coimbra et al., 2016; Huck et al. 2017; Zuo et al. 2018). Most studies focus on characteristic isotope signatures and stratigraphic trends rather than on absolute values (Immenhauser et al. 2003; Huck et al. 2011).

Chemostratigraphic studies dealing with Oxfordian strata are comparatively rare, and only a limited amount of carbon isotope data is currently available (Wierzbowski et al., 2017). During this time period, the western European archipelago and its adjacent shallow seas experienced significant ecological changes, expressed in the onset of widespread carbonate sedimentation and the global spread of coral

reefs (Leinfelder 2001; Helm et al. 2001; Betzler et al. 2007; Martin-Garin et al. 2012). However, precise dating and correlation of such changes in carbonate platform ecology at different sites (e. g. Jura Mountains, North German basin, Paris basin, England Yorkshire and Cambridgeshire) are problematic due to insufficient temporal resolution (Helm et al. 2003a).

In the LSB, regional synsedimentary salt tectonism and induced fluctuations in sedimentation rates complicate stratigraphic comparison and correlation with the Boreal Ocean during the Oxfordian (Hoyer, 1965; Betz et al. 1987; Gramann et al., 1997). The combination of chemostratigraphic (carbon isotopes) data with biostratigraphic information represents a promising approach to better date and correlate strata across different local depositional environments (Huck et al. 2011; Horikx et al. 2014; Frijia et al. 2015; Schmitt et al. 2020).

Up to now, some high-resolution carbon isotope stratigraphic records have been established for the Upper Jurassic strata of the LSB (Kästner et al., 2010; Bai et al. 2017; Zuo et al. 2018), but only Zuo et al. (2018) used chemostratigraphy to establish a refined stratigraphic framework for the investigated successions. Carbon isotope records covering the Oxfordian deposits within the LSB are scarce, with only three publications reporting continuous carbon isotope curves from outcrop or core material (Kästner et al., 2010; Bai et al. 2017, 2020), and a convincing carbon isotope-based intrabasinal correlation of the Korallenoolith Fm. across the LSB is still lacking. In this study, new data from the lower part of the Bisperode section, the lower Langenberg section, the Osterwald section, and the Konrad #101 core will be compared with existing data sets from the Eulenflucht 1 (Heunisch and Luppold, 2015; Bai et al., 2017). The overall objective of this study is the development of a high-resolution carbon isotope stratigraphic record for Oxfordian successions in the LSB. The new and refined correlation will shed light on the stratigraphic development of the Korallenoolith depositional system within the LSB and beyond.

5.3 Geological setting

The LSB located on the southern margin of the Central European Basin is one of several rift- and wrench-induced “marginal troughs”, that formed a series of E-W trending horst-and-graben structures (Voigt 1962; Betz et al., 1987; Ziegler 1990; Senglaub et al., 2006). The LSB has a length of ~300 km and a width of ~65 km and was bordered by the Rhenish Massif to the S and the Ringkøbing-Fyn High to the N (Zuo et al. 2018) (Fig. 1a). Sediment thickness reaches a maximum of ~4000 m (Betz et al. 1987; Kästner et al., 2010). Stratigraphic sections located on the uplifted horst regions may contain fewer small- and medium-scale cycles compared to the adjacent graben areas (Kästner et al. 2008). During the Oxfordian, the LSB was located at a palaeolatitude of about ~ 35°N (van Hinsbergen et al. 2015) and formed a tributary sea of the Tethys, which allowed the interchange of fauna and flora between the Boreal and the Tethyan realms (Helm et al. 2001; Căsar, 2012). Upper Jurassic deposits are mainly exposed in the E' part of the LSB with good and well accessible outcrops in the low mountain ranges of S' Lower Saxony. The studied stratigraphic sections include the Langenberg section, which is located in an active quarry about 5 km E of Goslar, the Bisperode section accessible in an abandoned quarry located about 2 km SW of the village Lauenstein, and the Osterwald section located in an abandoned quarry about 3 km SW of the village Springe Holtensen. The new results are compared with

Chapter 5

carbon isotope data from the scientific drill core Konrad #101, which was drilled close to the village Salzgitter-Beddingen (Fig. 1).

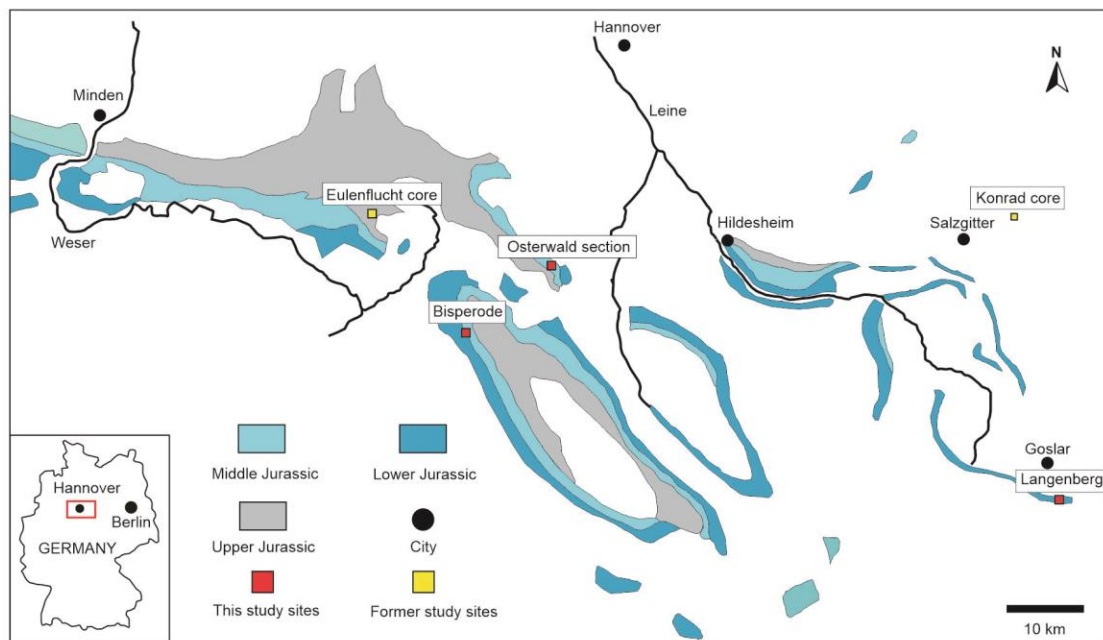


Fig. 1. Simplified geological map of Lower to Upper Jurassic strata cropping out in the central part of the southern Lower Saxony Basin. Locations of the investigated study sites and sites used for comparison are marked by red and yellow dots, respectively.

In the LSB, the Upper Jurassic succession includes the lithological units of the Upper Ornatenton Fm. (Callovia), Heersumer and Korallenoolith Fm. (Oxfordian), the Süntel Fm. (Kimmeridgian), Holzen Fm. and Eimbeckhausen Fm. (Tithonian). Focus of this study is on the limestones of the Oxfordian Korallenoolith Fm. (Middle to Late Oxfordian) (Fig. 2). The Korallenoolith Fm. consists predominantly of oolitic limestones with coral reef-bearing intercalations, assigned to a shallow-marine subtropical environment with limited terrestrial influx, which was deposited on a homoclinal carbonate ramp system (Helm et al. 2003; Betzler et al. 2007; Kästner et al. 2008; Cäsar et al. 2012; Zuo et al. 2018).

The biostratigraphic subdivision of the Upper Jurassic strata in Northern Germany was developed based on ammonites, ostracods, dinoflagellate cysts, charophytes, spores, and pollen (Schudack 1994; Weiß 1995; Gramann et al. 1997; Hardenbol et al. 1998). Due to the rare occurrence of age-diagnostic ammonites, the Oxfordian strata in the LSB is divided based on ostracods with the ostracod zones 1 to 8 covering the Ornatenton Fm. (zone 1), the Heersumer Fm. (zones 2 and 3), and the Korallenoolith Fm. (zones 4 to 8). The correlation between the ostracod zones from Gramann et al. (1997) and the sub-boreal ammonite zones as well as the diachronous character of the lower and upper boundaries of the Korallenoolith Fm. are shown in Fig. 2.

| Stage | Boreal realm Hardenbol et al. (1998) | | Ostracod zonation (LSB) | Lithostratigraphy Northwest Germany | |
|--------------|---|------------------------|-------------------------------|--|-----------------------------|
| | Ammonites | Sequence | | | |
| Kimmeridgian | Cymodoce | JKi2 | Zone 9 | Süntel Fm | |
| | Baylei | JKi1 | Zone 8 | | |
| 154.8 | | JOx8 | Zone 7 | Humeralis-Schichten | |
| Oxfordian | Upper | Pseudocordata | JOx7 | Zone 6 | Upper Korallenoolith Fm. |
| | | | JOx6 | Zone 5 | |
| | | Cautisnigrae | | Zone 4 | |
| | Middle | Transversarium/Pumilus | JOx5 | Zone 3 | Lower |
| | | Plicatilis | JOx4 | | |
| | Lower | Cordarum | JOx3 | Zone 2 | Upper Lower |
| Mariae | | JOx1 | | | |
| 161.5 | | JCa6 | Zone 1 | Hersumer Fm. | |
| Callovian | Lamaerti | | | Ornatenton Fm. | |

Fig. 2. Lithostratigraphic scheme of the Late Jurassic and its correlation with the standard zonation of the sub-boreal ammonite provinces (modified from Gramann et al. 1997; Hardenbol et al. 1998; Schulze 1975; Gradstein and Ogg 2020) and Ostracod zonation (Schudack 1994; Weiß 1995).

5.4 Lithostratigraphy and carbonate facies description

5.4.1 Bisperode section

For the Bisperode section, we focus on the lower 126 m of the accessible section (Fig. 3), assigned to the Korallenoolith Fm. (Betzler et al. 2007; Cäsar 2012), detailed sedimentology and sequence-stratigraphy are presented in Chapter 2. The lowermost interval (0.0–5.5 m) are represented by thick-bedded oolitic grainstones with large-scale cross-bedding and abundant shell detritus. Above, (5.5–45.0 m) characterized by boundstone horizons alternate with bioclastic-rich rudstone. The boundstone layers show distinct variations in terms of growth form (ramose, flat sheet-like, dome-shaped, hemispheric) and texture of the dominant reef builders. and bioclastic-rich rudstone beds (>1 m thickness) typically show fining-upward units and trough cross-bedding. In the third interval (45.0–65.0 m), grain- and packstone textures dominate the succession, with some intervals showing a high portion (>50%) of large benthic agglutinated *Reophaecidae cf. Reophaex* foraminifera. The marl-limestone alternation intervals at 52.6–60.0 m, 99.5 m–103.5, and 112.5 m–121.5 m are characterized by wacke- to mudstone beds. The upper part of the section (66.0 to 125.5 m) is essentially composed of ooid-rich pack- and grainstones with intercalations of bioclastic-rich wackestone.

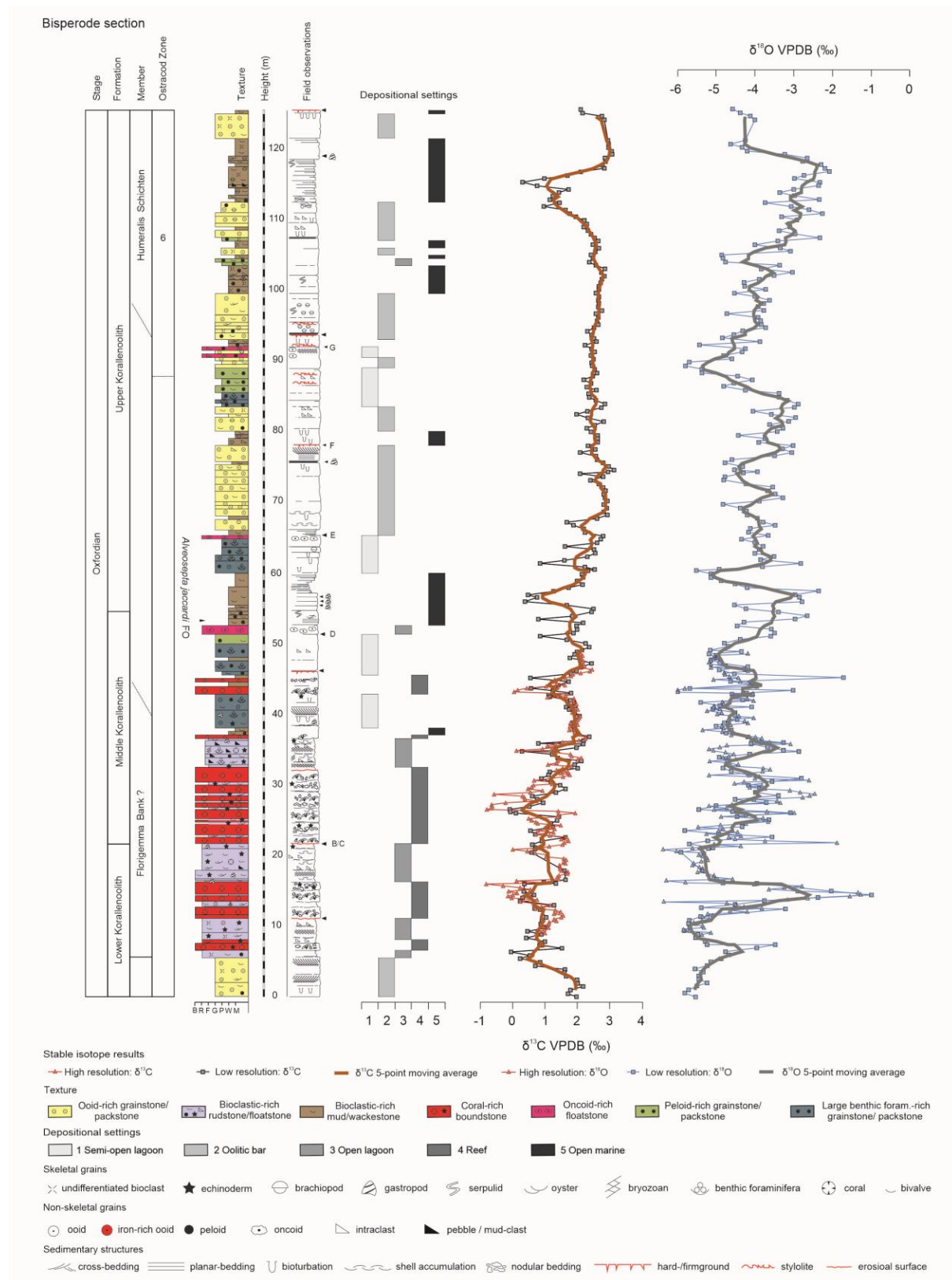


Fig. 3. Lithostratigraphy, sedimentological observations, erosional profile, inferred depositional settings, $\delta^{13}\text{C}$ and $\delta^{18}\text{O}$ values of the Bisperode section illustrated against stratigraphic height (m).

5.4.2 Osterwald section

Based on characteristic microfacies associations, biota content, and the position of discontinuity surfaces, the 46 m thick Osterwald section can be divided into 3 stratigraphic members (Mbs.) (Helm et al. 2003) (Fig. 4). The lower part is assigned to the Ahrensberg-Mb. (0.0–26.0 m), which is composed of two types of lithologies. The basal, 4 m thick part is composed of alternating thick grainstone beds alternating with thin marly layers, containing abundant fossil fragments incl. echinoderms, oysters, serpulids, plant remains, and rarely belemnites. This interval characterizes the very base of the Korallenoolith Fm. and its transition towards the underlying Heersum Fm. (Kaiser 1979; Schormann and Zawischa 1990). The upper 22 m thick part is composed of high-energy shoal limestones, which are represented by thick-bedded grainstones with large-scale cross-bedding and abundant shell detritus (echinoderm and mollusk fragments). This interval is bound by a hardground with strong bioturbation and high fossil density. The middle Hainholz Mb. (26.0–38.0 m) includes coral boundstones, intercalated with reef flank bioclastic rud- to floatstones. The boundstone intervals are dominated by flat, sheet-like, and strongly recrystallized corals, often showing abundant bioerosion features (for more details see Helm et al. 2003). The uppermost Barenburg-Member (38.0–46.0 m) is made up of ooid-rich packstones. In this study, the focus is on Ahrensberg and Hainholz Mbs. A detailed sedimentological study incl. a sequence-stratigraphic interpretation of the Osterwald section is provided by Helm et al. (2003).

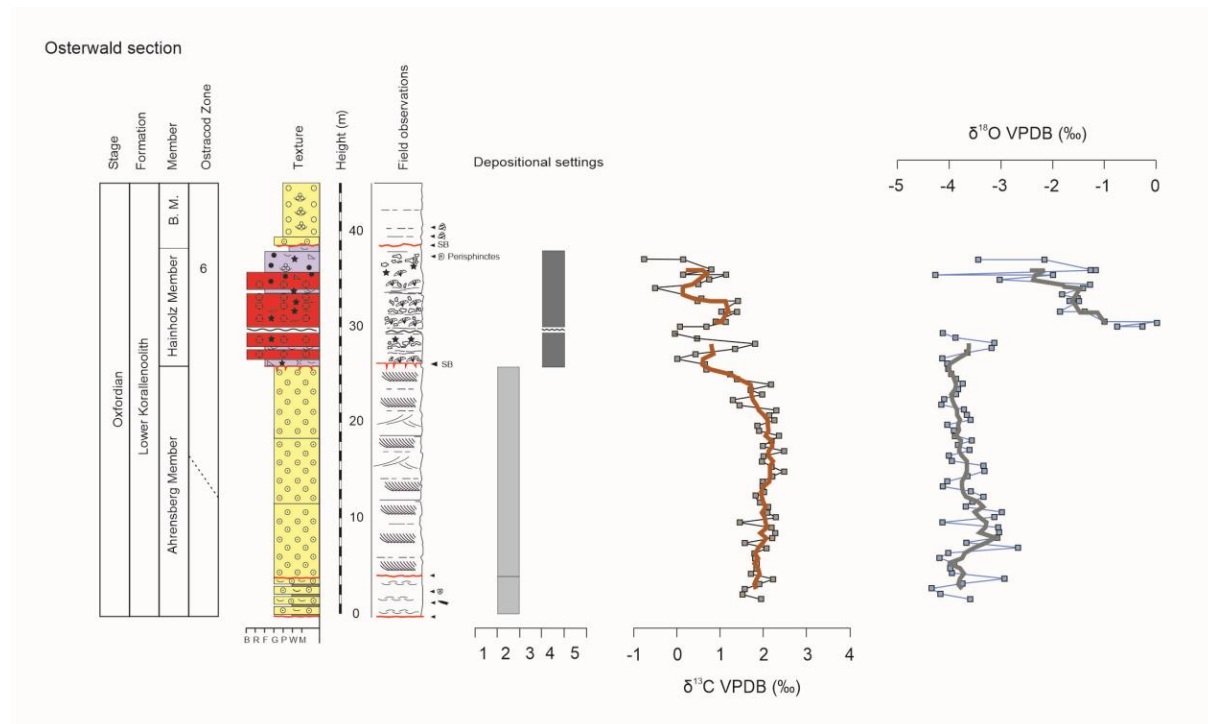


Fig. 4. Lithostratigraphy, sedimentological observations, erosional profile, inferred depositional settings, $\delta^{13}\text{C}$ and $\delta^{18}\text{O}$ values of the Osterwald section illustrated against stratigraphic height (m).

5.4.3 Langenberg section

In the studied part of the Langenberg section, 3 different lithostratigraphic units were identified within the 16 m thick section of the Korallenoolith Fm. (Fig. 4). The lowermost interval (0.0–2.0 m) is characterized by a thin-bedded, dark-grey clay to marlstone with rare shell fragments. This unit is bound by an erosional surface and overlain sharply by the second unit (2.0–10.0 m). This unit is mainly composed of well-developed oncoides, with individual beds showing large-scale cross-bedding and abundant shell fragments (bivalve and serpulid fragments), rare quartz, and Fe-rich peloids. Above, unit 3 (10.0–14.0 m) is characterized by thick-bedded oolitic grainstones. Common sedimentary features include cross-bedding, channel structures, and burrows. The fossil content in unit 3 comprises allochthonous macrofauna (echinoderms, bivalve shells) as well as abundant unidentified shell fragments. Unit 4 (14.0–16.0 m) is again composed of well-developed oncoides, similar to unit 2. The uppermost unit 5 (16.0–19.0 m) is made up of thick-bedded oolitic grainstones, which resemble unit 4.

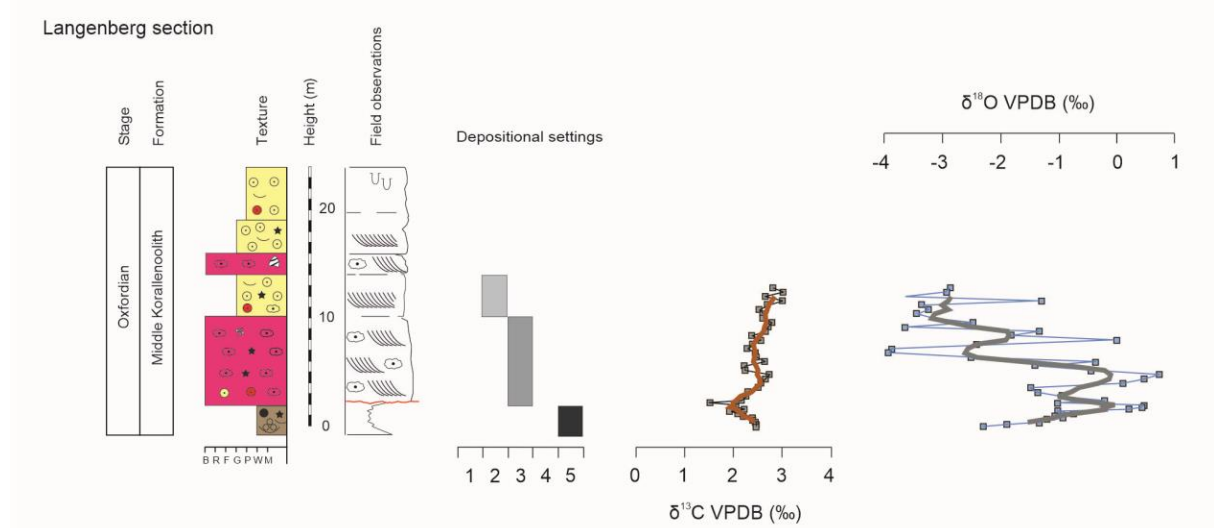


Fig. 5. Lithostratigraphy, sedimentological observations, erosional profile, inferred depositional settings, $\delta^{13}\text{C}$ and $\delta^{18}\text{O}$ values of the Langenberg section illustrated against stratigraphic height (m).

5.5 Materials and methods

5.5.1 Fieldwork and sampling

Fieldwork was carried out in three well-accessible quarries. Individual sections were logged in stratigraphic order and on the scale of individual beds incl. detailed macroscopic descriptions. Bulk samples taken with the hammer and drilled powder samples were taken with a battery-driven driller. Samples were taken bed by bed with a sampling interval of ~0.5 m or less. Higher density sampling was performed across facies boundaries and discontinuities. A total of 257 bulk samples were collected across the ~126.0 m thick Bisperode section. In addition, 164 drilled powder samples were obtained from the lower part of the section (at a spacing of ~0.25 m) for comparison. In the ~46 m thick Osterwald section, 14 bulk rock samples and 53 drilled powder samples were collected. The ~16 m thick

Langenberg section was covered with 39 drilled powder samples. For limestone classification, the scheme of Dunham (1962), including the modifications by Embry and Klovan (1971), was used. Bulk samples were washed and air-dried on the sample shelves, and subsequently cut into slabs for petrographic thin-sections.

Bulk rock sample powders were obtained (i) directly in the field using a hand-held battery-driven driller (163 samples from Bisperode, 53 from Osterwald, 39 from Langenberg), (ii) in the laboratory using a vibrating ball mill (258 samples from Bisperode), (iii) in the laboratory using a micro-driller equipped with tungsten drill bits (37 from Osterwald).

5.5.2 Isotope analysis

Carbon and oxygen isotopic analyses were carried out on a total of 577 powder samples at the stable isotope laboratory of the Institute of Geology at Leibniz University Hannover, Germany. All sample powders were treated with 100% phosphoric acid at 72 °C for at least 45 min. Stable isotope analysis were conducted using a Thermo Fisher Scientific Gasbench II carbonate device connected to a Thermo Fisher Scientific Delta 5 Advantage isotope ratio mass spectrometer. Repeated analyses of certified carbonate standards (NBS 19, IAEACO-1, NBS 18, and Carrara Marble) show an external reproducibility of ≤ 0.06 ‰ for $\delta^{13}\text{C}$ and 0.08 ‰ for $\delta^{18}\text{O}$. Values are expressed in conventional delta notation relative to the Vienna-Pee Dee Formation belemnite (VPDB) international standard, in parts per mil (‰). For more details on the analytical procedure, we refer to Schmitt et al. (2020). For the purpose of chemostratigraphic correlation, a 5-point moving average stratigraphic trend was calculated from all measured carbon and oxygen isotope values ($\delta^{18}\text{O}$).

5.6 Stable isotope results

5.6.1 Bisperode section

The $\delta^{13}\text{C}$ record of the Bisperode section varies between -0.1 ‰ and 3.1 ‰ (mean: 1.6 ‰) and shows distinct variations across the studied section (Fig. 3). In general, carbon isotope fluctuations are stronger in the lower and middle Korallenoolith Fm. compared to the upper Korallenoolith Fm. The lower part (0.0–68.0 m) is characterized by alternating negative and positive shifts with $\delta^{13}\text{C}$ values ranging between -0.1 ‰ and 3.0‰, with a superimposed stepwise increase. In the upper part (68.0–109.0 m), the carbon isotope record shows a pronounced plateau with relatively stable values of ~ 2.5 ‰, and only the top part of the section (109.0–125.0 m) is characterized by a well-developed negative anomaly with an amplitude in the range of 1.5 ‰.

In more detail, the $\delta^{13}\text{C}$ trend in the lowermost interval (0.0–5.5 m) is characterized by a distinct negative $\delta^{13}\text{C}$ shift of ~ 2.2 ‰, which is followed by some robust oscillations (5.5–27 m) between -0.1 and 2 ‰. The overlying interval (27.0–38.5 m) exhibits a noticeable stepwise increase with values reaching up to 2.4 ‰. This is followed by a relatively stable trend (38.5–56.5 m), which is interrupted by several smaller-scale negative excursions. The above interval (56.5–70.0 m) is

Chapter 5

marked by a sharp negative shift (with an amplitude of 1.6 ‰) and then exhibits a stepwise increase to maximum values of up to 3.1 ‰. The following interval (70.0–99.0 m) is characterized by a distinct $\delta^{13}\text{C}$ plateau with values oscillating around 2.6 ‰. The uppermost segment (99.0–126.0 m) shows a gradual $\delta^{13}\text{C}$ decline, reaching a minimum as low as -0.1 ‰, followed by a sharp $\delta^{13}\text{C}$ increase (up to 3 ‰).

The $\delta^{18}\text{O}$ values from the Bisperode section vary significantly between -6.4 ‰ and -1 ‰ (mean: -4.3 ‰) (Fig. 3). The $\delta^{18}\text{O}$ record is characterized by high-amplitude fluctuations of up to 1.5 ‰ within 60 m of section (0.0–60.0 m). Overall, a trend towards less negative values is observed upsection.

5.6.2 Osterwald section

The $\delta^{13}\text{C}$ values of samples derived from the Osterwald section range between -0.8 ‰ and 2.5 ‰ (mean: 1.7 ‰) (Fig. 4). The lower part of the section (0.0–26.0 m) shows relatively stable $\delta^{13}\text{C}$ values, of ~2 ‰ with only minor oscillations. The subsequent segment (26.0–33.0 m) is characterized by a noticeable stepwise negative shift reaching values of ~0.5 ‰. The uppermost part (33.0–37.0 m) shows strong fluctuations around values of ~0.8 ‰.

The $\delta^{18}\text{O}$ values from the Osterwald section vary between 0 ‰ and -4.4 ‰ (mean: -3.7 ‰) (Fig. 4). The lower part (0.0–33.0 m) displays relatively negative values with a trend toward more negative values upsection. This contrasts with the upper segment (33.0–37 m), which shows the highest $\delta^{18}\text{O}$ values (0 ‰) at its base, followed by a gradual shift towards more negative values as low as -4.3 ‰.

5.6.3 Langenberg section

The $\delta^{13}\text{C}$ values of the Langenberg section show only minor variability and range between 1.4 ‰ and 3.0 ‰ (mean: 2.4 ‰) (Fig. 5). The lowermost part (0.0–2.0 m) is characterized by an apparent gradual decline, reaching 1.4 ‰. The overlying segment (2.0–13.0 m) shows a stepwise increase toward more positive $\delta^{13}\text{C}$ values reaching 3 ‰.

$\delta^{18}\text{O}$ values from the Langenberg section vary between -4 ‰ and +0.7 ‰ (mean: -1.6 ‰) and are characterised by strong fluctuations. Records a positive excursion (0.0–6.0 m) and then a stepwise negative shift (6.0–13 m) (Fig. 5).

5.7 Discussion

5.7.1 Reliability of the carbonate carbon and oxygen isotope data

In general, $\delta^{18}\text{O}$ values of shallow marine carbonates have to be treated with caution due to potential diagenetic modification (compared to carbon) given the rapid exchange with the oxygen from the surrounding pore fluids (Allan and Matthews, 1982; Banner and Hanson, 1990; Jenkyns et al. 1994; Immenhauser et al., 2002; Weissert et al., 2008; Huck et al. 2013). Meteoric as well as burial diagenesis can lead to concomitant decrease in the ^{18}O content of carbonate rocks (Colombié et al., 2011). This may explain why the analyzed $\delta^{18}\text{O}$ values depart from typical Late Jurassic marine $\delta^{18}\text{O}$

signatures derived from well-preserved Oxfordian belemnites (Padden 2001; Nunn and Price 2010; Price and Rogov 2009; Benito et al. 2012), diagenetically unaltered ammonites (Wierzbowski et al., 2013), and oysters (Brigaud et al., 2008). The observed trend towards more depleted $\delta^{18}\text{O}$ values observed in the Osterwald and Bisperode sections indicates a certain diagenetic overprint (Fig. 6). Hence, due to a clear diagenetic influence on the $\delta^{18}\text{O}$ signatures, this type of data will not be further discussed in this study.

The analyzed bulk carbonate samples derived from the Bisperode section show $\delta^{13}\text{C}$ values between -0.8 ‰ and 3.1 ‰, between -0.8 ‰ and 2.5 ‰ for the Osterwald section and between 1.4 ‰ and 3.0 ‰ for the Langenberg section (Fig. 6). Such values are considered within the typical range of well-preserved and diagenetically unaltered Oxfordian belemnites (Padden 2001; Nunn and Price 2010; Price and Rogov 2009; Benito et al. 2012), ammonites (Wierzbowski et al., 2013) and oysters (Brigaud et al., 2008). A strong positive correlation between $\delta^{18}\text{O}$ and $\delta^{13}\text{C}$ values is commonly taken as indication of diagenetic alteration under the influx of meteoric waters within the mixing zone (Allan and Matthews, 1982), or during burial diagenesis (Derry, 2010). The stable isotope records from the studied Korallenoolith sections show only low covariance between $\delta^{13}\text{C}$ and $\delta^{18}\text{O}$ values (Bisperode section: $r^2=0.0038$; Osterwald section: $r^2=0.1955$; Langenberg section: $r^2=0.1253$), which is interpreted to reflect the absence of strong diagenetic alteration of the stable isotope ratios, potentially exhibiting reliable patterns useful for chemostratigraphic correlation. Relatively low and strongly fluctuating $\delta^{13}\text{C}$ values underlying sedimentary discontinuities have often been linked to meteoric diagenesis below subaerial exposure surfaces (Allan and Matthews, 1982; Lohmann, 1988). Although in the coral reef-rich lithologies of the Bisperode section (5.5–46.0 m) and upper part of the Osterwald section (26.0–38.0 m), $\delta^{13}\text{C}$ shows extensive fluctuations characterized by stronger dolomitization. Also, the inspection of petrographic thin-sections from these intervals indeed reveals the occurrence of vadose diagenetic fabrics typically associated with subaerial exposure episodes. Carbonates underlying subaerial exposure surfaces show negative carbon isotope values, which is likely the result of meteoric diagenesis due to incorporation of light, soil-derived carbon. However, this type of alteration is stratigraphically restricted to a few distinct horizons and did not significantly alter the overall $\delta^{13}\text{C}$ trend. Based on the above evidence, the $\delta^{13}\text{C}$ signatures of the studied carbonates are considered to represent the $\delta^{13}\text{C}$ of the marine dissolved inorganic carbon during the time of carbonate precipitation and therefore can serve as chemostratigraphic signal.

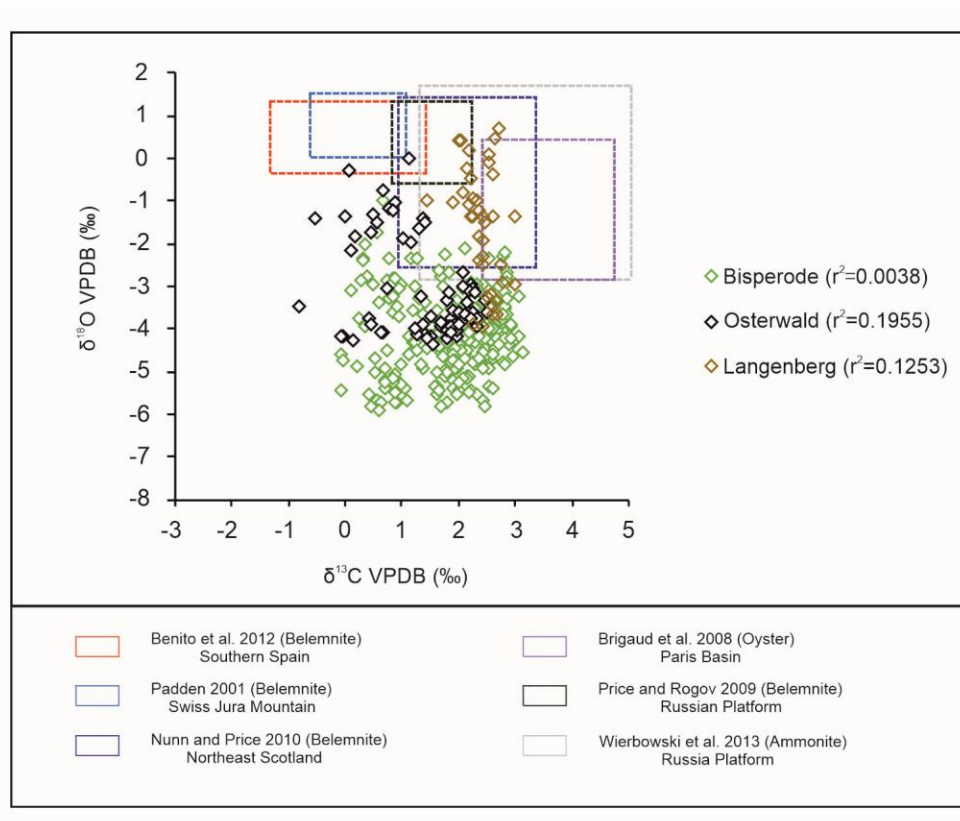


Fig. 6. Cross-plot of $\delta^{13}\text{C}$ and $\delta^{18}\text{O}$ values derived from the Bisperode, Langenberg and Osterwald sections compared with data obtained from well-preserved Oxfordian belemnites (Padden 2001; Nunn and Price 2010; Price and Rogov 2009; Benito et al. 2012), ammonites (Wierzbowski et al., 2013) and oysters (Brigaud et al., 2008).

5.7.2 Local environmental effects on carbon isotope signatures

Coastal depositional settings often receive sedimentary contributions from multiple sources and may record the superposition of local and global geochemical signals (Immenhauser et al., 2003; Colombié et al., 2011; Coimbra et al., 2016; Zuo et al. 2018). By comparing the $\delta^{13}\text{C}$ composition in relation to different sedimentary settings, facies-dependent variability of carbon isotope ratios can be identified.

The $\delta^{13}\text{C}$ values obtained from the semi-open lagoon depositional setting show only a slight deviation between the different sections (Fig.7, Bisperode, Langenberg). In such depositional environments with limited connectivity to open marine waters and low freshwater input, along with a high burial rate of organic matter and an oxygen-limited environment, also microscope inspections suggest good preservation of larger benthic foraminifera and other fossils which implies that they are good isotopic markers? The oolitic bar depositional setting shows consistently high $\delta^{13}\text{C}$ values in all three sections. Deposition of ooids occurred in a high-energy shoal environment located between the semi-open and the open lagoon environment. The porous and permeable ooid shoals may potentially generate a localized diagenetic-controlled interval. Due to relatively early stabilization of ooid-forming minerals during diagenesis by marine pore waters with only a minor contribution from organically derived light carbon (Armstrong-Altrin et al. 2009), the $\delta^{13}\text{C}$ signals from those ooid-rich lithologies are expected to

represent the marine DIC isotopic composition (Eltom et al. 2018). The carbon isotope data derived from the open lagoonal setting (restricted to Bisperode) shows a much broader scatter and exhibits more depleted $\delta^{13}\text{C}$ values, compared with the semi-open lagoon and ooid bar setting. The coral reef deposits exhibit the most depleted $\delta^{13}\text{C}$ values. In these two types of settings (open lagoon, reef), early meteoric diagenesis due to subaerial exposure, local changes in the organic matter source, and dolomitization are probably the most important processes affecting the carbon isotope ratios. Carbon isotope values from open marine strata (Bisperode, Langenberg) show moderate variability and relatively similar values between the two sites. Those off-shore deposits are predominantly composed of fine-grained micrites, which are usually compacted and cemented during a very early stage. Given the relatively low initial porosity of those fine-grained sediments, subsequent cementation, and diagenetic alteration are typically low resulting in only moderate diagenetic overprint (Marshall 1992; Immenhauser et al., 2003; Föllmi et al., 2006; Louis-Schmid et al. 2007; Eltom et al. 2018). In consequence, such kind of deposits is considered to preserve the most primary isotopic signal. Despite a certain degree of local environmental effects on the $\delta^{13}\text{C}$ signature, the studied carbonate sections are considered reliable recorders of the DIC of the ambient water masses during carbonate precipitation and allow for robust chemostratigraphic correlation.

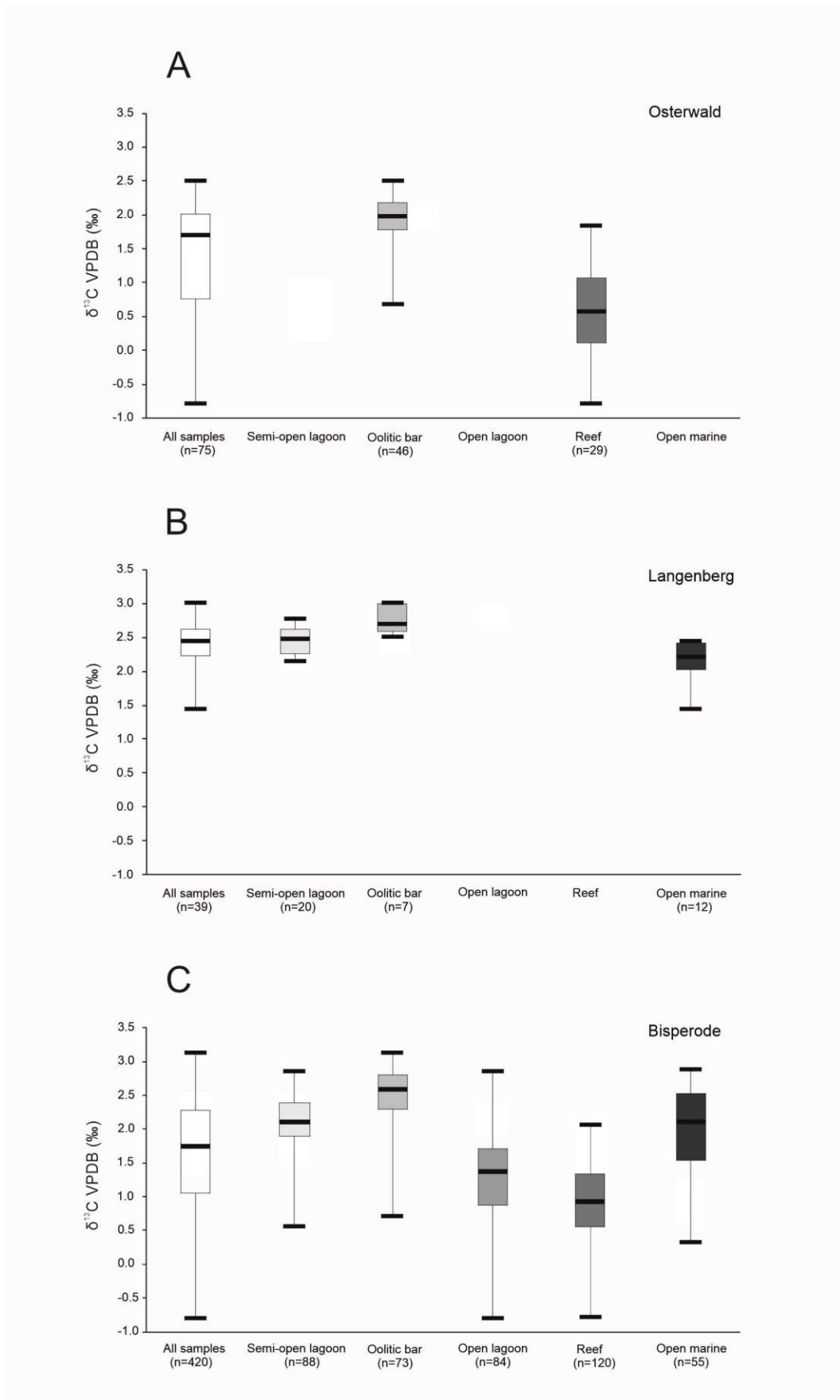


Fig. 7. Variability of $\delta^{13}\text{C}$ values within different carbonate depositional settings for the three studied sections with (A) Osterwald, (B) Langenberg and (C) Bisperode.

5.7.3 Carbon isotope-based correlation within the LSB

The age assignment of the Oxfordian successions within the LSB is primarily based on ostracod biostratigraphy (Heunisch and Luppold 2015; Zuo et al. 2017), with some additional calibration based on $^{87}\text{Sr}/^{86}\text{Sr}$ ratios for the late Oxfordian to early Kimmeridgian transition (Zuo et al. 2018). However, due to limited biostratigraphic and chemostratigraphic data, as well as due to strong small-scale depositional variability, it remains challenging to correlate core and outcrop data of the Korallenoolith Fm. In order to address this problem, a carbon isotope-based framework has been established, which can be used to strengthen the existing biostratigraphic correlation scheme of the LSB.

The ostracod biostratigraphic zonation for the Korallenoolith Fm. is essentially based on previous studies. For the Eulenflucht-1 core, the zonation was developed by Heunisch and Luppold (2015). Based on the work of Schudack (1994) and Weiß (1995), Zuo et al. (2017) identified zones 6 to 10 in the upper part of the Bisperode section. Additionally, zones 7-14 could be assigned for the upper Langenberg section using new data (Zuo et al. (2017)). However, the biostratigraphic zonation for the Lower and Middle Korallenoolith Fm. of both sections remains unclear. Regarding the Konrad #101 core, preliminary recognition of zones 3, and 6 to 12 was based on research by Kemper (1985) and Weiss (1985) (for further details see Chapter 3). In the Osterwald section, the ostracod zone 6 was recently identified (pers. com. J. Erbacher).

Based on the existing biostratigraphic framework and lithostratigraphic constraints, chemostratigraphic segments can be defined and correlated among the different sections across the studied area (Fig. 8). Based on a comparative analysis, the carbon isotope curve covering the Korallenoolith Fm. is subdivided into five distinct units. The lowermost unit 1 is defined based on the lithological expression of the Callovian/Oxfordian transition, which is described as an erosional surface cutting into the offshore marine claystones of the Ornatenton Fm. (Mönnig 2006; Mönnig et al. 2018). The deposits underlying this surface are mainly composed of claystones with very low carbonate content. In the SE part of the basin, those fine-grain offshore deposits are directly overlain by the shallow-marine Korallenoolith limestones (Mönnig 1989; Fischer 1991). Unit 2 includes the Heersum Fm. and the Lower Korallenoolith Fm. (Helm et al. 2003; Betzler et al. 2007; Bai et al. 2017) and is characterized by a distinct $\delta^{13}\text{C}$ positive shift followed by a rapid $\delta^{13}\text{C}$ decrease in the upper Lower Korallenoolith Fm. This positive carbon isotope excursion represents an important chemostratigraphic indicator for the inter-basinal correlation of the Lower Korallenoolith Fm. and is considered to be synchronous with the globally recorded Middle Oxfordian carbon isotope excursion (MOxE) (Jenkyns 1996; Weissert and Mohr 1996; Padden et al. 2001, 2002; Rais et al. 2007; Louis-Schmid et al. 2007; O'Dogherty et al. 2018; Eltom et al. 2018; Carneille et al. 2020; Eldrett 2022) (for discussion see Chapter 3). In the study area, this positive carbon isotope shift is well expressed in the Konrad #101 core and, though less pronounced, in the Eulenflucht core and Osterwald section. Unit 3 is characterised by an overall negative $\delta^{13}\text{C}$ trend overlying the positive MOxE, which varies in amplitude and shape. In the more W' part of the basin, this interval is characterized by the appearance of a coral-rich boundstone interval. Based on rare and poorly preserved ammonite findings, this interval can be placed within the *variocostatus* subzone (for discussion see Helm et al. 2003c). At Osterwald, the coral-rich interval can be placed within the ostracod

Chapter 5

zone 6 (pers. com. J. Erbacher). In the Konrad #101 core, unit 3 corresponds to two negative shifts in the $\delta^{13}\text{C}$ trend separated by a small positive bulge, which encompasses the transition from the Lower to Middle Korallenoolith Fm. This interval is placed within the lower ostracod zone 6 (Kemper, E. 1985; Weiss, W. 1985). The spatial occurrence of coral reef facies appears to be mainly controlled by local small-scale tectonic movements (Mönnig 2005) with this type of facies being restricted to the western part of the southern LSB. In the southeastern part of the basin, coral reef facies is replaced by other shallow-marine carbonate deposits (marls and oolitic limestones). Within unit 3, the $\delta^{13}\text{C}$ trend shows more fluctuations compared to the upper part of Korallenoolith Fm., but still enables a tentative correlation. Unit 4 is defined based on the occurrence of a pronounced emersion surface at its base, which is well-recognized in an increase in quartz content and peaks in gamma-ray logs (Kästner et al. 2008). This sequence boundary can be observed in other European basins during Oxfordian times (e.g., Gygi et al. 1998, Jacquin et al. 1998; Kästner et al. 2008). Above this unconformity, the carbon isotope record shows a relatively stable trend forming a plateau, which is terminated by a distinct negative shift. This interval of stable $\delta^{13}\text{C}$ values covers large parts of ostracod zone 6 and can be well correlated between the Bisperode section, Konrad #101 and Eulenflucht cores. Unit 5 is defined based on the existing correlation proposed by Zuo et al. (2018), who used ostracods and $^{87}\text{Sr}/^{86}\text{Sr}$ ratios to place this interval into the Süntel Fm. of the Lower Kimmeridgian (for Bisperode and Langenberg). For Konrad #101 core this interval is placed within the lower ostracod zone 7-12 (Kemper, E. 1985; Weiss, W. 1985) and with a similar carbon-isotopic trend to Eulenflucht-1 core and Bisperode, proposes a time-equivalent of Late Kimmeridgian. Within this interval, the $\delta^{13}\text{C}$ curve shows a bit of fluctuation, overall shows a relatively decreasing $\delta^{13}\text{C}$ tendency, which is comparable to the Oxfordian-Kimmeridgian boundary has also been reported from the Polish Jura Chain and the Swabian Alb in SW Germany (Wierzbowski, 2015). In summary, the combined geochemical and biostratigraphic data enable a tentative stratigraphic correlation of the Korallenoolith Fm. across the southern margin of the LSB. However, some differences and deviations are also observed, and further investigations are needed to better constrain the stratigraphic position and sedimentary expression of the Oxfordian strata within the studied section.

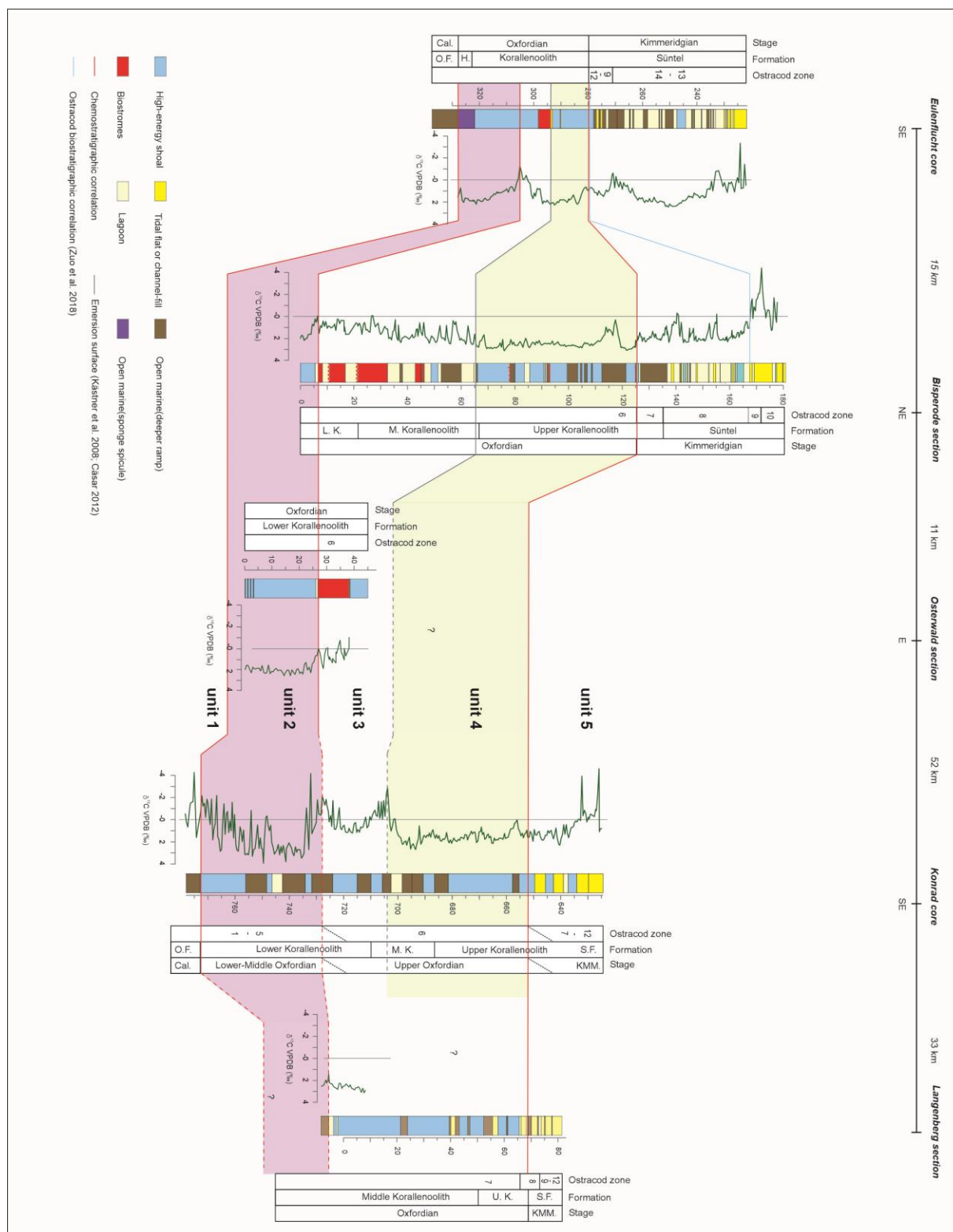


Fig. 8. Chemostratigraphic correlation based on carbon isotope trends across the southern LBS. For each section, lithostratigraphy, ostracod zonation, height, depositional setting and carbon isotope stratigraphic trends are shown. Correlation lines are based on chemostratigraphic (red), sedimentological (grey) and biostratigraphic (blue) constraints. The $\delta^{13}\text{C}$ record of the Eulenflucht core is based on Bai et al. (2017), and the upper part of the Bisperode section (125 m–180 m) is based on Zuo et al. (2018).

5.8 Conclusions

Chapter 5

This study provides detailed lithological logs of three Upper Jurassic sections (Bisperode, Osterwald, Langenberg) located in the LSB in northern Germany. While open-marine marker fossils, such as ammonites, are rare in the Oxfordian strata of the LSB, precise age assignment and correlation of the studied sections can be achieved using ostracod biostratigraphy. Chemostratigraphy, specifically the use of carbon isotopes, proved to be a valid and practical approach for regional correlation within the LSB, especially in the Korallenoolith Fm. where age-diagnostic fossils are scarce. A high-resolution study using carbon isotopes was conducted for the first time to correlate the different Oxfordian sections in the LSB. The observed $\delta^{13}\text{C}$ pattern between sections, even in the rather shallow-marine environments, was consistent, allowing for the establishment of a high-resolution carbon isotope stratigraphic record for Oxfordian successions in the LSB.

5.9 Acknowledgements

This research was supported by a CSC scholarship (201808510183) granted and by an LUH PhD completion grant to Deyan Zhang. Fritz-Lukas Stoeckle, Johanna Hansen, and Pascal Terbezniak are thanked for their assistance during fieldwork and sample collection. We also thank Jochen Erbacher for providing valuable information on the ostracod biostratigraphy of the Osterwald succession. The authors thank Christiane Wenske (Leibniz University Hannover) for support with the stable isotope analysis.

5.10 References

- Allan, J.R., Matthews, R.K. (1982). Isotope signatures associated with early meteoric diagenesis. *Sedimentology*, 29, 797–817.
- Armstrong-Altrin, J.S., Lee, Y.I., Verma, S.P., Worden, R.H. (2009). Carbon, oxygen, and strontium isotope geochemistry of carbonate rocks of the upper Miocene Kudankulam Formation, southern India: Implications for paleoenvironment and diagenesis. *Geochemistry*, 69, 45–60.
- Banner, J.L., Hanson, G.N. (1990). Calculation of simultaneous isotopic and trace element variations during water-rock interaction with applications to carbonate diagenesis. *Geochimica et Cosmochimica Acta*, 54, 3123–3137.
- Bai, H., Betzler, C., Erbacher, J., Reolid, J., Zuo, F. (2017). Sequence stratigraphy of Upper Jurassic deposits in the North German Basin (Lower Saxony, Süntel Mountains). *Facies*, 63, 1–20.
- Bai, H., Betzler, C., Huang, W., Zuo, F., Wu, F. (2020). Sequence stratigraphy of the Upper Jurassic mixed siliciclastic-carbonate deposits in the North German Basin (Lower Saxony, Hildesheimer Wald). *International Journal of Earth Sciences*, 109, 893–910.
- Benito, M.I., Reolid, M. (2012). Belemnite taphonomy (Upper Jurassic, Western Tethys) part II: Fossil-diagenetic analysis including combined petrographic and geochemical techniques. *Palaeogeography, Palaeoclimatology, Palaeoecology*, 358, 89–108.
- Betz, D., Führer, F., Greiner, G., Plein, E.M. (1987). Evolution of the Lower Saxony Basin. *Tectonophysics*, 137, 127–170.
- Betzler, C., Pawellek, T., Abdullah, M., Kossler, A. (2007). Facies and stratigraphic architecture of the Korallenoolith Formation in North Germany (Lauensteiner Pass, Ith Mountains). *Sedimentary Geology*, 194, 61–75.

- Bover-Amal, T., Moreno-Bedmar, J.A., Frijia, G., Pascual-Cebrian, E., Salas, R. (2016). Chronostratigraphy of the Barremian – Early Albian of the Maestrat Basin (E Iberian Peninsula): integrating strontium-isotope stratigraphy and ammonoid biostratigraphy. *Newsletters on Stratigraphy*, 49, 41–68.
- Buonocunto, F.P., Sprovieri, M., Bellanca, A., D'Argenio, B., Ferreri, V., Neri, R., Ferruzza, G. (2002). Cyclostratigraphy and high-frequency carbon isotope fluctuations in Upper Cretaceous shallow-water carbonates, southern Italy. *Sedimentology*, 49.
- Brigaud, B., Pucéat, E., Pellenard, P., Vincent, B., Joachimski, M.M. (2008). Climatic fluctuations and seasonality during the Late Jurassic (Oxfordian–Early Kimmeridgian) inferred from $\delta^{18}\text{O}$ of Paris Basin oyster shells. *Earth and Planetary Science Letters*, 273, 58–67.
- Carneille, M., Bourillot, R., Pellenard, P., Dupias, V., Schnyder, J., Riquier, L., Mathieu, O., Brunet, M.F., Énay, R., Grossi, V., Gaborieau, C., Razin, P., Visscher, P.T. (2020). Formation of microbial organic carbonates during the Late Jurassic from the Northern Tethys (Amu Darya Basin, Uzbekistan): Implications for Jurassic anoxic events. *Global and Planetary Change*, 186, 103–127.
- Colombié, C., Lécuyer, C., Strasser, A. (2011). Carbon- and oxygen-isotope records of palaeoenvironmental and carbonate production changes in shallow-marine carbonates (Kimmeridgian, Swiss Jura). *Geological Magazine* 148, 133–15
- Coimbra, R., Azerêdo, A.C., Cabral, M.C., Immenhauser, A. (2016). Palaeoenvironmental analysis of mid-Cretaceous coastal lagoonal deposits (Lusitanian Basin, W Portugal). *Palaeogeography, Palaeoclimatology, Palaeoecology*, 446, 308–325.
- Cäsar, S. (2012). Sequenzstratigraphie und Sedimentologie oberjurassischer Karbonate von Norddeutschland (Oxfordium/Kimmeridgium, Niedersächsisches Becken). Dissertation, Universität Hamburg.
- Derry, L.A. (2010). A burial diagenesis origin for the Ediacaran Shuram–Wonoka carbon isotope anomaly. *Earth and Planetary Science Letters*, 294, 152–162.
- Dunham, R.J. (1962). Classification of carbonate rocks according to depositional texture. *AAPG Mem*, 1, 108–121.
- Embry, A.F., Klován, J.E. (1971). A Late Devonian Reef Tract on Northeastern Banks Island, N.W.T. *Bulletin of Canadian Petroleum Geology*, 19, 730–781.
- Eldrett, J.S. (2021). Middle Oxfordian carbon cycle perturbation expressed in the Smackover Formation, Gulf of Mexico. *Geology*, 50, 500–505.
- Eltom, H.A., González, L.A., Hasiotis, S.T., Rankey, E.C., Cantrell, D.L. (2018). Paleogeographic and paleoceanographic influences on carbon isotope signatures: Implications for global and regional correlation, Middle–Upper Jurassic of Saudi Arabia. *Sedimentary Geology*, 364, 89–102.
- Fischer, R. (1991). Die Oberjura- Schichtfolge vom Langenberg bei Oker. *Arbeitskreis Paläontologie Hannover*, pp. 21–36.
- Föllmi, K.B., Godet, A., Bodin, S., Linder, P. (2006). Interactions between environmental change and shallow water carbonate buildup along the northern Tethyan margin and their impact on the Early Cretaceous carbon isotope record. *Paleoceanography*, 21, 1–16.
- Frijia, G., Parente, M., Lucia, M.D., Mutti, M. (2015). Carbon and strontium isotope stratigraphy of the Upper Cretaceous (Cenomanian-Campanian) shallow-water carbonates of southern Italy:

Chapter 5

- Chronostratigraphic calibration of larger foraminifera biostratigraphy. *Cretaceous Research*, 53, 110–139.
- Glumac, B., & Walker, K.R. (1998). A Late Cambrian positive carbon-isotope excursion in the Southern Appalachians; relation to biostratigraphy, sequence stratigraphy, environments of deposition, and diagenesis. *Journal of Sedimentary Research*, 68, 1212–1222.
- Gradstein, J. G. Ogg, M. D. Schmitz, G. M. Ogg (Eds.). 2020. *Geologic time scale*, Elsevier.
- Grötsch, J., Billing, I., & Vahrenkamp, V.C. (1998). Carbon - isotope stratigraphy in shallow - water carbonates: implications for Cretaceous black - shale deposition. *Sedimentology*, 45.
- Gramann, F., Heunisch, C., Klassen, H., Kockel, F., Dulce, G., Harms, F., Katschorek, T., Mönnig, E., Schudack, M., Schudack, U., Thies, D., Weiss, M. (1997). Das Niedersächsische Oberjura-Becken -Ergebnisse Interdisziplinärer Zusammenarbeit. *Zeitschrift der Deutschen Geologischen Gesellschaft*, 148, 165–236.
- Gygi R.A., Coe A.L., Vail P.R. (1998). Sequence stratigraphy of the Oxfordian and Kimmeridgian (Late Jurassic) in northern Switzerland. In: Graciansky PC, Hardenbol JT, Vail PR (eds), *Mesozoic and Cenozoic sequence stratigraphy of European Basins*, SEPM Special Publication 60:527–544
- Hardenbol, J., Thierry, J., Farley, M.B., Jacquin, T., de Graciansky, P.C., Vail, P.R. (1998). Jurassic chronostratigraphy. In: de Graciansky PC, Hardenbol J, Jacquin T, Vail PR (eds) *Mesozoic and Cenozoic sequence stratigraphy of European Basins*. SEPM Special Publication, Tulsa, pp 3–13.
- Helm, C., Schülke, I., Fischer, I. (2001). Paläobiogeographie des Korallenooliths (Mittleres Oxfordium Unteres Kimmeridgium): Tethyale Faunen- und Florenelemente auf höherer Paläobreite (Niedersächsisches Becken, NW-Deutschland). *Geologische Beiträge Hannover*, 2, 51–64.
- Helm, C., Reuter, M., Schülke, I. (2003). Die Korallenfauna des Korallenooliths (Oxfordium, Oberjura, NW-Deutschland): Zusammensetzung, Stratigraphie und regionale Verbreitung. *Paläontologische Zeitschrift*, 77, 77–94.
- Heunisch, C., Luppold, F.W. (2015). Mitteljura bis Unterkreide in den Bohrungen Eulenfucht 1 und Wendhausen 6-litho- und biostratigraphische Ergebnisse. In: Fischer et al (eds) *Neue Erkenntnisse zu Quartär, Jura und Unterkreide in Niedersachsen*. Landesamt für Bergbau, Energie und Geologie, Hannover, pp 40–69.
- Horikx, M., Heimhofer, U., Dinis, J., Huck, S. (2014). Integrated stratigraphy of shallow marine Albian strata from the southern Lusitanian Basin of Portugal. *Newsletters on Stratigraphy*, 47, 85–106.
- Hoyer, P. (1965). Fazies, Paläogeographie und Tektonik des Malm im Deister-Osterwald und Süntel. *Beih Geol Jb*, 61, 249.
- Huck, S., Heimhofer, U., Rameil, N., Bodin, S., Immenhauser, A. (2011). Strontium and carbon-isotope chronostratigraphy of Barremian–Aptian shoal-water carbonates: Northern Tethyan platform drowning predates OAE 1a. *Earth and Planetary Science Letters*, 304, 547–558.
- Huck, S., Heimhofer, U., Immenhauser, A., Weissert, H. (2013). Carbon isotope stratigraphy of Early Cretaceous (Urgonian) shoal-water deposits: Diachronous changes in carbonate-platform production in the north-western Tethys. *Sedimentary Geology*, 290, 157–174.
- Huck, S., Heimhofer, U. (2015). Improving shallow-water carbonate chemostratigraphy by means of rudist bivalve sclerochemistry. *Geochemistry, Geophysics, Geosystems*, 16(9), 3111–3128.
- Huck, S., Wohlwend, S.P., Coimbra, R., Christ, N., Weissert, H. (2017). Disentangling shallow-water

- bulk carbonate carbon isotope archives with evidence for multi-stage diagenesis: An in-depth component-specific petrographic and geochemical study from Oman (mid-Cretaceous). *The Depositional Record*, 3, 233–257.
- Immenhauser, A., Kenter, J.A.M., Ganssen, G., Bahamonde, J.R., Van Vliet, A., Saher, M.H. (2002). Origin and significance of isotope shifts in Pennsylvanian carbonates (Asturias, NW Spain). *Journal of Sedimentary Research* 72, 82–94
- Immenhauser, A., Della Porta, G., Kenter, J., Bahamonde, J.R. (2003). An alternative model for positive shifts in shallow-marine carbonate $\delta^{13}\text{C}$ and $\delta^{18}\text{O}$. *Sedimentology*, 50, 953–959.
- Jach, R., Djerić, N., Goričan, Š., Reháková, D., 2014. Integrated stratigraphy of the Middle Upper Jurassic of the Krížna Nappe, Tatra Mountains. *Annales. Societatis Geologorum Poloniae* 1–33.
- Jacquín, T., Dardeau, G., Durllet, C, Graciansky, P.C., Hantzpergue, P. (1998). The North sea cycle: an overview of 2nd-order transgressive/regressive facies cycles in Western Europe. In: Graciansky, P.C., Hardenbol, J., Jacquín, T., Vail, P.R. (eds) *Mesozoic and Cenozoic sequence stratigraphy of European Basins*, SEPM Special Publication 60:445–466
- Jenkyns, H.C., Gale, A.S., Corfield, R.M. (1994). Carbon- and oxygen-isotope stratigraphy of the English Chalk and Italian Scaglia and its palaeoclimatic significance. *Geological Magazine*, 131, 1–34.
- Jenkyns, H.C. (1996). Relative sea-level change and carbon isotopes: data from the Upper Jurassic (Oxfordian) of central and Southern Europe. *Terra Nova*, 8, 75–85.
- Kaiser, C. (1979). Einführung in die Geologie des Naturschutzgebietes Hohenstein. - 82 S., Hessisch-Oldendorf (Nds. L.-forstverw., Staatl. Forstamt Oldendorf).
- Kemper, E. (1985). Paläontologischer Bericht über die Kernbohrung Konrad 101. Bundesanstalt für Geowissenschaften und Rohstoffe (BGR), Hannover, 7 pp.
- Kästner, M., Schülke, I., Winsemann, J., Böttcher, J. (2010). High-resolution sequence stratigraphy of a Late Jurassic mixed carbonate-siliciclastic ramp, Lower Saxony Basin, Northwestern Germany. *Zeitschrift Der Deutschen Gesellschaft Für Geowissenschaften*, 161, 263–283.
- Kästner, M., Schülke, I., Winsemann, J. (2008). Facies architecture of a Late Jurassic carbonate ramp: the Korallenoolith of the Lower Saxony Basin. *International Journal of Earth Sciences*, 97, 991–1011.
- Krull, E.S., Lehmann, D.J., Druke, D., Kessel, B.J., Yu, Y., Li, R. (2004). Stable carbon isotope stratigraphy across the Permian-Triassic boundary in shallow marine carbonate platforms, Nanpanjiang Basin, south China. *Palaeogeography, Palaeoclimatology, Palaeoecology*, 204, 297–315.
- Leinfelder, R.R. (2001). Jurassic reef ecosystems, in Stanley, G.D., Jr. (ed.), *The History and Sedimentology of Ancient Reef Systems*: Boston, Springer, p. 251–309.
- Lohmann, K.C. (1988). *Geochemical Patterns of Meteoric Diagenetic Systems and Their Application to Studies of Paleokarst*.
- Louis-Schmid, B., Rais, P., Schaeffer, P., Bernasconi, S.M., Weissert, H. (2007a). Plate tectonic trigger of changes in pCO_2 and climate in the Oxfordian (Late Jurassic): Carbon isotope and modeling evidence. *Earth and Planetary Science Letters*, 258, 44–60.
- Luppold, F.W. (2003). Neue und seltene Index-Foraminiferen und -Ostrakoden aus dem Jura NW-Deutschlands. *Senckenb Lethaea* 83:15–37
- Martin-Garin, B., Lathuilière, B., Geister, J. (2012). The shifting biogeography of reef corals during the Oxfordian (Late Jurassic). A climatic control. *Palaeogeography, Palaeoclimatology, Palaeoecology*,

Chapter 5

- 365, 136–153.
- Marshall, J. (1992). Climatic and oceanographic isotopic signals from the carbonate rock record and their preservation. *Geological Magazine*, 129(2), 143–160.
- Mönnig, E. (1989). Stratigraphie und Fazies des Calloviums in NW-Deutschland. *Clausthaler Geowiss. Diss.*, 37, 1–183.
- Mönnig, E. (2006). Ornatenton-Formation. In: LithoLex (online databank), Hannover (BGR), Record no: 4012001. <http://www.bgr.bund.de/litholex>
- Mönnig, E., Franz, M., Schweigert, G. (2018). Der Jura in der Stratigraphischen Tabelle von Deutschland (STD 2016) The Stratigraphic Chart of Germany (STD 2016): Jurassic]. *Z Dtsch Ges Für Geowiss* 169:225–246
- Mudroch, A., Thies, D., Baumann, A. (1999). $^{87}\text{Sr}/^{86}\text{Sr}$ analysis on Late Jurassic fish teeth. Implication for paleosalinity of fossil habitats. In: Arratia G (ed) *Mesozoic Fishes—Systematics and Fossil Record*. Proceedings of the 2nd International Meeting, Buckow 1997, pp 595–604.
- Nunn, E.V., Price, G.D., Hart, M.B., Page, K.N., Leng, M.J. (2009). Isotopic signals from Callovian–Kimmeridgian (Middle–Upper Jurassic) belemnites and bulk organic carbon, Staffin Bay, Isle of Skye, Scotland. *Journal of the Geological Society*, 166, 633–641.
- O’Dogherty, L., Aguado, R., Baumgartner, P.O., Bill, M., Goričan, Š., Sandoval, J., Sequeiros, L. (2018). Carbon-isotope stratigraphy and pelagic biofacies of the Middle–Upper Jurassic transition in the Tethys–Central Atlantic connection. *Palaeogeography, Palaeoclimatology, Palaeoecology*, 507, 129–144.
- Padden, M., Weissert, H., Rafelis, M.D. (2001). Evidence for Late Jurassic release of methane from gas hydrate. *Geology*, 29, 223–226.
- Patterson, W.P., Walter, L.M. (1994). Depletion of ^{13}C in seawater ΣCO_2 on modern carbonate platforms: Significance for the carbon isotopic record of carbonates. *Geology*, 22, 885–888.
- Price, G.D., Rogov, M.A. (2009). An isotopic appraisal of the Late Jurassic greenhouse phase in the Russian Platform. *Palaeogeography, Palaeoclimatology, Palaeoecology*, 273, 41–49.
- Rais, P., Louis-Schmid, B., Bernasconi, S.M., Weissert, H. (2007). Palaeoceanographic and palaeoclimatic reorganization around the Middle–Late Jurassic transition. *Palaeogeography, Palaeoclimatology, Palaeoecology*, 251, 527–546.
- Schmitt, K.E., Heimhofer, U., Frijia, G., Lucia, M.D., Huck, S. (2020). Deciphering the fragmentary nature of Cretaceous shallow-water limestone archives: A case study from the subtropical Apennine carbonate platform. *Newsletters on Stratigraphy*, 53, 389–413.
- Schormann, J., Zawischa, D. (1990). Fundstellenbericht: Die “Grenzschichten im Oberen Jura des Süntel.” - Arbkr. *Paläontol.* Hannover, 18 (4), 92–96.
- Schudack, U. (1994). Revision, Dokumentation und Stratigraphie der Ostracoden des Nordwestdeutschen Oberjura und Unter-Berriasium. *Berliner Geowissenschaftliche Abhandlungen*, 11, 1–193.
- Senglaub, Y., Brix, M.R., Adriasola, A.C., Littke, R. (2005). New information on the thermal history of the southwestern Lower Saxony Basin, northern Germany, based on fission track analysis. *International Journal of Earth Sciences*, 94, 876–896.
- Swart, P.K., Eberli, G.P. (2005). The nature of the $\delta^{13}\text{C}$ of periplatform sediments: Implications for stratigraphy and the global carbon cycle. *Sedimentary Geology*, 175, 115–129.

- Vahrenkamp, V.C. (1996). Carbon Isotope Stratigraphy of the Upper Kharaib and Shuaiba Formations: Implications for the Early Cretaceous Evolution of the Arabian Gulf Region. *AAPG Bulletin*, 80, 647–662.
- Van Hinsbergen, D.J., de Groot, L.V., van Schaik, S.J., Spakman, W., Bijl, P.K., Sluijs, A., Langereis, C.G., Brinkhuis, H. (2015). A Paleolatitude Calculator for Paleoclimate Studies. *PLoS ONE*, 10.
- Voigt, E. (1962). Über Randtröge und Schollenränder und ihre Bedeutung im Gebiet der Mitteleuropäischen Senke und angrenzender Gebiete. *Zeitschrift dt Geol Ges* 114:378–41.
- Weiß, M. (1995). Stratigraphie und Mikrofauna im Kimmeridge SE-Niedersachsens unter besonderer Berücksichtigung der Ostracoden. *Clausthaler Geowiss Diss*, 48, 1–274.
- Weiss, W. (1985). Mikropaläontologischer Bericht. Bundesanstalt für Geowissenschaften und Rohstoffe (BGR), Hannover, 4 pp.
- Weissert, H., Mohr, H.M. (1996). Late Jurassic climate and its impact on carbon cycling. *Palaeogeography, Palaeoclimatology, Palaeoecology*, 122, 27–43.
- Weissert, H., Lini, A., Föllmi, K.B., Kuhn, O. (1998). Correlation of Early Cretaceous carbon isotope stratigraphy and platform drowning events: a possible link? *Palaeogeography, Palaeoclimatology, Palaeoecology*, 137, 189–203.
- Weissert, H., Joachimski, M., Sarnthein, M. (2008). Chemostratigraphy. *Newsletters on Stratigraphy*, 42, 145–179.
- Wierzbowski, H., Rogov, M.A., Matyja, B.A., Kiselev, D.N., Ippolitov, A.P. (2013). Middle–Upper Jurassic (Upper Callovian–Lower Kimmeridgian) stable isotope and elemental records of the Russian Platform: Indices of oceanographic and climatic changes. *Global and Planetary Change*, 107, 196–212.
- Wierzbowski, H. (2015). Seawater temperatures and carbon isotope variations in central European basins at the Middle–Late Jurassic transition (Late Callovian–Early Kimmeridgian). *Palaeogeography, Palaeoclimatology, Palaeoecology*, 440, 506–523.
- Wierzbowski, H., Anczkiewicz, R., Pawlak, J., Rogov, M.A., Kuznetsov, A. (2017). Revised Middle–Upper Jurassic strontium isotope stratigraphy. *Chemical Geology*, 466, 239–255.
- Ziegler, P. A. (1990). *Geological Atlas of Western and Central Europe*. 2nd Edition, Shell International Petroleum Mij. B.V. and Geological Society, London.
- Zuo, F., Heimhofer, U., Huck, S., Luppold, F.W., Wings, O., Erbacher, J. (2018). Sedimentology and depositional sequences of a Kimmeridgian carbonate ramp system, Lower Saxony Basin, Northern Germany. *Facies*, 64:1–25.
- Zuo, F., Heimhofer, U., Huck, S., Bodin, S., Erbacher, J., Bai, H. (2018). Coupled $\delta^{13}\text{C}$ and $^{87}\text{Sr}/^{86}\text{Sr}$ chemostratigraphy of Kimmeridgian shoal-water deposits: A new composite record from the Lower Saxony Basin, Germany. *Sedimentary Geology*, 376, 18–31.

6. Conclusions

This study focuses on refining the depositional setting and stratigraphy of the limestones of the Oxfordian Korallenoolith Fm. within the LSB. In order to achieve such a goal, an integrated approach combining sedimentological, sequence stratigraphic, biostratigraphic, and chemostratigraphic analysis has been applied to several Oxfordian sections and one scientific drill core. The major results of the current thesis include the following:

Analysis of the carbonate microfacies and establishment of a sequence stratigraphic framework

A total of seven superordinate carbonate facies types - composed of 14 different microfacies types - were distinguished throughout the Bisperode section and attributed to different paleoenvironments. Based on these findings a homoclinal ramp setting composed of different juxtaposed facies belts, ranging from semi-open lagoonal to open marine settings, is reconstructed. On the basis of microfacies types, diagnostic bedding surfaces, and the vertical lithofacies stacking pattern, a total of 15 small-, 8 medium-, and 3 large-scale sequences are identified. Detailed facies analysis and sequence stacking pattern of the Bisperode section suggest that eustatic fluctuations might have controlled the medium- and large-scale sequences preserved within the Korallenoolith Fm. based on their good match with well-established eustatic models (e.g., Hardenbol, 1998). Regional synsedimentary salt tectonism and sedimentation rate fluctuations may have played an additional role in relative sea-level changes within the LSB and as such influenced most of the small-scale sequences. Although it is clear that the lack of strong biostratigraphic markers limits the significance the correlation between regional and global sequence-stratigraphic schemes in the LSB, this work provides a general framework, which will help to better understand the link between the stacking pattern of Oxfordian strata in the LSB and allocyclic processes providing support for future chemo- and sequence-stratigraphic correlations.

First record of the Middle Oxfordian positive CIE within the Korallenoolith Formation

A new high-resolution inorganic $\delta^{13}\text{C}$ record illustrating a pronounced variation in the carbon isotope trend, which is obtained from a scientific borehole (Konrad #101 core) located in the LSB. Our $\delta^{13}\text{C}$ record is the first record of the Middle Oxfordian positive CIE within the LSB and is interpreted to reflect global $\delta^{13}\text{C}$ changes in ocean-atmosphere system. The positive CIE observed in the Konrad #101 core is an important chemostratigraphic marker for the inter-basinal correlation of the Lower Korallenoolith Fm. and considered to be synchronous with the globally recorded Middle Oxfordian carbon isotope excursion (MOxE). Our dataset, which is supported by well-defined tie points, further proves the usefulness of isotope variations recorded in shallow-water bulk carbonates as chemostratigraphic proxy.

$^{87}\text{Sr}/^{86}\text{Sr}$ chemostratigraphy of Oxfordian shallow-water carbonate deposits

New biocalcite-derived $^{87}\text{Sr}/^{86}\text{Sr}$ data from the Oxfordian Korallenoolith Fm. from the LSB are used to identify secular trends in seawater Sr ratios in order to better constrain the depositional age of the Korallenoolith Fm. Sr isotope ratios obtained from brachiopod, oyster and trichites shell calcite are within the range of values reported for Late Jurassic seawater. However, closer inspection shows distinct deviations from the Oxfordian open marine Sr isotope signature, indicating that the depositional setting

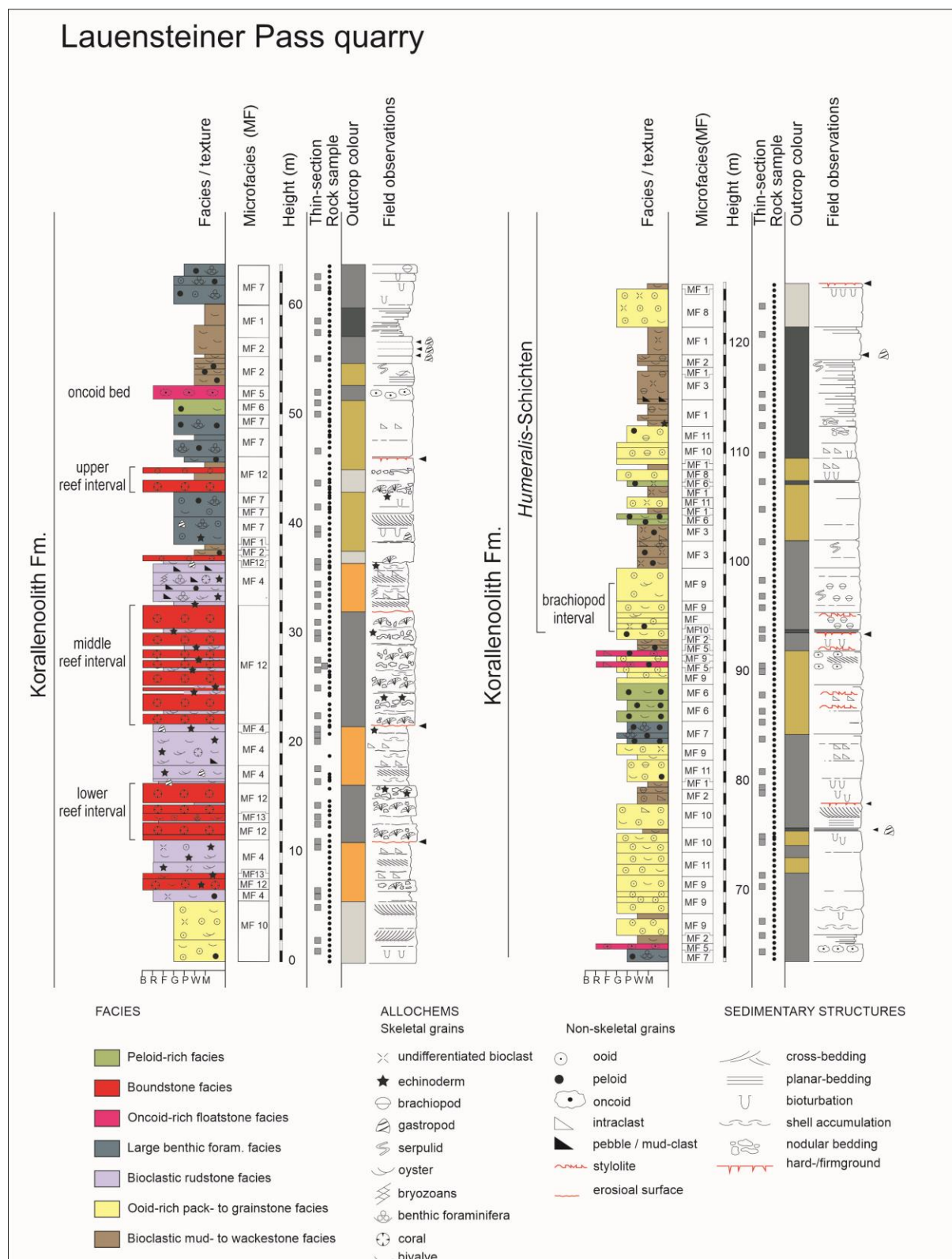
was probably influenced by freshwater input with a continental Sr isotope signature. The analyzed shells may have captured local, more radiogenic $^{87}\text{Sr}/^{86}\text{Sr}$ signatures derived from riverine waters and hence failed to provide a more precise age assignment. Our $^{87}\text{Sr}/^{86}\text{Sr}$ results indicate that shells from shallow marine settings showing no diagenetic overprint can still deviate from the open marine Sr isotope signature.

High-resolution carbon isotope stratigraphic records for Oxfordian successions in the LSB

High-resolution $\delta^{13}\text{C}$ analysis of bulk carbonate samples from three outcrop sections (Langenberg, Osterwald, and Bisperode) and one scientific borehole (Konrad #101 core) are studied and compared. Through the application of rigorous criteria, the majority of the $\delta^{13}\text{C}$ dataset of bulk carbonate obtained from the studied sections has been deemed free from diagenetic alterations and local environmental effects, thereby providing a representation of the global marine signals. Based on litho- and biostratigraphic constraints, a $\delta^{13}\text{C}$ record correlation is presented for the southern LSB for the Oxfordian interval. Chemostratigraphy, specifically the use of carbon isotopes, proved to be a valid and practical approach for regional correlation within the LSB, especially in the Korallenoolith Fm. where age-diagnostic fossils are scarce. The chemostratigraphic data presented in this study enables the refinement of the pre-existing biostratigraphic framework and the establishment of a composite high-resolution $\delta^{13}\text{C}$ stratigraphic record. The $\delta^{13}\text{C}$ records improve the correlation ability between the western and eastern parts of the LSB. Overall, the new framework also allows to better assess the impact of carbon cycle disturbances on the shallow-marine carbonate systems in the LSB.

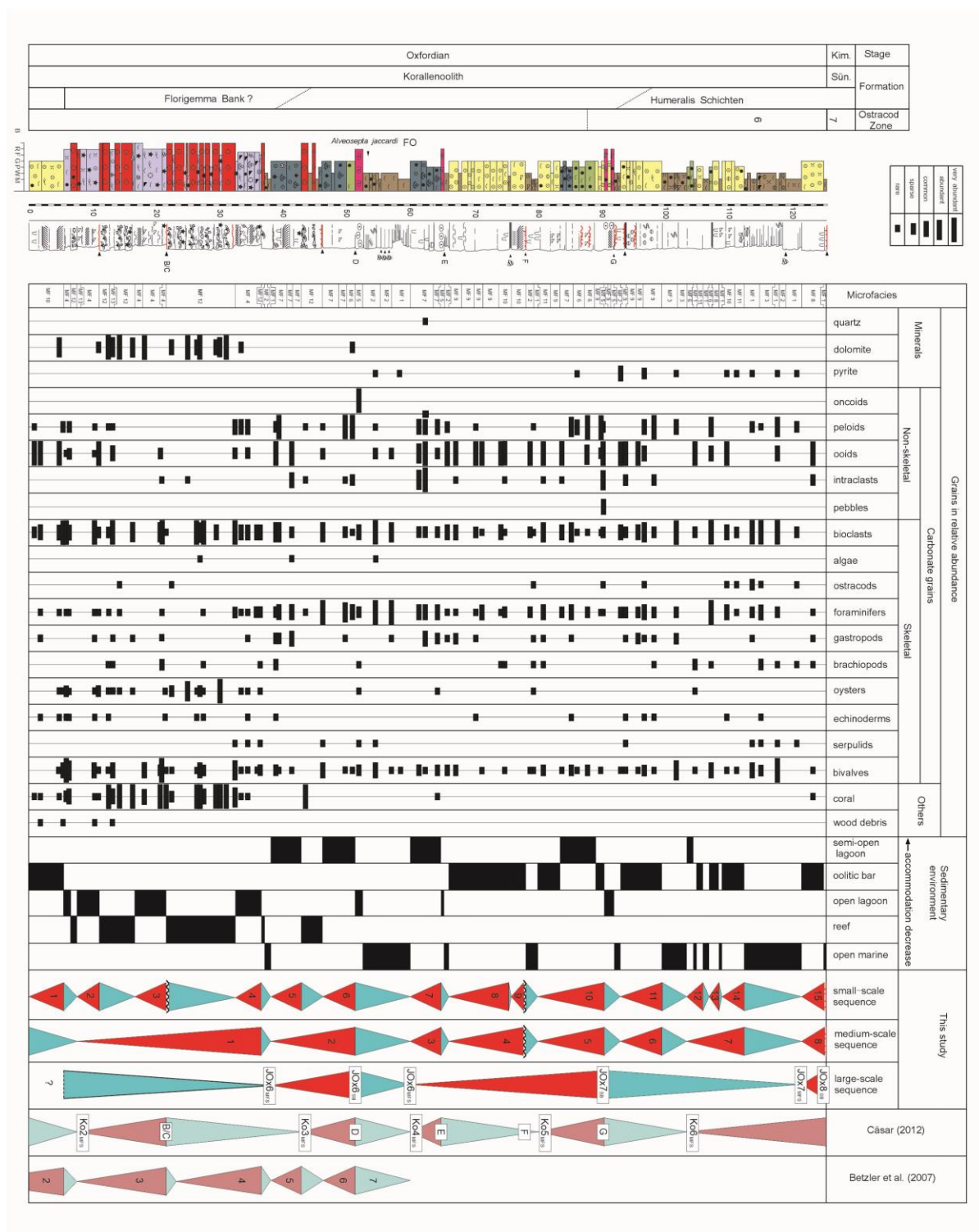
Appendix

Appendix 1 High-resolution log description of the Bisperode section (0–126 m)

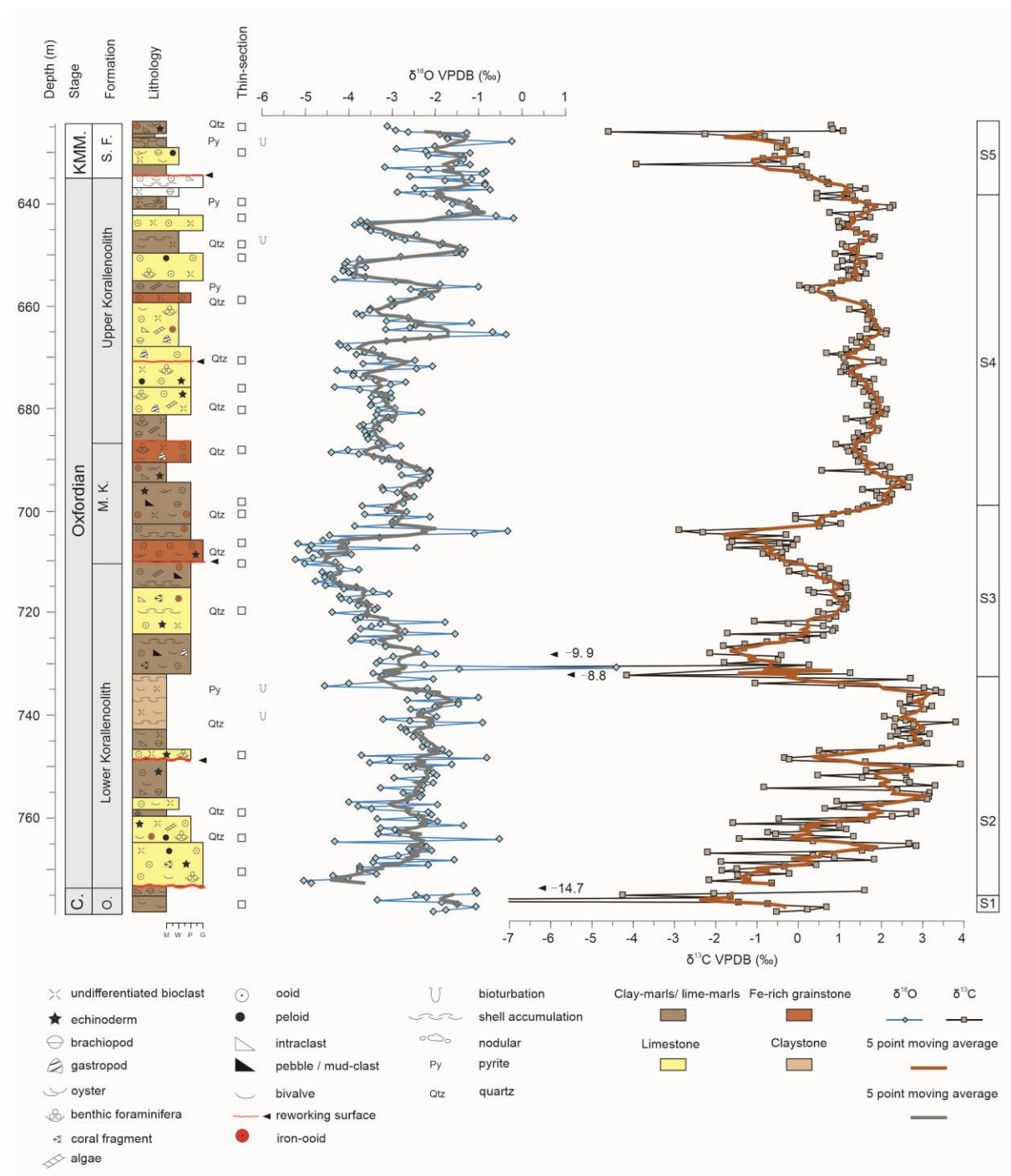


Appendix

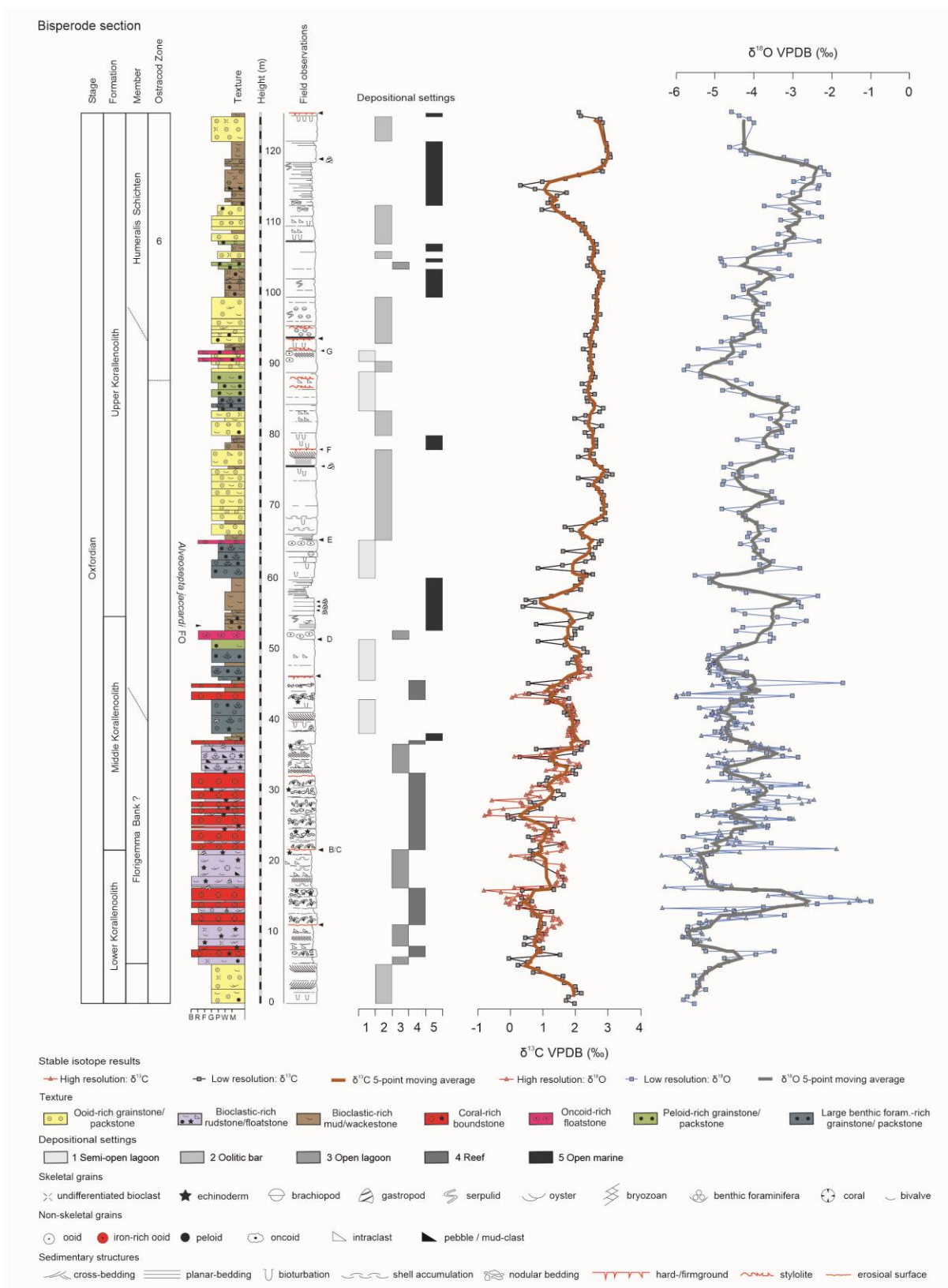
Appendix 2 Sedimentological description, depositional settings and sequence stratigraphic interpretation of the Bisperode section



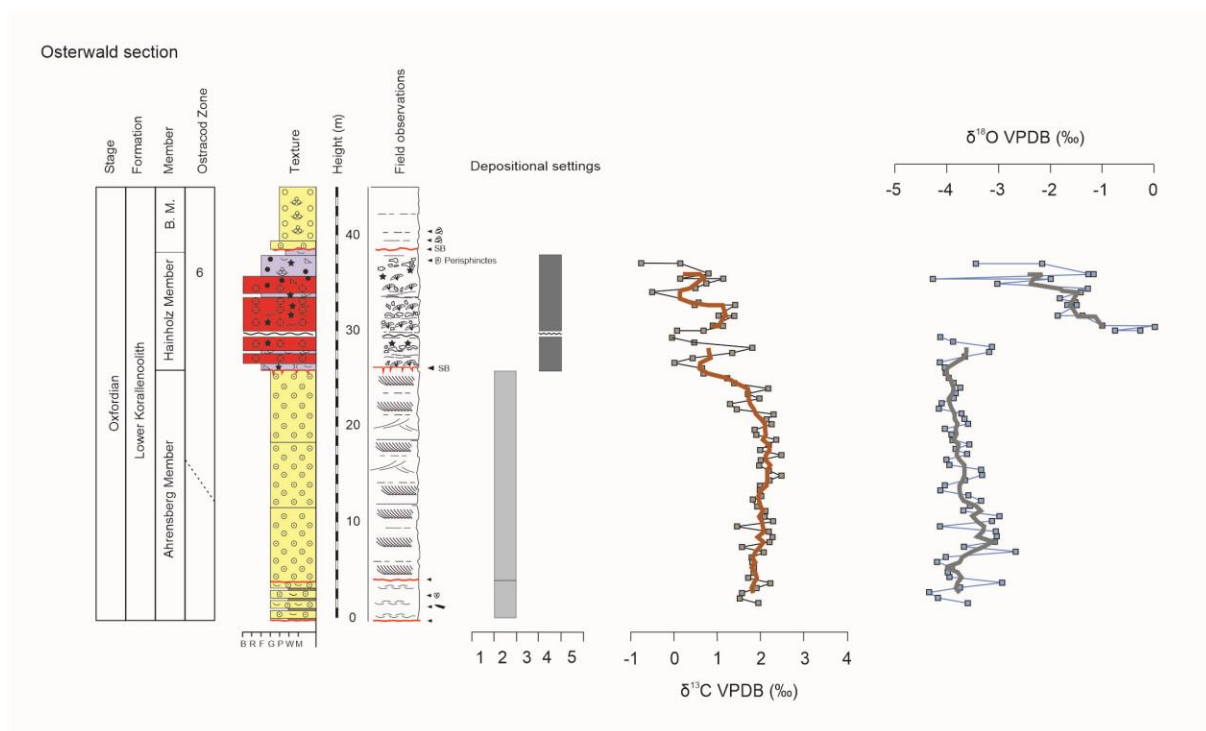
Appendix 3 Lithostratigraphy and high-resolution stable isotope stratigraphy ($\delta^{18}\text{O}$, $\delta^{13}\text{C}$) of the Konrad #101 core



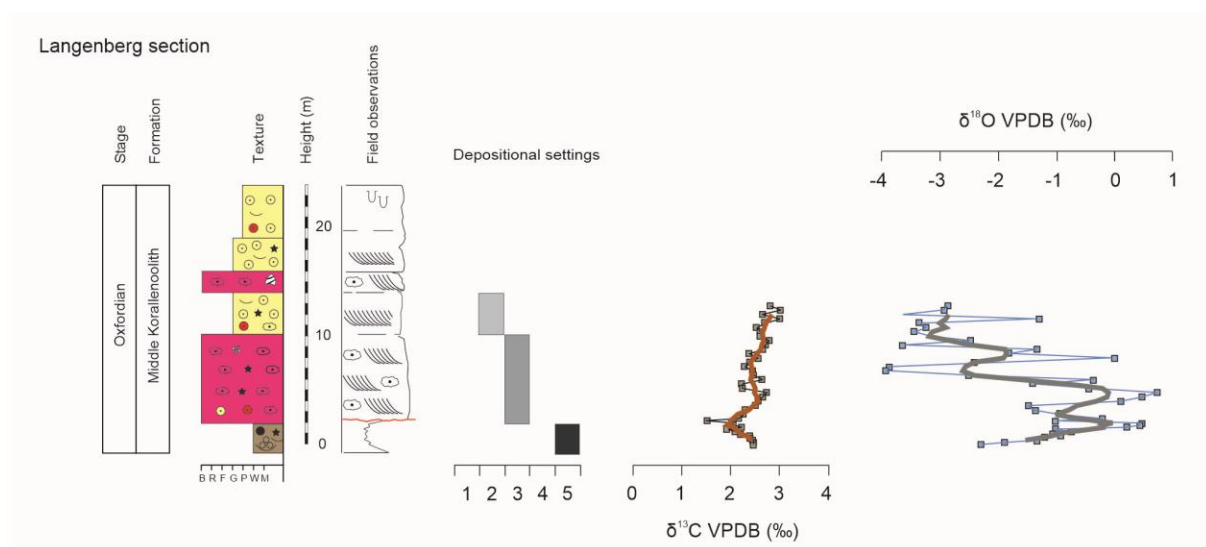
Appendix 4 Lithostratigraphy, high-resolution stable isotope stratigraphy ($\delta^{18}\text{O}$, $\delta^{13}\text{C}$) and inferred depositional settings of the Bisperode section (0–126 m)



Appendix 5 Lithostratigraphy, inferred depositional settings and high-resolution stable isotope stratigraphy ($\delta^{18}\text{O}$, $\delta^{13}\text{C}$) of Osterwald section (0–46 m)

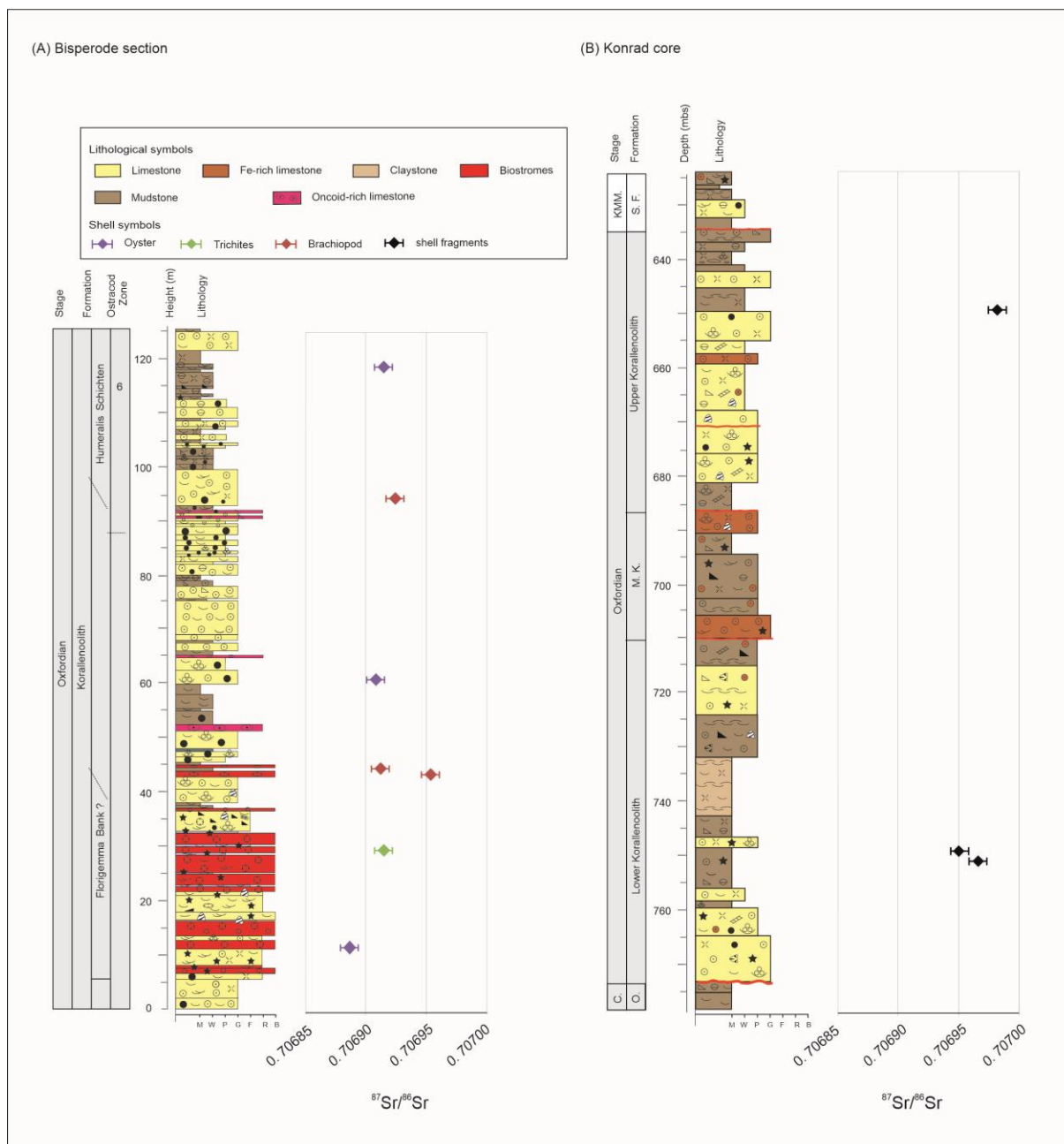


Appendix 6 Lithostratigraphy, inferred depositional settings and high-resolution stable isotope stratigraphy ($\delta^{18}\text{O}$, $\delta^{13}\text{C}$) of Langenberg section (0–16 m)



Appendix

Appendix 7 Lithostratigraphy versus $^{87}\text{Sr}/^{86}\text{Sr}$ ratios of selected calcite shell materials for (A) Bisperode section and (B) Konrad #101 core



Appendix 8 Carbon and oxygen isotope results of bulk material, Bisperode section

| Sample | Depth (m) | $\delta^{13}\text{C}$ VPDB | s.d. | $\delta^{18}\text{O}$ VPDB | s.d. | Sample | Depth (m) | $\delta^{13}\text{C}$ VPDB | s.d. | $\delta^{18}\text{O}$ VPDB | s.d. |
|----------|-----------|----------------------------|------|----------------------------|------|----------|-----------|----------------------------|------|----------------------------|------|
| DY0 | 0.00 | 1.98 | 0.08 | -5.53 | 0.06 | LPb 5,2 | 26.70 | -0.06 | 0.06 | -4.57 | 0.04 |
| DY0_5 | 0.50 | 1.70 | 0.06 | -5.81 | 0.04 | LPb 5,5 | 27.00 | -0.08 | 0.05 | -5.45 | 0.02 |
| DY1 | 1.00 | 1.79 | 0.09 | -5.72 | 0.04 | LPb 6 | 27.50 | 0.51 | 0.06 | -5.01 | 0.05 |
| DY1_5 | 1.50 | 2.17 | 0.06 | -5.51 | 0.03 | LPb 6,5 | 28.00 | 0.94 | 0.09 | -3.71 | 0.07 |
| DY2 | 2.00 | 2.01 | 0.06 | -5.23 | 0.05 | LPb 7 | 28.50 | 0.75 | 0.04 | -4.52 | 0.04 |
| DY2_5 | 2.50 | 1.99 | 0.09 | -5.45 | 0.06 | LPb 7,5 | 29.00 | 0.61 | 0.07 | -3.39 | 0.07 |
| DY3 | 3.00 | 1.65 | 0.08 | -5.44 | 0.06 | LPb 8 | 29.50 | 1.33 | 0.04 | -3.98 | 0.03 |
| DY3_5 | 3.50 | 1.60 | 0.06 | -5.34 | 0.07 | LPb 8,5 | 30.00 | 1.63 | 0.09 | -3.88 | 0.07 |
| DY4 | 4.00 | 1.61 | 0.11 | -5.55 | 0.05 | LPb 9 | 30.50 | 1.46 | 0.04 | -4.16 | 0.03 |
| DY4_5 | 4.50 | 0.70 | 0.07 | -5.24 | 0.07 | LPb 9,5 | 31.00 | 1.18 | 0.07 | -3.56 | 0.07 |
| DY5 | 5.00 | 0.85 | 0.05 | -5.14 | 0.03 | LPb 10 | 31.50 | 0.89 | 0.07 | -2.81 | 0.03 |
| DY5_5 | 5.50 | 0.23 | 0.09 | -4.88 | 0.07 | LPb 10,5 | 32.00 | 1.12 | 0.06 | -4.16 | 0.05 |
| DY6 | 6.00 | 0.53 | 0.09 | -4.68 | 0.06 | LPb 11 | 32.50 | 1.14 | 0.04 | -4.61 | 0.01 |
| DY6_5 | 6.50 | -0.04 | 0.02 | -4.75 | 0.02 | LPb 11,5 | 33.00 | 2.01 | 0.05 | -4.82 | 0.03 |
| DY7 | 7.00 | 1.52 | 0.04 | -3.95 | 0.05 | LPb 12 | 33.50 | 1.91 | 0.04 | -4.74 | 0.06 |
| DY7_5_1 | 7.50 | 0.91 | 0.06 | -3.47 | 0.03 | LPb 12,5 | 34.00 | 2.13 | 0.06 | -4.71 | 0.04 |
| DY7_5_2 | 7.50 | 0.84 | 0.07 | -5.24 | 0.05 | LPb 13 | 34.50 | 1.38 | 0.07 | -4.92 | 0.04 |
| DY8 | 8.00 | 1.00 | 0.09 | -5.28 | 0.10 | LPb 13,5 | 35.00 | 1.23 | 0.05 | -4.13 | 0.06 |
| DY8_5 | 8.50 | 0.42 | 0.06 | -5.53 | 0.06 | LPb 13,9 | 35.40 | 0.30 | 0.06 | -2.87 | 0.03 |
| DY9 | 9.00 | 0.89 | 0.06 | -5.47 | 0.05 | LPb 14 | 35.50 | 1.29 | 0.05 | -3.26 | 0.06 |
| DY9_5 | 9.50 | 0.46 | 0.06 | -5.83 | 0.05 | LPb 14,5 | 36.00 | 1.97 | 0.04 | -3.67 | 0.03 |
| DY10 | 10.00 | 1.08 | 0.05 | -5.67 | 0.04 | LPb 15 | 36.50 | 2.17 | 0.06 | -4.10 | 0.03 |
| DY10_5 | 10.50 | 0.87 | 0.06 | -5.71 | 0.04 | SB 0 | 36.60 | 0.79 | 0.05 | -3.26 | 0.07 |
| DY11 | 11.00 | 0.91 | 0.07 | -5.70 | 0.05 | SB 0,5 | 37.00 | 2.19 | 0.08 | -4.03 | 0.04 |
| DY11_5 | 11.50 | 1.04 | 0.04 | -5.40 | 0.05 | SB 1 | 37.50 | 2.36 | 0.06 | -4.19 | 0.03 |
| LPa 1 | 12.65 | 0.84 | 0.09 | -3.22 | 0.05 | SB 1,5 | 38.00 | 1.95 | 0.05 | -4.75 | 0.04 |
| LPa 2 | 12.80 | 0.69 | 0.06 | -5.38 | 0.01 | SB 2 | 38.50 | 1.92 | 0.05 | -4.61 | 0.04 |
| LPa 3 | 13.25 | 1.27 | 0.05 | -4.51 | 0.02 | SB 2,5 | 39.00 | 1.80 | 0.05 | -5.01 | 0.04 |
| LPa 4 | 13.85 | 0.23 | 0.05 | -3.76 | 0.01 | SB 3 | 39.50 | 1.85 | 0.06 | -4.79 | 0.03 |
| LPa 5 | 14.30 | 0.31 | 0.08 | -2.37 | 0.07 | SB 3,5 | 40.00 | 1.94 | 0.08 | -4.46 | 0.08 |
| LPa 6 | 14.70 | 0.66 | 0.09 | -0.98 | 0.03 | SB 4 | 40.50 | 2.06 | 0.07 | -4.51 | 0.06 |
| LPa 7 | 15.20 | 0.35 | 0.07 | -2.02 | 0.06 | SB 4,5 | 41.00 | 1.91 | 0.03 | -4.51 | 0.04 |
| LPa 8 | 16.30 | 0.37 | 0.08 | -3.95 | 0.06 | SB 5 | 41.50 | 1.75 | 0.07 | -5.09 | 0.05 |
| LPa 9 | 16.40 | 1.34 | 0.05 | -4.83 | 0.07 | SB 5,3 | 41.80 | 1.65 | 0.02 | -4.08 | 0.02 |
| LPa 10 | 16.55 | 0.97 | 0.04 | -4.83 | 0.03 | SB 5,5 | 42.00 | 1.94 | 0.05 | -4.90 | 0.04 |
| LPa 11 | 16.90 | 1.63 | 0.06 | -4.99 | 0.04 | SB 5,9 | 42.40 | 1.90 | 0.03 | -5.41 | 0.03 |
| LPa 12 | 18.20 | 1.60 | 0.02 | -5.36 | 0.06 | SB 6,3 | 42.80 | 1.79 | 0.05 | -4.32 | 0.06 |
| LPa 13 | 20.80 | 0.58 | 0.05 | -5.90 | 0.04 | SB 6,8 | 43.30 | 1.15 | 0.07 | -4.57 | 0.06 |
| LPa 14 | 21.40 | 0.70 | 0.09 | -5.20 | 0.06 | SB 7,0 | 43.50 | 1.30 | 0.09 | -4.07 | 0.09 |
| LPb 0 | 21.50 | 0.88 | 0.03 | -5.08 | 0.02 | SB 7,1 | 43.60 | 1.12 | 0.06 | -4.60 | 0.07 |
| LPb 0, 5 | 22.00 | 0.62 | 0.02 | -5.70 | 0.02 | SB 7,3 | 43.80 | 1.79 | 0.03 | -4.22 | 0.03 |
| LPb 1 | 22.50 | 0.90 | 0.05 | -5.22 | 0.06 | SB 7,7 | 44.20 | 1.24 | 0.05 | -3.01 | 0.04 |
| LPb 1, 5 | 23.00 | 1.63 | 0.04 | -3.56 | 0.02 | SB 8 | 44.50 | 0.58 | 0.03 | -5.69 | 0.04 |
| LPb 2 | 23.50 | 0.70 | 0.07 | -4.94 | 0.05 | SB 8,5 | 45.00 | 1.42 | 0.09 | -4.09 | 0.05 |
| LPb 2, 5 | 24.00 | 0.55 | 0.09 | -5.82 | 0.05 | SB 9,0 | 45.50 | 1.72 | 0.08 | -4.62 | 0.06 |
| LPb 3, 3 | 24.50 | 1.24 | 0.03 | -4.33 | 0.05 | SB 9,5 | 46.00 | 0.55 | 0.09 | -1.71 | 0.06 |
| LPb 3, 5 | 25.00 | 1.18 | 0.04 | -4.31 | 0.04 | SB 10,1 | 46.60 | 1.81 | 0.07 | -4.53 | 0.06 |
| LPb 4 | 25.50 | 1.37 | 0.08 | -3.65 | 0.07 | SB 10,6 | 47.10 | 1.97 | 0.07 | -4.92 | 0.05 |
| LPb 4, 5 | 26.00 | 1.43 | 0.05 | -4.47 | 0.06 | SB 11,1 | 47.60 | 2.11 | 0.06 | -4.18 | 0.04 |
| LPb 5 | 26.50 | 0.11 | 0.04 | -3.09 | 0.03 | SB 11,6 | 48.10 | 2.43 | 0.08 | -4.90 | 0.03 |

Appendix

| Sample | Depth (m) | $\delta^{13}\text{C}$ VPDB | s.d. | $\delta^{18}\text{O}$ VPDB | s.d. | Sample | Depth (m) | $\delta^{13}\text{C}$ VPDB | s.d. | $\delta^{18}\text{O}$ VPDB | s.d. |
|---------|-----------|----------------------------|------|----------------------------|------|---------|-----------|----------------------------|------|----------------------------|------|
| SB 12,1 | 48.60 | 2.09 | 0.04 | -5.14 | 0.02 | SB 36_5 | 73 | 2.87 | 0.01 | -3.67 | 0.05 |
| SB 12,4 | 48.90 | 1.77 | 0.07 | -4.99 | 0.04 | SB 37_0 | 73.5 | 2.79 | 0.03 | -3.54 | 0.04 |
| SB 12,9 | 49.40 | 1.91 | 0.03 | -5.19 | 0.05 | SB 37_5 | 74 | 2.66 | 0.04 | -4.23 | 0.06 |
| SB 13,3 | 49.80 | 2.00 | 0.07 | -4.35 | 0.04 | SB 38_0 | 74.5 | 2.39 | 0.03 | -4.81 | 0.03 |
| SB 13_5 | 50.00 | 2.14 | 0.03 | -5.15 | 0.08 | SB 38_5 | 75 | 2.79 | 0.05 | -4.77 | 0.03 |
| SB 14_0 | 50.50 | 2.36 | 0.05 | -4.7 | 0.04 | SB 38_9 | 75.5 | 2.08 | 0.07 | -4.30 | 0.03 |
| SB 14_5 | 51.00 | 2.25 | 0.03 | -4.79 | 0.07 | SB 39_2 | 75.7 | 2.94 | 0.05 | -3.93 | 0.02 |
| SB 15_0 | 51.50 | 1.66 | 0.09 | -4.39 | 0.04 | SB 35_5 | 76 | 3.12 | 0.03 | -4.53 | 0.02 |
| SB 15_5 | 52.00 | 0.84 | 0.03 | -3.6 | 0.04 | SB 40_0 | 76.5 | 2.96 | 0.01 | -4.32 | 0.07 |
| SB 16_0 | 52.50 | 1.87 | 0.04 | -3.5 | 0.03 | SB 40_5 | 77 | 2.79 | 0.05 | -4.77 | 0.03 |
| SB 16_5 | 53.00 | 1.99 | 0.06 | -3.57 | 0.04 | SB 41_0 | 77.5 | 2.61 | 0.06 | -4.60 | 0.05 |
| SB 17_0 | 53.50 | 1.96 | 0.02 | -4.47 | 0.05 | SB 41_5 | 78 | 2.56 | 0.04 | -3.49 | 0.03 |
| SB17_5 | 54.00 | 2.18 | 0.04 | -4.28 | 0.04 | SB 42_0 | 78.5 | 2.09 | 0.03 | -3.04 | 0.04 |
| SB 18_0 | 54.50 | 0.8 | 0.08 | -2.97 | 0.05 | SB 42_5 | 79 | 2.54 | 0.03 | -3.30 | 0.03 |
| SB 18_4 | 54.90 | 1.84 | 0.07 | -2.65 | 0.04 | SB 43_0 | 79.5 | 2.32 | 0.06 | -3.02 | 0.02 |
| SB 19_0 | 55.50 | 2.43 | 0.07 | -3.39 | 0.02 | SB 43_5 | 80 | 2.62 | 0.05 | -3.90 | 0.06 |
| SB 19_5 | 56.00 | 2.48 | 0.11 | -4.24 | 0.06 | SB 44_0 | 80.5 | 2.63 | 0.04 | -3.74 | 0.05 |
| SB 20_0 | 56.50 | 1.68 | 0.03 | -4.53 | 0.05 | SB 44_5 | 81 | 2.63 | 0.06 | -4.44 | 0.05 |
| SB 20_5 | 57.00 | 0.39 | 0.05 | -2.78 | 0.03 | SB 45_0 | 81.5 | 2.42 | 0.06 | -3.42 | 0.04 |
| SB 21_1 | 57.60 | 0.75 | 0.06 | -2.85 | 0.06 | SB 45_5 | 82 | 2.28 | 0.05 | -3.28 | 0.05 |
| SB 21_5 | 58.00 | 0.48 | 0.02 | -2.97 | 0.05 | SB 46_0 | 82.5 | 2.53 | 0.04 | -3.63 | 0.02 |
| SB 22_0 | 58.50 | 1.27 | 0.08 | -2.35 | 0.05 | SB 46_5 | 83 | 2.80 | 0.09 | -3.14 | 0.05 |
| SB 22_5 | 59.00 | 1.73 | 0.07 | -4.21 | 0.08 | SB 47_0 | 83.5 | 2.33 | 0.04 | -2.95 | 0.04 |
| SB 23_0 | 59.5 | 2.16 | 0.11 | -4.51 | 0.06 | SB 47_5 | 84 | 1.97 | 0.06 | -3.57 | 0.05 |
| SB 23_5 | 60 | 1.99 | 0.06 | -4.87 | 0.04 | SB 48_0 | 84.5 | 2.30 | 0.06 | -4.05 | 0.05 |
| SB 24_0 | 60.5 | 2.17 | 0.02 | -5.13 | 0.07 | SB 48_5 | 85 | 2.73 | 0.04 | -2.98 | 0.05 |
| SB 24_5 | 61 | 2.14 | 0.06 | -5.13 | 0.05 | SB 49_0 | 85.5 | 2.84 | 0.05 | -2.89 | 0.05 |
| SB 25_0 | 61.5 | 2.33 | 0.02 | -5.51 | 0.06 | SB 49_5 | 86 | 2.56 | 0.04 | -3.17 | 0.01 |
| SB 25_2 | 61.7 | 2.53 | 0.05 | -4.93 | 0.04 | SB 50_0 | 86.5 | 2.36 | 0.03 | -3.38 | 0.02 |
| SB 25_5 | 62 | 2.23 | 0.05 | -3.81 | 0.03 | SB 50_5 | 87 | 2.35 | 0.04 | -3.37 | 0.04 |
| SB 26_0 | 62.5 | 0.85 | 0.04 | -2.82 | 0.04 | SB 51_0 | 87.5 | 2.58 | 0.01 | -4.25 | 0.06 |
| SB 26_5 | 63 | 1.59 | 0.07 | -3.86 | 0.06 | SB 51_5 | 88 | 2.28 | 0.06 | -4.81 | 0.04 |
| SB 27_0 | 63.5 | 2.30 | 0.02 | -3.50 | 0.06 | SB 52_0 | 88.5 | 2.43 | 0.03 | -4.54 | 0.05 |
| SB 27_5 | 64 | 2.54 | 0.04 | -4.00 | 0.02 | SB 52_5 | 89 | 2.18 | 0.05 | -4.07 | 0.03 |
| SB 28_0 | 64.5 | 2.51 | 0.04 | -3.89 | 0.03 | SB 53_0 | 89.5 | 2.48 | 0.07 | -4.44 | 0.04 |
| SB 28_5 | 65 | 1.62 | 0.05 | -3.79 | 0.02 | SB 53_5 | 90 | 2.60 | 0.04 | -5.37 | 0.03 |
| SB 29_0 | 65.5 | 2.61 | 0.03 | -4.01 | 0.05 | SB 54_0 | 90.5 | 2.53 | 0.04 | -5.36 | 0.02 |
| SB 29_5 | 66 | 2.72 | 0.03 | -4.35 | 0.04 | SB 54_5 | 91 | 2.45 | 0.04 | -5.80 | 0.06 |
| SB 30_0 | 66.5 | 2.79 | 0.05 | -3.65 | 0.04 | SB 55_0 | 91.5 | 2.44 | 0.06 | -5.69 | 0.05 |
| SB 30_5 | 67 | 2.23 | 0.07 | -4.17 | 0.06 | SB 55_5 | 92 | 2.48 | 0.05 | -4.59 | 0.07 |
| SB 31_0 | 67.5 | 2.19 | 0.04 | -4.12 | 0.05 | SB 56_0 | 92.5 | 2.43 | 0.05 | -4.81 | 0.02 |
| SB 31_5 | 68 | 1.89 | 0.03 | -3.48 | 0.04 | SB 56_5 | 93 | 2.52 | 0.05 | -4.34 | 0.04 |
| SB 32_0 | 68.5 | 1.67 | 0.03 | -3.79 | 0.03 | SB 57_0 | 93.5 | 2.44 | 0.04 | -4.25 | 0.03 |
| SB 32_5 | 69 | 2.60 | 0.07 | -3.94 | 0.05 | SB 57_5 | 94 | 2.24 | 0.03 | -5.43 | 0.03 |
| SB 33_0 | 69.5 | 2.92 | 0.08 | -4.20 | 0.05 | SB 58_0 | 94.5 | 2.58 | 0.05 | -3.86 | 0.03 |
| SB 33_5 | 70 | 2.81 | 0.05 | -4.21 | 0.05 | SB 58_5 | 95 | 2.52 | 0.02 | -4.84 | 0.04 |
| SB 34_0 | 70.5 | 2.90 | 0.06 | -4.38 | 0.05 | SB 59_0 | 95.5 | 2.43 | 0.05 | -4.54 | 0.04 |
| SB 34_5 | 71 | 2.81 | 0.03 | -4.82 | 0.04 | SB 59_5 | 96 | 2.30 | 0.07 | -4.31 | 0.04 |
| SB 35_0 | 71.5 | 2.93 | 0.04 | -3.89 | 0.03 | SB 60_0 | 96.5 | 2.51 | 0.05 | -3.72 | 0.05 |
| SB 35_5 | 72 | 2.86 | 0.04 | -3.28 | 0.02 | SB 60_5 | 97 | 2.63 | 0.06 | -3.83 | 0.04 |
| SB 36_0 | 72.5 | 2.82 | 0.08 | -3.48 | 0.04 | SB 61_0 | 97.5 | 2.61 | 0.03 | -3.85 | 0.03 |

| Sample | Depth (m) | $\delta^{13}\text{C}$ VPDB | s.d. | $\delta^{18}\text{O}$ VPDB | s.d. | Sample | Depth (m) | $\delta^{13}\text{C}$ VPDB | s.d. | $\delta^{18}\text{O}$ VPDB | s.d. |
|---------|-----------|----------------------------|------|----------------------------|------|---------|-----------|----------------------------|------|----------------------------|------|
| SB 61_5 | 98 | 2.65 | 0.02 | -3.92 | 0.06 | SB 87_0 | 123.5 | 2.93 | 0.02 | -4.25 | 0.04 |
| SB 62_0 | 98.5 | 2.57 | 0.04 | -4.72 | 0.05 | SB 87_5 | 126.5 | 2.82 | 0.04 | -4.00 | 0.02 |
| SB 62_5 | 99 | 2.75 | 0.06 | -3.78 | 0.04 | SB 88_0 | 127 | 2.75 | 0.06 | -4.12 | 0.02 |
| SB 63_0 | 99.5 | 2.65 | 0.06 | -3.92 | 0.03 | SB 88_5 | 127.5 | 2.16 | 0.05 | -4.37 | 0.05 |
| SB 63_5 | 100 | 2.65 | 0.03 | -3.78 | 0.07 | SB 89_0 | 128 | 2.11 | 0.03 | -4.58 | 0.02 |
| SB 64_0 | 100.5 | 2.63 | 0.05 | -3.63 | 0.03 | | | | | | |
| SB 64_5 | 101 | 2.67 | 0.07 | -4.01 | 0.03 | | | | | | |
| SB 65_0 | 101.5 | 2.57 | 0.03 | -4.53 | 0.03 | | | | | | |
| SB 65_5 | 102 | 2.66 | 0.05 | -3.73 | 0.04 | | | | | | |
| SB 66_0 | 102.5 | 2.66 | 0.05 | -4.27 | 0.04 | | | | | | |
| SB 66_5 | 103 | 2.72 | 0.04 | -4.28 | 0.02 | | | | | | |
| SB 67_0 | 103.5 | 2.75 | 0.05 | -3.89 | 0.05 | | | | | | |
| SB 67_5 | 104 | 2.83 | 0.04 | -3.50 | 0.04 | | | | | | |
| SB 68_0 | 104.5 | 2.73 | 0.02 | -3.04 | 0.05 | | | | | | |
| SB 68_5 | 105 | 2.84 | 0.06 | -3.84 | 0.03 | | | | | | |
| SB 69_0 | 105.5 | 2.57 | 0.05 | -3.36 | 0.03 | | | | | | |
| SB 69_5 | 106 | 2.37 | 0.06 | -4.77 | 0.02 | | | | | | |
| SB 70_0 | 106.5 | 2.48 | 0.05 | -4.82 | 0.02 | | | | | | |
| SB 70_5 | 107 | 2.41 | 0.06 | -4.86 | 0.04 | | | | | | |
| SB 71_0 | 107.5 | 2.55 | 0.03 | -3.08 | 0.02 | | | | | | |
| SB 71_5 | 108 | 2.65 | 0.07 | -3.34 | 0.03 | | | | | | |
| SB 72_0 | 108.5 | 2.48 | 0.03 | -4.00 | 0.03 | | | | | | |
| SB 72_5 | 109 | 2.63 | 0.05 | -3.41 | 0.03 | | | | | | |
| SB 73_0 | 109.5 | 2.52 | 0.06 | -2.33 | 0.04 | | | | | | |
| SB 73_5 | 110 | 2.42 | 0.03 | -2.96 | 0.03 | | | | | | |
| SB 74_0 | 110.5 | 2.32 | 0.05 | -3.37 | 0.04 | | | | | | |
| SB 74_5 | 111 | 2.20 | 0.07 | -3.10 | 0.03 | | | | | | |
| SB 75_0 | 111.5 | 2.28 | 0.06 | -3.11 | 0.03 | | | | | | |
| SB 75_5 | 112 | 2.22 | 0.04 | -2.92 | 0.04 | | | | | | |
| SB 76_0 | 112.5 | 1.96 | 0.02 | -3.32 | 0.02 | | | | | | |
| SB 76_5 | 113 | 1.77 | 0.06 | -2.26 | 0.03 | | | | | | |
| SB 77_0 | 113.5 | 1.64 | 0.08 | -2.61 | 0.05 | | | | | | |
| SB 77_5 | 114 | 0.95 | 0.07 | -3.06 | 0.04 | | | | | | |
| SB 78_0 | 114.5 | 1.44 | 0.02 | -3.74 | 0.06 | | | | | | |
| SB 78_5 | 115 | 1.15 | 0.05 | -2.34 | 0.05 | | | | | | |
| SB 79_0 | 115.5 | 1.25 | 0.02 | -2.98 | 0.06 | | | | | | |
| SB 79_5 | 116 | 1.42 | 0.07 | -3.37 | 0.04 | | | | | | |
| SB 80_0 | 116.5 | 1.73 | 0.05 | -2.99 | 0.02 | | | | | | |
| SB 80_5 | 117 | 0.77 | 0.02 | -2.35 | 0.03 | | | | | | |
| SB 81_0 | 117.5 | 0.31 | 0.07 | -2.32 | 0.02 | | | | | | |
| SB 81_5 | 118 | 0.97 | 0.03 | -2.98 | 0.04 | | | | | | |
| SB 82_0 | 118.5 | 1.69 | 0.04 | -2.74 | 0.04 | | | | | | |
| SB 82_5 | 119 | 2.11 | 0.02 | -2.08 | 0.06 | | | | | | |
| SB 83_0 | 119.5 | 2.83 | 0.04 | -2.20 | 0.03 | | | | | | |
| SB 83_5 | 120 | 2.78 | 0.06 | -2.30 | 0.04 | | | | | | |
| SB 84_0 | 120.5 | 2.87 | 0.06 | -2.76 | 0.05 | | | | | | |
| SB 84_5 | 121 | 2.84 | 0.04 | -2.65 | 0.04 | | | | | | |
| SB 85_0 | 121.5 | 3.06 | 0.06 | -3.24 | 0.03 | | | | | | |
| SB 85_5 | 122 | 3.06 | 0.05 | -4.19 | 0.04 | | | | | | |
| SB 86_0 | 122.5 | 2.96 | 0.07 | -4.33 | 0.05 | | | | | | |
| SB 86_5 | 123 | 2.96 | 0.10 | -4.62 | 0.05 | | | | | | |

Appendix

Appendix 9 Carbon and oxygen isotope results of drilled powder, Bisperode section

| Sample | Depth (m) | $\delta^{13}\text{C}$ VPDB | s.d. | $\delta^{18}\text{O}$ VPDB | s.d. | Sample | Depth (m) | $\delta^{13}\text{C}$ VPDB | s.d. | $\delta^{18}\text{O}$ VPDB | s.d. |
|----------|-----------|----------------------------|------|----------------------------|------|----------|-----------|----------------------------|------|----------------------------|------|
| SA_10_25 | 9 | 0.72 | 0.04 | -5.37 | 0.04 | SA_22_75 | 21.5 | 0.92 | 0.05 | -5.62 | 0.04 |
| SA_10_5 | 9.25 | 0.99 | 0.05 | -5.13 | 0.03 | SA_23_0 | 21.75 | 1.14 | 0.09 | -4.37 | 0.02 |
| SA_10_75 | 9.5 | 0.84 | 0.04 | -5.70 | 0.03 | SA_23_25 | 22 | 1.55 | 0.04 | -5.06 | 0.04 |
| SA_11_0 | 9.75 | 0.98 | 0.03 | -5.85 | 0.03 | SA_23_5 | 22.25 | 1.59 | 0.06 | -1.87 | 0.04 |
| SA_11_25 | 10 | 1.11 | 0.06 | -5.32 | 0.02 | SA_23_75 | 22.5 | 1.72 | 0.02 | -3.74 | 0.05 |
| SA_11_5 | 10.25 | 0.88 | 0.01 | -5.35 | 0.06 | SA_24_0 | 22.75 | 1.50 | 0.03 | -4.52 | 0.03 |
| SA_11_75 | 10.5 | 1.12 | 0.04 | -5.54 | 0.03 | SA_24_25 | 23 | 1.67 | 0.03 | -4.68 | 0.02 |
| SA_12_0 | 10.75 | 1.13 | 0.04 | -5.59 | 0.02 | SA_24_5 | 23.25 | 1.15 | 0.02 | -4.37 | 0.04 |
| SA_12_25 | 11 | 1.35 | 0.06 | -5.37 | 0.03 | SA_24_75 | 23.5 | 0.73 | 0.04 | -5.26 | 0.03 |
| SA_12_5 | 11.25 | 1.27 | 0.05 | -5.19 | 0.05 | SA_25_0 | 23.75 | 1.27 | 0.07 | -4.45 | 0.05 |
| SA_12_75 | 11.5 | 1.51 | 0.04 | -5.35 | 0.03 | SA_25_25 | 24 | 0.77 | 0.04 | -4.93 | 0.04 |
| SA_13_0 | 11.75 | 1.56 | 0.05 | -5.09 | 0.04 | SA_25_50 | 24.25 | 1.30 | 0.07 | -4.82 | 0.04 |
| SA_13_25 | 12 | 1.28 | 0.06 | -5.22 | 0.04 | SA_25_75 | 24.5 | 1.17 | 0.06 | -5.46 | 0.05 |
| SA_13_5 | 12.25 | 1.48 | 0.02 | -4.19 | 0.08 | SA_26_0 | 24.75 | 1.49 | 0.08 | -4.88 | 0.06 |
| SA_13_75 | 12.5 | 1.31 | 0.05 | -4.65 | 0.05 | SA_26_25 | 25 | 0.78 | 0.05 | -4.24 | 0.04 |
| SA_14_0 | 12.75 | 0.70 | 0.02 | -3.81 | 0.05 | SA_26_50 | 25.25 | 0.71 | 0.02 | -3.66 | 0.04 |
| SA_14_25 | 13 | 0.88 | 0.03 | -4.28 | 0.03 | SA_26_75 | 25.5 | 0.58 | 0.03 | -3.99 | 0.03 |
| SA_14_5 | 13.25 | 1.16 | 0.03 | -4.50 | 0.04 | SA_27_0 | 25.75 | 0.49 | 0.06 | -3.78 | 0.03 |
| SA_14_75 | 13.5 | 0.64 | 0.07 | -4.72 | 0.04 | SA_27_25 | 26 | 1.40 | 0.07 | -4.88 | 0.07 |
| SA_15_0 | 13.75 | 0.23 | 0.02 | -6.36 | 0.06 | SA_27_50 | 26.25 | 1.41 | 0.06 | -4.23 | 0.02 |
| SA_15_25 | 14 | 0.76 | 0.03 | -3.16 | 0.06 | SA_27_75 | 26.5 | 1.92 | 0.06 | -2.98 | 0.03 |
| SA_15_5 | 14.25 | -0.03 | 0.07 | -2.64 | 0.03 | SA_28_0 | 26.75 | 1.41 | 0.04 | -3.68 | 0.02 |
| SA_15_75 | 14.5 | -0.14 | 0.05 | -1.56 | 0.05 | SA_28_25 | 27 | -0.79 | 0.05 | -5.06 | 0.02 |
| SA_16_0 | 14.75 | 0.01 | 0.06 | -1.27 | 0.02 | SA_28_5 | 27.25 | -0.67 | 0.06 | -4.73 | 0.04 |
| SA_16_25 | 15 | 0.14 | 0.06 | -1.33 | 0.04 | SA_28_75 | 27.5 | -0.63 | 0.06 | -5.19 | 0.03 |
| SA_16_5 | 15.25 | -0.11 | 0.04 | -2.89 | 0.04 | SA_29_0 | 27.75 | -0.65 | 0.07 | -4.60 | 0.05 |
| SA_16_75 | 15.5 | 0.55 | 0.06 | -3.64 | 0.05 | SA_29_25 | 28 | -0.21 | 0.05 | -3.35 | 0.03 |
| SA_17_0 | 15.75 | 0.23 | 0.02 | -3.24 | 0.06 | SA_29_5 | 28.25 | 0.74 | 0.04 | -3.43 | 0.04 |
| SA_17_25 | 16 | -0.28 | 0.03 | -2.78 | 0.03 | SA_29_75 | 28.5 | 0.38 | 0.04 | -4.03 | 0.03 |
| SA_17_5 | 16.25 | -0.80 | 0.05 | -4.02 | 0.02 | SA_30_0 | 28.75 | 0.37 | 0.01 | -2.77 | 0.05 |
| SA_17_75 | 16.5 | 0.94 | 0.08 | -5.79 | 0.04 | SA_30_25 | 29 | 0.32 | 0.06 | -2.59 | 0.03 |
| SA_18_0 | 16.75 | 0.13 | 0.03 | -6.28 | 0.02 | SA_30_5 | 29.25 | -0.57 | 0.06 | -2.45 | 0.03 |
| SA_18_25 | 17 | 1.43 | 0.07 | -4.58 | 0.03 | SA_30_75 | 29.5 | 0.56 | 0.04 | -2.84 | 0.04 |
| SA_18_5 | 17.25 | 1.37 | 0.04 | -5.07 | 0.03 | SA_31_0 | 29.75 | 0.92 | 0.03 | -3.10 | 0.05 |
| SA_18_75 | 17.5 | 1.43 | 0.05 | -5.05 | 0.04 | SA_31_25 | 30 | 0.48 | 0.05 | -3.73 | 0.04 |
| SA_19_0 | 17.75 | 1.70 | 0.04 | -5.22 | 0.04 | SA_31_5 | 30.25 | 0.59 | 0.06 | -4.14 | 0.04 |
| SA_19_25 | 18 | 1.71 | 0.06 | -5.48 | 0.03 | SA_31_75 | 30.5 | 0.65 | 0.06 | -3.83 | 0.04 |
| SA_19_5 | 18.25 | 1.50 | 0.03 | -5.35 | 0.06 | SA_32_0 | 30.75 | 1.22 | 0.03 | -4.53 | 0.05 |
| SA_19_75 | 18.5 | 1.46 | 0.04 | -5.34 | 0.03 | SA_32_25 | 31 | 1.26 | 0.04 | -4.29 | 0.05 |
| SA_20_0 | 18.75 | 1.46 | 0.04 | -5.44 | 0.01 | SA_32_5 | 31.25 | 0.65 | 0.05 | -2.61 | 0.06 |
| SA_20_25 | 19 | 1.45 | 0.02 | -5.62 | 0.03 | SA_32_75 | 31.5 | 1.17 | 0.07 | -4.01 | 0.02 |
| SA_20_5 | 19.25 | 1.64 | 0.03 | -5.58 | 0.02 | SA_33_0 | 31.75 | 1.56 | 0.08 | -3.89 | 0.04 |
| SA_20_75 | 19.5 | 1.58 | 0.03 | -5.39 | 0.03 | SA_33_25 | 32 | 1.77 | 0.04 | -5.18 | 0.05 |
| SA_21_0 | 19.75 | 1.65 | 0.06 | -5.22 | 0.05 | SA_33_5 | 32.25 | 1.48 | 0.05 | -4.19 | 0.05 |
| SA_21_25 | 20 | 1.59 | 0.07 | -5.23 | 0.04 | SA_33_75 | 32.5 | 1.71 | 0.04 | -3.80 | 0.03 |
| SA_21_5 | 20.25 | 1.04 | 0.06 | -5.35 | 0.03 | SA_34_0 | 32.75 | 1.36 | 0.05 | -3.60 | 0.04 |
| SA_21_75 | 20.5 | 1.05 | 0.05 | -5.45 | 0.04 | SA_34_25 | 33 | 1.54 | 0.05 | -3.79 | 0.03 |
| SA_22_0 | 20.75 | 0.70 | 0.03 | -5.32 | 0.03 | SA_34_5 | 33.25 | 1.82 | 0.02 | -4.62 | 0.04 |
| SA_22_25 | 21 | 0.47 | 0.04 | -6.02 | 0.03 | SA_34_75 | 33.5 | 1.09 | 0.04 | -4.44 | 0.03 |
| SA_22_5 | 21.25 | 0.01 | 0.05 | -6.37 | 0.03 | SA_35_0 | 33.75 | 1.35 | 0.07 | -4.67 | 0.06 |

| Sample | Depth (m) | $\delta^{13}\text{C}$ VPDB | s.d. | $\delta^{18}\text{O}$ VPDB | s.d. | Sample | Depth (m) | $\delta^{13}\text{C}$ VPDB | s.d. | $\delta^{18}\text{O}$ VPDB | s.d. |
|----------|-----------|----------------------------|------|----------------------------|------|----------|-----------|----------------------------|------|----------------------------|------|
| SA 35_25 | 34 | 1.39 | 0.07 | -5.17 | 0.04 | SA 48_0 | 46.75 | 2.11 | 0.04 | -4.79 | 0.04 |
| SA 35_5 | 34.25 | 2.00 | 0.04 | -4.50 | 0.02 | SA 48_25 | 47 | 2.37 | 0.04 | -4.18 | 0.04 |
| SA 35_75 | 34.5 | 2.13 | 0.08 | -4.83 | 0.07 | SA 48_50 | 47.25 | 2.45 | 0.06 | -4.25 | 0.04 |
| SA 36_0 | 34.75 | 1.83 | 0.03 | -4.68 | 0.01 | SA 48_75 | 47.5 | 2.06 | 0.02 | -5.13 | 0.02 |
| SA 36_25 | 35 | 1.78 | 0.05 | -4.55 | 0.01 | SA 49_0 | 47.75 | 2.21 | 0.03 | -4.72 | 0.03 |
| SA 36_5 | 35.25 | 1.31 | 0.07 | -4.75 | 0.04 | SA 49_25 | 48 | 2.10 | 0.07 | -5.14 | 0.05 |
| SA 36_75 | 35.5 | 0.12 | 0.05 | -5.08 | 0.04 | SA 49_50 | 48.25 | 2.13 | 0.03 | -5.19 | 0.03 |
| SA 37_0 | 35.75 | 0.92 | 0.05 | -5.19 | 0.04 | SA 49_75 | 48.5 | 2.17 | 0.07 | -5.14 | 0.03 |
| SA 37_25 | 36 | 1.23 | 0.07 | -4.91 | 0.05 | SA 50_0 | 48.75 | 2.13 | 0.07 | -4.90 | 0.05 |
| SA 37_5 | 36.25 | 1.07 | 0.06 | -4.73 | 0.03 | SA 50_25 | 49 | 2.10 | 0.06 | -5.02 | 0.03 |
| SA 37_75 | 36.5 | 1.32 | 0.09 | -3.09 | 0.03 | SA 50_50 | 49.25 | 2.15 | 0.04 | -5.03 | 0.04 |
| SA 38_0 | 36.75 | 1.54 | 0.08 | -3.62 | 0.04 | SA 50_75 | 49.5 | 2.10 | 0.06 | -4.18 | 0.04 |
| SA 38_25 | 37 | 2.05 | 0.09 | -4.10 | 0.05 | | | | | | |
| SA 38_5 | 37.25 | 2.26 | 0.03 | -3.82 | 0.03 | | | | | | |
| SA 38_75 | 37.5 | 2.25 | 0.05 | -3.99 | 0.04 | | | | | | |
| SA 39_0 | 37.75 | 1.90 | 0.03 | -4.61 | 0.02 | | | | | | |
| SA 39_25 | 38 | 2.02 | 0.03 | -4.58 | 0.04 | | | | | | |
| SA 39_5 | 38.25 | 1.92 | 0.04 | -4.83 | 0.05 | | | | | | |
| SA 39_75 | 38.5 | 1.75 | 0.05 | -5.35 | 0.05 | | | | | | |
| SA 40_0 | 38.75 | 1.97 | 0.02 | -4.81 | 0.05 | | | | | | |
| SA 40_25 | 39 | 1.77 | 0.06 | -4.86 | 0.03 | | | | | | |
| SA 40_5 | 39.25 | 2.00 | 0.02 | -4.64 | 0.05 | | | | | | |
| SA 40_75 | 39.5 | 1.78 | 0.06 | -4.19 | 0.05 | | | | | | |
| SA 41_0 | 39.75 | 1.97 | 0.05 | -4.27 | 0.04 | | | | | | |
| SA 41_25 | 40 | 2.00 | 0.09 | -4.69 | 0.05 | | | | | | |
| SA 41_5 | 40.25 | 2.05 | 0.05 | -4.03 | 0.03 | | | | | | |
| SA 41_75 | 40.5 | 2.08 | 0.06 | -4.42 | 0.03 | | | | | | |
| SA 42_0 | 40.75 | 1.92 | 0.07 | -4.97 | 0.05 | | | | | | |
| SA 42_25 | 41 | 1.84 | 0.03 | -4.87 | 0.03 | | | | | | |
| SA 42_5 | 41.25 | 1.92 | 0.02 | -5.23 | 0.03 | | | | | | |
| SA 42_75 | 41.5 | 2.01 | 0.04 | -4.91 | 0.04 | | | | | | |
| SA 43_0 | 41.75 | 1.83 | 0.05 | -5.07 | 0.04 | | | | | | |
| SA 43_25 | 42 | 1.84 | 0.04 | -5.06 | 0.04 | | | | | | |
| SA 43_50 | 42.25 | 1.96 | 0.06 | -4.81 | 0.05 | | | | | | |
| SA 43_75 | 42.5 | 1.89 | 0.03 | -4.85 | 0.05 | | | | | | |
| SA 44_0 | 42.75 | 1.87 | 0.06 | -4.04 | 0.06 | | | | | | |
| SA 44_25 | 43 | 1.89 | 0.06 | -4.19 | 0.04 | | | | | | |
| SA 44_50 | 43.25 | 1.07 | 0.05 | -4.50 | 0.05 | | | | | | |
| SA 44_75 | 43.5 | 1.63 | 0.06 | -4.21 | 0.02 | | | | | | |
| SA 45_0 | 43.75 | 1.68 | 0.06 | -4.05 | 0.04 | | | | | | |
| SA 45_25 | 44 | 0.05 | 0.05 | -5.99 | 0.03 | | | | | | |
| SA 45_50 | 44.25 | 0.15 | 0.02 | -5.99 | 0.02 | | | | | | |
| SA 45_75 | 44.5 | 0.44 | 0.05 | -5.81 | 0.04 | | | | | | |
| SA 46_0 | 44.75 | 1.03 | 0.04 | -3.95 | 0.04 | | | | | | |
| SA 46_25 | 45 | 1.61 | 0.06 | -4.13 | 0.06 | | | | | | |
| SA 46_50 | 45.25 | 1.38 | 0.02 | -4.07 | 0.02 | | | | | | |
| SA 46_75 | 45.5 | 1.31 | 0.03 | -4.38 | 0.02 | | | | | | |
| SA 47_0 | 45.75 | 1.30 | 0.06 | -5.06 | 0.05 | | | | | | |
| SA 47_25 | 46 | 1.63 | 0.07 | -4.42 | 0.04 | | | | | | |
| SA 47_50 | 46.25 | 1.80 | 0.08 | -4.65 | 0.06 | | | | | | |
| SA 47_75 | 46.5 | 1.86 | 0.05 | -4.78 | 0.07 | | | | | | |

Appendix

Appendix 10 Carbon and oxygen isotope results of drilled powder, Konrad #101 core

| Sample | Depth (m) | $\delta^{13}\text{C}$ VPDB | s.d. | $\delta^{18}\text{O}$ VPDB | s.d. | Sample | Depth (m) | $\delta^{13}\text{C}$ VPDB | s.d. | $\delta^{18}\text{O}$ VPDB | s.d. |
|----------|-----------|----------------------------|------|----------------------------|------|----------|-----------|----------------------------|------|----------------------------|------|
| K_624_96 | 624.96 | 0.80 | 0.09 | 3.10 | 0.06 | K_646_99 | 646.99 | 1.82 | 0.07 | -2.70 | 0.03 |
| K_625_46 | 625.46 | 0.84 | 0.08 | 2.91 | 0.03 | K_647_49 | 647.49 | 1.53 | 0.09 | -1.83 | 0.07 |
| K_625_77 | 625.77 | 1.09 | 0.05 | 2.62 | 0.02 | K_647_93 | 647.93 | 1.06 | 0.11 | -1.88 | 0.07 |
| K_625_90 | 625.90 | 4.60 | 0.03 | 1.26 | 0.06 | K_648_43 | 648.43 | 1.16 | 0.02 | -1.42 | 0.04 |
| K_626_37 | 626.37 | 2.25 | 0.06 | 1.89 | 0.07 | K_648_86 | 648.86 | 1.41 | 0.09 | -1.30 | 0.05 |
| K_626_87 | 626.87 | 0.81 | 0.11 | 1.71 | 0.06 | K_649_36 | 649.36 | 1.37 | 0.06 | -1.50 | 0.05 |
| K_627_15 | 627.15 | 0.93 | 0.07 | 1.70 | 0.05 | K_649_76 | 649.76 | 0.90 | 0.07 | -1.35 | 0.07 |
| K_627_65 | 627.65 | 0.78 | 0.08 | 0.77 | 0.06 | K_650_26 | 650.26 | 1.97 | 0.06 | -2.79 | 0.03 |
| K_628_16 | 628.16 | - | - | - | - | K_650_72 | 650.72 | 1.31 | 0.09 | -3.74 | 0.06 |
| K_628_66 | 628.66 | 0.44 | 0.03 | 1.99 | 0.04 | K_651_22 | 651.22 | 1.06 | 0.03 | -4.03 | 0.03 |
| K_629_08 | 629.08 | 0.51 | 0.05 | 2.88 | 0.06 | K_651_64 | 651.64 | 1.60 | 0.03 | -4.09 | 0.03 |
| K_629_58 | 629.58 | 0.06 | 0.05 | 2.71 | 0.05 | K_652_25 | 652.25 | 1.57 | 0.04 | -3.61 | 0.03 |
| K_629_85 | 629.85 | 0.71 | 0.08 | 1.19 | 0.08 | K_652_45 | 652.45 | 0.96 | 0.06 | -4.11 | 0.02 |
| K_630_35 | 630.35 | 0.20 | 0.09 | 2.14 | 0.05 | K_652_95 | 652.95 | 1.23 | 0.05 | -4.12 | 0.03 |
| K_630_78 | 630.78 | 0.56 | 0.05 | 1.33 | 0.04 | K_653_25 | 653.25 | 1.29 | 0.04 | -3.99 | 0.06 |
| K_631_28 | 631.28 | 0.85 | 0.08 | 1.34 | 0.04 | K_653_75 | 653.75 | 1.64 | 0.06 | -3.88 | 0.06 |
| K_631_78 | 631.78 | 0.36 | 0.05 | 1.57 | 0.04 | K_654_15 | 654.15 | 1.22 | 0.04 | -3.61 | 0.03 |
| K_632_23 | 632.23 | 3.93 | 0.08 | 1.18 | 0.04 | K_654_65 | 654.65 | 1.47 | 0.07 | -4.33 | 0.05 |
| K_632_68 | 632.68 | 0.08 | 0.02 | 3.15 | 0.03 | K_655_11 | 655.11 | 1.04 | 0.04 | -2.90 | 0.06 |
| K_633_18 | 633.18 | 0.03 | 0.05 | 2.15 | 0.03 | K_655_61 | 655.61 | 0.82 | 0.06 | -1.89 | 0.05 |
| K_633_53 | 633.53 | 0.03 | 0.10 | 0.82 | 0.08 | K_656_04 | 656.04 | 0.02 | 0.08 | -0.99 | 0.03 |
| K_634_03 | 634.03 | 0.21 | 0.07 | 0.90 | 0.03 | K_656_54 | 656.54 | 0.23 | 0.10 | -2.56 | 0.09 |
| K_634_50 | 634.50 | 0.11 | 0.06 | 2.58 | 0.01 | K_656_99 | 656.99 | 0.34 | 0.07 | -2.23 | 0.03 |
| K_635_00 | 635.00 | 0.29 | 0.05 | 1.14 | 0.03 | K_657_49 | 657.49 | 0.78 | 0.08 | -2.31 | 0.04 |
| K_635_25 | 635.25 | 0.59 | 0.06 | 1.76 | 0.05 | K_657_97 | 657.97 | 0.81 | 0.04 | -2.07 | 0.02 |
| K_635_80 | 635.80 | 0.70 | 0.07 | 0.84 | 0.04 | K_658_47 | 658.47 | 0.86 | 0.06 | -3.03 | 0.04 |
| K_636_15 | 636.15 | 0.73 | 0.05 | 0.83 | 0.02 | K_658_97 | 658.97 | - | - | - | - |
| K_636_75 | 636.75 | 1.26 | 0.02 | 2.47 | 0.05 | K_659_42 | 659.42 | 1.58 | 0.05 | -2.92 | 0.08 |
| K_637_08 | 637.08 | 1.63 | 0.07 | 0.72 | 0.07 | K_659_89 | 659.89 | 1.63 | 0.08 | -3.00 | 0.03 |
| K_637_53 | 637.53 | 1.26 | 0.06 | 2.86 | 0.04 | K_660_39 | 660.39 | 1.70 | 0.05 | -3.49 | 0.05 |
| K_637_98 | 637.98 | 0.45 | 0.07 | 2.27 | 0.05 | K_660_71 | 660.71 | 1.23 | 0.07 | -3.51 | 0.03 |
| K_638_48 | 638.48 | 1.31 | 0.12 | 1.96 | 0.06 | K_661_31 | 661.31 | 1.77 | 0.06 | -3.81 | 0.04 |
| K_638_91 | 638.91 | 0.46 | 0.02 | 1.79 | 0.05 | K_661_61 | 661.61 | 1.73 | 0.03 | -3.67 | 0.04 |
| K_639_41 | 639.41 | 1.37 | 0.11 | 1.20 | 0.05 | K_662_05 | 662.05 | 1.68 | 0.05 | -2.61 | 0.03 |
| K_639_82 | 639.82 | 1.68 | 0.05 | 1.60 | 0.02 | K_662_75 | 662.75 | 1.68 | 0.03 | -3.13 | 0.04 |
| K_640_32 | 640.32 | 2.30 | 0.11 | 1.18 | 0.04 | K_663_13 | 663.13 | 1.84 | 0.08 | -1.15 | 0.04 |
| K_640_78 | 640.78 | 2.22 | 0.06 | 1.06 | 0.04 | K_663_63 | 663.63 | 1.80 | 0.06 | -2.45 | 0.04 |
| K_641_33 | 641.33 | 1.65 | 0.10 | 1.05 | 0.04 | K_664_04 | 664.04 | 1.87 | 0.08 | -2.57 | 0.08 |
| K_641_73 | 641.73 | 0.76 | 0.06 | 1.67 | 0.03 | K_664_49 | 664.49 | 1.66 | 0.10 | -3.14 | 0.06 |
| K_642_23 | 642.23 | 1.30 | 0.06 | 0.59 | 0.07 | K_664_93 | 664.93 | 2.14 | 0.05 | -0.66 | 0.06 |
| K_642_68 | 642.68 | 1.74 | 0.02 | 0.17 | 0.03 | K_665_43 | 665.43 | 2.12 | 0.10 | -0.36 | 0.07 |
| K_643_22 | 643.22 | 1.31 | 0.05 | 3.77 | 0.03 | K_665_88 | 665.88 | 1.49 | 0.05 | -2.12 | 0.03 |
| K_643_49 | 643.49 | 0.98 | 0.03 | 3.57 | 0.07 | K_666_38 | 666.38 | 1.65 | 0.04 | -2.70 | 0.03 |
| K_643_94 | 643.94 | 1.07 | 0.07 | 3.85 | 0.04 | K_666_74 | 666.74 | 1.30 | 0.05 | -3.13 | 0.05 |
| K_644_25 | 644.25 | 1.21 | 0.07 | 3.60 | 0.06 | K_667_19 | 667.19 | 1.41 | 0.07 | -4.21 | 0.04 |
| K_644_75 | 644.75 | 0.99 | 0.03 | 3.48 | 0.04 | K_667_54 | 667.54 | 1.68 | 0.06 | -4.19 | 0.07 |
| K_645_15 | 645.15 | 1.42 | 0.04 | 3.48 | 0.04 | K_668_04 | 668.04 | 1.77 | 0.09 | -4.01 | 0.05 |
| K_645_65 | 645.65 | 1.41 | 0.06 | 3.14 | 0.05 | K_668_37 | 668.37 | 1.16 | 0.05 | -3.42 | 0.03 |
| K_645_98 | 645.98 | 1.65 | 0.13 | 2.43 | 0.06 | K_668_87 | 668.87 | 1.35 | 0.08 | -3.61 | 0.04 |
| K_646_48 | 646.48 | 1.85 | 0.07 | 2.98 | 0.07 | K_669_27 | 669.27 | 0.68 | 0.08 | -3.80 | 0.03 |

| Sample | Depth (m) | $\delta^{13}\text{C}$ VPDB | s.d. | $\delta^{18}\text{O}$ VPDB | s.d. | Sample | Depth (m) | $\delta^{13}\text{C}$ VPDB | s.d. | $\delta^{18}\text{O}$ VPDB | s.d. |
|----------|-----------|----------------------------|------|----------------------------|------|----------|-----------|----------------------------|------|----------------------------|------|
| K_669_53 | 669.53 | 1.05 | 0.03 | -3.22 | 0.02 | K_692_45 | 692.45 | 1.68 | 0.05 | -2.12 | 0.04 |
| K_670_08 | 670.08 | 1.11 | 0.05 | -3.26 | 0.03 | K_692_95 | 692.95 | 2.10 | 0.05 | -2.76 | 0.03 |
| K_670_55 | 670.55 | 1.95 | 0.07 | -2.47 | 0.02 | K_693_48 | 693.48 | 2.70 | 0.06 | -2.15 | 0.04 |
| K_671_05 | 671.05 | 2.07 | 0.07 | -3.66 | 0.04 | K_693_88 | 693.88 | 2.52 | 0.08 | -2.28 | 0.03 |
| K_671_54 | 671.54 | 1.15 | 0.09 | -2.06 | 0.04 | K_694_36 | 694.36 | 2.19 | 0.06 | -2.36 | 0.05 |
| K_672_04 | 672.04 | 1.11 | 0.07 | -2.42 | 0.05 | K_694_86 | 694.86 | 2.30 | 0.06 | -2.35 | 0.05 |
| K_672_45 | 672.45 | 1.29 | 0.06 | -4.25 | 0.04 | K_695_35 | 695.35 | 2.66 | 0.09 | -3.22 | 0.03 |
| K_672_95 | 672.95 | 1.04 | 0.06 | -3.87 | 0.06 | K_695_80 | 695.80 | 1.58 | 0.11 | -3.20 | 0.08 |
| K_673_35 | 673.35 | 1.31 | 0.05 | -3.89 | 0.03 | K_696_27 | 696.27 | 1.92 | 0.05 | -2.87 | 0.03 |
| K_673_85 | 673.85 | 1.47 | 0.06 | -3.67 | 0.04 | K_696_77 | 696.77 | 2.30 | 0.08 | -2.68 | 0.10 |
| K_674_35 | 674.35 | 1.84 | 0.09 | -3.37 | 0.11 | K_697_10 | 697.10 | 1.93 | 0.06 | -2.49 | 0.06 |
| K_674_70 | 674.70 | 1.38 | 0.04 | -2.67 | 0.05 | K_697_60 | 697.60 | 2.01 | 0.04 | -2.70 | 0.04 |
| K_675_24 | 675.24 | 1.35 | 0.08 | -3.01 | 0.07 | K_698_10 | 698.10 | 2.23 | 0.07 | -2.74 | 0.06 |
| K_675_69 | 675.69 | 1.74 | 0.08 | -4.31 | 0.06 | K_698_41 | 698.41 | 2.17 | 0.08 | -2.74 | 0.05 |
| K_676_19 | 676.19 | 1.65 | 0.06 | -3.74 | 0.02 | K_698_91 | 698.91 | 1.66 | 0.09 | -3.68 | 0.07 |
| K_676_79 | 676.79 | 1.58 | 0.06 | -3.02 | 0.03 | K_699_22 | 699.22 | 1.58 | 0.05 | -2.99 | 0.04 |
| K_677_24 | 677.24 | 1.88 | 0.02 | -3.23 | 0.04 | K_699_77 | 699.77 | 1.45 | 0.09 | -3.10 | 0.05 |
| K_677_59 | 677.59 | 1.80 | 0.04 | -3.46 | 0.05 | K_700_16 | 700.16 | 1.21 | 0.07 | -2.65 | 0.06 |
| K_677_77 | 677.77 | 1.78 | 0.06 | -3.00 | 0.14 | K_700_61 | 700.61 | 0.85 | 0.06 | -3.61 | 0.02 |
| K_678_32 | 678.32 | 1.98 | 0.06 | -3.13 | 0.04 | K_701_06 | 701.06 | -0.07 | 0.07 | -2.11 | 0.05 |
| K_679_03 | 679.03 | 1.84 | 0.02 | -3.46 | 0.03 | K_701_56 | 701.56 | -0.06 | 0.02 | -2.91 | 0.05 |
| K_679_38 | 679.38 | 1.66 | 0.08 | -3.48 | 0.04 | K_702_02 | 702.02 | 0.58 | 0.07 | -2.98 | 0.05 |
| K_679_75 | 679.75 | 1.84 | 0.07 | -2.93 | 0.05 | K_702_52 | 702.52 | 1.03 | 0.07 | -2.99 | 0.04 |
| K_680_25 | 680.25 | 2.14 | 0.11 | -3.32 | 0.07 | K_702_92 | 702.92 | 0.51 | 0.05 | -3.86 | 0.02 |
| K_680_65 | 680.65 | 1.82 | 0.07 | -2.31 | 0.05 | K_703_42 | 703.42 | | | | |
| K_681_15 | 681.15 | 2.10 | 0.09 | -3.34 | 0.06 | K_703_83 | 703.83 | -2.88 | 0.10 | -0.31 | 0.07 |
| K_681_55 | 681.55 | 1.89 | 0.08 | -3.09 | 0.04 | K_704_28 | 704.28 | -2.30 | 0.01 | -1.09 | 0.04 |
| K_682_05 | 682.05 | 1.16 | 0.06 | -2.98 | 0.04 | K_704_73 | 704.73 | -0.30 | 0.04 | -4.42 | 0.02 |
| K_682_49 | 682.49 | 1.57 | 0.04 | -3.40 | 0.07 | K_705_23 | 705.23 | -1.72 | 0.06 | -3.28 | 0.07 |
| K_682_99 | 682.99 | 1.80 | 0.10 | -3.65 | 0.08 | K_705_67 | 705.67 | -0.02 | 0.02 | -4.58 | 0.03 |
| K_683_43 | 683.43 | 1.73 | 0.05 | -3.73 | 0.01 | K_706_12 | 706.12 | -1.61 | 0.07 | -4.04 | 0.06 |
| K_683_93 | 683.93 | 1.94 | 0.07 | -3.27 | 0.04 | K_706_35 | 706.35 | -0.46 | 0.02 | -5.17 | 0.05 |
| K_684_37 | 684.37 | 1.91 | 0.08 | -3.63 | 0.05 | K_706_65 | 706.65 | -0.12 | 0.08 | -4.85 | 0.06 |
| K_684_87 | 684.87 | 1.46 | 0.10 | -3.45 | 0.05 | K_707_15 | 707.15 | -1.66 | 0.05 | -2.43 | 0.03 |
| K_685_28 | 685.28 | 1.69 | 0.04 | -3.58 | 0.03 | K_707_55 | 707.55 | -0.30 | 0.03 | -4.92 | 0.06 |
| K_685_78 | 685.78 | 1.37 | 0.06 | -3.55 | 0.04 | K_708_05 | 708.05 | -0.39 | 0.08 | -4.62 | 0.05 |
| K_686_25 | 686.25 | 1.68 | 0.06 | -3.25 | 0.06 | K_708_50 | 708.50 | -0.86 | 0.07 | -3.93 | 0.04 |
| K_686_75 | 686.75 | 1.37 | 0.09 | -3.32 | 0.03 | K_709_05 | 709.05 | -0.62 | 0.04 | -4.81 | 0.02 |
| K_687_10 | 687.10 | 0.92 | 0.10 | -2.80 | 0.04 | K_709_42 | 709.42 | -0.39 | 0.04 | -5.23 | 0.04 |
| K_687_60 | 687.60 | 1.19 | 0.06 | -3.21 | 0.05 | K_709_92 | 709.92 | 0.05 | 0.07 | -4.30 | 0.04 |
| K_687_93 | 687.93 | 1.58 | 0.04 | -4.02 | 0.05 | K_710_30 | 710.30 | -0.28 | 0.06 | -5.01 | 0.03 |
| K_688_43 | 688.43 | 1.22 | 0.06 | -4.39 | 0.06 | K_710_85 | 710.85 | 0.56 | 0.08 | -4.18 | 0.03 |
| K_688_75 | 688.75 | 1.50 | 0.09 | -3.75 | 0.06 | K_711_38 | 711.38 | 0.74 | 0.09 | -3.76 | 0.06 |
| K_689_25 | 689.25 | 1.39 | 0.04 | -3.41 | 0.05 | K_711_88 | 711.88 | -0.22 | 0.07 | -4.61 | 0.04 |
| K_689_63 | 689.63 | 1.61 | 0.03 | -3.05 | 0.02 | K_712_33 | 712.33 | 0.16 | 0.04 | -4.41 | 0.03 |
| K_690_18 | 690.18 | 1.46 | 0.05 | -3.21 | 0.03 | K_712_78 | 712.78 | 0.64 | 0.06 | -4.55 | 0.03 |
| K_690_45 | 690.45 | 1.44 | 0.07 | -2.77 | 0.03 | K_713_24 | 713.24 | 0.74 | 0.07 | -4.36 | 0.02 |
| K_691_20 | 691.20 | 2.04 | 0.02 | -2.83 | 0.03 | K_713_74 | 713.74 | 0.67 | 0.07 | -4.75 | 0.06 |
| K_691_56 | 691.56 | 2.21 | 0.07 | -2.42 | 0.04 | K_714_16 | 714.16 | 1.14 | 0.03 | -4.21 | 0.04 |
| K_692_11 | 692.11 | 0.57 | 0.07 | -2.12 | 0.05 | K_714_56 | 714.56 | 0.95 | 0.05 | -4.53 | 0.05 |

Appendix

| Sample | Depth (m) | $\delta^{13}\text{C}$ VPDB | s.d. | $\delta^{18}\text{O}$ VPDB | s.d. | Sample | Depth (m) | $\delta^{13}\text{C}$ VPDB | s.d. | $\delta^{18}\text{O}$ VPDB | s.d. |
|----------|-----------|----------------------------|------|----------------------------|------|----------|-----------|----------------------------|------|----------------------------|------|
| K_714_86 | 714.86 | 0.91 | 0.08 | -3.81 | 0.03 | K_737_78 | 737.78 | 2.96 | 0.07 | -1.45 | 0.06 |
| K_715_16 | 715.16 | 1.17 | 0.04 | -4.11 | 0.05 | K_738_25 | 738.25 | 2.46 | 0.06 | -1.45 | 0.04 |
| K_715_60 | 715.60 | 0.26 | 0.05 | -3.43 | 0.02 | K_738_75 | 738.75 | 3.25 | 0.07 | -1.99 | 0.04 |
| K_716_10 | 716.10 | 0.39 | 0.06 | -3.06 | 0.07 | K_739_18 | 739.18 | 3.04 | 0.08 | -2.55 | 0.06 |
| K_716_69 | 716.69 | 1.20 | 0.11 | -4.20 | 0.08 | K_739_68 | 739.68 | 2.56 | 0.06 | -2.27 | 0.06 |
| K_717_14 | 717.14 | 1.16 | 0.09 | -4.16 | 0.07 | K_740_15 | 740.15 | | | | |
| K_717_49 | 717.49 | 1.06 | 0.05 | -3.97 | 0.03 | K_740_65 | 740.65 | 2.09 | 0.08 | -1.96 | 0.06 |
| K_717_99 | 717.99 | 0.77 | 0.02 | -3.57 | 0.07 | K_741_05 | 741.05 | 2.36 | 0.09 | -3.20 | 0.04 |
| K_718_39 | 718.39 | 1.14 | 0.08 | -3.78 | 0.04 | K_741_28 | 741.28 | 2.60 | 0.06 | -2.58 | 0.04 |
| K_718_94 | 718.94 | 1.17 | 0.07 | -3.33 | 0.03 | K_741_83 | 741.83 | 3.81 | 0.08 | -0.90 | 0.06 |
| K_719_30 | 719.30 | 1.11 | 0.11 | -3.38 | 0.06 | K_742_25 | 742.25 | 2.80 | 0.08 | -2.08 | 0.07 |
| K_719_80 | 719.80 | 0.50 | 0.06 | -4.37 | 0.03 | K_742_70 | 742.70 | 2.34 | 0.09 | -2.78 | 0.04 |
| K_720_25 | 720.25 | 0.60 | 0.07 | -3.56 | 0.07 | K_743_12 | 743.12 | 2.98 | 0.09 | -2.67 | 0.05 |
| K_720_75 | 720.75 | 0.91 | 0.06 | -3.72 | 0.04 | K_743_62 | 743.62 | 2.42 | 0.11 | -2.65 | 0.06 |
| K_721_16 | 721.16 | 0.74 | 0.11 | -3.83 | 0.05 | K_744_08 | 744.08 | 3.17 | 0.12 | -2.32 | 0.12 |
| K_721_63 | 721.63 | -1.07 | 0.02 | -1.76 | 0.04 | K_744_58 | 744.58 | 2.25 | 0.11 | -2.50 | 0.05 |
| K_722_04 | 722.04 | -0.23 | 0.08 | -3.26 | 0.07 | K_745_03 | 745.03 | 2.73 | 0.04 | -2.28 | 0.03 |
| K_722_54 | 722.54 | 0.62 | 0.09 | -3.47 | 0.03 | K_745_53 | 745.53 | 2.93 | 0.09 | -2.25 | 0.05 |
| K_722_99 | 722.99 | 0.89 | 0.06 | -3.72 | 0.05 | K_746_03 | 746.03 | 3.12 | 0.06 | -2.17 | 0.07 |
| K_723_49 | 723.49 | 0.84 | 0.08 | -2.70 | 0.04 | K_746_48 | 746.48 | 2.49 | 0.09 | -2.30 | 0.06 |
| K_723_94 | 723.94 | -1.72 | 0.10 | -1.52 | 0.06 | K_746_87 | 746.87 | 2.04 | 0.11 | -1.82 | 0.08 |
| K_724_39 | 724.39 | 0.62 | 0.10 | -3.83 | 0.07 | K_747_35 | 747.35 | 0.51 | 0.06 | -1.95 | 0.04 |
| K_724_79 | 724.79 | -0.37 | 0.03 | -2.81 | 0.06 | K_747_72 | 747.72 | 1.01 | 0.08 | -1.67 | 0.04 |
| K_725_29 | 725.29 | 0.21 | 0.05 | -3.92 | 0.03 | K_748_27 | 748.27 | 0.60 | 0.05 | -3.69 | 0.05 |
| K_725_63 | 725.63 | -0.76 | 0.04 | -3.43 | 0.02 | K_748_64 | 748.64 | -0.34 | 0.11 | -0.79 | 0.06 |
| K_726_18 | 726.18 | -1.29 | 0.06 | -3.13 | 0.05 | K_749_14 | 749.14 | -0.21 | 0.07 | -3.04 | 0.04 |
| K_726_46 | 726.46 | -1.82 | 0.05 | -3.14 | 0.03 | K_749_53 | 749.53 | 1.63 | 0.04 | -3.51 | 0.02 |
| K_726_96 | 726.96 | -1.31 | 0.10 | -2.39 | 0.03 | K_749_93 | 749.93 | 3.92 | 0.07 | -1.62 | 0.06 |
| K_727_40 | 727.40 | | | | | K_750_25 | 750.25 | 2.64 | 0.05 | -2.65 | 0.06 |
| K_727_85 | 727.85 | -2.14 | 0.08 | -1.97 | 0.06 | K_750_75 | 750.75 | 2.63 | 0.04 | -2.49 | 0.03 |
| K_728_33 | 728.33 | -0.41 | 0.07 | -2.96 | 0.05 | K_751_18 | 751.18 | 1.64 | 0.04 | -2.15 | 0.04 |
| K_728_83 | 728.83 | | | | | K_751_68 | 751.68 | 2.60 | 0.07 | -2.04 | 0.07 |
| K_729_18 | 729.18 | -0.49 | 0.08 | -3.27 | 0.04 | K_752_15 | 752.15 | 0.48 | 0.05 | -1.96 | 0.03 |
| K_729_68 | 729.68 | -1.80 | 0.08 | -3.35 | 0.08 | K_752_65 | 752.65 | 1.54 | 0.04 | -2.95 | 0.05 |
| K_730_10 | 730.10 | 0.27 | 0.10 | -2.24 | 0.07 | K_753_14 | 753.14 | 2.62 | 0.07 | -2.25 | 0.04 |
| K_730_60 | 730.60 | -9.86 | 0.04 | 2.20 | 0.05 | K_753_64 | 753.64 | 2.69 | 0.07 | -2.04 | 0.05 |
| K_730_88 | 730.88 | -8.76 | 0.07 | -1.43 | 0.04 | K_754_07 | 754.07 | 3.32 | 0.05 | -2.27 | 0.07 |
| K_731_33 | 731.33 | | | | | K_754_62 | 754.62 | -0.84 | 0.09 | -3.25 | 0.05 |
| K_731_73 | 731.73 | 1.27 | 0.08 | -3.43 | 0.03 | K_755_08 | 755.08 | 2.40 | 0.13 | -2.30 | 0.07 |
| K_732_13 | 732.13 | -4.16 | 0.06 | -3.22 | 0.06 | K_755_53 | 755.53 | 3.18 | 0.04 | -2.73 | 0.04 |
| K_732_81 | 732.81 | 2.71 | 0.08 | -2.03 | 0.07 | K_755_95 | 755.95 | 3.06 | 0.08 | -2.31 | 0.07 |
| K_733_66 | 733.66 | -1.05 | 0.03 | -3.98 | 0.03 | K_756_40 | 756.40 | 3.16 | 0.07 | -2.34 | 0.02 |
| K_734_16 | 734.16 | 1.05 | 0.08 | -4.54 | 0.08 | K_756_85 | 756.85 | 3.13 | 0.10 | -2.63 | 0.07 |
| K_734_60 | 734.60 | 3.04 | 0.08 | -2.18 | 0.03 | K_757_35 | 757.35 | 0.94 | 0.10 | -3.98 | 0.05 |
| K_735_10 | 735.10 | 3.33 | 0.07 | -2.41 | 0.06 | K_757_73 | 757.73 | 1.99 | 0.10 | -1.95 | 0.03 |
| K_735_55 | 735.55 | 3.48 | 0.11 | -2.12 | 0.05 | K_758_18 | 758.18 | 1.11 | 0.08 | -3.78 | 0.07 |
| K_736_05 | 736.05 | 2.72 | 0.04 | -2.15 | 0.05 | K_758_79 | 758.79 | 0.65 | 0.11 | -3.46 | 0.10 |
| K_736_48 | 736.48 | 2.71 | 0.06 | -1.00 | 0.04 | K_759_34 | 759.34 | 2.85 | 0.12 | -2.14 | 0.09 |
| K_736_98 | 736.98 | 2.69 | 0.06 | -2.63 | 0.05 | K_759_70 | 759.70 | 2.74 | 0.07 | -2.08 | 0.07 |
| K_737_28 | 737.28 | 2.96 | 0.07 | -1.45 | 0.06 | K_760_20 | 760.20 | 2.28 | 0.07 | -2.38 | 0.06 |

| Sample | Depth (m) | $\delta^{13}\text{C}$ VPDB | s.d. | $\delta^{18}\text{O}$ VPDB | s.d. | Sample | Depth (m) | $\delta^{13}\text{C}$ VPDB | s.d. | $\delta^{18}\text{O}$ VPDB | s.d. |
|----------|-----------|----------------------------|------|----------------------------|------|--------|-----------|----------------------------|------|----------------------------|------|
| K_760_56 | 760.56 | 1.66 | 0.10 | -1.94 | 0.03 | | | | | | |
| K_761_06 | 761.06 | -1.57 | 0.08 | -2.25 | 0.06 | | | | | | |
| K_761_41 | 761.41 | 1.00 | 0.05 | -1.34 | 0.02 | | | | | | |
| K_761_86 | 761.86 | 0.11 | 0.06 | -3.26 | 0.04 | | | | | | |
| K_762_31 | 762.31 | 1.16 | 0.09 | -2.92 | 0.07 | | | | | | |
| K_762_81 | 762.81 | -0.74 | 0.05 | -2.81 | 0.04 | | | | | | |
| K_763_15 | 763.15 | -0.54 | 0.05 | -3.31 | 0.05 | | | | | | |
| K_763_65 | 763.65 | 1.33 | 0.07 | -2.49 | 0.05 | | | | | | |
| K_764_07 | 764.07 | -1.43 | 0.10 | -0.52 | 0.05 | | | | | | |
| K_764_57 | 764.57 | 0.35 | 0.02 | -4.32 | 0.07 | | | | | | |
| K_764_97 | 764.97 | 2.68 | 0.08 | -2.31 | 0.05 | | | | | | |
| K_765_47 | 765.47 | 2.86 | 0.10 | -2.18 | 0.03 | | | | | | |
| K_766_00 | 766.00 | 1.75 | 0.05 | -2.60 | 0.04 | | | | | | |
| K_766_40 | 766.40 | 1.54 | 0.04 | -2.06 | 0.03 | | | | | | |
| K_766_79 | 766.79 | -2.19 | 0.05 | -2.51 | 0.03 | | | | | | |
| K_767_34 | 767.34 | 0.36 | 0.12 | -2.84 | 0.06 | | | | | | |
| K_767_80 | 767.80 | 0.88 | 0.07 | -3.37 | 0.02 | | | | | | |
| K_768_20 | 768.20 | 1.83 | 0.10 | -1.56 | 0.07 | | | | | | |
| K_768_66 | 768.66 | -1.87 | 0.03 | -3.43 | 0.05 | | | | | | |
| K_769_16 | 769.16 | 0.44 | 0.09 | -2.15 | 0.05 | | | | | | |
| K_769_53 | 769.53 | -0.33 | 0.04 | -3.73 | 0.03 | | | | | | |
| K_769_98 | 769.98 | -1.48 | 0.07 | -3.74 | 0.05 | | | | | | |
| K_770_38 | 770.38 | -1.85 | 0.05 | -3.74 | 0.03 | | | | | | |
| K_770_88 | 770.88 | -0.22 | 0.02 | -3.35 | 0.03 | | | | | | |
| K_771_31 | 771.31 | -1.47 | 0.06 | -4.36 | 0.03 | | | | | | |
| K_771_76 | 771.76 | -1.22 | 0.05 | -4.01 | 0.03 | | | | | | |
| K_772_24 | 772.24 | -2.15 | 0.02 | -5.04 | 0.06 | | | | | | |
| K_772_74 | 772.74 | -0.65 | 0.07 | -4.85 | 0.05 | | | | | | |
| K_773_12 | 773.12 | | | | | | | | | | |
| K_774_25 | 774.25 | 1.62 | 0.07 | -1.08 | 0.06 | | | | | | |
| K_774_75 | 774.75 | -2.03 | 0.05 | -1.03 | 0.05 | | | | | | |
| K_775_08 | 775.08 | -4.26 | 0.02 | -2.44 | 0.04 | | | | | | |
| K_775_48 | 775.48 | -1.64 | 0.07 | -2.20 | 0.02 | | | | | | |
| K_776_08 | 776.08 | 14.73 | 0.06 | -3.33 | 0.09 | | | | | | |
| K_776_48 | 776.48 | -1.46 | 0.03 | -1.84 | 0.02 | | | | | | |
| K_776_89 | 776.89 | -0.74 | 0.06 | -1.47 | 0.05 | | | | | | |
| K_777_39 | 777.39 | 0.68 | 0.10 | -1.06 | 0.05 | | | | | | |
| K_777_92 | 777.92 | 0.22 | 0.07 | -1.74 | 0.03 | | | | | | |
| K_778_32 | 778.32 | -0.52 | 0.05 | -2.04 | 0.05 | | | | | | |

Appendix

Appendix 11 Carbon and oxygen isotope results of drilled powder, Osterwald section

| Sample | Depth (m) | $\delta^{13}\text{C}$ VPDB | s.d. | $\delta^{18}\text{O}$ VPDB | s.d. | Sample | Depth (m) | $\delta^{13}\text{C}$ VPDB | s.d. | $\delta^{18}\text{O}$ VPDB | s.d. |
|--------|-----------|----------------------------|------|----------------------------|------|--------|-----------|----------------------------|------|----------------------------|------|
| OSW 01 | 0 | 1.93 | 0.14 | -3.60 | 0.10 | OSW 47 | 25 | 1.83 | 0.15 | -3.15 | 0.11 |
| OSW 02 | 0.5 | 1.51 | 0.07 | -4.19 | 0.04 | OSW 48 | 25.5 | 0.45 | 0.21 | -3.89 | 0.09 |
| OSW 03 | 1 | 1.55 | 0.15 | -4.36 | 0.07 | OSW 49 | 26 | -0.07 | 0.12 | -4.15 | 0.11 |
| OSW 04 | 1.5 | 1.88 | 0.13 | -3.77 | 0.10 | | | | | | |
| OSW 05 | 2 | 2.22 | 0.21 | -2.95 | 0.11 | | | | | | |
| OSW 06 | 2.5 | 1.70 | 0.10 | -3.96 | 0.10 | | | | | | |
| OSW 07 | 3 | 1.83 | 0.18 | -4.00 | 0.10 | | | | | | |
| OSW 08 | 3.5 | 1.83 | 0.17 | -3.93 | 0.09 | | | | | | |
| OSW 09 | 4 | 1.79 | 0.17 | -4.20 | 0.11 | | | | | | |
| OSW 10 | 4.5 | 1.78 | 0.09 | -4.04 | 0.10 | | | | | | |
| OSW 11 | 5 | 2.07 | 0.13 | -2.66 | 0.12 | | | | | | |
| OSW 12 | 5.5 | 1.53 | 0.13 | -3.72 | 0.11 | | | | | | |
| OSW 13 | 6 | 2.19 | 0.20 | -3.09 | 0.10 | | | | | | |
| OSW 14 | 6.5 | 2.26 | 0.22 | -3.05 | 0.11 | | | | | | |
| OSW 15 | 7 | 2.18 | 0.21 | -3.07 | 0.09 | | | | | | |
| OSW 16 | 7.5 | 1.40 | 0.11 | -4.15 | 0.07 | | | | | | |
| OSW 17 | 8 | 2.30 | 0.12 | -3.14 | 0.10 | | | | | | |
| OSW 17 | 8.5 | 2.08 | 0.07 | -2.99 | 0.15 | | | | | | |
| OSW 18 | 9 | 2.11 | 0.20 | -3.73 | 0.12 | | | | | | |
| OSW 19 | 9.5 | 1.90 | 0.11 | -3.56 | 0.09 | | | | | | |
| OSW 19 | 10 | 1.80 | 0.07 | -3.35 | 0.08 | | | | | | |
| OSW 20 | 10.5 | 2.01 | 0.17 | -3.61 | 0.12 | | | | | | |
| OSW 21 | 11 | 1.97 | 0.20 | -4.16 | 0.10 | | | | | | |
| OSW 22 | 11.5 | 1.97 | 0.18 | -4.05 | 0.10 | | | | | | |
| OSW 23 | 12 | 2.18 | 0.16 | -3.65 | 0.09 | | | | | | |
| OSW 24 | 12.5 | 2.45 | 0.23 | -3.34 | 0.04 | | | | | | |
| OSW 24 | 13 | 2.16 | 0.05 | -3.36 | 0.07 | | | | | | |
| OSW 25 | 13.5 | 1.95 | 0.12 | -3.97 | 0.12 | | | | | | |
| OSW 26 | 14 | 1.98 | 0.16 | -4.03 | 0.13 | | | | | | |
| OSW 27 | 14.5 | 2.49 | 0.22 | -3.61 | 0.08 | | | | | | |
| OSW 28 | 15 | 1.95 | 0.07 | -3.88 | 0.12 | | | | | | |
| OSW 29 | 15.5 | 2.17 | 0.14 | -3.59 | 0.11 | | | | | | |
| OSW 30 | 16 | 2.34 | 0.13 | -3.92 | 0.10 | | | | | | |
| OSW 31 | 16.5 | 1.88 | 0.17 | -3.94 | 0.10 | | | | | | |
| OSW 32 | 17 | 1.85 | 0.13 | -4.06 | 0.12 | | | | | | |
| OSW 33 | 17.5 | 2.25 | 0.21 | -3.59 | 0.09 | | | | | | |
| OSW 34 | 18 | 2.13 | 0.07 | -3.68 | 0.10 | | | | | | |
| OSW 35 | 18.5 | 2.32 | 0.12 | -3.74 | 0.12 | | | | | | |
| OSW 36 | 19 | 1.43 | 0.16 | -4.20 | 0.11 | | | | | | |
| OSW 37 | 19.5 | 1.27 | 0.05 | -4.12 | 0.11 | | | | | | |
| OSW 38 | 20 | 1.99 | 0.19 | -3.90 | 0.09 | | | | | | |
| OSW 39 | 20.5 | 1.68 | 0.09 | -3.86 | 0.10 | | | | | | |
| OSW 40 | 21 | 2.21 | 0.23 | -3.75 | 0.06 | | | | | | |
| OSW 41 | 21.5 | 1.38 | 0.13 | -3.89 | 0.10 | | | | | | |
| OSW 42 | 22 | 1.22 | 0.12 | -3.99 | 0.13 | | | | | | |
| OSW 43 | 22.5 | 0.66 | 0.08 | -4.06 | 0.10 | | | | | | |
| OSW 44 | 23 | 0.64 | 0.09 | -4.06 | 0.11 | | | | | | |
| OSW 45 | 23.5 | -0.04 | 0.08 | -4.16 | 0.09 | | | | | | |
| OSW 46 | 24 | 0.42 | 0.11 | -3.73 | 0.08 | | | | | | |
| OSW 47 | 24.5 | 1.33 | 0.22 | -3.21 | 0.05 | | | | | | |

Appendix 12 Carbon and oxygen isotope results of drilled powder, Osterwald section

| Sample | Depth (m) | $\delta^{13}\text{C}$ VPDB | s.d. | $\delta^{18}\text{O}$ VPDB | s.d. | | |
|---------------|-----------|----------------------------|------|----------------------------|------|--|--|
| 2PT-1 | 0.1 | 1.18 | 0.15 | -2.77 | 0.14 | | |
| 2PT-1 | 0.1 | 1.12 | 0.18 | -2.94 | 0.12 | | |
| 2PT-2 | 0.55 | 0.60 | 0.14 | -1.57 | 0.11 | | |
| 2PT-3 | 1.1 | 0.62 | 0.13 | -1.98 | 0.10 | | |
| 2PT-4 | 1.9 | 1.27 | 0.11 | -2.81 | 0.10 | | |
| 1PT-21(2PT-4) | 1.9 | 0.28 | 0.12 | -3.09 | 0.14 | | |
| PT2-5 | 2.6 | 0.56 | 0.06 | -1.45 | 0.13 | | |
| 2PT-5 | 2.6 | 1.50 | 0.19 | -1.61 | 0.13 | | |
| 1PT-19(2PT-5) | 2.6 | 0.59 | 0.07 | -1.84 | 0.15 | | |
| PT2-6 | 3 | 0.82 | 0.09 | -0.94 | 0.14 | | |
| PT2-7 | 3.7 | 1.15 | 0.16 | -0.88 | 0.12 | | |
| PT2-8 | 4.2 | 0.30 | 0.12 | -1.91 | 0.13 | | |
| PT2-9 | 4.45 | 0.41 | 0.13 | -1.33 | 0.11 | | |
| PT2-10 | 4.75 | 0.82 | 0.13 | -1.23 | 0.14 | | |
| PT2-10 | 4.75 | 0.87 | 0.11 | -1.11 | 0.15 | | |
| PT2-11 | 5.52 | 0.37 | 0.12 | -0.47 | 0.12 | | |
| PT2-12 | 5.55 | 0.46 | 0.14 | -1.21 | 0.10 | | |
| PT2-12 | 6.05 | 0.80 | 0.11 | -1.82 | 0.11 | | |
| OSW-11 | | 1.85 | 0.13 | -4.06 | 0.10 | | |
| OSW-13 | | 1.37 | 0.14 | -4.82 | 0.10 | | |

Appendix

Appendix 13 Carbon and oxygen isotope results of drilled powder, Langenberg section

| Sample | Depth (m) | $\delta^{13}\text{C}$ VPDB | s.d. | $\delta^{18}\text{O}$ VPDB | s.d. | Sample | Depth (m) | $\delta^{13}\text{C}$ VPDB | s.d. | $\delta^{18}\text{O}$ VPDB | s.d. |
|--------|-----------|----------------------------|------|----------------------------|------|--------|-----------|----------------------------|------|----------------------------|------|
| LJ1 | 0 | 2.44 | 0.08 | -2.29 | 0.10 | | | | | | |
| LJ2 | 0.25 | 2.44 | 0.08 | -1.90 | 0.11 | | | | | | |
| LJ3 | 0.5 | 2.43 | 0.09 | -1.37 | 0.09 | | | | | | |
| LJ4 | 0.75 | 2.36 | 0.10 | -1.22 | 0.10 | | | | | | |
| LJ5 | 1 | 2.34 | 0.09 | -0.96 | 0.09 | | | | | | |
| LJ6 | 1.25 | 2.18 | 0.08 | -1.06 | 0.08 | | | | | | |
| LJ7 | 1.5 | 2.07 | 0.10 | -0.78 | 0.11 | | | | | | |
| LJ8 | 1.75 | 1.90 | 0.08 | -1.03 | 0.10 | | | | | | |
| LJ9 | 2 | 2.20 | 0.09 | 0.19 | 0.08 | | | | | | |
| LJ10 | 2.25 | 2.03 | 0.10 | 0.43 | 0.10 | | | | | | |
| LJ11 | 2.5 | 1.99 | 0.08 | 0.44 | 0.12 | | | | | | |
| LJ12 | 2.75 | 1.43 | 0.09 | -1.00 | 0.09 | | | | | | |
| LJD1 | 3 | 2.14 | 0.07 | -0.23 | 0.08 | | | | | | |
| LJD2 | 3.5 | 2.24 | 0.10 | -0.95 | 0.08 | | | | | | |
| LJD3 | 4 | 2.26 | 0.09 | -1.38 | 0.09 | | | | | | |
| LJD4 | 4.5 | 2.48 | 0.08 | -1.50 | 0.07 | | | | | | |
| LJD5 | 5 | 2.53 | 0.08 | 0.10 | 0.09 | | | | | | |
| LJD6 | 5.5 | 2.63 | 0.07 | 0.47 | 0.05 | | | | | | |
| LJD7 | 6 | 2.71 | 0.09 | 0.71 | 0.10 | | | | | | |
| LJD8 | 6.5 | 2.21 | 0.06 | -0.46 | 0.06 | | | | | | |
| LJD9 | 7 | 2.20 | 0.10 | -1.36 | 0.09 | | | | | | |
| LJD10 | 7.5 | 2.62 | 0.09 | -0.38 | 0.08 | | | | | | |
| LJD11 | 8 | 2.44 | 0.09 | -2.50 | 0.08 | | | | | | |
| LJD12 | 8.5 | 2.41 | 0.08 | -3.92 | 0.05 | | | | | | |
| LJD13 | 9 | 2.26 | 0.08 | -3.88 | 0.07 | | | | | | |
| LJD14 | 9.5 | 2.36 | 0.06 | -2.38 | 0.07 | | | | | | |
| LJD15 | 10 | 2.53 | 0.05 | -0.07 | 0.09 | | | | | | |
| LJD16 | 10.5 | 2.35 | 0.06 | -1.82 | 0.10 | | | | | | |
| LJD17 | 11 | 2.62 | 0.09 | -1.34 | 0.08 | | | | | | |
| LJD18 | 11.5 | 2.68 | 0.09 | -3.64 | 0.07 | | | | | | |
| LJD19 | 12 | 2.76 | 0.10 | -2.50 | 0.09 | | | | | | |
| LJD20 | 12.5 | 2.58 | 0.05 | -3.17 | 0.09 | | | | | | |
| LJD21 | 13 | 2.58 | 0.04 | -3.44 | 0.08 | | | | | | |
| LJD22 | 13.5 | 2.50 | 0.06 | -3.25 | 0.05 | | | | | | |
| LJD23 | 14 | 2.68 | 0.09 | -3.33 | 0.11 | | | | | | |
| LJD24 | 14.5 | 2.99 | 0.07 | -1.38 | 0.07 | | | | | | |
| LJD25 | 15 | 2.60 | 0.09 | -3.66 | 0.07 | | | | | | |
| LJD26 | 15.5 | 2.99 | 0.04 | -2.95 | 0.08 | | | | | | |
| LJD27 | 16 | 2.78 | 0.05 | -2.89 | 0.07 | | | | | | |

Appendix 14 Trace element data, Bisperode and Konrad core

| Sample | Depth (m) | Ca | | Mg | | Sr | | Fe | | Mn | | Unit |
|----------|-----------|-----------|---------|-----------|---------|-----------|---------|-----------|---------|-----------|---------|------|
| | | \bar{X} | $\pm S$ | \bar{X} | $\pm S$ | \bar{X} | $\pm S$ | \bar{X} | $\pm S$ | \bar{X} | $\pm S$ | |
| SB7.7 | 44 | 387760 | 4169 | 2634 | 10 | 592 | 2.5 | 68 | 0.6 | 16 | 0.3 | ppm |
| SB8.5-A | 45 | 370700 | 4347 | 5327 | 19 | 159 | 1.7 | 456 | 1.8 | 99 | 0.5 | ppm |
| SB8.5-B | 45 | 390570 | 3012 | 1756 | 6 | 566 | 2.1 | 218 | 1.8 | 19 | 0.1 | ppm |
| SB8.5-C | 45 | 386250 | 3273 | 3830 | 19 | 103 | 2.3 | 275 | 1.4 | 46 | 0.3 | ppm |
| SB8.5-D | 45 | 381560 | 2036 | 1623 | 11 | 542 | 4.9 | 94 | 0.8 | 12 | 0.0 | ppm |
| DY10 | 10 | 386790 | 1984 | 1364 | 6 | 537 | 3.3 | 293 | 0.6 | 23 | 0.1 | ppm |
| DY11.5 | 12.15 | 395480 | 4039 | 743 | 4 | 621 | 1.7 | 334 | 1.6 | 13 | 0.1 | ppm |
| SB25.2 | 61.5 | 362740 | 2160 | 3813 | 13 | 645 | 1.5 | 201 | 0.6 | 32 | 0.1 | ppm |
| SB57.2 | 94 | 388150 | 2727 | 1436 | 11 | 617 | 4.4 | 112 | 1.1 | 7 | 0.1 | ppm |
| SB58.5 | 95 | 385200 | 4927 | 3578 | 6 | 420 | 2.1 | 1285 | 2.2 | 73 | 0.1 | ppm |
| SB60.5-A | 97 | 393070 | 1426 | 2044 | 11 | 466 | 2.2 | 194 | 0.9 | 21 | 0.1 | ppm |
| SB60.5-B | 97 | 397700 | 3484 | 1079 | 6 | 618 | 2.6 | 90 | 1.1 | 9 | 0.2 | ppm |
| SB65-A | 101.5 | 395520 | 2659 | 4010 | 12 | 289 | 3.2 | 109 | 1.8 | 57 | 0.3 | ppm |
| SB65-B | 101.5 | 391500 | 2998 | 3763 | 17 | 189 | 2.5 | 269 | 15.1 | 76 | 0.5 | ppm |
| SB65-C | 101.5 | 372420 | 1671 | 3473 | 20 | 185 | 1.4 | 316 | 2.1 | 69 | 0.6 | ppm |
| D82.5-A | 119 | 390990 | 2985 | 6171 | 28 | 622 | 2.2 | 3885 | 20.8 | 70 | 0.2 | ppm |
| D82.5-B | 119 | 386050 | 3438 | 5093 | 27 | 666 | 4.5 | 252 | 1.4 | 29 | 0.2 | ppm |
| LPb-3 | 24.5 | 389840 | 3739 | 1778 | 10 | 450 | 2.8 | 686 | 4.1 | 31 | 0.3 | ppm |
| LPb-6.5A | 28 | 388210 | 4496 | 796 | 5 | 562 | 2.3 | 552 | 2.2 | 62 | 0.2 | ppm |
| LPb-6.5B | 28 | 385990 | 5816 | 2125 | 10 | 571 | 2.6 | 216 | 1.5 | 23 | 0.1 | ppm |
| LPb-8.5 | 30 | 395050 | 2215 | 704 | 7 | 530 | 3.9 | 319 | 2.5 | 34 | 0.1 | ppm |
| LPb-8.5B | 30 | 390350 | 3336 | 1189 | 6 | 600 | 3.8 | 275 | 1.2 | 29 | 0.1 | ppm |
| LPb-8.5D | 30 | 361870 | 2938 | 5658 | 18 | 48 | 1.0 | 1477 | 6.2 | 95 | 0.7 | ppm |
| K649.5A | 649.5 | 384440 | 3839 | 1845 | 5 | 666 | 3.7 | 2073 | 6.2 | 99 | 0.4 | ppm |
| K649.5B | 649.5 | 360690 | 4180 | 3181 | 16 | 775 | 2.9 | 5592 | 17.8 | 136 | 0.4 | ppm |
| K655.79A | 655.79 | 315340 | 1686 | 3089 | 18 | 248 | 2.7 | 2102 | 123. | 316 | 1.7 | ppm |
| K655.79B | 655.79 | 359550 | 1122 | 2638 | 14 | 440 | 1.9 | 11660 | 68.4 | 235 | 1.1 | ppm |
| K748.2 | 748.2 | 369010 | 2540 | 1288 | 7 | 914 | 3.0 | 4078 | 17.3 | 380 | 1.4 | ppm |
| K753.5 | 753.5 | 373700 | 5010 | 697 | 7 | 584 | 4.3 | 3240 | 12.6 | 259 | 1.3 | ppm |
| K776.48 | 776.48 | 346380 | 3110 | 234 | 2 | 480 | 3.7 | 221 | 0.7 | 50 | 0.3 | ppm |
| K776.7 | 776.7 | 394910 | 4134 | 380 | 3 | 503 | 3.3 | 1380 | 4.0 | 59 | 0.1 | ppm |
| K777.45 | 777.45 | 376450 | 3575 | 3643 | 14 | 567 | 5.1 | 10110 | 38.6 | 142 | 0.7 | ppm |
| K777.7 | 777.7 | 372010 | 3855 | 423 | 7 | 485 | 3.5 | 559 | 1.3 | 66 | 0.2 | ppm |
| K778.40A | 778.40 | 394080 | 1943 | 637 | 8 | 518 | 1.1 | 677 | 2.6 | 76 | 0.4 | ppm |
| K778.40B | 778.40 | 388340 | 3822 | 502 | 8 | 496 | 3.1 | 4994 | 15.6 | 77 | 0.3 | ppm |

Appendix

Appendix 15 Strontium isotope values

| Section | Sample | Depth (m) | $^{87}\text{Sr}/^{86}\text{Sr}$ measured | $\pm 2 \text{ s mean}$ | $^{87}\text{Sr}/^{86}\text{Sr}$ sample corrected to difference: NBS 987 value measured with sample | $^{87}\text{Sr}/^{86}\text{Sr}$ sample corrected to difference: USGS EN-1 value and USGS EN-1 measured with sample | $^{87}\text{Sr}/^{86}\text{Sr}$ sample corrected to difference: NBS 987 value and NBS 987 Bochum mean value | $^{87}\text{Sr}/^{86}\text{Sr}$ sample corrected to difference: USGS EN-1 value and USGS EN-1 Bochum mean value |
|-------------|----------|-----------|--|------------------------|--|--|---|---|
| Bisperode | DY11.5 | 11.5 | 0.706873 | 0.000005 | 0.706857 | 0.706869 | 0.706878 | 0.706887 |
| | LPb-8.5B | 30 | 0.706900 | 0.000005 | 0.706884 | 0.706896 | 0.706905 | 0.706914 |
| | SB8.5-B | 45 | 0.706898 | 0.000005 | 0.706899 | 0.706906 | 0.706903 | 0.706913 |
| | SB7.7 | 44.2 | 0.706939 | 0.000005 | 0.706923 | 0.706935 | 0.706944 | 0.706954 |
| | SB25.2 | 61.7 | 0.706894 | 0.000005 | 0.706878 | 0.706890 | 0.706899 | 0.706909 |
| | SB60.5-B | 97 | 0.706909 | 0.000005 | 0.706893 | 0.706905 | 0.706914 | 0.706923 |
| | D82.5-B | 119 | 0.706900 | 0.000005 | 0.706884 | 0.706896 | 0.706905 | 0.706914 |
| Konrad core | K748.2 | 748.2 | 0.706935 | 0.000005 | 0.706919 | 0.706931 | 0.706940 | 0.706950 |
| | K753.5 | 753.5 | 0.706951 | 0.000005 | 0.706952 | 0.706959 | 0.706956 | 0.706966 |
| | K649.5A | 649.5 | 0.706967 | 0.000005 | 0.706951 | 0.706963 | 0.706972 | 0.706981 |
| | K649.5B | 649.5 | 0.707178 | 0.000007 | 0.707162 | 0.707174 | 0.707183 | 0.707193 |

Acknowledgments

I am extremely grateful to my supervisor, Prof. Dr. Ulrich Heimhofer, for providing me with the wonderful opportunity to conduct my Ph.D. project in the amazing and spectacular Jurassic world. Despite the disruptions caused by the COVID-19 pandemic, Ulrich has been a constant source of guidance and support throughout my research journey, and I could not have asked for a better mentor.

I would also like to express my appreciation to Dr. François-Nicolas Krencker for co-guiding this project and injecting fresh ideas into the group. François has been a great friend during field trips and in the office, and his support during the last months has been invaluable.

A special mention goes to Dr. Stefan Huck for his exceptional expertise in carbonate sedimentary. His advice and support have been crucial to my start in our group, and I am grateful for his assistance. Christiane Wenske, thank you for your help and professional work in the measurement of the stable isotopes.

I also want to express my heartfelt appreciation to all my colleagues at the Institute of Geology, including Doris, Jeanette, Jörg, Christian, Jutta, Fanfan, Runa, Andreas, Alexandra, Katharina Müller, Katharina Schmitt, Suping, Gang, Falko, Nils, Julia, Jill, Yvonne, Geert, Alexander, and Armin. Their help and assistance have been invaluable to me during my Ph.D. study, and the happy memories I have shared with them will always be treasured.

I am particularly thankful to Prof. Dr. Andrea Hampel for her support in helping me apply for the completion grant. Thanks also go to Prof. Dr. Jörg Mutterlose for being co-examiner.

I would also like to extend my gratitude to Fritz, who has been instrumental in assisting me with fieldwork and sample preparation. Runa thank you for checking my thesis.

Furthermore, I would like to acknowledge the generous financial support provided by the China Scholarship Council (CSC) and the Leibniz University Hannover Ph.D. completion grant. Without their support, my Ph.D. study in Germany would not have been possible.

Last, but not least, I am deeply indebted to my parents for their unwavering love and support. Their encouragement and sacrifices have been instrumental in my academic journey. I would also like to thank my brother and sister for their patience, encouragement, and assistance throughout my Ph.D. study.

Curriculum Vitae

Personal information

Name: Deyan Zhang
 Birthday: 02.02.1989 in Huining, China
 Nationality: Chinese

Education and professional career

09, 2005–0, 2008 Huining Nr. 2 High School, China

09, 2008–07, 2012 Bachelor of Science, Geo-information. Hebei GEO University, China
 Thesis: *GIS-based Geological conditions of Molybdenum mineralization, Dongwuqi, Inner Mongolia*

09, 2012–07, 2015 Master of Science, Sedimentary Geology. Chengdu University of Technology, China
 Thesis: *Further research on chlorite rims in sandstones: Evidence from the Triassic Yanchang Formation in the Ordos basin, China*

07, 2015–09, 2017 Assistant Engineer, (geological mapping in the Tibet Plateau), Sichuan Bureau of Geology and Mineral Resources, China

09, 2017–09, 2018 Ph.D. student at Chengdu University of Technology, China (quit)

Since 10, 2018 Ph.D. student at Institut für Geologie, Leibniz Universität Hannover
 Thesis: *Carbon ($\delta^{13}C$) and Strontium ($^{87}Sr/^{86}Sr$)-based chemostratigraphy of the Oxfordian series in the Lower Saxony Basin of Northern Germany*

Publications

Publications, submitted papers and manuscripts in preparation

1. **Zhang Deyan**, Xiang Fang, Chen Kang, Feng Qin, He Dejun. Characteristics of Dolomite Reservoir of Upper Silurian Dengying 4 Formation, Yankong Area, Jinsha County, Guizhou Province. *Natural Gas Exploration and Development*. 2015, 38 (1), 12-15. (In Chinese)
2. Xiang Fang, **Zhang Deyan**, Chen Kang, Feng Qin. Early Cretaceous Paleoclimate Characteristics of China: Clues from Continental Climate-indicative sediments. *Acta Geologica Sinica*. 2015, 04:1307-1318.
3. Fang Xiang, Yuwan Wang, Qin Feng, **Deyan Zhang** & Junxing Zhao. Further research on chlorite rims in sandstones: evidence from the Triassic Yanchang Formation in the Ordos basin, China. *Arabian Journal of Geosciences*, 2016, 9(7):1-11
4. Huang, Hengxu, Fang Xiang, **Deyan Zhang**, Yuming Guo, Qi Yang and Li-Xue Ding. New evidence from heavy minerals and detrital zircons in Quaternary fluvial sediments for the evolution of the upper Yangtze River, South China. *Quaternary Research*, 1-20, 2022
5. Fang Xiang, Xiantao Yu, Hengxu Huang, **Deyan Zhang**, Xiang Zhu. Mineralogical characterization and diagenetic history of Permian marine tuffaceous deposits in Guangyuan area, northern Sichuan basin, China, *Marine and Petroleum Geology*, Volume 123, 2021
6. Xiantao Yu, Fang Xiang, Zhongtang Su, **Deyan Zhang**, Gary G. Lash, Kunmei Yang, Wenzhi You. Miniaturized trace fossils in microbialites from the Cambrian Series 2 Qingxudong Formation in the Panshi area, eastern Guizhou, China. *Paleogeography, Palaeoclimatology, Palaeoecology*, Volume 576, 2021
7. **Deyan Zhang**, François-Nicolas Krencker, Stefan Huck, Ulrich Heimhofer. Carbonate microfacies and transgressive-regressive cycles of Oxfordian shallow-water limestones (Korallenoolith, Lower Saxony Basin). In preparation for *ZDGG*
8. **Deyan Zhang**, François-Nicolas Krencker, Stefan Huck, Philipp Ulke, Michael Schramm, Ulrich Heimhofer. First record of the middle Oxfordian positive carbon isotope excursion within the Korallenoolith formation, Lower Saxony Basin, Germany. In preparation for *TERRA NOVA*.
9. **Deyan Zhang**, François-Nicolas Krencker, Stefan Huck, Ulrich Heimhofer. Sedimentology and carbon isotope chemostratigraphy of an Oxfordian carbonate ramp system, Lower Saxony Basin, Germany. In preparation for *PALEO3*

Conference contributions

2nd Early Career Sedimentologist Meeting (ECSM), Nov. 12– 13, 2021

Poster: Deyan Zhang, Stefan Huck, Ulrich Heimhofer. Carbonate microfacies and transgressive-regressive cycles of Oxfordian shallow-water limestones (Korallenoolith, Lower Saxony Basin)

11th International Congress on the Jurassic System, Aug. 29– Sept. 02, 2022

Poster: Deyan Zhang, François-Nicolas Krencker, Stefan Huck, Philipp Ulke, Michael Schramm, Ulrich Heimhofer. First record of the middle Oxfordian positive carbon isotope excursion within the Korallenoolith formation, Lower Saxony Basin, Germany

The 21st International Sedimentological Congress (ISC), Aug. 22– 26, 2022

Poster: Deyan Zhang, François-Nicolas Krencker, Stefan Huck, Ulrich Heimhofer. Sedimentology and carbon isotope record of an Oxfordian carbonate ramp system, Lower Saxony Basin, Germany